

Sustainable sulfur polymers for environmental remediation and multifunctional composite materials

By

Nicholas A. Lundquist

*Thesis
Submitted to Flinders University
for the degree of*

Doctor of Philosophy

College of Science and Engineering
27th August 2021

CONTENTS

<i>SUMMARY</i>	<i>i</i>
<i>DECLARATION</i>	<i>iii</i>
<i>ACKNOWLEDGEMENTS</i>	<i>iv</i>
<i>PUBLICATIONS</i>	<i>v</i>
1.0 Introduction	1
1.1 Waste valorisation and sustainable polymers	1
1.2 Food waste and recycling of used cooking oils	2
1.3 Valorisation of waste sulfur from petroleum refining process	4
1.3 Sulfur polymers history	5
1.4 Sulfur and heavy metal remediation	8
1.5 Methods for reforming, recycling, and re-using sulfur polymers	10
1.6 Multifunctional materials and sulfur polymers	12
1.7 Outline of thesis	13
2.0 Sulfur polymers and iron remediation	15
2.1 Acknowledgements	15
2.2 Abstract	15
2.3 Introduction	16
2.3.1 Sulfur polymers as sustainable heavy metal sorbent materials.....	16
2.3.2 Previous studies on heavy metal sorbents prepared using inverse vulcanisation	16
2.3.3 Iron pollution and its associated problems	17
2.3.4 50-poly(S- <i>r</i> -canola) polymer as an iron sorbent material.....	19
2.4 Experimental	20
2.4.1 General considerations.....	20
2.4.2 Poly(S- <i>r</i> -canola) sorbents preparation and Fe(III) treatment	21
2.4.3 Porous 50-poly(S- <i>r</i> -canola) sorbent preparation and Fe(III) treatment.....	23
2.4.4 Fe(II) treatment using 50-poly(S- <i>r</i> -canola) sorbent	26

2.4.5 Effect of pH and presence of H ₂ O ₂ on Fe(III) treatment using 50-poly(S- <i>r</i> -canola) sorbent.....	26
2.4.6 Porous 50-poly(S- <i>r</i> -canola) sorbent from waste cooking oil	27
2.4.7 Microwave synthesis of porous 50-poly(S- <i>r</i> -canola) sorbent	28
2.5 Results and discussion	30
2.5.1 Poly(S- <i>r</i> -canola) synthesis and characterisation.....	30
2.5.2 Fe(III) sorption with 50-poly(S- <i>r</i> -canola) polymer	35
2.5.3 Fe(II) sorption with 50-poly(S- <i>r</i> -canola) polymer	38
2.5.4 Effect of H ₂ O ₂ on Fe(III) sorption efficiency of the 50-poly(S- <i>r</i> -canola)	39
2.5.5 Porous 50-poly(S- <i>r</i> -canola) stability at varying pH	42
2.5.6 Large scale Fe(III) treatment	44
2.5.7 Comparison to elemental sulfur.....	45
2.5.8 Porous 50-poly(S- <i>r</i> -canola) synthesis and characterization	45
2.5.9 Fe(III) treatment with porous 50-poly(S- <i>r</i> -canola) sorbent.....	49
2.5.10 Langmuir isotherm for Fe(III) sorption using porous 50-poly(S- <i>r</i> -canola).....	50
2.5.11 Effect of pH and competing ions on Fe(III) removal	51
2.5.12 Kinetic analysis of Fe(III) sorption onto the porous polysulfide.....	53
2.5.13 Porous poly(S- <i>r</i> -canola) synthesis from waste cooking oil	54
2.5.14 Microwave induced 50-poly(S- <i>r</i> -canola) synthesis and characterization.....	57
2.6 Conclusion	62
Appendices.....	64
3.0 Powdered activated carbon / 50-poly(S-<i>r</i>-canola) blend	65
3.1 Acknowledgements	65
3.2 Abstract.....	65
3.3 Introduction.....	66
3.3.1 50-poly(S- <i>r</i> -canola) as an activated carbon support polymer.....	66
3.3.2 PFAS pollution	67
3.3.3 PFAS remediation.....	69

3.4 Experimental	69
3.4.1 General considerations.....	69
3.4.2 Material synthesis and characterization.....	70
3.4.3 PFOA batch sorption studies	72
3.4.4 PFOA continuous sorption studies	74
3.5 Results and discussion	75
3.5.1 Synthesis and characterization of PAC / 50-poly(<i>S-r</i> -canola) blend sorbent.....	75
3.5.2 PFOA treatment using 50-poly(<i>S-r</i> -canola) sorbent.....	81
3.5.3 PFOA treatment using PAC / 50-poly(<i>S-r</i> -canola) blend sorbent (batch).....	83
3.5.4 PFOA treatment using PAC / 50-poly(<i>S-r</i> -canola) blend sorbent (batch).....	88
3.6 Conclusion	91
Appendices.....	92
4.0 Reactive compression moulding	93
4.1 Acknowledgements	93
4.2 Abstract.....	93
4.3 Introduction.....	94
4.3.1 Recycling of thermoset polymers	94
4.3.2 Exchangeable cross linkers.....	94
4.3.3 Use of sulfur exchange reaction in polymers made via inverse vulcanization....	96
4.3.4 Reactive compression moulding.....	97
4.3.5 Composite preparation using reactive compression moulding	98
4.4 Experimental	101
4.4.1 General considerations.....	101
4.4.2 First generation reactive compression moulding.....	102
4.4.3 Second generation reactive compression moulding	102
4.4.4 Effect of free sulfur and formation of high sulfur content surface layer	104
4.4.5 Recycling, reforming and re-use facilitated by reactive compression moulding	105
4.4.6 Composite material preparation facilitated by reactive compression moulding	106

4.4.7 Confining spent pollution sorbents in a safe medium	108
4.5 Results and discussion	110
4.5.1 First-generation reactive compression moulding.....	110
4.5.2 Second-generation reactive compression moulding	113
4.5.3 Optimizing reaction conditions.....	114
4.5.4 Sulfur surface layer.....	124
4.5.5 Effect of free sulfur on the moulding process	126
4.5.6 Free sulfur content analysis	128
4.5.7 Reactive compression moulding of canola oil and elemental sulfur	131
4.5.8 Theoretical considerations regarding S-S metathesis of organic polysulfides ..	132
4.5.9 Reactive compression moulding for recycling and repurposing	134
4.5.10 Reactive compression moulding on a 15.0 gram scale.....	139
4.5.11 Preparation of composite materials using reactive compression moulding.....	141
4.5.12 Encapsulation of spend sorbent for safer handling, transport, and storage	148
4.6 Conclusions.....	151
Appendices.....	152
5.0 Multi-functional 50-poly(S-r-canola) / Fe₂O₃ composites	153
5.1 Acknowledgements	153
5.2 Abstract.....	153
5.3 Introduction.....	154
5.3.1 Composite materials from reactive compression moulding	154
5.3.2 Magnetic materials and composites.....	155
5.3.3 Magnetic composites in filtration and separation.....	156
5.3.4 Microwave heating of ferromagnetic composite materials.....	157
5.3.5 Magnetic composites in electrical and mechanical applications	158
5.4 Experimental	159
5.4.1 General considerations.....	159
5.4.2 Composite synthesis design.....	160

5.4.3 Characterisation of composites.....	161
5.4.4 Magnetic filtration	163
5.4.5 Microwave heating	165
5.4.6 Microwave induced reactive compression moulding	167
5.4.7 Composites use in mechanical and electronical systems.....	168
5.5 Results and Discussion.....	169
5.5.1 Preparation of 50-poly(<i>S-r</i> -canola) / γ -Fe ₂ O ₃ composite	169
5.5.2 Direct preparation of composite materials with varying Fe ₂ O ₃ content	173
5.5.3 Characterisation of 50-poly(<i>S-r</i> -canola) / γ -Fe ₂ O ₃ nanoparticles	174
5.5.4 Applications: Magnetic filtration.....	185
5.5.5 Applications: Microwave heating.....	189
5.4.6 Applications: Electrical and mechanical components	198
5.5 Conclusions.....	199
6.0 Conclusions and outlook.....	201
7.0 References.....	203

SUMMARY

Historically elemental sulfur, a waste product of the petroleum refining process, has been difficult to process into useful polymeric forms. The recent development of inverse vulcanisation has allowed for the stabilisation of high sulfur content polymers leading to a wide variety of new sulfur-based materials with interesting chemical and physical properties. In this thesis inverse vulcanisation was utilised to prepare sustainable high sulfur content polymers from renewable plant oils (canola oil) and waste cooking oils. Porous versions of these polymers were prepared by using a NaCl porogen during the inverse vulcanisation reaction. This porogen was then removed after synthesis by washing the product with water, leaving behind a high surface area porous polymer structure. This was an important step for increasing the efficiency of these materials in sorption-based applications. Another important development was the use of microwave irradiation to facilitate the rapid inverse vulcanisation of sulfur and canola oil in 5 minutes, compared to the 30 minutes required under conventional heating. The ability to use household microwaves to prepare this material make it far more accessible to remote areas with limited resources. This is especially true for the application of environmental remediation whereby remote areas with limited resources require access to efficient water treatment technologies. Sulfur polymers have previously been investigated as sorbent materials for heavy metal remediation with most studies focusing on mercury pollution remediation. This thesis focused on using a sorbent material prepared from the inverse vulcanisation of sulfur with canola oil for the remediation of iron pollution. These sorbents were shown to effectively reduce the Fe(III) concentrations to below regulation limits. Removal of Fe(II) was also achieved by oxidising the Fe(II) to Fe(III) using H₂O₂ followed by treatment with the polymer sorbent. The use of waste cooking oil instead of food grade canola oil to prepare the polymer was shown not to impact the performance of the sorbent material. This was an important discovery as it means that waste cooking oil can be used instead of food grade oil, demonstrating a further advancement in the field of waste valorisation. To further the scope of these sulfur materials in the field of environmental remediation, their use as polymeric support materials for the stabilisation of powdered activated carbon (PAC) was demonstrated. The poly(S-*r*-canola) support facilitated the effective use of PAC in continuous flow treatment processes as well as increased its safety profile by suppressing the generation of flammable PAC dust plumes. The PAC / poly(S-*r*-canola) blend was demonstrated to be an effective sorbent material for the remediation of the persistent organic pollutants perfluorooctanoic acid (PFOA) and perfluorooctanesulfonic acid (PFOS), outperforming the current industry standard, granular activated carbon (GAC). Although a wide variety of important applications for these sulfur polymers have been investigated, efficient end of life recycling strategies have not been yet developed. In this thesis a new

method for reforming, repurposing, and recycling sulfur polymers termed reactive compression moulding was developed. This process involved compressing poly(*S-r*-canola) particles reactive interfaces into direct contact under heat, whereby a sulfur exchange reaction would occur facilitating the chemical binding of neighbouring particles. Different types and amounts of filler materials were combined with the polymer during reactive compression moulding to allow for the mechanical properties of the resulting mats/blocks to be tailored for specific applications. This simple recycling/reforming process was then further utilized to prepare multifunctional magnetic composite materials. To achieve this, magnetic γ -Fe₂O₃ nanoparticles were combined with poly(*S-r*-canola) particles before undergoing reactive compression moulding to effectively encapsulate the nanoparticles. The resulting composite materials were shown to maintain their ability to remove HgCl₂ from solution whilst also allowing for magnetic filtration to be used to isolate the spent sorbent from other solids in solution reducing the quantities of solid waste being produced. The inclusion of the magnetic particles also facilitated the heating of these composites through microwave irradiation. The heating rate was shown to be directly proportional to the amount of γ -Fe₂O₃ nanoparticle in the composite material allowing for the determination of optimized irradiation times for each composite. Using this information rapid reactive compression moulding of the composite material, forming composite disks and cylinders, was demonstrated under microwave irradiation. Finally, the use of these magnetic composites in electrical and mechanical systems was demonstrated by replacing the active magnetic component in a solenoid valve with the magnetic composite material. This reduced the weight of the component by an order of magnitude and demonstrated one of many potential uses within electrical and mechanical systems.

DECLARATION

I certify that this thesis does not incorporate without acknowledgment any material previously submitted for a degree or diploma in any university; and that to the best of my knowledge and belief it does not contain any material previously published or written by another person except where due reference is made in the text.

Signed.....Nicholas Lundquist.....

Date.....12th June 2021.....

ACKNOWLEDGEMENTS

Associate professor Justin Chalker for the all the guidance, advice and help with experimental design. Martin Johnston for assistance in using the laboratory microwave reactor. Dr. Max Worthington for running ^1H NMR samples for chapters 2 and 4 as well as assistance in SEM / EDX analysis of porous 50-poly(*S-r*-canola) polymer in chapter 2. Nick Adamson for XRD analysis of porous and non-porous 50-poly(*S-r*-canola) polymers in chapter 2. Salah Alboaji for performing the initial PFOA sorption experiment which resulted in the direct observation of PFOA hemi-micelle formation of the poly(*S-r*-canola) surface in chapter 3. Kymberley Scroggie for assistance with ^{19}F NMR analysis of PFOA. Christopher Gibson for all Raman spectroscopy. Louisa Esdaile for developing and optimising the up scaling of polymer synthesis in chapter 3. Alfrets Tikoalu for assistance with origin pro software in chapter 3 as well as composite preparation, and compression testing of the poly(*S-r*-canola) composites in chapter 4. Sam Tonkin for running three-point bending tests on poly(*S-r*-canola) composites. Jonathan Campbell for assistance with DMA analysis and instrument training. Dr. Filip Stojcevski and Prof. Luke C. Henderson for supplying waste carbon fibre for composite synthesis, running nano-indentation analysis as well as contact angle experiments on carbon fibre composites in chapter 4. Dr. Amir Karton for all theoretical calculations of S-S bond strengths. Israa Bu Najmah for assistance with thermal conductivity measurements for the 50-poly(*S-r*-canola) polymer in chapter 5. Dr Yanting Yin for XPS characterisation of all magnetic composite samples.

PUBLICATIONS

This work in this thesis has formed the basis for 8 peer reviewed publications:

1. Lundquist, N. A., et al. "Polysulfides made from re-purposed waste are sustainable materials for removing iron from water." *RSC Adv.* **2018** 8, 1232-1236.
2. Worthington, M. J. H., et al. "Sustainable Polysulfides for Oil Spill Remediation: Repurposing Industrial Waste for Environmental Benefit." *Adv. Sustain. Syst.* **2018**, 2, 1800024.
3. Lundquist, N. A., et al. "Polymer Supported Carbon for Safe and Effective Remediation of PFOA- and PFOS-Contaminated Water." *ACS Sustain. Chem. Eng.* **2019**, 7, 11044-11049.
4. Chalker, J. M., et al. "Synthesis and Applications of Polymers Made by Inverse Vulcanization." *Topics in Current Chem.* **2019**, 377 16.
5. Tikoalu, A. D., et al. "Mercury Sorbents Made By Inverse Vulcanization of Sustainable Triglycerides: The Plant Oil Structure Influences the Rate of Mercury Removal from Water." *Adv. Sustain. Syst.* **2020**, 4, 1900111.
6. Lundquist, N. A. et al. "Reactive compression moulding Post-Inverse vulcanization: A Method To Assemble, Recycle, and Repurpose Sulfur Polymers and Composites" *Chem. Eur. J.* **2020**, 26, 10035-10044.
7. Lundquist, N. A.; Chalker, J. M. "Confining a spent lead sorbent in a polymer made by inverse vulcanisation prevents leaching," *Sustain. Mater. Technol.* **2020**, 26, e00222.
8. Bu Najmah, I., et al. "Insulating Composites Made from Sulfur, Canola Oil, and Wool." *ChemSusChem* **2021**, 14, 2352-2359.

1.0 Introduction

1.1 Waste valorisation and sustainable polymers

Modern life is dependent on polymeric materials. Polymeric materials have become important components in multiple industries including clothing, transport, construction, medicine, diagnostics and electronics.¹ In recent years the industrial scale manufacturing of new products, a large percentage of which are made from polymeric materials, has exponentially increased.² This exponential increase in manufacturing results in the production of large quantities of unwanted waste. Sustainable uses for these waste products must be developed or else the waste will accumulate and lead to potential contamination and damage to local environment.² Efficient green methods for re-using, recycling and re-forming these materials must therefore be developed in order to reduce waste and move towards a circular economy (Figure 1). Industrial waste products are typically readily available and inexpensive making them potentially useful as starting blocks in the preparation of new sustainable polymeric materials.

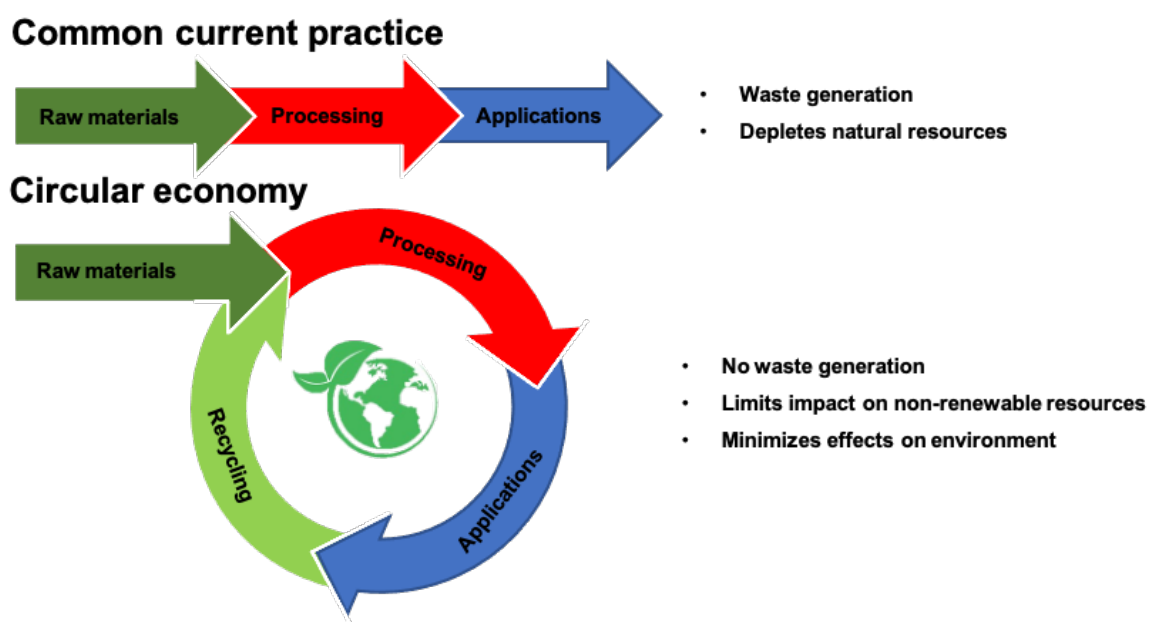


Figure 1 – Figure showing typical current manufacturing scheme vs a circular economy model.

Examples of waste products produced in significant quantities include food waste, electronics waste, glass waste, plastic waste, and chemical waste.³⁻⁷ The depletion of natural resources, increasing waste generation and the need to reduce the practice of landfilling has resulted in an increasing interest in recycling and waste valorisation.⁸ The vast majority of the polymers currently utilised on an industrial scale are prepared directly from petrochemicals. There are concerns about the environmental impacts of both the starting materials and the end of use waste products.¹ In 2014 only 0.56% of global polymer production was from bio-derived

sources.¹ Investigating both renewable alternatives to petrochemicals and new strategies for end of life waste management such as recycling and re-use, have become important endeavours in tackling the potential negative environmental impacts associated with petrochemical based polymers.¹ Many examples of waste valorisation are present in literature converting waste from different industries into useful final products. Waste from the food industry is typically converted into either biofuel or useful chemicals such as fats and oils.⁹ Recycling strategies for waste products from the construction industry such as glass, recycled wood, paper, cardboard, metal, glass, mineral wool, gypsum, concrete, and ceramics have previously been demonstrated.^{5, 10} Some materials, such as thermoset polymers are unable to undergo typical melt processing methods limiting the potential for recycling. One method by which their recycling has been achieved is through their use in various composite materials. Some examples of waste products recycled for use as reinforcement materials in polymer composites include bagasse, bamboo, hemp, rice husks, kenaff, groundnut shells, wool, etc.^{11, 12} Petrochemical waste in the form of elemental sulfur has been converted into sulfur polymers and been used as an oil sorbent material for oil spill remediation.⁷ This is an example whereby the waste from the petrochemical industry was used to prepare a material used to clean up the waste generated by the same industry. Another example of this is where a functional catalyst was prepared from food waste in the form of corncob residue and then used to catalyse a reaction converting another type of food waste, waste cooking oil, into new useful products.¹³ This example demonstrated the ability to not only create useful materials from waste, but to utilise those materials to aid in further waste valorisation efforts.¹³ This thesis will focus of two major forms of waste: food waste in the form of waste cooking oil and waste sulfur produced from the desulfurization of petroleum during its refining process.

1.2 Food waste and recycling of used cooking oils

The global food industry is a significant contributor to global solid waste productions. Food waste can be defined as waste produced during the production, processing, distribution and consumption of food.¹⁴ Concerns into the disposal of global food waste have been increasing. Studies show that up to 50% of the world's food produced ends up as food waste, equating to approximately 1.3 billion tonnes annually.⁸ This has negative impacts on the environment, the economy and society.¹⁵ Issues associated with food waste include pathogen growth, rapid autoxidation of fats into foul smelling fatty acids, degradation and microbial contamination.^{8, 14, 16, 17} Therefore there is a growing need for efficient methods at both reducing and recycling the food waste to make the food industry more sustainable and prevent the potential negative

impacts stated. Types of food waste include organic crop wastes (i.e. fruits and vegetables not suitable for sale), catering wastes (cooking oils), animal by-products (inedible waste from slaughter), packaging and mixed food wastes.¹⁸ Typically, these waste products are produced during the preparation of a meal. The most common method used to cook food around the world is frying.¹⁹ Because of this, waste cooking oils (WCOs) represent a significant portion of the food waste produced globally every year. The global production of used vegetable oils (including used cooking oils) exceed 190 million tonnes annually.¹⁹ WCOs are typically disposed of down the drain and through public sewage systems resulting in increases to water treatment costs and extra maintenance requirements for treatment equipment.²⁰ The presence of WCOs in water systems results in a series of mass transfer issues as well as promoting the formation of foams and the floatation of sludges.²⁰ Current methods for recycling WCOs are limited. Some sellers re-use their cooking oil multiple times before disposing of it to increase the oil's lifespan. Whilst methods for the efficient recycling and valorisation of WCOs require more investigation, several strategies for recycling WCOs do exist. WCOs are typically composed of a mixture of triglycerides, diglycerides, monoglycerides and varying amounts of free fatty acids produced throughout the frying process.²⁰ The major components are the saturated and unsaturated fatty acids. These can be used as a platform for synthesis and manufacture of new value-added products.²⁰ One major application of WCOs has been in the production of biodiesel.²¹⁻²⁶ Other applications for WCOs include as bio-lubricants,²⁷ additives for asphalts,²⁸ biosolvents for pollutants and raw materials in the synthesis of bio-plasticisers, syngas and a number of other value added materials.^{20, 29-31} Oxidative polymerization²⁹ and microwave processing techniques^{30, 31} have been utilised to convert WCOs into value added polymeric products. Finding new methods for preparing different polymeric products from WCOs would substantially increase the range and types of polymeric products formed. This would increase the scope of potential applications of WCO based polymers helping to solve the issue related to sulfur over-production. Inverse vulcanisation is a new strategy used to prepare high sulfur content polymer materials from elemental sulfur and alkene cross-linkers.³² This thesis will investigate the valorisation of waste cooking oil in the form of canola oil, through polymerisation with sulfur to create new value-added materials. Canola oil is the third largest plant oil produced behind soybean oil and palm oil, with approximately 26 million tonnes of canola oil being produced annually.^{33, 34} Canola oil is produced from rapeseed crops and sold commercially as cooking oil (Figure 2).



Figure 2 – Rapeseed crop used to produce canola oil (left), Canola oil products (middle) and canola oil being used in deep frying (right).

We will investigate the use of canola oil (and waste canola oil) as a starting block for the synthesis of new sustainable polymeric materials through inverse vulcanisation with elemental sulfur.

1.3 Valorisation of waste sulfur from petroleum refining process

Another industry which produces substantial amounts of waste products is the petroleum industry. As sampled directly from the ground, typically less than half a barrel of crude oil is able to be used for transportation fuels.³⁵ Crude oil is a complex mixture of hydrocarbon compounds contaminated with small amounts of water, salts and other oxygen, nitrogen and sulfur related compounds with trace quantities of inorganic contaminants also present.³⁵ The presence of these contaminants means the oil must undergo a refined process before being used as fuel.³⁵ During the petroleum refining process hydrogen sulfide gas is produced in high concentrations. This gas is then converted into elemental sulfur using the Claus process, which involves first converting the H_2S into SO_2 by reaction with air.³⁵ This was followed by reaction between the SO_2 and H_2S using a bauxite catalyst to form elemental sulfur.³⁵ This elemental sulfur is the major waste product produced during the petroleum refining process with over 60 million tons produced annually.³² It has found use in the preparation of sulfuric acid, fertilizers and other commodity chemicals as well as in the production of synthetic rubber through classic vulcanization.³² Although these applications consume a lot of sulfur they only account for approximately 88% of the sulfur produced leaving an excess of sulfur (7 million tons) left unused annually.³² This sulfur must be stored somewhere and therefore massive above ground deposits have been created to stockpile this abundance of sulfur.³² Elemental sulfur is also produced naturally during volcanic eruptions however the amount produced annually by petroleum refining far exceeds this amount. Figure 3 shows the two major sources of sulfur production, petroleum refining and volcanic eruptions, as well as a site where sulfur is being stockpiled.



Figure 3 – Images showing the two major sources of sources; petroleum refining (Left) and natural sources such as volcanoes (middle). Stockpiles of sulfur remaining unused (right).

Elemental sulfur has several useful properties making it a potential candidate for use in several important applications. Upon heating, sulfur demonstrates a high tendency to react with itself to form S-S bonds.³⁶ Depending on the conditions it can be in ring or chain form with chains forming from between 2 sulfur atoms to up to 10^5 sulfur atoms.³⁶ These different forms are present in equilibrium depending on the conditions. This variety in sulfur structure leads to a wide variety of interesting reaction possibilities.³⁶ Unfortunately difficulties in controlling reaction outcomes and forming stable products arise due to the high reactivity of sulfur and the photosensitivity of S-S bonds.³⁶ These difficulties have limited sulfurs use in many applications. To alleviate the growing amount of land and resources required to store the sulfur and limit the potential environmental impacts these stockpiles could result in, new innovative methods for using this sulfur must be investigated.⁵ Developing new sulfur processing methods and new sulfur materials could also help alleviate the use of less available natural resources.⁵ One strategy that has gained popularity in recent years is using elemental sulfur as a feedstock material for the preparation of high sulfur content polymers.³²

1.3 Sulfur polymers history

Although sulfur has useful electrochemical and optical properties, historically, the utilization of sulfur as a feedstock material for material preparation was scarce.³² This is mostly due to the difficulties, outlined above, in controlling reaction outcomes for sulfur compounds.³⁶ Another reason for this scarcity of use is due to difficulties in processing elemental sulfur and other sulfur based compounds into useful forms.³⁷ Elemental sulfur is insoluble in most common solvents showing limited solubility in cyclohexane, chlorobenzene, p-xylene and toluene.³⁸ Elemental sulfur has a melting point at $119\text{ }^{\circ}\text{C}$ forming a yellow molten liquid phase consisting primarily of S_8 rings but can also contain sulfur rings with between 6 and 35 sulfur atoms.³⁹ Once the temperature is increased to $159\text{ }^{\circ}\text{C}$ a transition occurs whereby the properties of the liquid dramatically change.⁴⁰ Properties effected by this transition include viscosity,

specific heat, material density, refractive index and dielectric permittivity.⁴⁰⁻⁴³ Raman, ESR and neutron diffraction analysis confirmed that this transition is due to the ring opening polymerization of elemental sulfur initiated by homolytic cleavage of S-S bonds.⁴⁰⁻⁴⁴ This transition temperature has been termed the floor temperature or polymerization temperature for sulfur.³⁷ The polymeric sulfur formed is an insoluble semicrystalline solid with poor mechanical properties and inability to be melt processed.⁴⁵ By comparing the soluble fractions in CS₂, the extent of polymerization was shown to increase with an increase in reaction temperature.⁴⁰ This polymeric form of sulfur is unstable and depolymerizes over a period of time to form the thermodynamically favoured α -S₈.⁴⁵ This depolymerization is accelerated when in the presence of heat, light or a number of chemical compounds including H₂O, NH₃, S₂Cl₂ and H₂S_x (x = 1, 2, 3, ...).⁴⁵ This means the state of polymeric sulfur depends on its age, its storage conditions, and the presence of any contaminants. Its high reactivity with contaminants suggests interesting chemical properties however its instability renders it impractical for use in most applications. Creating stabilized polymeric forms of sulfur would open up a number of new potential applications of sulfur based materials due to sulfurs favourable weathering characteristics, chemical reactivity, high availability and low costs.³⁶ A process termed classical vulcanisation is used to incorporate small quantities into polymeric materials.³² This process involves the addition of small quantities of sulfur to cross-link a pre-formed polymer.⁴⁶ Methods for the co-polymerisation of sulfur with other monomers have also been investigated. One study used copolymerisation with dienes to quench the radicals and stabilize the polymeric sulfur. Whilst this worked to stabilize the polymeric sulfur the product was a brittle crystalline material with poor mechanical properties.⁴⁷ Other studies utilized copolymerization with propylene sulfide,^{48, 49} styrene,⁵⁰ diynes,⁵¹ cyclic disulfides,⁵² sodium sulfide⁵³ as well as a number of transition metals to form stable polysulfide.^{54, 55} Whilst these studies demonstrated the capability to utilize sulfur in the production of new materials, they suffered from low degrees of sulfur incorporation or formed polymeric materials with limited ability to process or tune their properties reducing the scope of potential applications. In 2013 Pyun and collaborators investigated using molten sulfur as a medium for the copolymerization of polymeric sulfur with a divinyl crosslinker, 1,3-diisopropenylbenzene (DIB), to form stable high sulfur content polymers.³² This method termed inverse vulcanisation had not previously been investigated and is the inverse of the classical vulcanisation process used in the rubber industry.³² Since the first study by Pyun, a variety of cross-linkers have been investigated producing a multitude of different sulfur polymers with unique properties.⁵⁶ The process involves heating elemental sulfur to above 120 °C, where it melts to form a yellow molten

phase.³⁹ The molten sulfur is then further heated to above 159 °C (floor temperature of S₈) whereby homolytic cleavage of the S-S bonds in sulfur occurs forming polysulfide chains with radicals ends.³⁹ These chains combine to propagate the polysulfide chain forming longer polysulfide chains with radical ends (Figure 4).

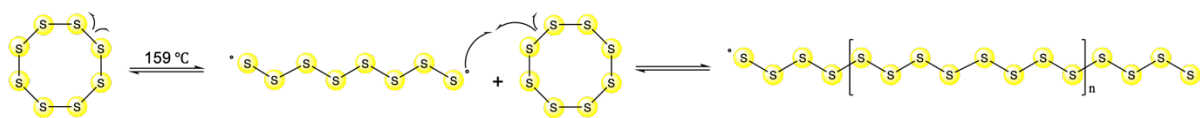


Figure 4 – Thermal ring opening polymerization of elemental sulfur (S₈).

This propagation is halted by termination through quenching with a divinyl cross-linker.³² The S-S bonds of this terminated polysulfide chain will continue to undergo homolytic cleavage followed by radical termination with another cross-linker molecule until the molecular weight of the polymer is high enough that the polymer vitrifies. This is shown in Figure 5.

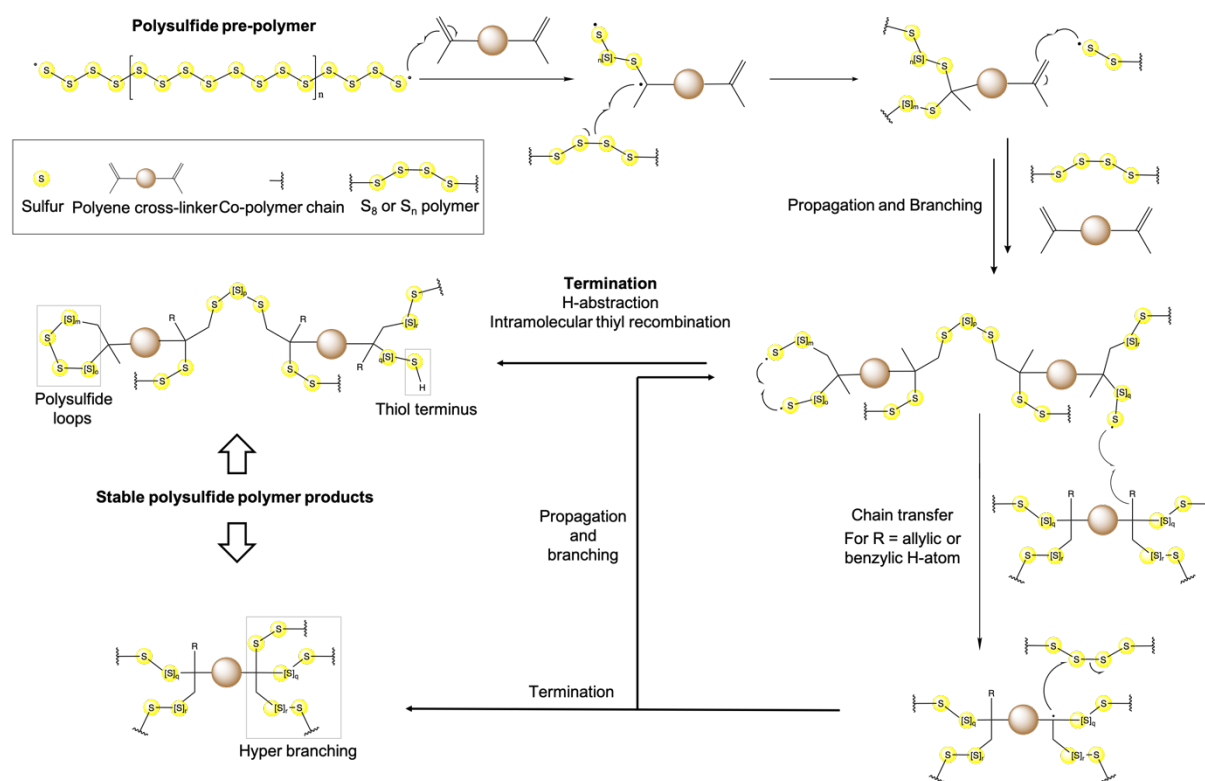


Figure 5 – Proposed mechanism for inverse vulcanization

Termination of copolymerization could also occur via hydrogen abstraction, intramolecular and intermolecular polysulfide recombination.⁴⁶ Intermolecular polysulfide recombination occurs between polysulfide chains attached to different monomer units whilst intramolecular recombination occurs between polysulfide chains connected to the same monomer unit. Intramolecular recombination terminates chain growth forming cyclic copolymer chains whereas intermolecular recombination extends the polymer chain forming higher molecular

weight polymer chains with higher degrees of cross linking. It's important to note that although H-abstraction does terminate the sulfur chain propagation, it forms a carbon radical which can result in branching off a non-alkene carbon. The polysulfide chains can also depolymerize through a process called 'back-biting' to form the thermodynamically favoured S₈.⁴⁶ This process results in unreacted free sulfur remaining in the final product after reaction. The mechanism for depolymerization through 'back-biting' is shown in Figure 6.⁵⁷

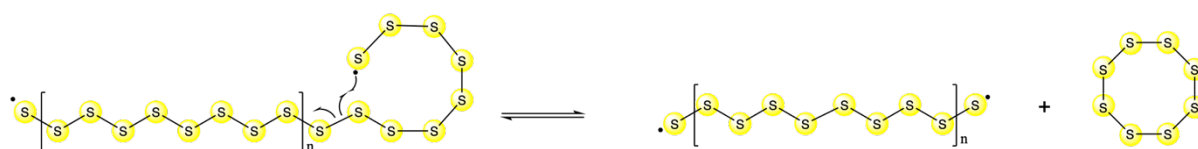


Figure 6 – Depolymerizations of polymeric sulfur through backbiting.

The first application for these sulfur polymers, investigated by Pyun, was as cathode materials for lithium sulfur batteries.³² This study demonstrated that these new sulfur polymers displayed comparable electrochemical properties to elemental sulfur and could be effectively used as cathode materials for Li-S batteries.³² These cathodes exhibited high specific heat capacities of 823 mA.h.g⁻¹ at 100 cycles and enhanced capacity retention compared with typical sulfur cathodes.³² They also highlighted the ability to process this polymer into useful forms by using imprint lithography to prepare micropatterned films, something not possible with typical polymeric sulfur. The vast majority of follow up studies related to inverse vulcanisation investigate the use of these materials as cathode materials in Lithium-Sulfur batteries.⁵⁸⁻⁸⁶ Other applications investigated for high sulfur content polymers prepared by inverse vulcanisation include IR imaging lens materials,^{87, 88} materials for hydrogen splitting, hole-transport materials for dye sensitives solar cells,⁸⁹ mediums for nanoparticle synthesis,⁹⁰⁻⁹³ fertilizers,⁹⁴⁻⁹⁷ oil spill sorbent materials,⁷ heavy metal sorbent materials,⁹⁸⁻¹⁰³ porous materials for natural gas sweetening,¹⁰⁴ antibacterial surfaces,¹⁰⁵ starting materials for sulfur doped porous carbon synthesis,¹⁰⁶⁻¹⁰⁹ polymeric mediums for composite materials,^{12, 110-112} photoactive catalysts,¹¹³ and as additives to improve cement strength and durability.^{114, 115} This thesis will focus on heavy metal remediation and recycling/healing applications for sulfur polymers.

1.4 Sulfur and heavy metal remediation

Another important application of high sulfur content polymer is environmental remediation. Sulfur polymers and other sulfur related compounds have been investigated in the past for environmental remediation strategies especially in heavy metal remediation.¹¹⁶ Of these sulfur based compounds, dithiocarbamic acids have been the most popular.^{117, 118} The selectivity of metal adsorption for dithiocarbamic acid is low and the slow emission of toxic carbon disulfide

is another limitation preventing this compounds large scale practical use.¹¹⁸ Thiol and thiocarbonyl sorbents do not have this issue and have been demonstrated as effective functional groups for heavy metal sorption materials.¹¹⁸⁻¹²⁴ Its important to note that whilst thiols can act as metal scavengers forming stable thiolates in the process, they are also susceptible to oxidative coupling to form disulfides instead of metal adsorption.¹²² Thioamides,¹²⁵⁻¹³⁶ thiourethane¹³⁷⁻¹⁴⁰ and thiourea¹⁴¹⁻¹⁴⁹ have also been investigated as stable sulfur based heavy metal sorbent materials. Thiocarbonyl groups demonstrate high affinity toward the noble metals due to sulfur's excellent affinity towards soft cations.^{126, 138-140, 150-152} Studies have demonstrated the removal of Hg,¹⁵³ Au,¹⁵⁰ Ag,¹⁵⁰ Pd,¹⁵⁰ Cd¹⁵⁴ from solution using thiocarbonyl moieties. Sulfur based compounds have also been utilized for the removal of heavy metals from biological samples. This process is called detoxification and has been investigated for mercury, arsenic, lead, cadmium and copper pollutants by mono-, di- and polythiols, dithiocarbamates and cysteine derivatives.¹⁵⁵ This suggests that new sulfur polymers prepared by inverse vulcanisation could find application as heavy metal sorbent materials for both environmental remediation and heavy metal detoxification applications. Previous studies have demonstrated the use of sulfur polymers for environmental applications.^{99, 101, 102, 156-162} The recent invention of inverse vulcanisation has led to the creation of a vast variety of new stable sulfur polymers which could be utilized as heavy metal sorbent materials. Chalker and co-workers were the first to investigate the use of these polymers in heavy metal remediation. A sulfur polymer was prepared by the inverse vulcanisation of D-limonene, a by-product of the citrus industry.⁹⁸ This wax-like sulfur polymer was shown to effectively remove both mercury and palladium salts. Treatment of mercury(II) salts resulted in their conversion to mercury metal and sulfur rich nanoparticles on the materials surface. This resulted in the material changing colour from red to yellow. This colour change is useful as it could be utilized for potential sensing applications or be used to determine the point at which the sorbent is spent.⁹⁸ The rate of mercury uptake for this polymer was slow taking up to several hours.⁹⁸ To increase both the rate of mercury uptake and overall capacity Wu *et al.* tested mercury uptake using a high surface area silica gel coated with the limonene polysulfide.¹⁵⁷ The mercury uptake capacity was show to increase to 716 mg of Hg per gram of sorbent material which is among the highest mercury uptake capacity reported in the literature.¹⁵⁷ Other methods for increasing the surface area of these materials to enhance the mercury uptake capacity include; foaming S-DIB,¹⁵⁸ salt-templating followed by a water wash^{100, 159, 161} as well as electrospinning into nanofibers.¹⁶⁰ It was demonstrated that the electro spun nanofibers were capable of removing over 98% of the mercury(II) from aqueous solution (20 ppm) within only seconds of contact.¹⁶⁰ Other studies have demonstrated

that mercury sorbents could be prepared by the inverse vulcanisation of low cost and renewable cross-linkers. After the initial study using D-limonene, Chalker and associates investigated mercury sorption using polymers prepared by the inverse vulcanisation of unsaturated triglycerides such as canola oil, sunflower oil, olive oil and even used cooking oil.^{100, 163} Types of mercury investigated included; inorganic mercury, liquid mercury metal, mercury gas, organic mercury, and mercury bound to natural organic matter. These polymers were demonstrated to be reactive sorbents oxidising the mercury metal into mercury sulfide (non-volatile and very insoluble) unlike typical mercury sorbent materials that rely on physical adsorption.¹⁰⁰ Both the uptake of inorganic mercury and mercury metal resulted in an observable colour change that could be utilised in sensing applications and to monitor the lifetime of air or water filters.¹⁰⁰ Chalker's study also demonstrated that the same sorbent material could be used to remove mercury metal from soil by milling the polymer and soil together and then separated using a sieve.¹⁰⁰ Other sustainable crosslinkers used to prepare heavy metal sorbent materials by inverse vulcanisation include, myrcene and diallyl disulfide.¹⁶² Most studies focus on the use of high sulfur content polymers in mercury remediation however there are many other pollutants which need investigating.

1.5 Methods for reforming, recycling, and re-using sulfur polymers

Polymers prepared by inverse vulcanisation are characterised by a large amount of S-S bonds. These bonds are dynamic and can break and reform by application of heat, light or use of chemical initiators.¹⁶⁴ This unique property facilitates a mechanism by which the repair, recycling and reformation can occur.⁸⁸ Sulfur compounds previously investigated as self-healing materials include poly(dimethylsiloxane) crosslinked with disulfide bonds,¹⁶⁵ aryl disulfides¹⁶⁶ and sulfur polymers.¹⁶⁷ Several studies have demonstrated initiator free sulfur exchange in aromatic disulfides at room-temperature.¹⁶⁸ Unfortunately this room temperature sulfur exchange reaction has only been observed to occur for aryl disulfides. Different methods used for initiating sulfur exchange include chemical,¹⁶⁹⁻¹⁷¹ thermal¹⁷² and UV irradiation.^{173, 174} Chemical initiators have been shown to catalyse this reaction under mild conditions and polar solvents such as tertiary amines and phosphines.¹⁶⁹ Tonkin *et al.* demonstrated the ability to induce the repair, adhesion and recycling of inverse vulcanised polymers using chemical initiators.¹⁶⁷ They demonstrated that two surfaces of inverse vulcanised polymers could be chemically adhered at room temperature through treatment with a phosphine or amine-catalysed sulfur-sulfur exchange reaction. The use of pyridine or triethylamine showed exchange at room temperature for polysulfides with more than 2 sulfur atoms bonded

consecutively in a chain.¹⁶⁷ Another study also demonstrated the use of tri-n-butylphosphine as an effective catalyst for initiating the sulfur exchange reaction at room temperature.¹⁷⁵ Both studies employ the use of room temperature compression to facilitate the remoulding of the materials into new shapes and forms.^{167, 170} Whilst these methods facilitate the sulfur exchange reaction, they require the use of an added solvent, further complicating the process as well as substantially increasing the costs involved for large scale recycling processes. On top of this the most effective catalysts (amines and phosphines) are generally hazardous adding further safety concerns to the process. Light and heat-initiated sulfur exchange reactions are advantageous as no added solvents or catalysts are required for the process. Light initiated sulfur exchange has been demonstrated at room temperature. Photodegradable and photo adaptable hydrogels have been prepared which utilize light initiated sulfide exchange reactions as their primary mechanism for 'adaption'.¹⁷⁴ A number of other studies have also demonstrated the use of light-initiated sulfur exchange reaction for material healing, reforming and/or recycling.^{173, 175} Whilst these methods are interesting and useful for soluble polymers, insoluble polymers suffer from the issue that the reaction is limited to areas in direct contact with the light, which in this case is only the surface. Whilst this issue may be overcome in lab scale reactions, large scale recycling processes would be significantly impacted. Whilst heat-initiated sulfur exchange reactions consume more energy over the course of the reaction compared to light-initiated, it overcomes the apparent issues with scaling up light-initiated sulfur exchange for a large-scale recycling process. Heat-initiated sulfur exchange has also been shown to occur at a faster rate than light-initiated, increasing the speed (and in turn the viability) of the recycling process. For these reasons heat-initiated sulfur exchange will be investigated as a practical method for the large-scale recycling of sulfur polymers. With regards to sulfur polymers prepared from inverse vulcanisation, a number have studies related to sulfur exchange reactions have been published. Most of these studies utilize these reactions for healing applications.^{88, 176-179} The first demonstration of sulfur-exchange based healing in inverse vulcanised polymers was by Pyun and collaborators in 2015.⁸⁸ They prepared a copolymer from 1,3-diisopropenylbenzene (DiB), scratched its surface and then cured it for 3 hours.⁸⁸ This curing was enough to initiate sulfur exchange reactions at the defects and facilitate the repair of the scratch's through the formation of new covalent bonds.⁸⁸ In this case whilst the material must be converted into the molten phase for efficient repair to occur, it differs from typical melt processing because it also breaks and reforms covalent bonds through S-S exchange reactions. Sulfur exchange reactions therefore offer a convenient new method for recycling sulfur polymers.¹⁸⁰⁻¹⁸³ This study will focus on the recycling of sulfur polymers

prepared by inverse vulcanisation into new shapes/forms by initiating S-S exchange using heat and compression. This method, outlined in Figure 7, will also be investigated for use in preparing polymer composites.

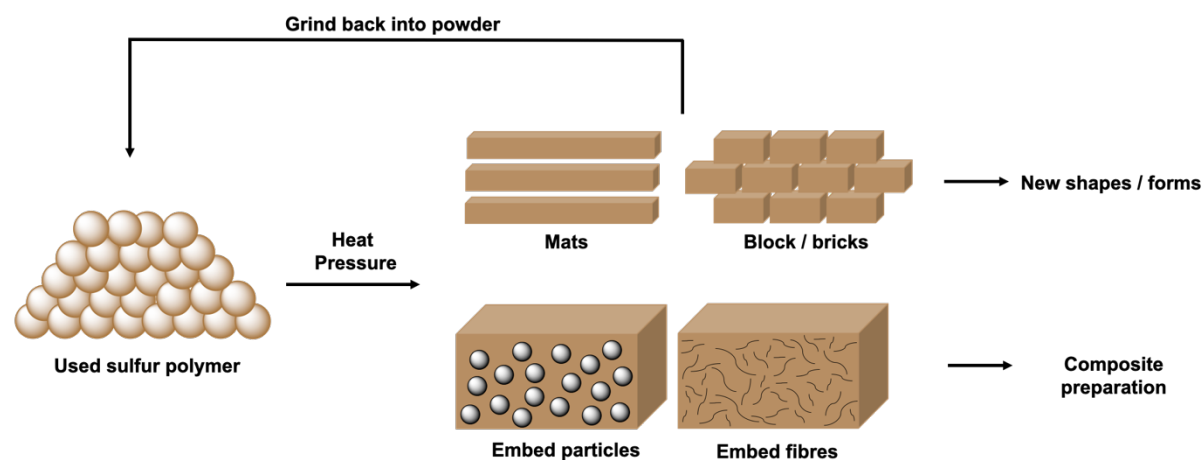


Figure 7 – Strategy for recycling used sulfur polymers into useful forms and the formation of sulfur polymer composite materials.

1.6 Multifunctional materials and sulfur polymers

‘Smart materials’ is a general term encompassing a wide range of materials that are capable of changing one (or more) of their properties in response to a certain stimulus.¹⁸⁴ The definition of smart materials was expanded to include any material capable of receiving, transmitting, or processing a stimulus and responding in a manner which produces some useful effect.¹⁸⁴ The ‘smart’ title describes the ability of the material to be self-adaptive, self-sensing, have some form of memory and multiple functionalities. The complex functionalities of these smart materials make them useful in applications such as manufacturing, electronics, robotics, civil infrastructure systems, aerospace, biomechanics, and the environment.¹⁸⁴ The stimuli used for different smart materials include electromagnetic radiation, pH, temperature, water, chemical as well as mechanical stress, strain and pressure.¹⁸⁴ The types of smart materials can be categorized into piezoelectric materials, thermo-responsive materials, chromogenic systems, pH-sensitive materials, electro-responsive and magneto-restrictive materials.¹⁸⁴ Magneto-restrictive materials are those that activate and respond to magnetic stimuli. They are typically used in low frequency / high power applications such as sonar transducers, motors, hydraulic actuators, active vibrational dampeners and shape memory alloys such as Nitinol.¹⁸⁴ The need to save energy and the demand for cheaper materials and manufacturing processes is driving the increase in research into new magnetic materials to be used in these systems.¹⁸⁵ Due to the low costs, high availability and useful chemical properties of sulfur and its resulting polymers,

the preparation of multifunctional magnetic composites from 50-poly(*S-r*-canola) polymer and magnetic nanoparticles will be investigated in this thesis. Sulfur polymers on their own display useful chemical properties resulting from their dynamic S-S bonds, facilitating their healing and repair by heat, light or chemical initiators. By combining these properties with the magnetic properties of the nanoparticles a multifunctional magnetic sulfur composite will be prepared and its potential applications investigated. Another interesting application arising from the dynamic S-S bonds is shape memory materials. In one study a material was prepared from sulfur and pentaerythritol tetra(3-mercaptopropionate) that demonstrated both thermo-induced and photo-induced solid-state plasticity. These abilities give this material a complex 3D shape memory mechanism initiated by heat or light.¹⁸⁶ Sulfur polymers could also be combined with other useful materials to form multifunctional composite materials. One example of a multifunctional sulfur polymer composite is a sulfur-liquid metal composite material able to undergo room temperature self-healing. The liquid metal (gallium-indium-zinc eutectic alloy) binds with the surface sulfur upon direct contact facilitating the healing between the two pieces.¹⁸⁷ The mechanism for self-healing in this case is due to the polymer's affinity towards the liquid metal instead of sulfur exchange.¹⁸⁷ In this thesis, magnetic nanoparticles will be imbedded within the 50-poly(*S-r*-canola) polysulfide forming multifunctional magnetic composite materials.

1.7 Outline of thesis

In this thesis sulfur polymers prepared from sulfur and canola oil will be investigated in several different applications. In chapter 2, the synthesis and characterisation of 50-poly(*S-r*-canola) polymer sorbent materials was demonstrated and their use in iron remediation was investigated. The 50-poly(*S-r*-canola) was shown to bind to Fe(III) and facilitate its removal from water. To increase the surface area of these sorbents, NaCl was added into the reaction mixture as a porogen. This porogen was removed after inverse vulcanisation by dissolving the NaCl porogen in water. The porous 50-poly(*S-r*-canola) polymer was more effective at Fe(III) removal than the non-porous polymer. The rapid inverse vulcanisation (~5 mins) of the 50-poly(*S-r*-canola) polymer using microwave heating was also demonstrated. This is an important development in the field of inverse vulcanised polymers. By replacing food grade cooking oil with waste cooking oil, the material appeared identical and no loss in Fe(III) uptake capacity was observed. In chapter 3 the 50-poly(*S-r*-canola) polymer was investigated as a support polymer for powdered activated carbon. Simply mixing the 50-poly(*S-r*-canola) with PAC resulted in a homogenous mixture whereby the PAC adhered to the surface of the 50-

poly(*S-r*-canola) particles. The optimum ratio for PAC to 50-poly(*S-r*-canola) was determined to be 20:80. The ability of this blend to remove PFAS from solution was investigated. In chapter 4, a new method for recycling and reforming sulfur polymers was investigated. This method utilised compression to bring the reactive polysulfide interfaces into direct contact and heat (100 °C) to initiate S-S exchange reactions facilitating the binding process. With a wide variety of applications for these new sulfur polymers, this is an important discover to increase the viabilities of these materials. Reactive compression moulding was then investigated for the synthesis of composite materials with coco-fibres, waste PVC, sand, and waste carbon fibres. By changing the amount and type of filler material the properties of the resulting composites could be tailored for specific applications. In chapter 5 the reactive compression moulding process developed in chapter 4 was used to prepare magnetic $\gamma - \text{Fe}_2\text{O}_3$ /50-poly(*S-r*-canola) composites. These composites were prepared with $\gamma - \text{Fe}_2\text{O}_3$ contents of between 25-90 wt%. These composites were determined to retain their magnetic properties after preparation. Powdered composite particles were shown to efficiently undergo magnetic filtration and physical magnetic separation allowing its isolation from both liquids and solids. By combining this ability with the chemical properties of the 50-poly(*S-r*-canola) polymer, the efficient removal of HgCl_2 from a slurry of fine tailings was demonstrated. The numerous heat loss mechanisms for $\gamma - \text{Fe}_2\text{O}_3$ nanoparticles under microwave irradiation facilitated the microwave heating of these composite materials. Microwave heating was then utilized to perform reactive compression moulding of these composites into new shapes and forms. The synthesis of the magnetic composite by reactive compression moulding was also achieved using microwave irradiation. Use of these magnetic composites in mechanical and electrical systems was demonstrated with the composite material effectively replacing the active magnetic component in a solenoid valve. This reduced the components weight tenfold and demonstrates one of many potential applications for this material.

2.0 Sulfur polymers and iron remediation

2.1 Acknowledgements

Dr. Max Worthington for assistance in SEM/EDX and ^1H NMR analysis of samples. Dr. Christopher Gibson for Raman Spectroscopy. Nick Adamson for XRD analysis. Justin Chalker and Amanda Ellis for assistance with experimental design and data interpretation. Martin Johnston for assistance in using the laboratory microwave reactor.

2.2 Abstract

Although iron is not highly toxic, its emission results in a number of negative consequences for the environment, industry and critical infrastructure, leading to its regulation by water authorities and government agencies. To aid water treatment facilities in meeting the regulation limits for iron, new low-cost and sustainable iron sorbent materials were prepared entirely from industrial waste products. Inverse vulcanisation was used to convert waste elemental sulfur (from petroleum refining process) and waste cooking oil (canola oil) into a high sulfur content rubber. This rubbery polymer demonstrated the ability to act as a sorbent for Fe(III) remediation from water at industry relevant levels. The sorbent was shown to be used effectively, both individually and in conjunction with current iron remediation strategies to reduce the levels below regulation limits. Microwave irradiation was utilized to prepare the 50-poly(S-*r*-canola) sorbent material instead of typical conventional heating methods. This is the first-time microwave irradiation has been demonstrated to facilitate the inverse vulcanisation reaction. This method allowed for rapid synthesis of the sorbent material in under 5 minutes, far quicker than typical polymerization methods which can take hours to complete. Microwave heating also provided a more uniform heating of the material in comparison to conventional methods. This is an important advancement in the field of sulfur polymers and provides access to this sorbent to areas in need but with limited resources.

2.3 Introduction

2.3.1 Sulfur polymers as sustainable heavy metal sorbent materials

A new method for preparing high sulfur polymers, termed inverse vulcanisation has opened the door to a wide variety of new materials with useful chemical properties. The low costs (<\$0.1 per kg) and high abundance (>70 million tonnes per year) of elemental sulfur make it an ideal feedstock material for new material synthesis.^{188, 189} High sulfur content polysulfide materials, prepared using inverse vulcanisation have been investigated for a wide variety of applications.⁵⁶ One application of growing global importance is environmental remediation. Elemental sulfur and other sulfur containing compounds have been shown to react with heavy metal compounds including Fe, Mn, Zn, Cu, Pb, Cd, Hg and As.^{116, 155, 190, 191} Although these chemical properties would be ideal for potential heavy metal sorbent materials, its physical properties limit practical use. Elemental sulfur is known to cake onto the walls of pipes and tanks when it is stored and shipped, and it can block filters and membranes during filtration. This makes it impractical for use in both batch and continuous flow treatment systems.¹⁹² Sulfur polymers, prepared from inverse vulcanisation, have been shown to demonstrate comparable or greater chemical reactivity to elemental sulfur, whilst allowing for tuneable mechanical properties based upon the cross-linker used and its ratio with sulfur.¹⁹³ Therefore by choice of an appropriate cross-linker, high sulfur content polymers could be prepared that are efficient as heavy metal sorbent materials in both batch and continuous flow treatment processes. Environmental remediation is a relatively new yet important application of sulfur polymers.

2.3.2 Previous studies on heavy metal sorbents prepared using inverse vulcanisation

Previous studies have shown that these sulfur polymers can be utilised in the remediation of heavy metals⁹⁹⁻¹⁰⁷ as well as in oil spill remediation.⁷ Using a wax-like polymer prepared from D-limonene using inverse vulcanisation, Chalker *et al.* demonstrated that both mercury and palladium salts could be effectively removed from solution. The mercury(II) salts reacted with the material to produce mercury and sulfur rich nanoparticles on the material's surface resulting in a colour change from red to yellow.⁹⁸ In the case of elemental mercury, the high sulfur content sorbents oxidised the toxic metal mercury into mercury sulfide (non-volatile and very insoluble). This is an added benefit over classical mercury sorbent materials which typically relies on physical adsorption to remove the mercury.¹⁰⁰ Wu *et al.* recently demonstrated that it is possible to coat high surface area silica gel with the limonene polysulfide, increasing both the rate of uptake and the overall capacity of mercury capture.¹⁵⁷ Other methods for increasing

the surface area of these materials to enhance the mercury uptake capacity include; foaming,¹⁵⁸ salt-templating followed by a water wash,^{100, 159, 161} and electrospinning to form high surface area nanofibers.¹⁶⁰ Chalker and associates, in align with the goals of green chemistry, investigated the preparation of other sustainable sorbent materials using low cost and renewable cross-linkers. They investigated sorbent materials prepared from unsaturated triglycerides such as canola oil, sunflower oil, olive oil and even used cooking oil.^{100, 163} The effect of mercury compound type on its sorption capacity and uptake rate were also investigated. Several other studies have also investigated mercury remediation using polymers prepared from inverse vulcanisation.^{101-103, 194, 195} Whilst these high sulfur content sorbent materials have been demonstrated to efficiently remove all forms of mercury, they have yet to be heavily investigated as sorbent materials for other heavy metal pollutants.

2.3.3 Iron pollution and its associated problems

Iron is the fourth most abundant element by weight within the Earth's crust and because of this its actively found in significant concentrations in groundwater.¹⁹⁶ Aqueous iron is typically present in one of two oxidation states, the divalent Fe(II) and trivalent Fe(III). In aqueous solution, Fe(III) undergoes a hydrolysis reaction progressively forming FeOH^{2+} , Fe(OH)_2^+ , $\text{Fe}_2(\text{OH})_2^{4+}$ and finally Fe(OH)_3 .¹⁹⁷ These products become increasingly less soluble, with Fe(OH)_3 being the least soluble and precipitating out of solution.¹⁹⁷ The relative concentrations of these iron species in solution are dependent on pH, ionic strength and total iron concentration.¹⁹⁷ Even at lower concentrations precipitation of Fe(OH)_3 will occur when $\text{pH} > 4$. Between the range of pH 2 and 3, the major iron species present were Fe^{3+} and Fe(OH)^{2+} .¹⁹⁷ Under oxidising conditions the majority of the iron in groundwater is precipitated as ferric hydroxide.¹⁹⁶ Most water treatment facilities employ the use of aeration or a chemical oxidant to oxidise the Fe(II) into Fe(III) which is then precipitated at $\text{pH} > 4$ and removed using aggregation and filtration.¹⁹⁶ This process is known as oxidative precipitation. High iron concentrations found in natural groundwater have been known to cause significant issues in water treatment facilities as its removal is essential for making aesthetically acceptable drinking water.¹⁹⁶ Most studies into heavy metal sorbent materials, focus on the more toxic heavy metals (mercury, lead, arsenic, etc).¹⁹⁸⁻²⁰⁰ Although iron is less toxic, its presence in high concentrations is still associated with a number negative consequences. These consequences, highlighted below, are of major concern to water authorities, industry, and environmental agencies. The trivalent form of iron, Fe(III), also known as ferric iron, is of particular interest as it leads to discolouring of plumbing fixtures and containers, promotes the growth of bacteria

which lead to fouling and clogging of pipes as well as imparting an undesirable odour and taste to drinking water.²⁰¹⁻²⁰³ High iron concentrations also result in the formation of rust leading to damage in pipes, tanks and other critical infrastructures. These issues are highlighted in Figure 8. Some evidence also suggests that high Fe(III) concentration could have some negative health effects for certain aquatic organisms.^{204, 205} In order to prevent potential environmental consequences and ensure clean drinking water, total iron levels in water are regulated by the government.^{206, 207} The regulation discharge limit is defined for the total iron content (Fe(II) + Fe(III)) as 3 mg/L per day.

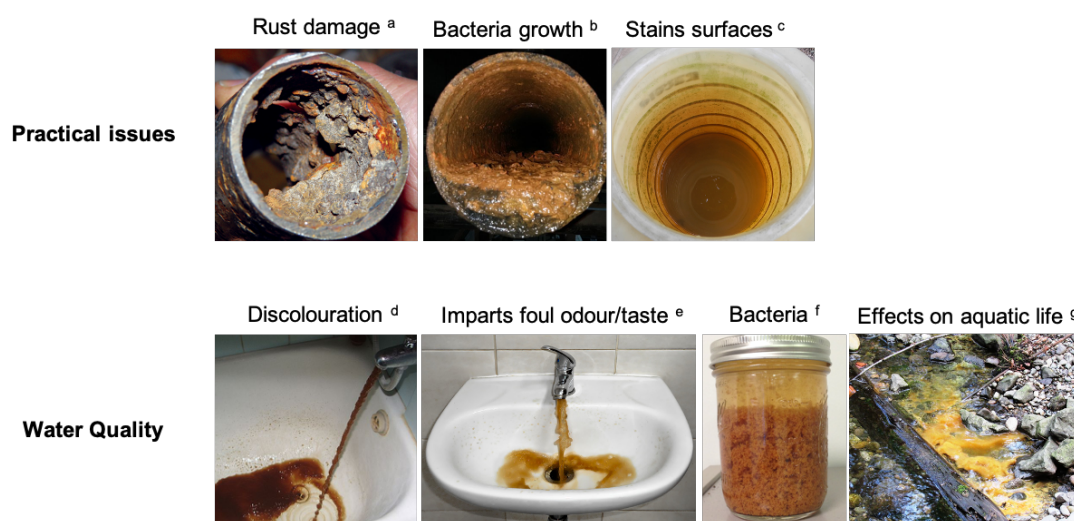


Figure 8 – Image depicting the issues related to iron pollution. All images are used with a permission under a Creative Commons Licence.

Current iron removal strategies include oxidative precipitation followed by aggregation/filtration, ion exchange and adsorption using a sorbent material, typically activated carbon.^{208, 209} These methods typically suffice to reduce the total iron concentration to below regulation limit on small scales and low iron content however when the concentration is high and the water volume is large, their performance is hindered, or the process becomes too expensive. An industry partner, who was treating groundwater contaminated with iron from an underground operations centre, used a process which combines oxidative conversion of Fe(II)_(aq) to Fe(III)_(aq) with precipitation at high pH followed by separation using flocculants and filtration.¹⁵⁶ Whilst this method is mostly capable of achieving these regulation limits, discharge volumes of over 150 000 L per day with Fe(III) levels between 35 and 60 mg L⁻¹ make the process expensive creating the need for low cost alternatives.¹⁵⁶

2.3.4 50-poly(S-*r*-canola) polymer as an iron sorbent material

Previous studies suggest that aqueous forms of iron may react with high sulfur content polymers. Reactions between $\text{Fe}^{2+}_{(\text{aq})}$ and $\text{Fe}^{3+}_{(\text{aq})}$ ions with various sulfur species have been reported in literature.²¹⁰⁻²¹³ Dissolved forms of sulfur have been shown to rapidly reduce organic Fe(III) species and form $\text{FeS}_{(\text{aq})}$ and elemental sulfur (S^0).²¹⁰ This can further react at low pH with H_2S to form pyrite (FeS_2). Fe(II) has also been shown to effectively remove dissolved sulfide species from solution.²¹¹ Iron is also known to form a number of iron-sulfide and iron-polysulfide species in nature.²¹² We therefore hypothesised that the high sulfur content of the 50-poly(S-*r*-canola) sorbent may facilitate binding with iron species and their subsequent removal from solution. Whilst the polysulfide chains are hypothesised to bind with the iron, it is also possible that the triglyceride ester in the 50-poly(S-*r*-canola) polymer could also help bind to Fe through oxygen. Sulfur polymers, prepared using inverse vulcanisation, have previously been investigated for use as heavy metal sorbent materials, however none have focused on iron pollution. Thielke *et al.* demonstrated that a blend of poly(sulfur statistical polysulfide isopropenylbenzene) and poly(methyl methacrylate) showed some affinity towards Fe(III) suggesting other high sulfur content polymer may show similar affinities.¹⁹⁹ This discovery lead us to investigate if high sulfur content polymers, prepared using inverse vulcanisation, could effectively remove iron from solution. The 50-poly(S-*r*-canola) polymer has previously been investigated as a sustainable sorbent material for mercury sorption.^{99, 100} Mercury (Hg^{2+}) is softer than the harder iron (Fe^{3+}) species suggesting that the affinity of the sorbent towards iron would be lower than that of mercury. While this may be the case, the low costs and simplicity of preparation may still make this sorbent a viable alternative to current treatment options.

2.4 Experimental

2.4.1 General considerations

3.4.1.1 IR Spectroscopy

Infrared (IR) spectra were recorded on a Fourier Transform Spectrophotometer using the ATR method. Transmission maxima (ν_{\max}) are reported in wavenumbers (cm^{-1}).

3.4.1.2 Raman Spectroscopy

Raman spectra were acquired using a Witec alpha300R Raman microscope at an excitation laser wavelength of 532 nm with a 40X objective (numerical aperture 0.60). Typical integration times for single Raman spectra were between 20 to 60 s and averaged from 1 to 3 repetitions.

3.4.1.3 SEM and EDX

Scanning Electron Microscopy (SEM) images were obtained using an FEI F50 Inspect system, while corresponding EDS spectra were obtained using an EDAX Octane Pro detector. All samples were coated in 10 nm platinum before imaging.

3.4.1.4 Simultaneous Thermal Analysis (STA)

Simultaneous Thermal Analysis (STA) was carried out on a Perkin Elmer STA8000 simultaneous thermal analyzer (STA). A sample size between 11 and 15 mg was used in each run. The furnace was purged at 20 mL/min with nitrogen gas and equilibrated for 1 minute at 30 °C before each run. Heating was carried out up to 700 °C using a 20 °C/min heating rate. The temperature was held isothermally at 700 °C at the end of each experiment to oxidize remaining organic matter.

3.4.1.5 X-ray diffraction

Powder X-ray diffraction (XRD) patterns were recorded on a Bruker D8 Advance Eco diffractometer (Bragg-Brentano geometry) using Co-K α radiation ($\lambda = 1.78897 \text{ \AA}$). The Bragg angle (2θ) was varied from 15° to 90° with a step size of 0.019°, measurement time of 0.45 s per step and sample rotation at 15 rpm. The XRD patterns were collected on a silicon low background sample holder, where powder samples were deposited onto the surface of the holder.

3.4.1.6 UV/Vis spectroscopy

UV/Vis spectroscopy was performed using an Agilent Technologies Cary 60 UV-vis spectrometer. A sample size of 1 ml was used for each measurement. All measurements

were initially referenced to pure water before sample measurement. Fe(III) was monitored at 306 nm.

3.4.1.7 Atomic Absorption Spectroscopy (AAS)

Atomic absorption spectroscopy was performed using a GBC 933 plus atomic absorptions spectrometer with a Fe hollow cathode lamp. Analysis of total iron concentrations between 2-9 mg/L was performed at a wavelength of 248.3 nm. Analysis of total iron concentrations between 20-80 ppm was performed using a wavelength of 372 nm. A sample size of approximately 3-5 ml was required for each measurement. Every sample was first referenced to pure water before sample analysis.

2.4.2 Poly(*S-r*-canola) sorbents preparation and Fe(III) treatment

2.4.2.1 Synthesis of 50-, 60- and 70-poly(*S-r*-canola) sorbents

Sulfur (technical grade, 20.0 g) was added to a 250 mL round bottom flask and then melted, with stirring, before heating further to 180 °C. Canola oil (20.0 g) was then added over 3-5 minutes, resulting in a two-phase mixture. The reaction was stirred vigorously to ensure efficient mixing of the two phases. The mixture appeared to form one phase after approximately 10 minutes. Heating was continued for an additional 10 minutes at 180 °C. Over this time, the product formed a rubbery solid. The material was then removed from the flask and then blended for 2-3 minutes (8.5 cm rotating blade) to provide rubber particles less than 12 mm in diameter. The particles were then transferred to a beaker and treated with enough 0.1 M NaOH to cover the particles entirely. This mixture was stirred for 90 minutes at room temperature to remove any residual hydrogen sulfide. Care was taken to submerge any polymer particles that floated on the NaOH solution. After this time, the particles were isolated by filtration and then washed on the filter with deionised water ($3 \times \sim 50$ mL). The particles were then collected from the filter and air dried at room temperature and pressure for 24 hours. Typically, this procedure provided a final mass between 39.2 and 40.0 g of the washed and dried 50-poly(*S-r*-canola) particles (>98% yield). The polymer particles were then partitioned into various size distributions using sieves. The particle size ranges obtained were < 0.5 mm, 0.5-1.0 mm, 1.0-2.5 mm, and 2.5 - 5.0 mm, and > 5.0 mm. For all subsequent experiments, the particles ranging from 1.0-2.5 mm were used. This size was selected to balance the need for higher surface area (smaller particles), but also to minimize caking and hydraulic resistance associated with smaller particles. A similar protocol was used for the synthesis of the 60- and 70-poly(*S-*

r-canola) sorbents. For the 60-poly(*S-r*-canola), 16.0 g canola oil and 24.0 g of sulfur were used. For the 70-poly(*S-r*-canola), 12.0 g canola oil and 28.0 g of sulfur were used.

2.4.2.2 Fe(III) calibration curve for UV/Vis analysis

An aqueous Fe(III) solution was prepared by adding 50 mg FeCl₃ to a 1.0 L volumetric flask and then adding water up to 1.0 L mark. The solution was then equilibrated at room temperature for 48 hours. The pH of this solution was measured to be 3.04, using a pH meter. Samples of concentrations varying from 0.2 mg/L Fe(III) to 50.0 mg/L were then prepared and used to construct a calibration curve based on the absorbance at 306 nm. This calibration curve was used to monitor removal of Fe(III) from solution in subsequent experiments.

2.4.2.3 Fe(III) treatment using 50-, 60- and 70-poly(*S-r*-canola) sorbent

20 mL aliquots of FeCl₃ solution (50 mg/L) were added to 12 × 50 mL centrifuge tubes. Three samples served as controls in which no polymer was added. To the remaining samples, 2.0 g of the 50-poly(*S-r*-canola) was added: 3 samples were treated with the 50-poly(*S-r*-canola), 3 samples were treated with the 60-poly(*S-r*-canola), and 3 samples were treated with the 70-poly(*S-r*-canola). The particles size for all polymer samples was 1.0-2.5 mm. All samples were then placed on a rotating mixer (25 RPM) at room temperature. The concentration of Fe(III) was monitored for all samples by taking a 1 mL aliquot and removing any solids using a benchtop centrifuge. The absorbance of the supernatant at 306 nm was then recorded for the sample. The measurements were recorded at 24 and 48 hours.

2.4.2.4 Fe(III) treatment varying amount of 50-poly(*S-r*-canola)

The stock solution of FeCl₃ was prepared at 50 mg/L and equilibrated for 48 hours. This solution had a pH = 3.0, as prepared. Various masses of the 50-poly(*S-r*-canola) were added to 20 mL samples of the Fe(III) solution (run in triplicate). The particle size of the polymer was 1.0-2.5 mm. The samples were incubated on a rotary mixer at room temperature for 24 hours, as described in the previous iron capture experiment. The absorbance was monitored at 306 nm to determine Fe(III) concentration for all samples.

2.4.2.5 Optimized Fe(III) treatment process

The stock solution of FeCl₃ was prepared at 45 mg/L and equilibrated for 48 hours. This solution had a pH = 3.0, as prepared. 2.0 grams of the 50-poly(*S-r*-canola) was added into 20 mL of Fe(III) solution (run in triplicate). The particle size was 1.0-2.5 mm. Another three solutions acted as controls where no polymer was used. The samples were incubated

on a rotary mixer at room temperature for 24 hours, as described in the previous Fe(III) capture experiment. The absorbance was monitored at 306 nm to determine Fe(III) concentration.

2.4.2.6 Litre-scale Fe(III) removal from water using the 50-poly(S-*r*-canola) sorbent

The stock solution of FeCl₃ was prepared at 50 ppm as described previously. This solution had a pH = 3.0, as prepared. 200 g of the 50-poly(S-*r*-canola) was added to 1.0 L of Fe(III) solution. The particle size range for the 50-poly(S-*r*-canola) particles was 1.0-2.5 mm. The solution was stirred at room temperature for 24 hours, after which time the polymer was removed by filtration. The absorbance was monitored at 306 nm to determine Fe(III) concentration. Atomic Absorption Spectroscopy was used as an independent measurement of total iron concentration.

2.4.3 Porous 50-poly(S-*r*-canola) sorbent preparation and Fe(III) treatment

2.4.3.1 Porous 50-poly(S-*r*-canola) synthesis

NaCl (14.0 grams) was ground into a fine powder using a mortar and pestle. Sulfur (technical grade, 3.00 g) was added to a 250 mL round bottom flask and then melted, with stirring, before heating further to 180 °C. Canola oil (3.00 g) was added drop wise over 2 minutes. The reaction mixture was stirred at a rate that ensured efficient mixing of the two phases. The NaCl powder was then added over 5-10 minutes, and the stirring rate was continually adjusted to ensure efficient mixing. Heating was continued for an additional 10-15 minutes at 180 °C, over which time the reaction mixture formed a brown solid. The reaction was cooled to room temperature and removed from the flask. The product (20.0 g) was milled for 1 minute in a blender (8.0 cm rotating blade) to give various particle sizes (typically between 0.1 mm and 3.0 cm). The particles were then transferred to a beaker and washed with 150 mL of water for 1 hour with stirring. The washing process was repeated at least one more time to remove as much sodium chloride as possible. Drying in a desiccator under vacuum provided the porous 50-poly(S-*r*-canola) polymer as a soft rubbery sponge. If NaCl was visible as a white solid on the surface of the polymer, the washing and drying steps were repeated until a constant mass was obtained.

2.4.3.2 Fe(III) removal from water using the porous 50-poly(S-*r*-canola)

20 mL aliquots of 50 mg/L Fe(III) solution were added to 6 × 50 mL centrifuge tubes. The pH of this solution was measured to be 2.80. Three samples served as control experiments in which no porous polymer was added. To the remaining samples, 2.00 g of the porous 50-poly(S-*r*-canola) was added. The polymer particle size is between 1.0-2.5 mm. All

samples were then placed on a rotating mixer (25 RPM) at 23 °C for 24 hours. After this time, the concentration of Fe(III) in solution was measured by taking a 1 mL aliquot and removing any solids using a benchtop centrifuge. The absorbance at 306 nm was then recorded for the sample. The results are plotted below, indicating that the porous 50-poly(S-*r*-canola) reduced the Fe(III) concentration to less than 2 mg/L. The pH of the water after treatment was 6.95.

2.4.3.3 Fe(III) removal from water: porous vs non-porous 50-poly(S-*r*-canola)

20 mL aliquots of 50 mg/L Fe(III) solution were added to 12 × 50 mL centrifuge. Three samples served as control experiments in which no polymer was added. Into three of the tubes, 2.00 g of the porous 50-poly(S-*r*-canola) was added. In the final three tubes, 2.0 grams of the non-porous 50-poly(S-*r*-canola) was added. All polymer particles were 1.0-2.5 mm in diameter. All samples were then placed on a rotating mixer (25 RPM) at room temperature for 24 hours. The concentration of Fe(III) was monitored for all samples by taking a 1 mL aliquot and removing any solids using a benchtop centrifuge. The absorbance at 306 nm was then recorded over a period of 24 hours.

2.4.3.4 Fe(III) treatment varying mass of porous 50-poly(S-*r*-canola) sorbent

The stock solution of FeCl₃ was prepared at 50 mg/L as described previously. This solution had a pH = 3.0, as prepared. Various masses of the porous 50-poly(S-*r*-canola) were added to 20 mL samples of the FeCl₃ solution (run in triplicate). The particles were 1.0-2.5 mm in diameter. The samples were incubated on a rotary mixer at room temperature for 24 hours, as described in the previous Fe(III) capture experiment. The absorbance was monitored at 306 nm to determine iron concentration for all samples.

2.4.3.5 Langmuir isotherm for porous 50-poly(S-*r*-canola)

A stock solution of Fe(III) was prepared at 50 mg/L as previously described. This solution has a pH = 3.0, as prepared. Fe(III) solutions with concentrations of 2, 5, 10, 20, 30 and 40 mg/L were then prepared by diluting the stock solution with deionized water. 20 mL aliquots at each Fe(III) concentration were added to 50 mL centrifuge tubes (run in triplicate). 100 mg of the porous 50-poly(S-*r*-canola) was added to each solution. All samples were then placed on a rotating mixer (25 RPM) at 23 °C for 6 hours. The concentration of Fe(III) was monitored for all samples by taking a 1 mL aliquot after 6 hours of treatment and removing any solids using a bench top centrifuge and then recording the absorbance at 306 nm. The Langmuir sorption isotherm for the sorption of Fe(III) by the 50-poly(S-*r*-canola) sorbent was then plotted.

2.4.3.6 Solubility of Fe(III) in presence of competing ions

A 20 mL aliquot of an FeCl₃ solution (50 mg/L, pH 3.0) was added to 5 × 20 mL glass vials. One of the following ‘contaminant’ salts was then added to the Fe(III) solution such that their concentration was 10 mg/L: NaCl, CaCl₂, KCl, Na₂SO₄. The vials were incubated at 23 °C for 16 hours.

2.4.3.7 Effect of competing ions on porous 50-poly(S-*r*-canola)’s Fe(III) sorption

A solution of FeCl₃ was prepared at 50 mg/L and then NaCl, MgCl₂, CaCl₂, and KCl were all added such that the final concentration of the ‘contaminant’ salts was 10 mg/L. No iron precipitated from this solution. 20 mL of this solution was transferred into 6 × 50 mL centrifuge tubes. 2.0 grams of porous 50-poly(S-*r*-canola) was added to three of the solutions, with the remaining three solutions acting as controls in which no polymer was added. All samples were then placed on a rotating mixer (25 RPM) at 23 °C for 6 hours. After this time, a 1 mL aliquot was transferred into a centrifuge tube. Any remaining solids were then removed using a bench top centrifuge. The concentrations of these samples were then monitored by recording the UV/Vis absorbance at 306 nm.

2.4.3.8 Kinetic analysis of Fe(III) sorption onto the porous 50-poly(S-*r*-canola)

A stock solution of Fe(III) was prepared at 50 mg/L as previously described. 20 mL of this solution was transferred into 12 × 50 mL centrifuge tubes. The pH was recorded to be 2.8. Next, 2.0, 1.0 and 0.5 grams of porous 50-poly(S-*r*-canola) polymer were added into three solutions each, while the remaining three solutions acted as controls to which no polymer was added. All samples were then placed on a rotating mixer (25 RPM) at 23 °C for 6 hours. Every hour a 1 mL aliquot was transferred into a centrifuge tube and any remaining solids were then removed using a bench top centrifuge. The concentrations of these samples were then monitored by recording the UV/Vis absorbance at 306 nm. At the end of the treatment, the pH of the water after Fe(III) removal was measured to be 6.95.

2.4.3.9 Re-use of the porous 50-poly(S-*r*-canola) sorbent in Fe(III) treatment

A stock solution of Fe(III) was prepared at 50 mg/L as described previously. 1.5 grams of the porous 50-poly(S-*r*-canola) was added into a tube containing 20 mL of the Fe(III) solution. The polymer particles were 1.0-2.5 mm in diameter. A control in which no polymer sorbent was present was also included. The samples were incubated on a rotary mixer at room temperature for 2 hours. After 2 hours, 1 mL was transferred into a centrifuge tube and centrifuged for 2 minutes to remove any suspended solids. The absorbance was then monitored at 306 nm to determine the Fe(III) concentration. The

sorbent was then removed from the tube via vacuum filtration and dried in air overnight. Once dry, the same sorbent sample was transferred to a fresh 50 mg/L Fe(III) solution. This re-use was repeated 10 times and the concentration of Fe(III) in solution was measured after each re-use step.

2.4.4 Fe(II) treatment using 50-poly(S-*r*-canola) sorbent

2.4.4.1 Fe(II) removal from water using the 50-poly(S-*r*-canola) sorbent

The stock solution of FeCl₂ was prepared at 50 mg/L. 20 mL of this solution was transferred into 6 × 50 mL centrifuge tubes. A pH meter was used to determine the initial pH of the solution. 2.0 grams of non-porous 50-poly(S-*r*-canola) polymer was added to three of the solutions, while the remaining three solutions were controls to which no polymer was added. All samples were then placed on a rotating mixer (25 RPM) at 23 °C for 6 hours. After 6 hours, the pH of each solution was recorded using a pH meter and 1.0 mL aliquots of each solution were transferred into a centrifuge tube. Any remaining solids were then removed using a bench top centrifuge. The concentrations of these samples were then monitored by atomic absorption spectroscopy (AAS).

2.4.5 Effect of pH and presence of H₂O₂ on Fe(III) treatment using 50-poly(S-*r*-canola) sorbent

2.4.5.1 Treatment of 50-poly(S-*r*-canola) with H₂O₂

1.0 g of 50-poly(S-*r*-canola) was added to 20 mL samples of 15% H₂O₂ (run in triplicate samples). The samples were incubated on a rotary mixer at room temperature for 24 hours. The 50-poly(S-*r*-canola) sorbent was then filtered, washed with 3 × 40 mL of water and dried in air overnight.

2.4.5.2 Fe(III) treatment using 50-poly(S-*r*-canola) previously treated with H₂O₂

The stock solution of Fe(III) was prepared at 50 mg/L at a pH of 3.0 as described previously. The H₂O₂ treated 50-poly(S-*r*-canola) sorbent (2.0 g) was added to 20 mL samples of the Fe(III) solution. The samples were incubated on a rotary mixer at room temperature for 24 hours, as described previously. The absorbance was monitored at 306 nm to determine the Fe(III) concentrations. Control experiments with no polymer and also 2.0 g of 50-poly(S-*r*-canola) sorbent that was not treated with H₂O₂ were also used for comparison.

2.4.5.3 Stability of 50-poly(*S-r*-canola) sorbent at different pH

The stability of the 50-poly(*S-r*-canola) was tested in 3 solutions at different pH over a period of 7 days.

Solution 1 (pH ~13): 92 mg NaOH was dissolved in 2.31 mL D₂O to afford a 1.0 M solution of NaOH in D₂O. 600 μL of this solution was transferred to a separate vial containing 5.4 mL of D₂O, diluting the sample to 0.1 M NaOH. Finally, 30 μL of 1,4-dioxane was added as an internal standard. The pH was measured to be approximately 13 using a pH strip.

Solution 2 (pH ~1): 59.2 μL HCl (37% HCl in water) was added to 6.0 mL D₂O to afford a 0.1 M HCl solution. 30 μL dioxane was added as an internal standard. The pH was measured to be 1 by pH strip.

Solution 3 (pH ~6): 30 μL dioxane was added to 6 mL D₂O. The pH was measured to be 6 by pH strip.

2 mL of each solution was pipetted into separate glass vials containing 100 mg porous polysulfide. 2 mL of each solution were kept as controls. All solutions were incubated at 25 °C for seven days. After this time, the resultant solutions were separated from the polymer and ¹H NMR spectrum of the solution was acquired.

2.4.5.4 Effect of pH on the efficiency of Fe(III) removal using the porous 50-poly(*S-r*-canola)

A stock solution of Fe(III) was prepared at 50 mg/L as described previously. This solution has a pH = 3.0, as prepared. Fe(III) solutions were then adjusted to pH 1, 7 and 10 by the addition of 3.0M HCl or 3.0M NaOH until the desired pH was indicated by a pH meter. 20 mL of each solution was then transferred into 50 mL centrifuge tubes along with 2.0 grams of the porous 50-poly(*S-r*-canola). Control experiments in which no polymer was added were also carried out. All samples were then placed on a rotating mixer (25 RPM) at 23 °C for 6 hours. After this time a 1 mL aliquot was transferred into a centrifuge tube. Any remaining solids were then removed using a bench top centrifuge. The concentrations of these samples were monitored by recording the UV/Vis absorbance at 306 nm.

2.4.6 Porous 50-poly(*S-r*-canola) sorbent from waste cooking oil

2.4.6.1 Synthesis of the porous 50-poly(*S-r*-canola) using recovered cooking oil

NaCl (70.0 grams) was ground into a fine powder using a mortar and pestle. Waste cooking oil (used, unsaturated cooking oil from fryer, 15.0 g) was added into a 500 mL reaction

vessel, which was then heated to 170 °C. Sulfur (technical grade, 15.00 g) was added to the reaction pot over a period of 5 minutes. The reaction mixture was stirred at a rate that ensured efficient mixing of the two phases. The ground up NaCl was then added over 10 minutes, and the stirring rate was continually adjusted to ensure efficient mixing. Heating was continued for an additional 10 minutes at 180 °C, over which time the reaction mixture formed a brown solid. The reaction was cooled to room temperature and removed from the reactor. The product (100.0 g) was milled for 1 minute in a blender (8.0 cm rotating blade) to give various particle sizes (typically between 0.1 mm and 3.0 cm). The particles were then transferred to a beaker and washed with 1.0 L of water for 4 hours with stirring. The particles were then isolated via vacuum filtration and dried in a desiccator under vacuum overnight. This washing process was repeated two more times to ensure all NaCl had been removed from the polymer. This left a porous 50-poly(*S-r*-canola) polymer remaining.

2.4.6.2 Fe(III) treatment using the porous 50-poly(*S-r*-canola) sorbent prepared from waste cooking oil.

A 20 mL portion of 50 mg/L Fe(III) solution was added to 6 × 50 mL centrifuge tubes. Three samples served as control experiments in which no polymer was added. To the remaining samples, 2.00 g of the porous 50-poly(*S-r*-canola) prepared from waste cooking oil was added. All samples were then placed on a rotating mixer (25 RPM) at room temperature for 24 hours. After this time, the concentration of Fe(III) in solution was measured by taking a 1.0 mL aliquot and removing any solids using a benchtop centrifuge. The absorbance at 306 nm was then recorded for all samples.

2.4.7 Microwave synthesis of porous 50-poly(*S-r*-canola) sorbent

2.4.7.1 Porous 50-poly(*S-r*-canola) synthesis using a microwave reactor (6.0 g scale)

3.0 grams of elemental sulfur was added to a 500 mL RBF equipped with an oval-shaped stirring bar (12 × 15 mm). 3.0 grams of canola oil was then added to the flask followed by the addition of 14.0 grams of sodium chloride. The flask was placed into a Startsynth front-loading microwave reactor on top of a Weflon flask holder with a condenser attached to the flask. The stirred mixture was then irradiated with microwaves. The power of the microwave was set 1200 W and the reaction was heated at constant power for approximately 8 minutes and 50 seconds. The heating profile is shown below. The mixture was stirred at 10% of the maximum speed until the sulfur had melted. At this point the stirring rate was increased to 70% of the maximum speed and maintained at this level for

the remainder of the synthesis. After 8 minutes and 50 seconds had passed the irradiation was stopped but stirring was continued until the cross-linking prevented further stirring (approximately 1 minute after irradiation ceased). The flask was then lifted off the Weflon stand to cool the reaction vessel. The product was then removed from the flask using a metal spatula. The product was then transferred into a 500 mL beaker with 250 mL of DI H₂O and stirred for 24 hours to remove sodium chloride from the 50-poly(S-*r*-canola) polymer. After 24 hours the product was filtered by vacuum filtration and rinsed with 200 mL of distilled water. The product was then re-washed by stirring in 200 mL DI water for 1 hour. The product was then isolated by vacuum filtration and dried in air over night.

Notes: For 6.0 gram scale synthesis a 500 mL round bottom flask must be used so that the reaction mixture is evenly distributed around the bottom of the flask and heated evenly. The stirring rate must be monitored throughout the reaction because of the changes in viscosity. It is critical to ensure efficient mixing of the sulfur and canola oil. If the mixture isn't stirred efficiently, the reaction can phase separate and gel in a non-uniform manner.

2.4.7.2 Porous 50-poly(S-*r*-canola) synthesis using a household microwave (30.0 g scale)

15.0 grams of elemental sulfur was mixed with 15.0 grams of canola oil in a 10.5 cm diameter Pyrex dish, followed by the addition of 70.0 grams of NaCl. All components were mixed with a spatula to form a viscous paste. The mixture was then placed into a household microwave (1100W) and irradiated for 4 minutes and 30 seconds. The mixture was then removed from the microwave and mixed using a metal spatula for 30 seconds, before being returned to the microwave. The mixture was then irradiated for a further 30 seconds and then mixed with a metal spatula for 30 seconds or until the product solidified.

Notes: Do not let the temperature exceed 200 °C, otherwise the polymer can decompose and emit H₂S. The temperature can be monitored periodically (between irradiations) by using a non-contact hand-held IR thermometer. Limit the amount of time during the stirring steps to prevent the reaction from cooling down too much. Ensure thorough mixing of the reaction has occurred, as insufficient mixing will result in phase separation and a non-uniform gel formation. Microwaves with lower power than 1100W will require longer irradiation times for the reaction to reach completion. In this case a similar procedure is used whereby the sample is irradiated until the initial colour change is noted. After this point, 30 second periods of irradiation, followed by 30 seconds of stirring, are performed until the product is formed.

2.4.7.3 Fe(III) treatment using sorbent prepared using microwave irradiation

A 50 ppm Fe(III) solution was prepared as previously described. 20 ml of the Fe(III) solution was transferred into 9 × 50 mL centrifuge tubes. Into 3 tubes, 1.0 grams of the porous 50-poly(S-*r*-canola) polymer, prepared using microwave irradiation, was added. Into another 3 tubes, 1.0 grams of porous 50-poly(S-*r*-canola) polymer, prepared using conventional heating, was added. The final 3 tubes acted as negative controls with no sorbent present. All nine tubes were placed in a rotary mixer and mixed at 25 rpm for 2 hours. Finally, 1 mL aliquots of each sample were transferred into 1 mL centrifuge tubes and centrifuged for 1-2 minutes. These samples were transferred into cuvettes and their UV/Vis absorbance at 306 nm was recorded to determine the Fe(III) concentration.

2.5 Results and discussion

2.5.1 Poly(S-*r*-canola) synthesis and characterization

Inverse vulcanisation was utilized to prepare a high sulfur content sorbent material, termed poly(S-*r*-canola), directly from elemental sulfur and canola oil. To achieve this, elemental sulfur was heated to 180 °C promoting radical ring-opening polymerisation to form a polysulfide pre-polymer. The addition of canola oil effectively cross links the sulfur pre-polymer by reaction of its alkene groups with the sulfur radical chains. The reaction typically reached its gel point within approximately 20 minutes under these conditions. Adjusting the ratio of sulfur and canola oil used in the synthesis provided rubbery materials with varying sulfur contents. Poly(S-*r*-canola) particles with sulfur contents of 50, 60 and 70 wt% sulfur contents are shown in Figure 9.

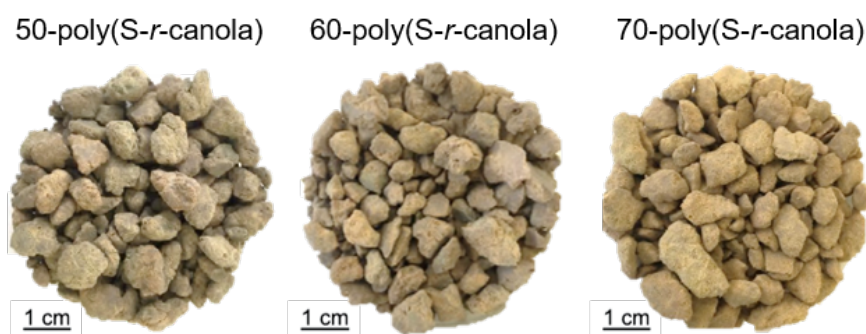


Figure 9 - Images of 50-, 60- and 70-poly(S-*r*-canola).

To characterise the physical and chemical properties of these materials; FTIR, Raman, STA, SEM and EDX characterisation were performed. FTIR analysis was performed on all samples but no significant difference was observed between the samples. This suggests that the sulfur content didn't significantly affect the chemical composition of the resulting polymer.

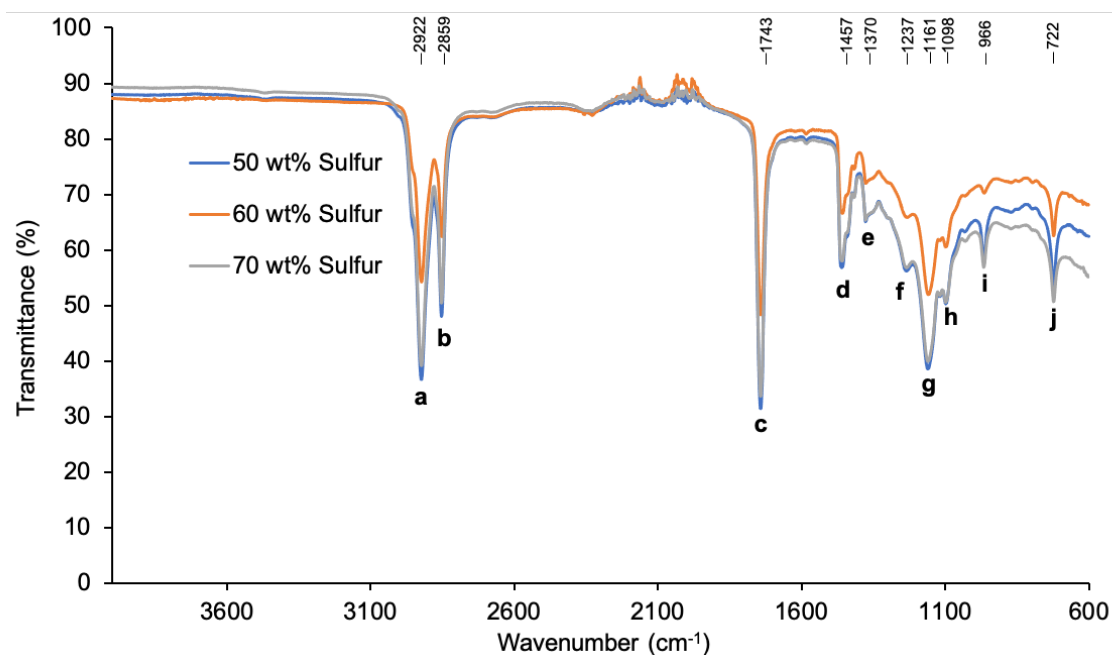


Figure 10 - FTIR spectrum for 50-, 60- and 70-poly(*S-r*-canola) polymer.

Peak	Wavenumber (cm ⁻¹)	Assignment
a	2922	Symmetric sp ³ C-H stretch
b	2859	Asymmetric sp ³ C-H stretch
c	1743	C=O stretch
d	1457	CH ₂ bend (adjacent to carbonyl)
e	1370	CH ₃ bend
f	1237	C-O stretch
g	1161	C-O stretch or skeletal C-C vibrations
h	1098	C-O stretch
i	996	C=C-H stretch (out of plane) for trans-linoleic acid
j	722	C=C-H stretch (out of plane) for cis-linoleic acid

Table 1 – Peak assignment for FTIR spectrum of 50-, 60- and 70-poly(*S-r*-canola) polymers.²¹⁴

Further analysis of the FTIR spectra (Figure 10) reveals that the reaction was likely incomplete as vibrations corresponding with alkene functional groups were observed. Peaks **i** and **j** correspond to vibrations characteristic of cis and trans isomers of linoleic acid. As linoleic acid is a major component of canola oil triglyceride ester, the presence of these vibrations suggests that unreacted alkene groups remain in the material. Although no distinct peak was observed for C=C-H stretch vibrations a small shoulder on the left of peak **a** occurs at approximately 3012 cm⁻¹. This corresponds with C=C-H stretch vibrations suggesting that the peak for these vibrations is masked by peak **a**.²¹⁴ Characteristic peaks for ester groups (**c**, **d**, **e** and **f**) are also

observed suggesting that these groups remained unreacted after poly(*S-r*-canola) synthesis.²¹⁴ Skeletal C-C stretching vibrations are also known to occur around 1160 cm⁻¹, however the signals are likely masked by the C-O stretch vibrations. Peaks **g** and **h** are due to bending vibrations of CH₂ group (adjacent to the carbonyl group) and CH₃ groups respectively. Although FTIR revealed information of the canola oil domain of the polymer, little information is gathered on the sulfur domain. This is because S-S bonds don't typically absorb within the IR region. They are however strong Raman scatterers, making Raman spectroscopy a useful tool for probing the sulfur domain of the polymer.²¹⁵ The 50-, 60- and 70-poly(*S-r*-canola) polymers were analysed and compared using Raman spectroscopy.

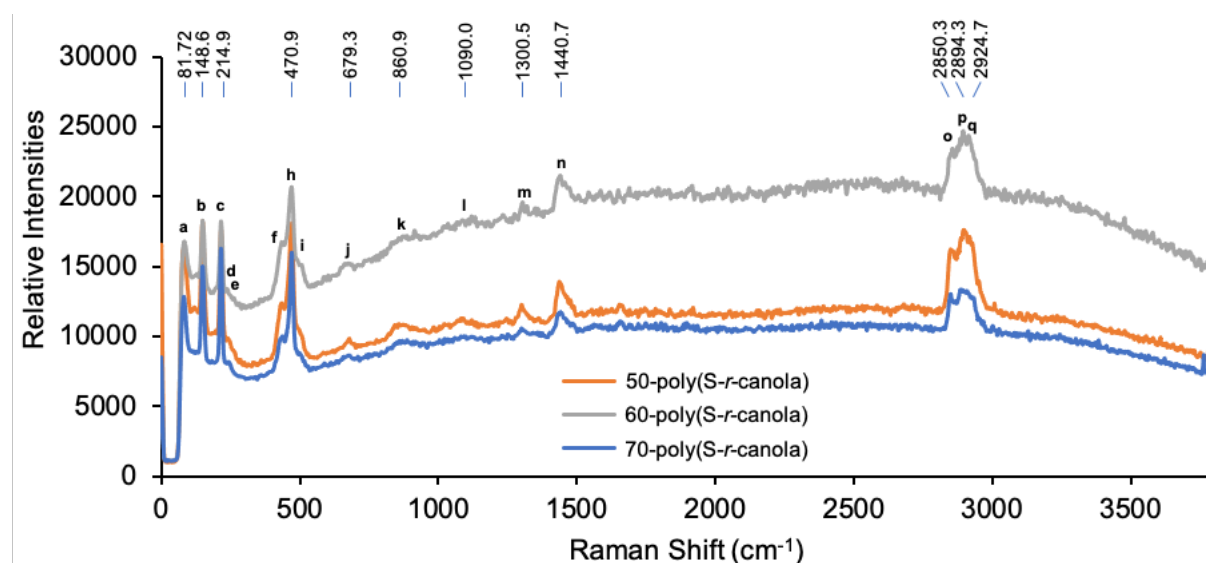


Figure 11 - Raman spectrums for 50-, 60- and 70-poly(*S-r*-canola).

Shown in Figure 11, no significant difference is observed between the samples, all of which displayed the same peaks. These peaks are known from literature to correspond to peaks for rhombic S₈ and polysulfide ions.²¹⁶ The peaks corresponding with rhombic S₈ (**a**, **b** and **c**) increase in relative area as the sulfur content increases. This suggests that the amount of unreacted sulfur remaining in the polymer increases as the sulfur content increases. The signal corresponding to a polysulfide stretch vibration (**h**) decreases in relative intensity as the sulfur content increases, suggesting that the percentage of polysulfide to sulfur decreases. This offers further evidence to suggest that not all the sulfur is completely reacted and remains encapsulated inside the polymer after synthesis. This corresponds to previous results indicating an amorphous poly(*S-r*-canola) polymer with unreacted S₈ particles embedded. The series of peaks above 800 cm⁻¹ correspond to the Raman signals for unreacted canola oil.¹⁰⁰ As expected, these signals decreased in area as sulfur content increased. The peak occurring at 679 cm⁻¹ was assigned to C-S stretch vibrations. This value corresponds with literature values for C-S stretch

vibrations and is not present in either the sulfur or canola oil starting material.²¹⁷ To investigate the thermal properties of these materials, simultaneous thermogravimetric analysis (STA) were performed on all polymers. The mass loss is shown in Figure 12 below. Two major regions of mass loss were observed. The first mass loss is rapid and initiates around 210 °C. The reduction in mass observed during this degradation, in all cases, is approximately 7-10 % less than the suggested sulfur content. This degradation step is likely due to the thermal degradation of S-S bonds and mass loss from the polysulfide domain, as they are converted to SO₂.²¹⁸ As C-S bonds are stronger than S-S bonds, they break at higher temperatures.²¹⁹ This difference in bond energy is likely the reason the 7-10 % difference in mass was observed. The second major mass loss begins at around 320 °C and is due to the thermal decomposition of the canola oil domains, which include the triglyceride regions of the polymer and the sulfurised fatty acid esters. It was noticed that for all polymers, the mass was not reduced to zero. Approximately 10% of the 50- and 60-poly(S-*r*-canola) polymers remained after heating to 800 °C however approximately 18% was remaining for the 70-poly(S-*r*-canola) sample. Previous studies showed a similar result whereby the amount of mass remaining after heating was larger for the samples containing high sulfur content.¹⁰⁰

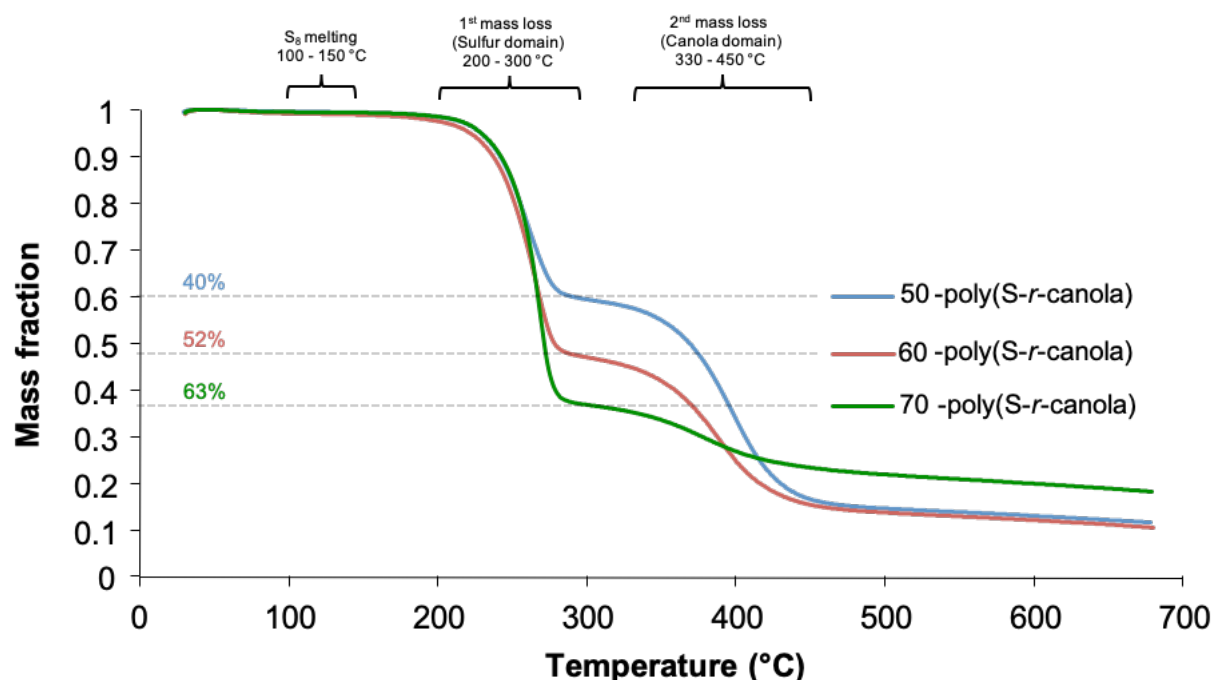


Figure 12 - TGA for 50-, 60- and 70-poly(S-*r*-canola) measured using STA.

Under DSC analysis (Figure 13), an endotherm was observed between 100 and 130 °C. This endotherm corresponds to the transition of orthorhombic S₈ into monoclinic crystalline state followed by its melting and is highlighted in yellow.¹⁰⁰ The area under this endotherm is proportional to the amount of unreacted sulfur in the sample. The presence of some unreacted

sulfur was expected as previous studies have demonstrated that for poly(*S-r*-canola) above 30 wt% sulfur, free sulfur particles are observed.¹⁰⁰ A second endotherm was observed between 210 and 280 °C. This endotherm corresponds to the mass loss observed within the same temperature range in the TGA curve shown above. As this endotherm is due to the heat energy required to break the S-S bonds in the material, the area of this peak corresponds to the total sulfur content in the material, both unreacted S₈ and polysulfide chains. It was therefore not surprising to see that the area under the curve for this endotherm appeared to increase as the total sulfur content rose from 50 to 70 wt% sulfur. No significant changes in the heat flow were observed in the temperature range for the second mass loss event.

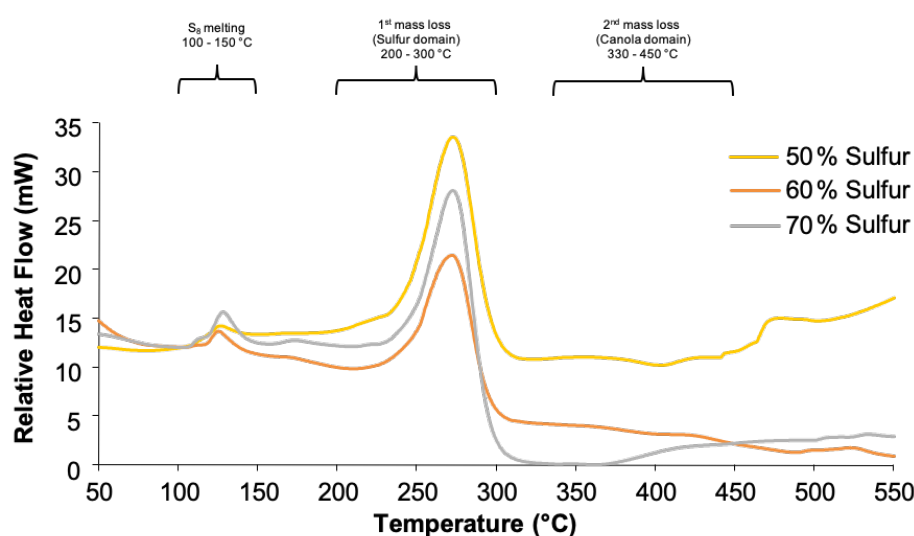


Figure 13 – DSC for 50-, 60- and 70-poly(*S-r*-canola) polymers measured using STA.

Both DSC and TGA results were consistent with previous studies using these poly(*S-r*-canola) polymers.¹⁰⁰ Now that the thermal and chemical properties have been characterised, SEM / EDX analysis was performed to probe the physical and chemical structure of the poly(*S-r*-canola) surface. In all samples, two distinct regions of surface morphology are observed: areas with a smooth amorphous surface and areas whereby small crystalline particles cover the surface. These crystalline particles have previously been shown to be free sulfur which remained unreacted after synthesis.¹⁰⁰ Analysis revealed the 50-poly(*S-r*-canola)'s surface was covered in these crystalline particles. The coverage of these particles was not uniform and areas with no particle coverage, are observed.

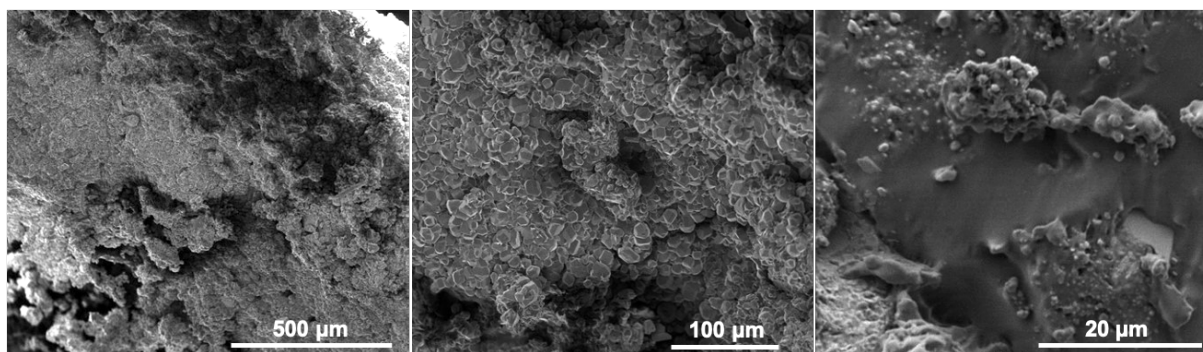


Figure 14 – SEM images for 50-poly(*S-r-canola*) polymer.

All though free particles were still observable in the bulk and protruding through the surface, the 60-poly(*S-r-canola*) polysulfide (Figure 15) contained significantly less surface coverage than observed in the 50-poly(*S-r-canola*) initial sample (Figure 14). It does appear that larger aggregates of the free sulfur appear in the bulk suggesting that potentially the sulfur free particles are simply more aggregated, and these larger aggregates are distributed throughout the materials bulk instead of the surface.

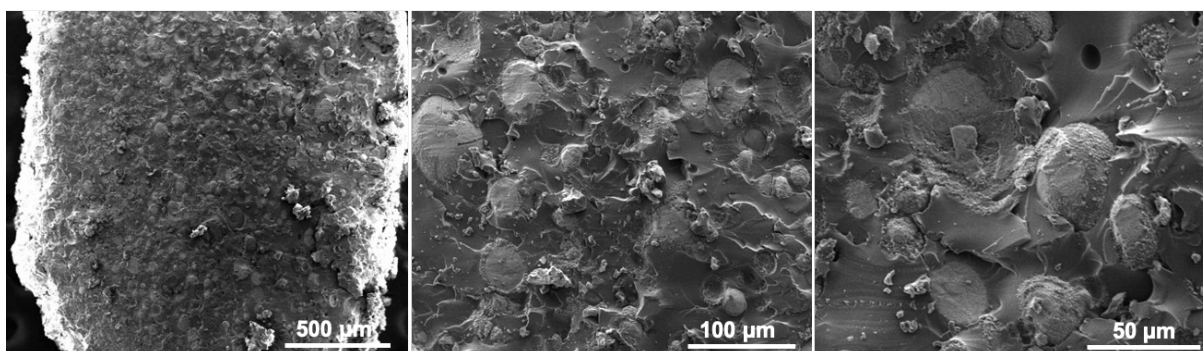


Figure 15 - SEM images for 60-poly(*S-r-canola*) polymer.

Finally, for the 70-poly(*S-r-canola*) sample, minimal amorphous surface region was observed with the entire surface of the polymer being coated in these crystalline particles (Figure 16). This suggests that at 70 wt% sulfur, a larger percentage of free sulfur is remaining after synthesis.

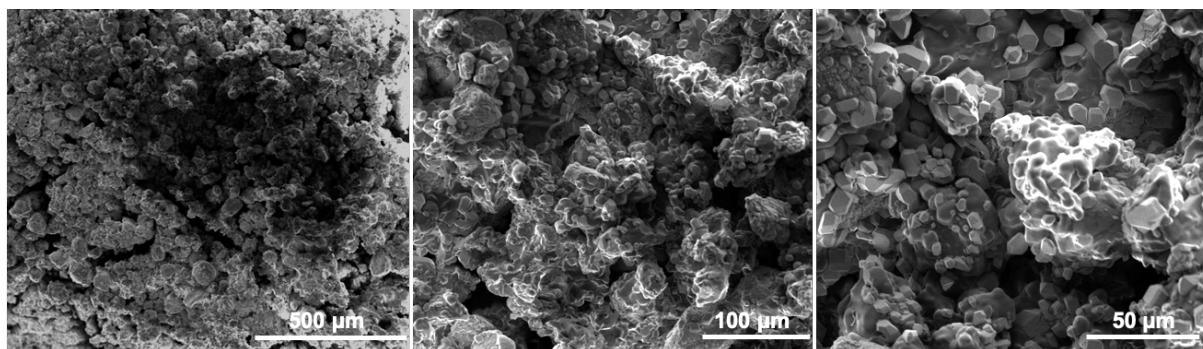


Figure 16 - SEM images for 70-poly(*S-r-canola*) polymer.

2.5.2 Fe(III) sorption with 50-poly(*S-r-canola*) polymer

Now that the 50-, 60- and 70-poly(*S-r-canola*) sorbents have been prepared and characterised their ability to act as a Fe(III) sorbent was investigated. Fe(III) chloride shows a characteristic UV/Vis absorbance peak at 306 nm. In order to evaluate the Fe(III) concentration in solution, a UV/Vis calibration curve for Fe(III) chloride was prepared (Figure 17).

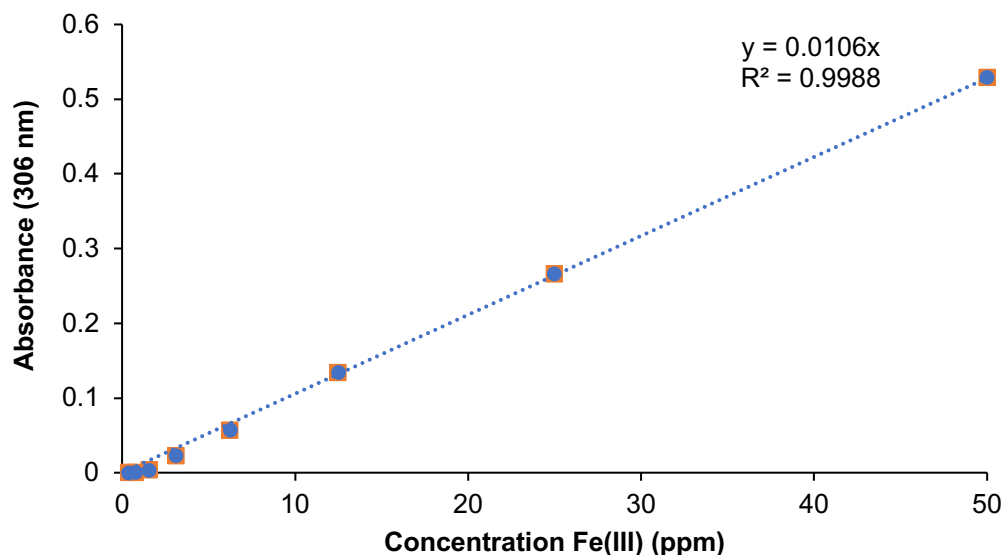


Figure 17 - UV/Vis absorbance calibration curve for Fe(III) in water.

Therefore, by re-arranging the equation for the trendline in Figure 17, the following equation can be formed and then used to determine the Fe(III) concentration from its UV/Vis absorbance at 306 nm:

$$[\text{Fe(III)}] = \frac{\text{Absorbance}(306 \text{ nm})}{0.0106} \quad \text{Equation 1}$$

This equation was then used to evaluate the Fe(III) concentrations in further experiments. Initially, to show if Fe(III) sorption occurs, a solution of Fe(III) chloride (50 ppm) was treated with 2.0 grams of 50-, 60- and 70-poly(*S-r-canola*) for 24 hours. A colour change was observed with all solutions turning colourless after treatment. This is shown in Figure 18a. All three polymers reduced the Fe(III) concentration to below 10 ppm. Figure 18b shows the Fe(III) solution before and after treatment with 50-poly(*S-r-canola*).

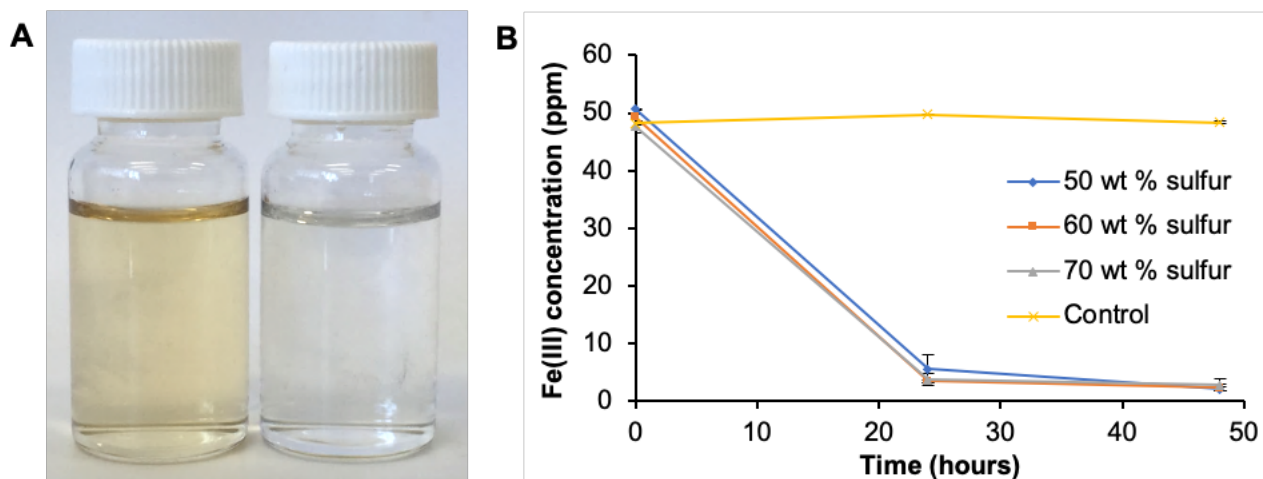


Figure 18 – A) Fe(III) solution (50 ppm) before (left) and after treatment (right) with 50-poly(*S-r-canola*), B) Fe(III) concentration against time for 50, 60 and 70 wt % sulfur polysulfides

No significant difference was observed between the samples after 24 hours treatment. 60- and 70-poly(*S-r-canola*) did remove slightly more on average after 24 hours however this was still within the range of error. Due to the similarity in results and a desire to limit the amount of unreacted sulfur in the sorbent, the 50-poly(*S-r-canola*) was the only sorbent considered for further investigation. To determine how much 50-poly(*S-r-canola*) is required to reduce the Fe(III) concentration (50 ppm) of a 20 mL solution to below regulation limits, the treatment was repeated varying the amount of 50-poly(*S-r-canola*) used. The results are shown below in Figure 19.

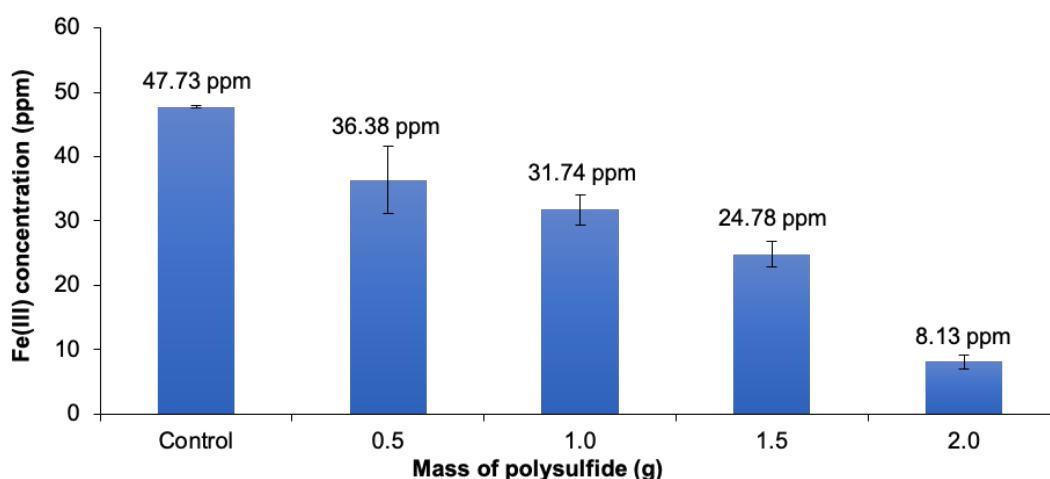


Figure 19 – Fe(III) treatment varying the mass of 50-poly(*S-r-canola*).

To get the concentration to below 10 ppm, 2.0 grams of 50-poly(*S-r-canola*) had to be used. To validate these results Fe(III) treatment was repeated, in triplicate, using 2.0 grams of 50-poly(*S-r-canola*) to treat a 20 mL 50 ppm Fe(III) solution. The samples were analysed using

Atomic Absorption Spectroscopy (AAS). The results (Figure 20) correlated well with UV/Vis measurements and demonstrated the consistency in the treatment results with a small error value.

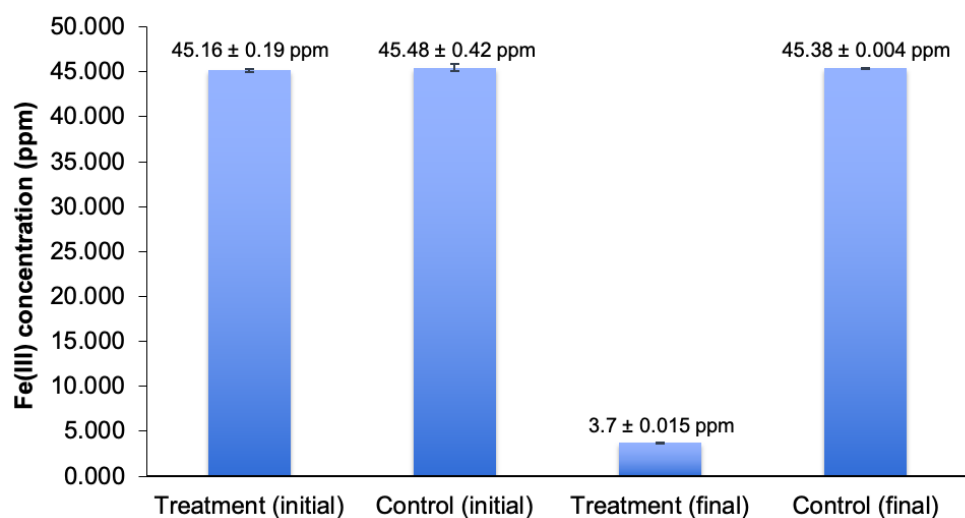


Figure 20 - Optimized treatment process results

To investigate any possible changes in the materials surface after treatment, SEM analysis was performed on the sample. The SEM micrographs of the 50-poly(*S-r*-canola) before and after treatment with Fe(III) is shown below in Figure 21. The 50-poly(*S-r*-canola) polymer was identical under SEM after treatment with Fe(III) solution with no observable changes to the surface present.

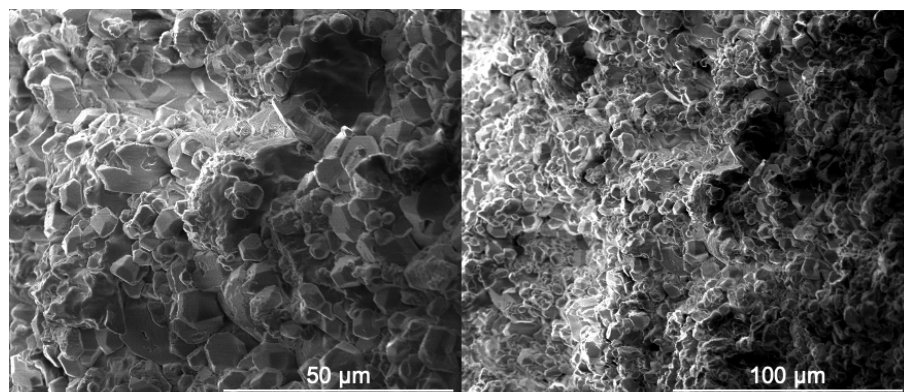


Figure 21 - SEM of 50-poly(*S-r*-canola) after Fe(III) treatment for 24 hours.

2.5.3 Fe(II) sorption with 50-poly(*S-r*-canola) polymer

Now that the ability to remove Fe(III) from water has been established, Fe(II) removal was investigated. To do this, 2.00 g of the 50-poly(*S-r*-canola) sorbent material was added to 20 mL of the Fe(II) solution (50 ppm) and mixed for 24 hours. The results, shown in Figure 22, were recorded using atomic adsorption spectroscopy (AAS).

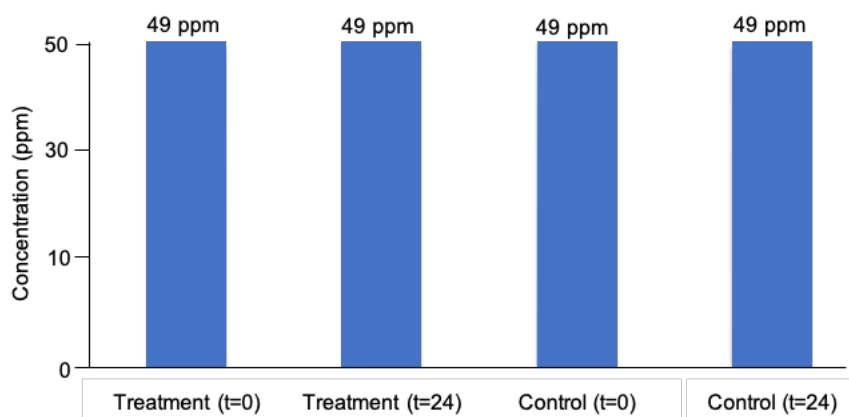


Figure 22 – Results from Fe(II) treatment with 50-poly(S-*r*-canola).

It revealed that negligible amounts of Fe(II) were bound to the polymer. Although Fe(II) was not removed via treatment with 50-poly(S-*r*-canola) most treatment processes start by oxidising all Fe(II) into Fe(III) with the aid of an oxidising agent such as H₂O₂. The second step involves precipitating out the Fe(III) by increasing the pH. Therefore the 50-poly(S-*r*-canola) could be implemented to remove Fe(II) if it was first oxidised to Fe(III) by an oxidant such as H₂O₂.

2.5.4 Effect of H₂O₂ on Fe(III) sorption efficiency of the 50-poly(S-*r*-canola) sorbent

Incorporation of 50-poly(S-*r*-canola) into an already established treatment process not only allows for treatment of Fe(II) as well as Fe(III), but also reduces the amount of 50-poly(S-*r*-canola) sorbent required for a treatment process to reach regulation limits. Therefore the effects of both pH and presence of H₂O₂ on Fe(III) reduction must be investigated. To investigate the effects of H₂O₂ on the process, 50-poly(S-*r*-canola) was treated with 15% H₂O₂ for 24 hours.

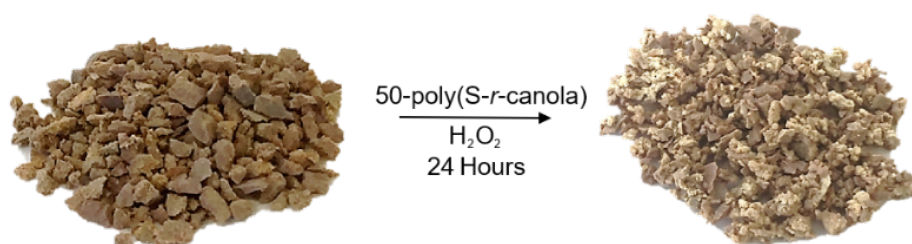


Figure 23 – Image of 50-poly(S-*r*-canola) after treatment with H₂O₂.

As shown in Figure 23, H₂O₂ treatment resulted in a slight discolouration of the polymer particles. To further analyse any differences to the polymers surface, SEM / EDX analysis was performed on the polymer before and after treatment with H₂O₂.

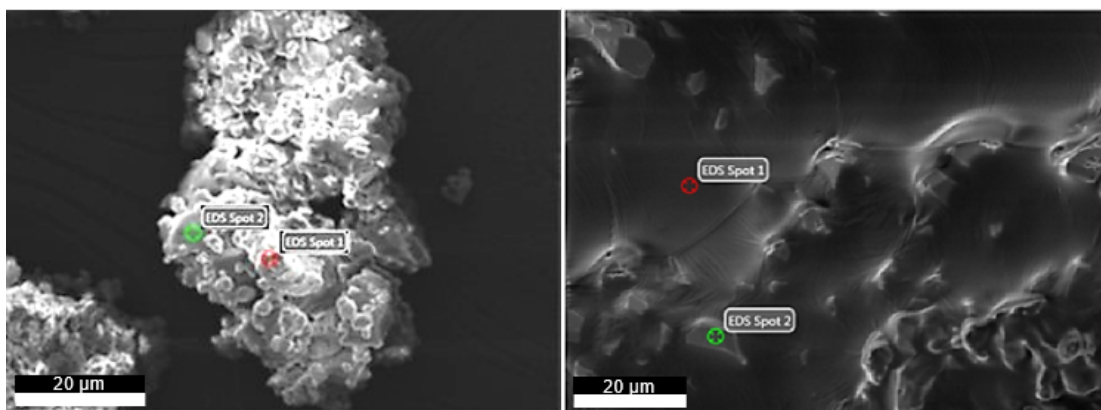


Figure 24 – 50-poly(*S-r-canola*) particles before (left) and after (right) treatment with H₂O₂.

It can be seen in Figure 24 that before treatment the 50-poly(*S-r-canola*) polymers surface was covered in unreacted sulfur particles. After treatment with H₂O₂ no unreacted free sulfur particles were observed on the surface. EDX analysis (Figure 25) was performed on the samples before and after treatment with H₂O₂ revealing a small increase in oxygen and carbon content and a small decrease in sulfur content. This could be due to the conversion of S₈ into sulfate.

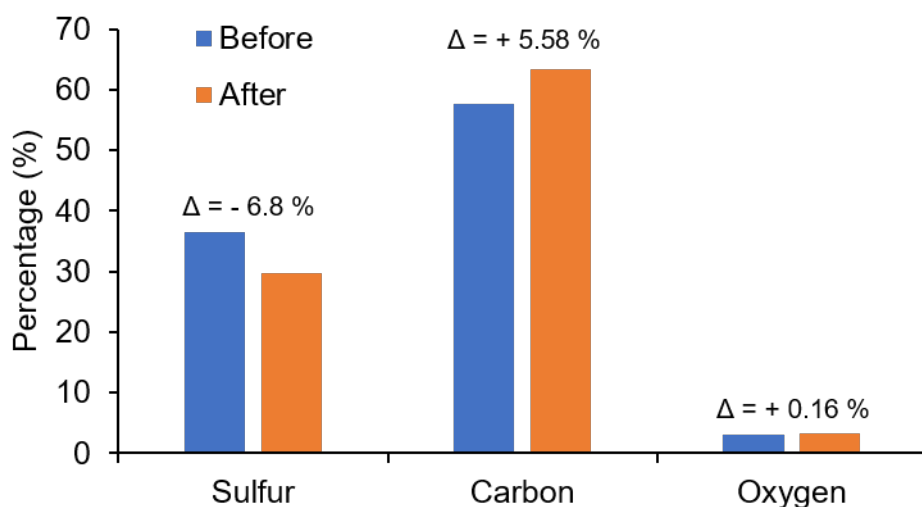


Figure 25 – EDX results for sulfur, carbon, and oxygen in 50-poly(*S-r-canola*) before and after treatment with H₂O₂.

It appears that treatment with H₂O₂ resulted in the removal of free sulfur particle from the surface. H₂O₂ is known to oxidize persulfide species, meaning it could potentially be reacting with the S₈ oxidising it into a sulfate and removing the free sulfur from the surface. As the S-S bonds have been shown to be weaker in polymeric sulfur than in the stable S₈ form, if the H₂O₂ oxidised the free sulfur the polysulfide surface could have also been oxidised into sulfate species.²²⁰ This hypothesis is consistent with both the SEM results showing no sulfur particles on the materials surface and EDX results revealing an increase in oxygen signal and decrease

in sulfur signal after treatment. To investigate whether this influenced the 50-poly(*S-r*-canola) polymers ability to remove Fe(III), H₂O₂ treated 50-poly(*S-r*-canola) was used to treat a 50 ppm Fe(III) solution. The results, shown in Figure 26, were compared with the untreated 50-poly(*S-r*-canola) polysulfide.

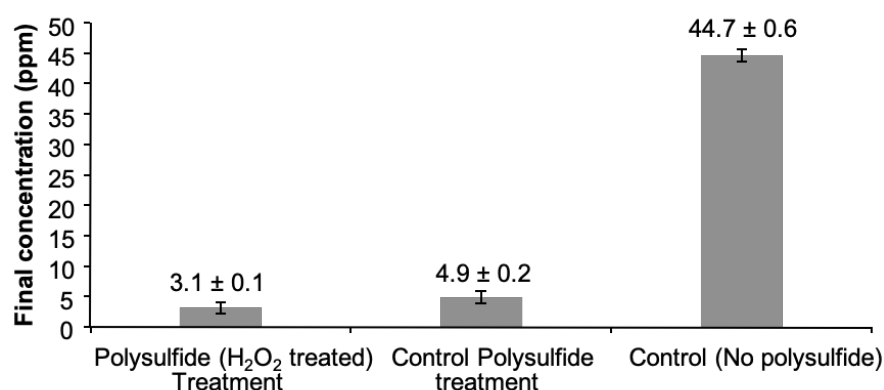


Figure 26 – Results for Fe(III) treatment using 50-poly(*S-r*-canola) previously treated with H₂O₂.

Therefore, prior treatment of 50-poly(*S-r*-canola) with 15% aqueous hydrogen peroxide does not impair its ability to remove Fe(III) from water to any significant degree. To investigate whether the Fe(II) oxidation and Fe(III) sorption steps could be performed simultaneously, a Fe(II) solution (50 ppm) was treated with both 15% H₂O₂ and the 50-poly(*S-r*-canola) sorbent simultaneously.

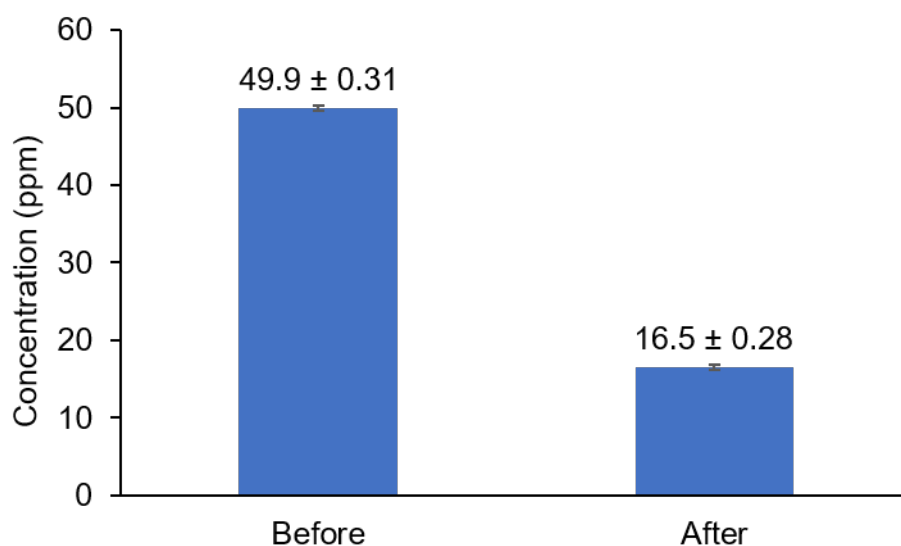


Figure 27 – Results from simultaneous treatment of Fe(II) with H₂O₂ and 50-poly(*S-r*-canola) polymer.

The results in Figure 27 show that when the Fe(II) was treated in tandem with both H₂O₂ and the 50-poly(*S-r*-canola) sorbent the levels of Fe(II) removal only reached 67.9%. This is far

lower than observed for Fe(III). This is likely due to the H₂O₂ reacting with both the 50-poly(*S-r*-canola) sorbent and the Fe(III). As the efficiency of the polymer was previously shown to be the same after treatment with H₂O₂, the reduction in iron removal efficiency is likely due to the competing reactions between both the H₂O₂ and Fe(III) with the 50-poly(*S-r*-canola) sorbent leading to a decreased Fe(II) oxidation rate. This means that the polymer's capacity did not decrease but the iron did not get fully oxidised from Fe(II) into Fe(III). Therefore oxidation of Fe(II) to Fe(III) should preferentially occur before treatment with the 50-poly(*S-r*-canola) sorbent for maximum Fe(II) removal to be achieved.

2.5.5 Porous 50-poly(*S-r*-canola) stability at varying pH

Iron treatment strategies typically employ specific pH levels to achieve the desired reduction levels. To evaluate the stability of the 50-poly(*S-r*-canola) polymer, samples were treated with water at pH 3, 7 and 13 for 7 days. A slight colouration of the water was observed at pH 13, whilst the water remained colourless at pH 3 and 7. ¹H NMR analysis was performed on the samples before and after treatment for 7 days. Results are shown below in Figure 28 and Figure 29. All samples show the peaks corresponding to D₂O (4.79 ppm) and 1,4 – dioxane (3.73 ppm).

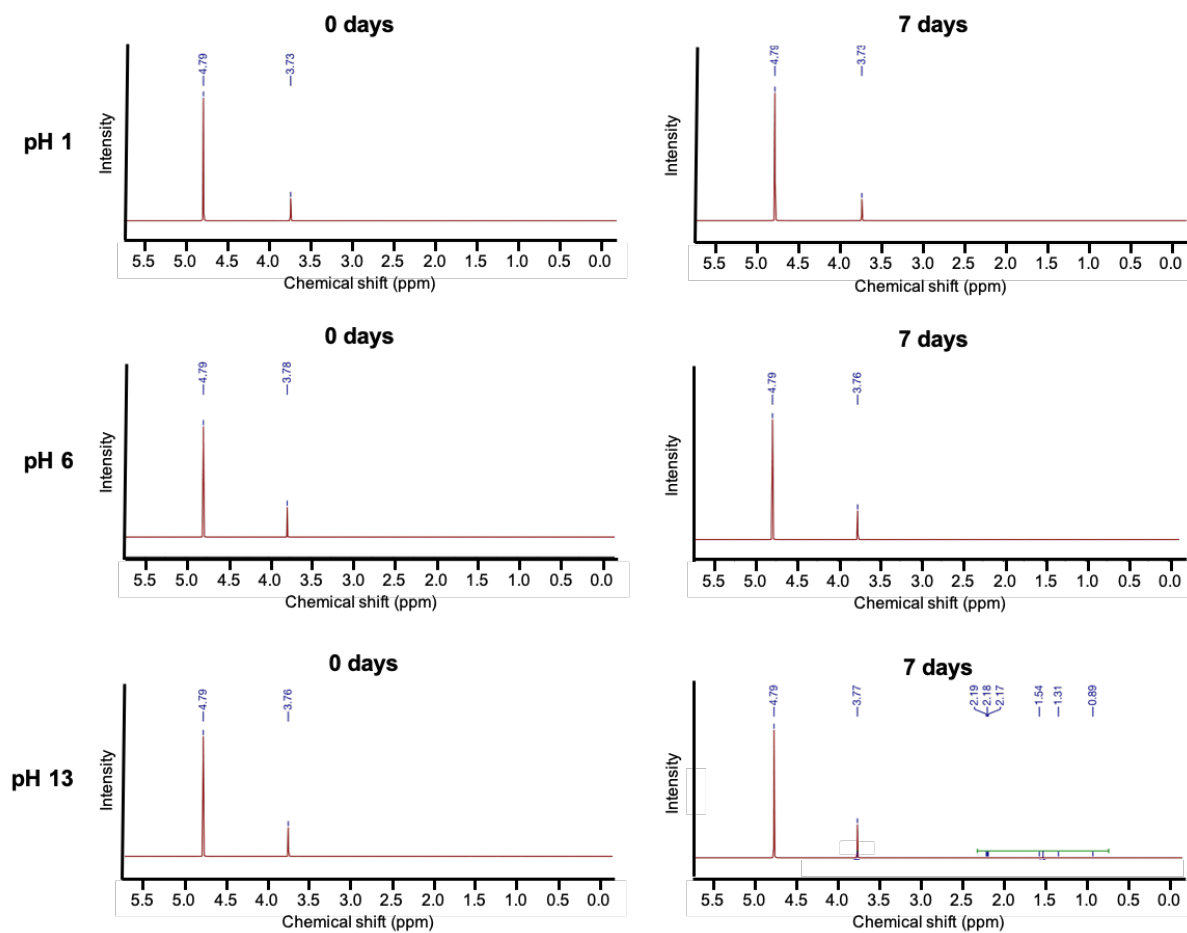


Figure 28 – ^1H NMR results for degradation of 50-poly(*S-r*-canola) over 7 days. $\delta = 4.79$ ppm (D_2O), 3.77 ppm (1,4-dioxane), 2.19 ppm (a), 2.18 ppm (a), 2.17 ppm (a), 1.54 ppm (b), 1.31 ppm (c), 0.89 ppm (d).

^1H NMR analysis revealed that no observable change occurred after treatment for 7 days at pH 1 and however trace amounts of degradation products were observed at pH 13. These products appeared as a triplet (2.19, 2.18 and 2.17 ppm) and three singlets at 1.54, 1.31 and 0.89 ppm. A close up of these signals is shown below in Figure 29.

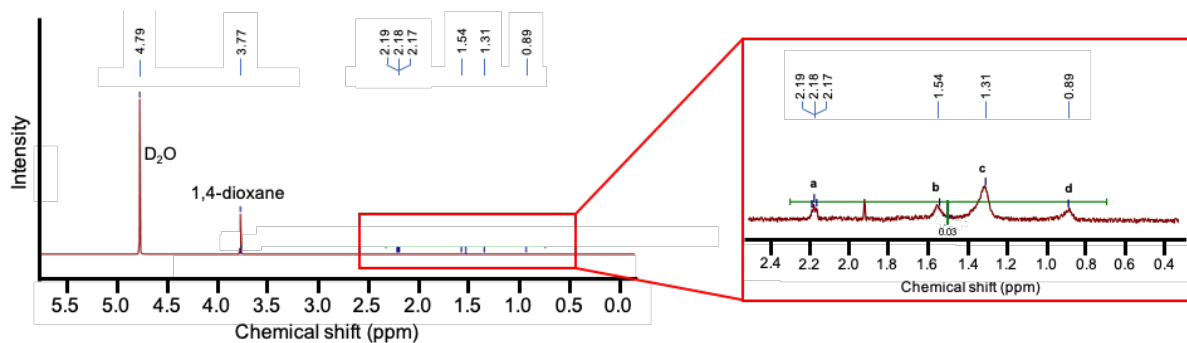


Figure 29 – ^1H NMR spectrum for 50-poly(*S-r*-canola) polymer after degradation at pH 13 for 7 days. (600 MHz, D_2O): $\delta = 4.79$ ppm (D_2O), 3.77 ppm (1,4-dioxane), 2.19 ppm (a), 2.18 ppm (a), 2.17 ppm (a), 1.54 ppm (b), 1.31 ppm (c), 0.89 ppm (d).

This suggests that the 50-poly(*S-r-canola*) Fe(III) sorbent is compatible with acidic and neutral environments but may undergo minor degradation when exposed to basic environments for extended periods of time. This is important information to consider when implementing this 50-poly(*S-r-canola*) sorbent into an already established iron removal process.

2.5.6 Large scale Fe(III) treatment

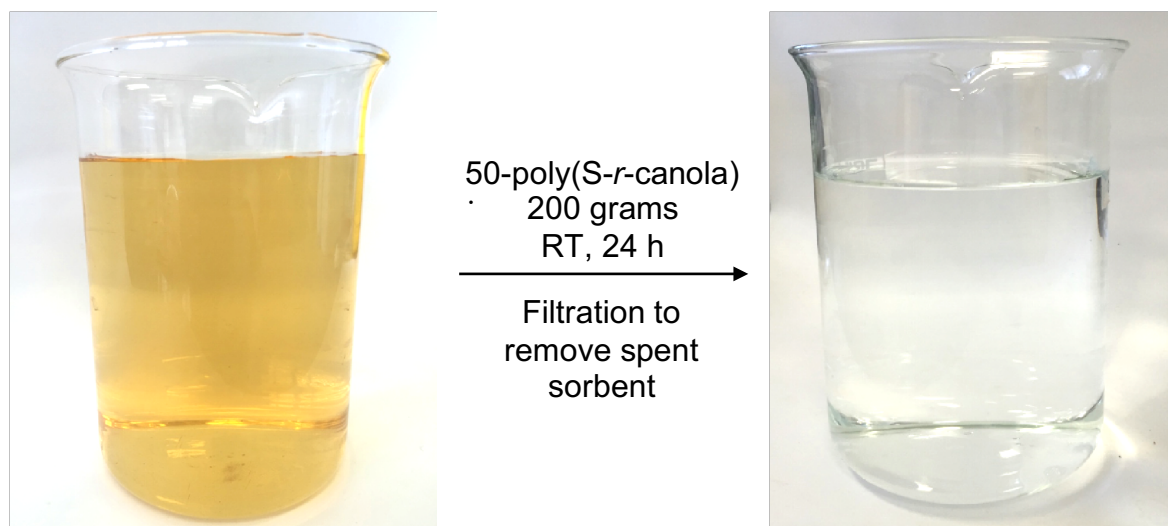


Figure 30 – FeCl_{3(aq)} (50 ppm, 1.0 L) before and after treatment with 50-poly(*S-r-canola*) sorbent.

The discoloration of iron contaminated water disappeared after treatment with 50-poly(*S-r-canola*) polymer (Figure 30). To ensure the results were accurate, both UV/Vis and AAS analysis were performed. The measurements were equivalent within the margin of error.

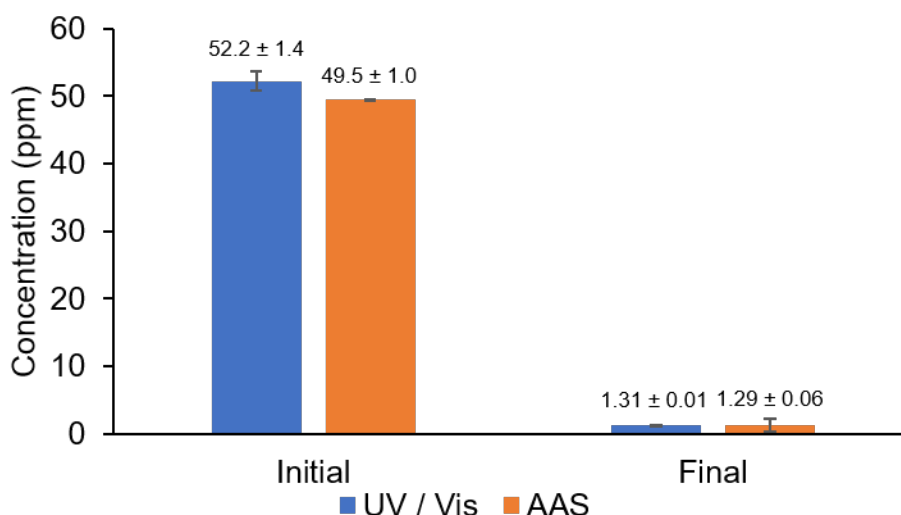


Figure 31 – UV / Vis and AAS results from large scale treatment experiment.

These results (Figure 31) prove that the 50-poly(*S-r-canola*) polymer is capable of reducing the Fe(III) concentration down to below the regulation limit and further prove that the UV/Vis method is achieving similar results to the AAS method.

2.5.7 Comparison to elemental sulfur

To highlight the differences between the 50-poly(*S-r-canola*) sorbent and elemental sulfur a comparison experiment was performed. Elemental sulfur was used (1.0 g) to treat a 50 ppm Fe(III) solution (20 mL, run in triplicate). It was observed that treatment with sulfur resulted in similar levels of Fe(III) reduction. Results are shown in Figure 32.

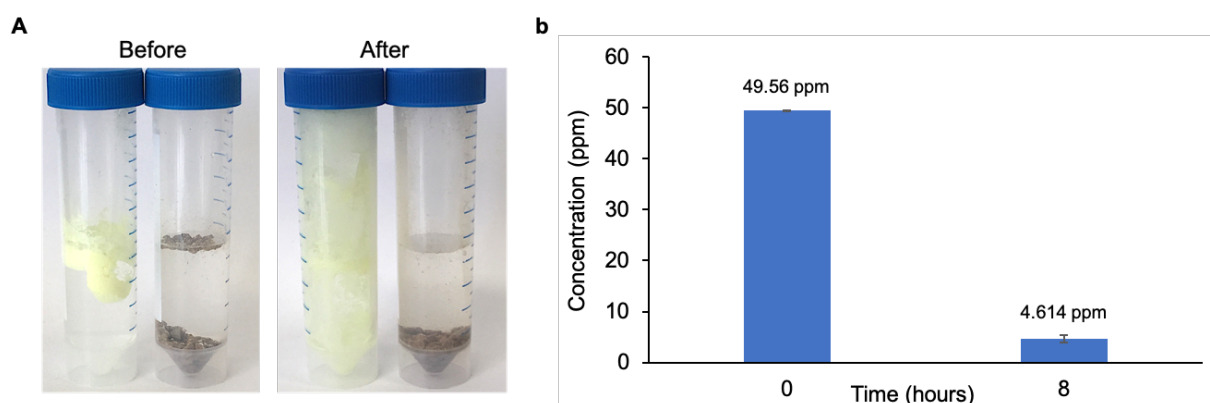


Figure 32 – A) Elemental sulfur and 50-poly(*S-r-canola*) polymer before (right) and after (left) mixing, B) Results for Fe(III) remediation using elemental sulfur.

Although elemental sulfur was shown to be effective in Fe(III) binding, it stuck to the container walls making it difficult to remove from solution. In comparison, the 50-poly(*S-r-canola*) simply sunk to the bottom and was easily separated by simple filtration. This demonstrates that by forming sulfur into 50-poly(*S-r-canola*), the Fe(III) removal efficiency is maintained however the issues with caking, blocking and adhering are resolved. This makes 50-poly(*S-r-canola*) more practical than sulfur for large scale implementation.

2.5.8 Porous 50-poly(*S-r-canola*) synthesis and characterization

Although the 50-poly(*S-r-canola*) sorbent was capable of removing Fe(III) from solution its capacity was impractical for large scale practical use. To enhance the capacity of the 50-poly(*S-r-canola*) polymer as a sorbent material, its surface area was increased by preparing a porous version of the material. Sodium chloride (NaCl) was incorporated into the synthesis as a porogen. The 50-poly(*S-r-canola*) reacts as usual and eventually vitrifies forming the polymer around the NaCl porogen. Washing the NaCl / polymer composite with water dissolved the NaCl effectively removing it from the 50-poly(*S-r-canola*) and leaving behind a series of pores

and microchannels. Once all the remaining sodium chloride has been washed away, a porous 50-poly(*S-r*-canola) polymer remains. A large excess of NaCl (70 wt%) was required to form the highly porous 50-poly(*S-r*-canola) sponge material shown in Figure 33. This large excess of NaCl was required so that the NaCl would form microchannels and allow for a highly porous product. Using less than 70 wt% NaCl resulted in more encapsulation of NaCl than microchannel formation. In the case of the encapsulated salt, water was unable to reach it and remove it.

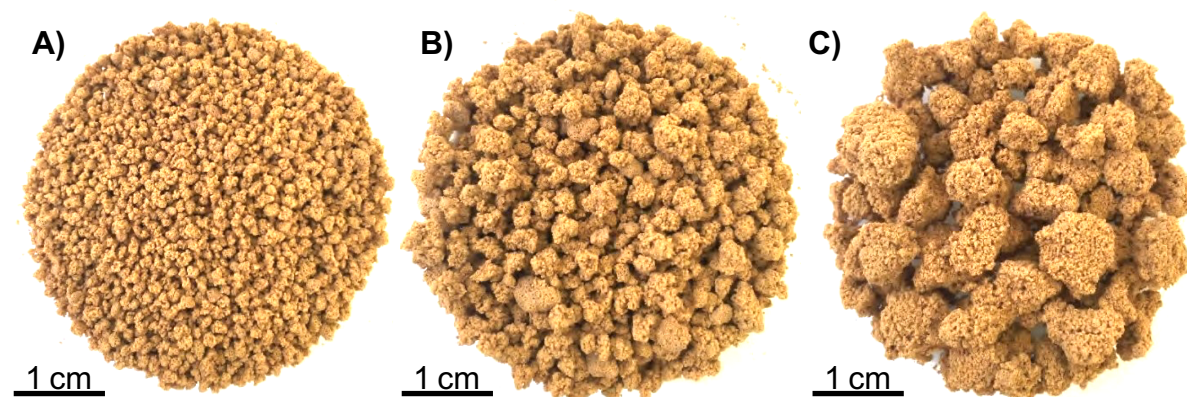


Figure 33 - Porous 50-poly(*S-r*-canola) particles of size ranges: **A)** 1.0-2.5 mm, **B)** 2.5-5 mm, **C)** >5.0 mm.

The resulting polymer particles, shown in Figure 33, were porous and acted like sponges when compressed. Although the NaCl was washed out post-synthesis, the synthesis may have been affected by its presence. The porous 50-poly(*S-r*-canola) material was compared with the non-porous polymer using FTIR, STA, XRD and SEM analysis. Under FTIR analysis (Figure 34), all peaks previously assigned to 50-poly(*S-r*-canola) polymer were present in both the porous and non-porous 50-poly(*S-r*-canola) samples. No significant difference is observed between the porous and non-porous polymers under FTIR analysis.

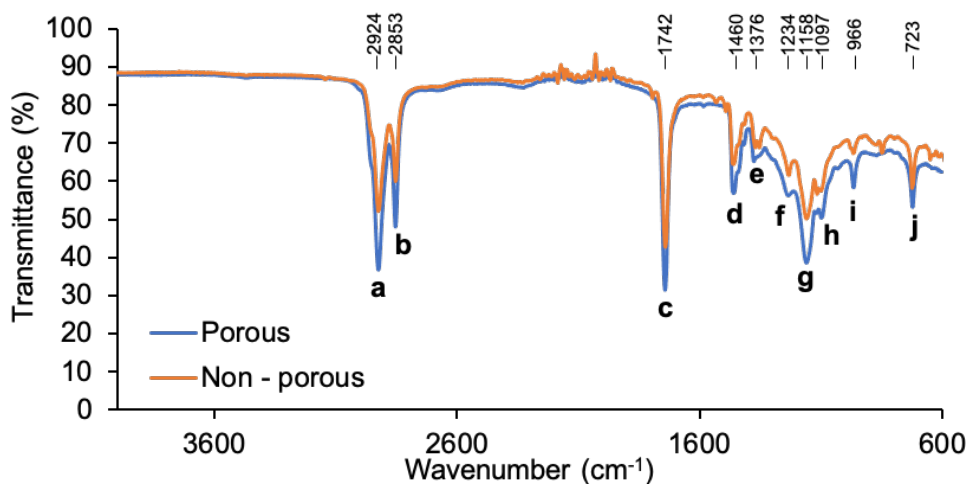


Figure 34 – FTIR analysis of porous and non-porous 50-Poly(*S-r-canola*) polysulfides

This suggests that the addition of NaCl into the reaction only effects the physical structure of the polymer not its chemical structure. NaCl doesn't adsorb IR radiation and its presence is therefore unable to be determined using FTIR analysis. To better characterise any differences and to investigate the presence of any remaining NaCl which wasn't removed during the washing step, X-Ray Diffraction (XRD) was performed.

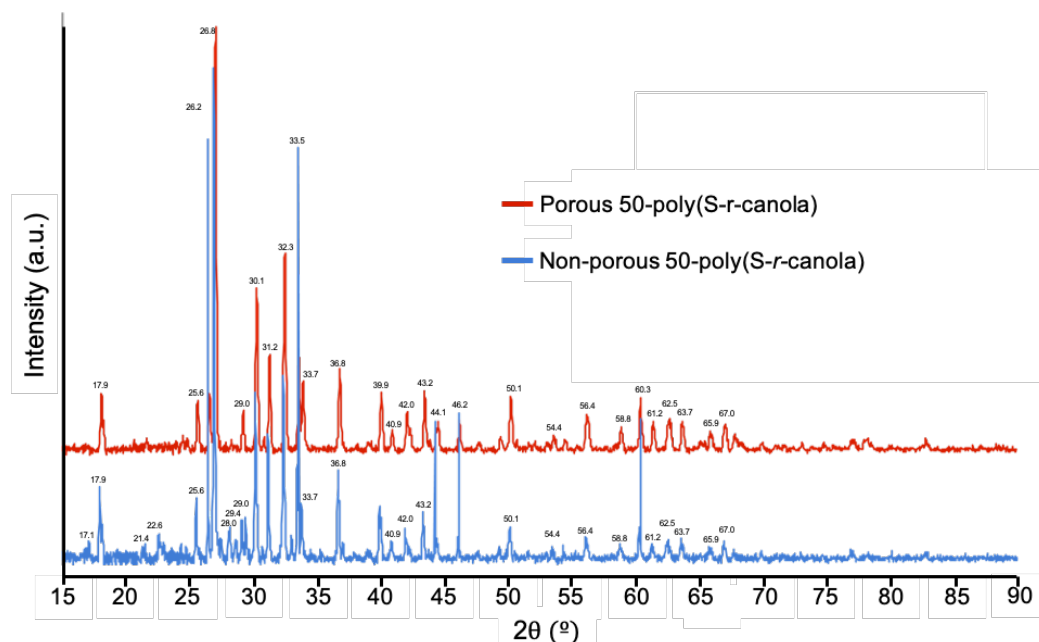


Figure 35 - XRD of porous and non-porous 50-poly(*S-r-canola*).

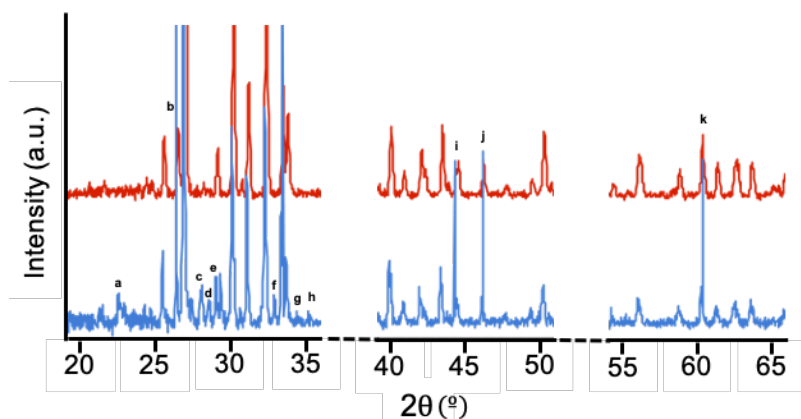


Figure 36 – Close up of peaks of interest from XRD in figure 35.

The XRD analysis (Figures 35 and 36) revealed no significant differences in the porous and non-porous 50-poly(*S-r*-canola) polymers. It appears as if there are some small extra peaks present in the non-porous canola oil polymer which aren't observed in the porous canola oil polymer sample. This suggests a difference in crystalline structure. FTIR revealed no difference in chemical structure suggesting that the porous 50-poly(*S-r*-canola) polysulfide was chemically identical to the non-porous polysulfide. SEM analysis was used to observe the extent of porosity of the polymer. The SEM micrograph of the porous 50-poly(*S-r*-canola) polysulfide is shown below in Figure 37.

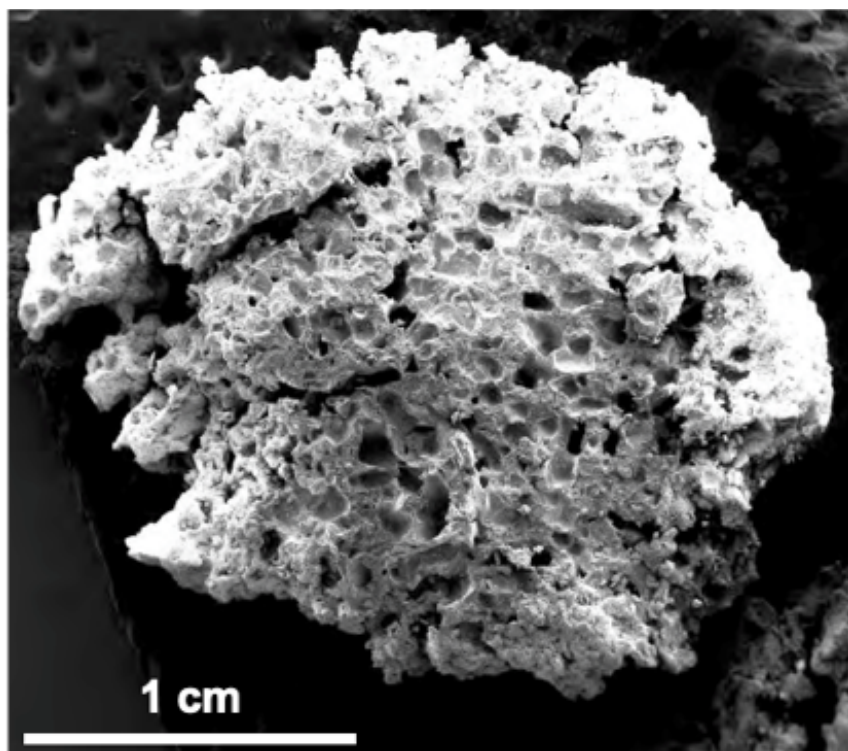


Figure 37 – Representative SEM images of porous 50-poly(*S-r*-canola).

Pores can clearly be observed in the 50-poly(*S-r-canola*) sponge. For a random sample of 50 pores, the diameter of the pores was measured, and the average was found to be approximately $119 \pm 53 \mu\text{m}$.

2.5.9 Fe(III) treatment with porous 50-poly(*S-r-canola*) sorbent

Now that a porous version of the 50-poly(*S-r-canola*) has been prepared, its efficiency at Fe(III) removal was evaluated. To achieve this, porous and non-porous 50-poly(*S-r-canola*) were used to treat Fe(III) solution over 24 hours. The results are shown below in Figure 38.

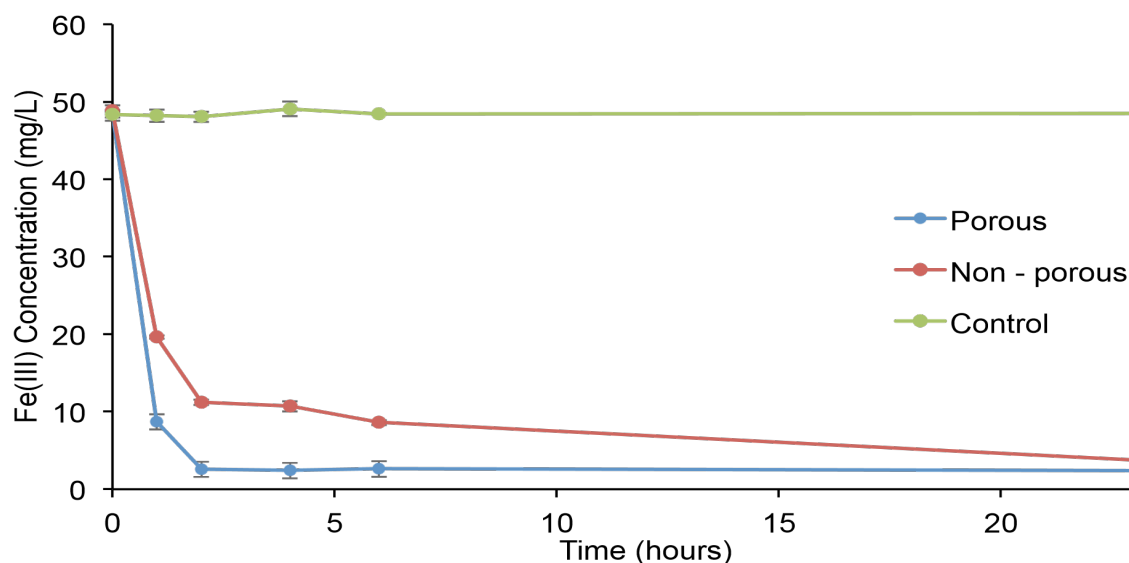


Figure 38 – Fe(III) treatment using porous and non-porous 50-poly(*S-r-canola*) sorbents over 24 hours.

Although the porous and non-porous 50-poly(*S-r-canola*) polymers demonstrated the same overall reduction in Fe(III) concentration over 24 hours, the porous sorbent achieves this concentration at a significantly faster rate than the non-porous sorbent. This is important for large scale implementation as it increases the rate of water treatment increasing its viability.

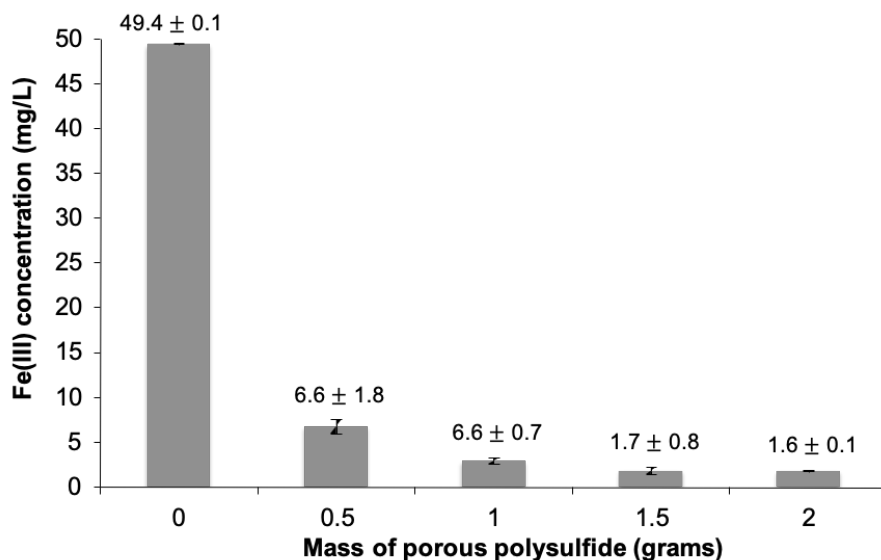


Figure 39 - Fe(III) removal from water using varying mass of the porous 50-poly(*S-r*-canola)

These results (Figure 39) show that by using just 0.5 grams of 50-poly(*S-r*-canola) sorbent, similar levels of Fe(III) reduction were achieved to 2.0 grams of the non-porous sorbent. 2.0 grams was enough to reduce the Fe(III) levels to below regulation limits (3 mg L^{-1}).²²¹ It should also be noted that this sorbent was able to reduce the iron concentration by up to 96.8%, higher than reports using activated carbon (90%).²⁰⁸

2.5.10 Langmuir sorption isotherm for Fe(III) sorption using porous 50-poly(*S-r*-canola)

In order to determine the Fe(III) sorption capacity of the porous 50-poly(*S-r*-canola), a Langmuir sorption isotherm experiment was performed. The Langmuir adsorption isotherm describes the equilibrium between the 50-poly(*S-r*-canola) sorbent and the Fe(III) in solution. The Langmuir adsorption isotherm assumes that adsorption is limited to one molecular layer.²²² The process involves treating a series of Fe(III) solutions with the same mass of 50-poly(*S-r*-canola) polymer. The initial (C_0) and equilibrium (C_{eq}) concentrations were used to calculate the amount of Fe(III) adsorbed per gram of sorbent (Y). This value was then plotted against C_{eq} producing the isotherm shown in Figure 40. The linearized Langmuir isotherm for Fe(III) sorption using the porous 50-poly(*S-r*-canola) polymer is shown below (Figure 40).

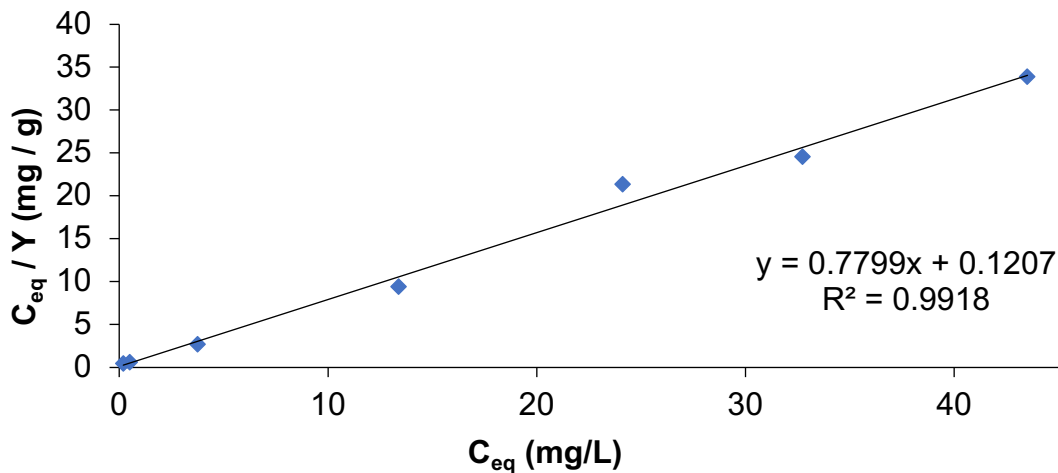


Figure 40 – Linearized Langmuir sorption isotherm for Fe(III) sorption using porous 50-poly(S-r-canola) sorbent.

From this isotherm the maximum sorption capacity and the Langmuir sorption constant were calculated:

$$\frac{C_{eq}}{Y} = C_{eq} \frac{1}{Y_{max}} + \frac{1}{Y_{max}k_L} = 0.7799C_{eq} + 0.1207$$

Therefore:

$$\frac{1}{Y_{max}} = 0.78 \leftrightarrow Y_{max} = \frac{1}{0.78} = 1.28 \text{ mg } g^{-1}$$

And

$$\frac{1}{Y_{max}k_L} = 0.1207 \leftrightarrow k_L = \frac{1}{0.1207 \times 0.78} = 10.62 \text{ L } g^{-1}$$

to be $Y_{max} = 0.89 \text{ mg / g}$ and $K_L = 10.6 \text{ L / g}$.

2.5.11 Effect of pH and competing ions on Fe(III) removal

For practical use in Fe(III) treatment, it's important to determine the effect of pH removal efficiency. This is also an important factor when considering implementing this within a current Fe(III) removal system as many are pH dependant.^{209, 223} To achieve this Fe(III) removal experiments were repeated at varying pH values and the results are shown in Figure 41.

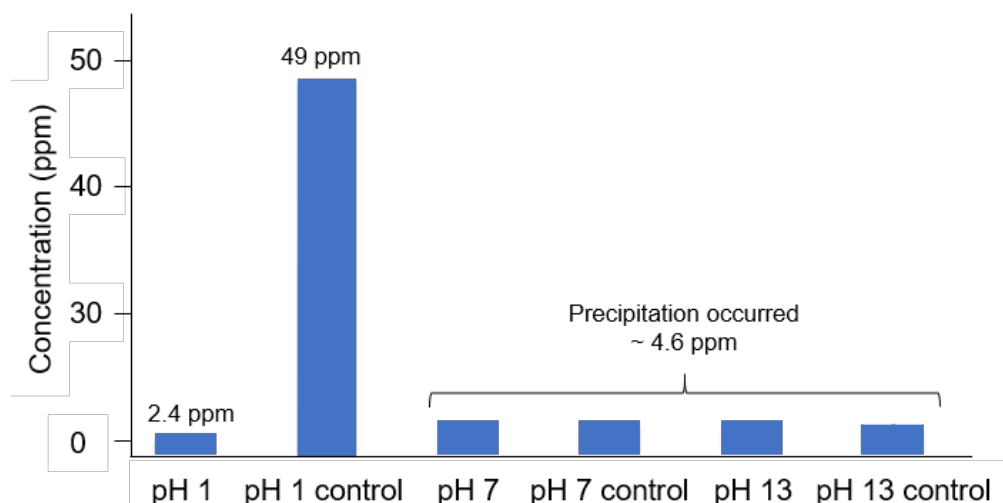


Figure 41 – Fe(III) concentrations after treatment from porous 50-poly(*S-r-canola*) at pH 1, 7 and 13.

The highest extent of Fe(III) removal was observed at pH 1 with the concentration dropping from 50 ppm to 2.4 ppm (95.2%). Treatment at pH of 7 and 10 showed reduction down to approximately 4.6 ppm, however the control solutions showed the same reduction. This is because at pH above 3, Fe(III) is oxidised and precipitates out of solution. These results show that the 50-poly(*S-r-canola*) sorbent removes more Fe(III) than simple precipitation and that Fe(III) removal should be performed at a pH below 3 for maximum reduction. Another factor known to affect the efficiency of metal ion absorption are competing ions. In order to determine whether competing ions would affect the Fe(III) removal efficiency, a 50 ppm Fe(III) solution at pH 3 was prepared containing 10 mg/L: NaCl, CaCl₂, MgCl₂, KCl and Na₂SO₄. These solutions were left to incubate for 16 hours. After which, all of the Fe(III) had precipitated from the solution containing 10 mg/L Na₂SO₄. This can be seen in Figure 42. The solution containing Na₂SO₄ was therefore not considered further in this experiment.



Figure 42 - Images of 50 ppm Fe(III) solutions containing either 10 ppm of MgCl₂, CaCl₂, KCl, Na₂SO₄, or NaCl.

Next a Fe(III) solution (50 ppm) was prepared at pH 3 containing 10 mg/L of NaCl, CaCl₂, MgCl₂ and KCl. This solution was then treated with the 50-poly(S-*r*-canola) sorbent and the Fe(III) concentration was determined using AAS. Results shown in Figure 43 indicate the presence of Na⁺, K⁺, Mg²⁺, Ca²⁺ and Cl⁻ ions does not affect the Fe(III) removal efficiency of the 50-poly(S-*r*-canola) sorbent.

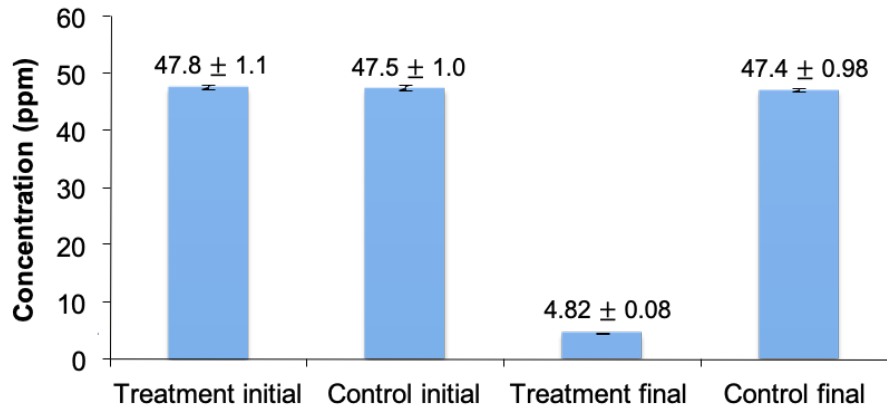


Figure 43 – Results for Fe(III) sorption using 50-poly(S-*r*-canola) sorbent in the presence of Na⁺, K⁺, Mg²⁺, or Ca²⁺ and Cl⁻ ions.

2.5.12 Kinetic analysis of Fe(III) sorption onto the porous polysulfide

The sorption kinetics are important in order to determine the treatment time required for a given Fe(III) concentration. To test the kinetics, Fe(III) solutions (50 ppm) were treated with different amounts of 50-poly(S-*r*-canola) sorbent. The concentration was monitored over 6 hours. The results for this are plotted below in Figure 44.

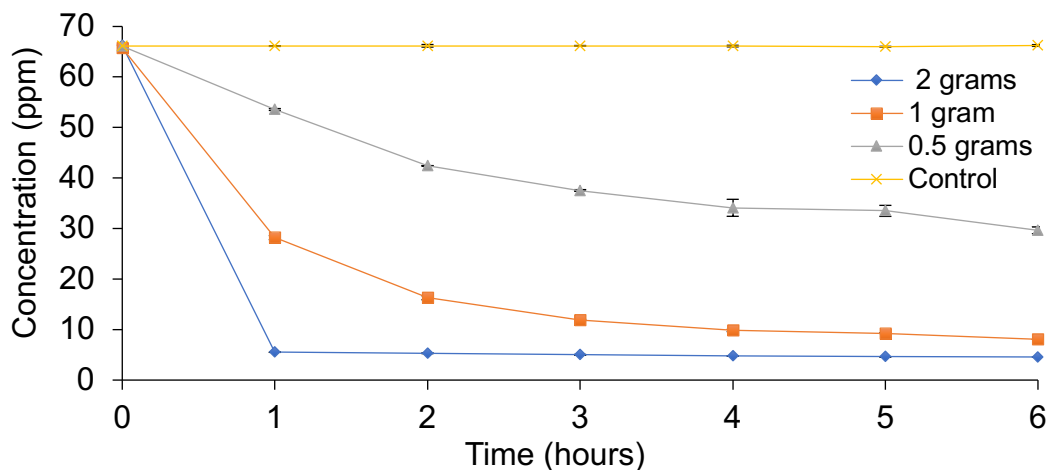


Figure 44 – Kinetic data for Fe(III) removal using porous 50-poly(S-*r*-canola) sorbent.

Using the data obtained for treatment of Fe(III) solution (50 ppm) using 2.0 grams of porous 50-poly(S-*r*-canola) polysulfide, the kinetics were analysed. The initial Fe(III) concentration (Q_0) and Fe(III) concentration at time t (Q) were used to evaluate the kinetics. The reaction

involves two reactants, Fe(III) and 50-poly(S-*r*-canola), whereby the Fe(III) concentration decreases whilst the 50-poly(S-*r*-canola) concentrations remains constant. The reaction is therefore a second order reaction however the rate is dependent on only one reactant, Fe(III). This is classified as a pseudo first order reaction. The data was therefore fitted to a pseudo-first order equation (eq 2).

$$\ln\left(\frac{1}{Q_0-Q}\right) = k_{ad}t \quad \text{Equation 2}$$

By fitting the Q_0 and Q values along with their corresponding t values using equation 2, the slope of the resulting line is equivalent to the rate constant, k_{ad} .

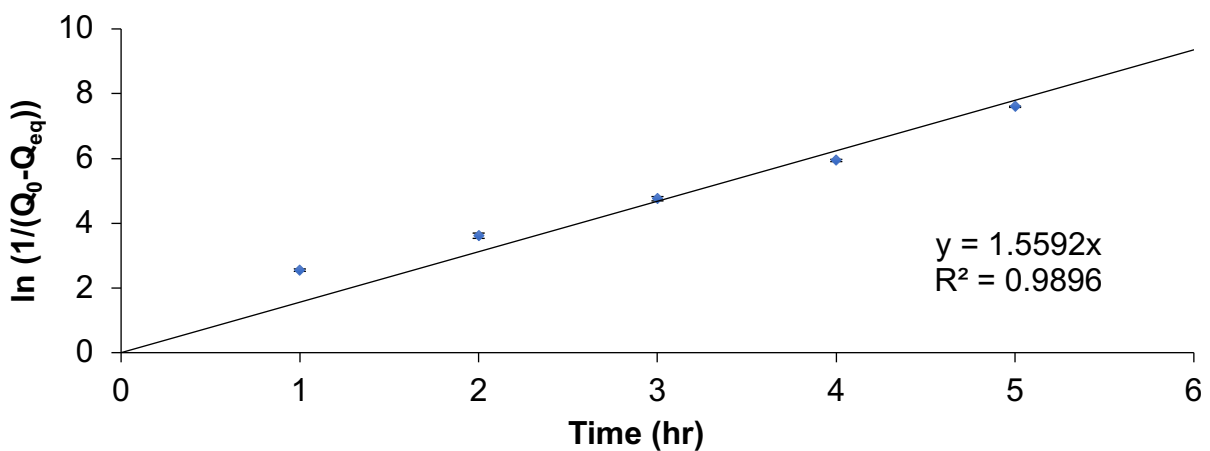


Figure 45 – Kinetic analysis for Fe(III) treatment with porous 50-poly(S-*r*-canola) sorbent.

The equation of the trendline in Figure 45 was re-arranged to form the following equation:

$$\ln\frac{1}{(Q_0-Q)} = 1.5592 \times \text{Time} \quad \text{Equation 3}$$

The slope of this line is equivalent to the rate constant for the sorption of Fe(III) onto 50-poly(S-*r*-canola) sorbent.

$$k_{ad} = 1.56 \text{ mg L}^{-1} \text{ Hr}^{-1}$$

2.5.13 Porous poly(S-*r*-canola) synthesis using waste cooking oil

Earlier syntheses of the key 50-poly(S-*r*-canola) polymer used food grade canola oil. Next, to increase the sustainability of the sorbent, its preparation from waste cooking oil was investigated. This is important as it extends the lifetime of plant oils and ensures that large scale polymer production wouldn't cut into food and land resources. The synthesis proceeds the same as that using food grade oil producing a rubbery polymer after around 30 minutes

reaction time. To investigate any differences in the polymer prepared from food grade and waste cooking oil, the materials were first characterised using FTIR spectroscopy.

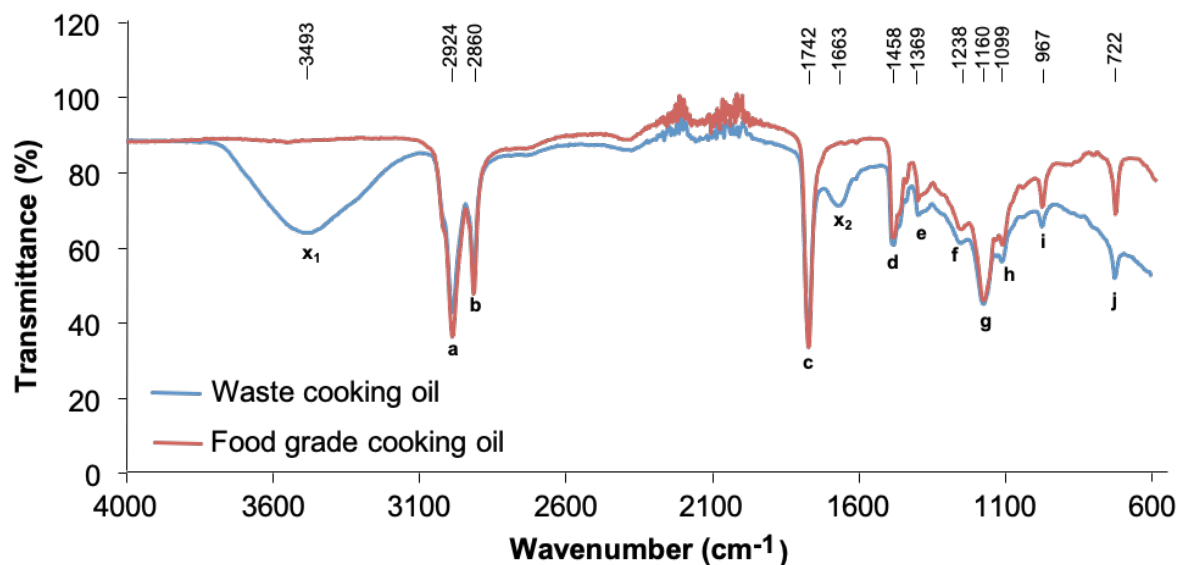


Figure 46 – FTIR analysis of 50-poly(*S-r*-canola) prepared using waste cooking oil

FTIR analysis (Figure 46) revealed the presence of all peaks previously assigned to 50-poly(*S-r*-canola) polymers (**a-j**). The waste cooking oil sample did however exhibit two extra peaks located at 3459 cm^{-1} (**x₁**) and 1663 cm^{-1} (**x₂**) corresponding to -OH group vibrations for alcohols groups. The presence of alcohol groups in the waste cooking oil polymer was not surprising. During the frying process, cooking oils, are known to undergo oxidation resulting in the formation of peroxides, epoxides, aldehydes, carboxylic acids and alcohols.²¹⁹ Water and partially hydrolysed triglycerides could also be present. Although the cooking oil was chemically different to the food grade cooking oil, the resulting polymers were visibly identical and other than the presence of OH vibrations, identical under IR analysis. This suggests that the OH groups didn't not adversely impact the formation of the sorbent material. Although FTIR analysis reveals a difference in chemical structure, the 50-poly(*S-r*-canola) appeared identical under SEM analysis containing two distinct regions: a smooth amorphous surface and crystalline sulfur particles coating the surface.

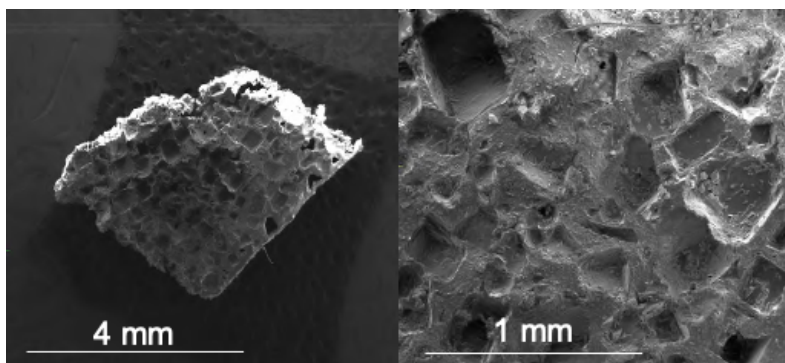


Figure 47 - Representative SEM of 50-poly(S-*r*-canola) made from waste cooking oil.

The cross-section is shown to illustrate the pores and pits formed in the synthesis (Figure 47). Whilst some microchannels were observed, large pores and divots were the main features on the surface. This is likely due to larger grain size of the salt used and insufficient mixing resulting in aggregation and less microchannel formation.

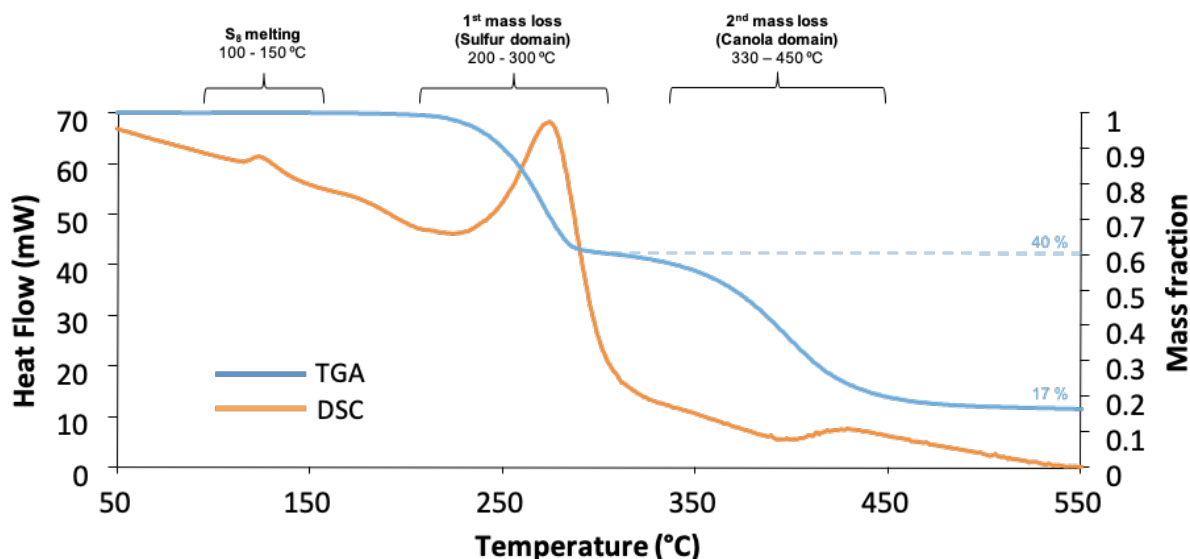


Figure 48 – TGA and DSC of 50-poly(S-*r*-canola) polymer prepared from waste cooking oil (canola oil).

Although some changes were observed under FTIR, the 50-poly(S-*r*-canola) polymer prepared from waste cooking oil displays the same features under STA analysis (Figure 48). Both the endotherms, for S₈ melting and the mass loss due to sulfur, are present and correspond with those previously observed for the 50-poly(S-*r*-canola) material. This suggests that the use of waste cooking oil did not affect the thermal properties of the material. The sorbent prepared from waste cooking oil was then tested in Fe(III) removal.

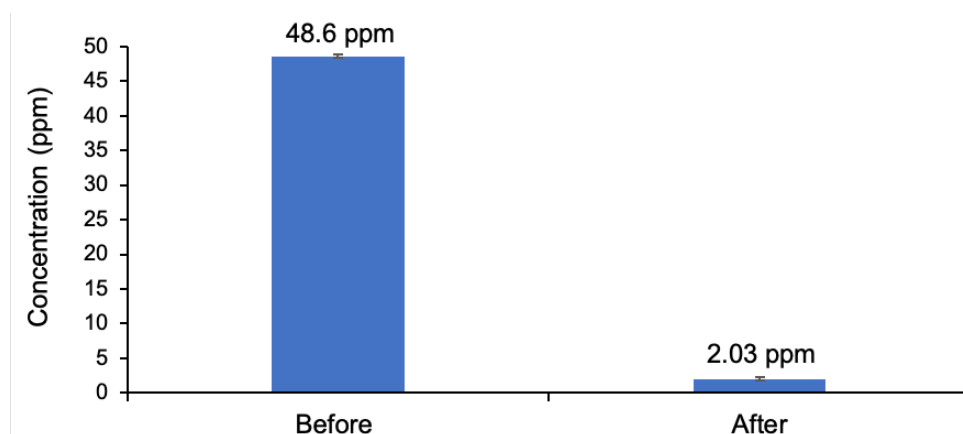


Figure 49 – Results for Fe(III) treatment using 50-poly(S-*r*-canola) polymer prepared using waste cooking oil.

The sorbent prepared from waste cooking oil demonstrated similar Fe(III) removal ability to the sorbent prepared from food grade cooking oil (Figure 49). This is important as it shows that food grade canola oil can be replaced with waste cooking oils, making it more sustainable and increasing the lifetime of the plant oils.

2.5.14 Microwave induced 50-poly(S-*r*-canola) synthesis and characterization

Sulfur polymers have been suggested for use in water purification and environmental chemistry purposes. To facilitate a scalable method by which someone could easily prepare poly(S-*r*-canola) sorbents rapidly and on demand without the need for expensive equipment, microwave irradiation was investigated. Sulfur based polymers are known to be excellent thermal insulators making it difficult to apply reliable and uniformly distributed heating during polymerisation. Canola oil and triglycerides are capable of being heated at rapid rates using microwave irradiation. As canola oil is a major component of the reaction mixture, we hypothesised that microwave irradiation could be used to facilitate heating of the reaction mixture. To investigate this, the reaction was carried out using a laboratory microwave reactor with precise temperature and power control (Startsynth front-loading microwave reactor). The microwave reactor was set to heat up at constant power for approximately 8 minutes and 50 seconds. The mixture was stirred using a magnetic stir bar and the temperature and pressure were monitored throughout the reaction. The results are shown in Figure 50.

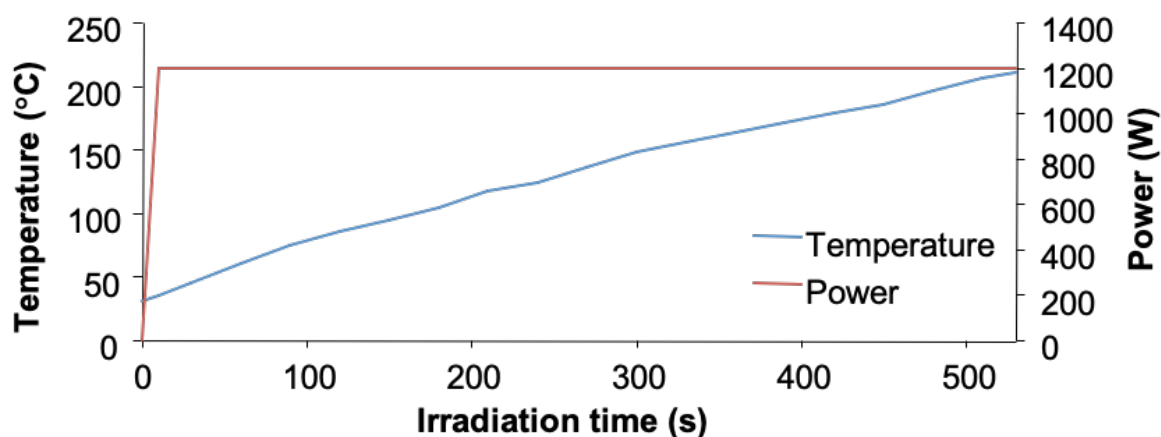


Figure 50 - Heating and power profile for microwave-based synthesis of 50-poly(*S-r*-canola). As shown in Figure 51, the resulting polymer looked visually equivalent to the polymer prepared using conventional heating.

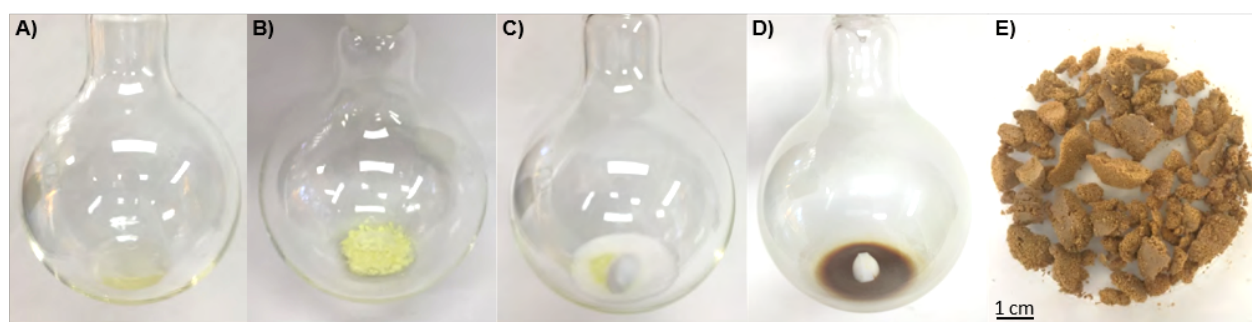


Figure 51 – A) Canola oil in round bottom flask B) Sulfur added to canola oil, C) Sodium chloride porogen added, D) Product as formed in flask from microwave irradiation. E) Isolated porous polysulfide after washing out sodium chloride.

Now that the concept has been validated, it was repeated using a 1100 W household microwave. Using this simple method, the polymer was able to be formed in just 5 minutes (compared to 20 minutes for conventional heating). The resulting polymer was shown in Figure 52. The ability to prepare these materials in conventional microwaves could be important for scaling up the synthesis as several batches could be prepared in rapid succession or by using multiple inexpensive microwave reactors in parallel and implementing continuous flow reaction systems.²¹⁹ This makes preparation of this polysulfide polymer accessible to areas with limited resources. This is an especially important point with regards to using this material as sorbents for water remediation.



Figure 52 – Images of reaction mixture in bowl before (left) and after (middle) inverse vulcanization in a household microwave for ~5 minutes and the porous 50-poly(*S-r*-canola) product after washing to remove salt.

This biggest limitation in this method was the inability to efficiently mix the reaction during the heating process. Poor mixing results in phase separation and inconsistent final product. To avoid this issue, the sample was initially irradiated for 4 minutes and 30 seconds, so that the reaction reached approximately 180 °C. This was then followed by 30 second stirring and 30 second irradiation cycles. This was repeated until the 50-poly(*S-r*-canola) polymer vitrified and formed in the reaction bowl.

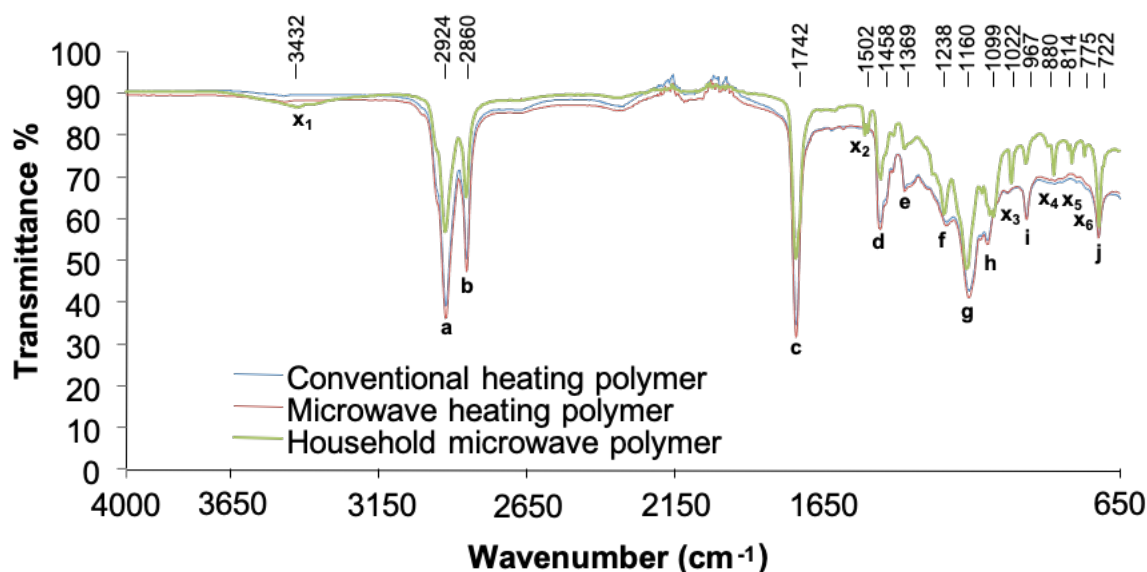


Figure 53 – FTIR analysis of 50-poly(*S-r*-canola) material prepared by conventional heating, controlled microwave heating, and household microwave heating.

FTIR analysis (Figure 53) reveals that along with the peaks previously assigned to 50-poly(*S-r*-canola) polymer (a-j), a series of new peaks occurred for the microwave heated sample (x₁-x₆). Although microwave heating is typically more uniform than conventional heating, the sulfur and canola oil were not mixed sufficiently. The magnetic stir bar in the laboratory microwave reactor wasn't strong enough to mix the reagents efficiently enough. This could have led to areas with higher canola oil content which would result in inconsistent heating and

hot spots. These hot spots may have far exceeded the intended reaction temperature leading to areas in which further reactions were taking place. To determine if the changes, observed under FTIR, had any effect on the surface morphology, SEM analysis was performed. The results are shown in Figure 54.

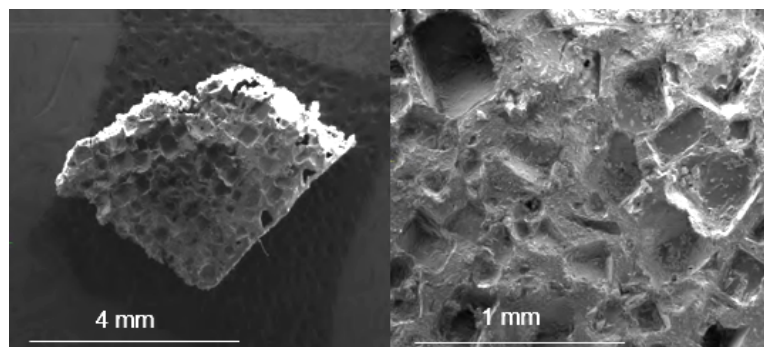


Figure 54 – SEM images of porous 50-poly(*S-r*-canola) prepared using a household microwave.

SEM analysis revealed that the 50-poly(*S-r*-canola) polymer prepared using the household microwave did not appear as porous as previous samples. This was likely due to the inability to efficiently mix the reaction whilst heating in a microwave oven. Poor mixing would have led to a poor distribution of porogen throughout the material. This is likely the reason which the poor size is so large and the typical microchannels are not observed. The method still worked to increase the surface area and introduce pores and microchannels however not to the extent shown in the standard method. Next simultaneous thermogravimetric analysis (STA) was performed on the samples. The results are shown in Figure 55.

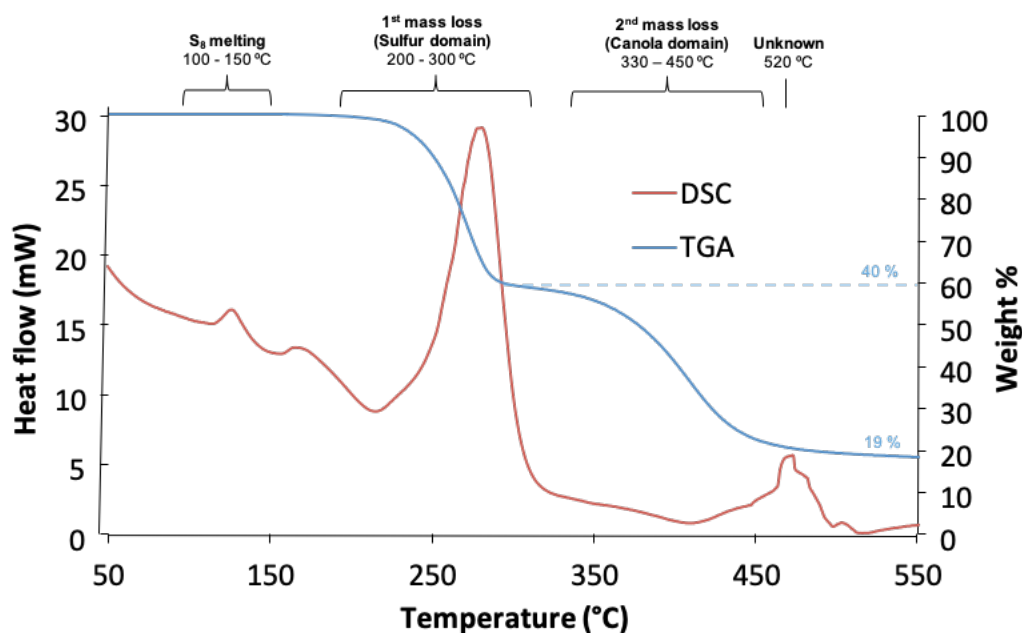


Figure 55 – STA analysis (TGA and DSC) of 50-poly(S-*r*-canola) polysulfide prepared using a laboratory microwave reactor.

The endotherms between 100 – 130 °C and 210 - 300 °C were due to S₈ melting and the mass loss due to the sulfur domain, respectively. Differences were observed however with two extra isotherms centred around 175 °C and 475 °C. This is consistent with the differences observed under FTIR analysis. Now that characterisation was complete, the Fe(III) removal ability was investigated. The efficiency of the sorbent prepared using microwave irradiation was compared to the sorbent prepared using conventional heating (Figure 56).

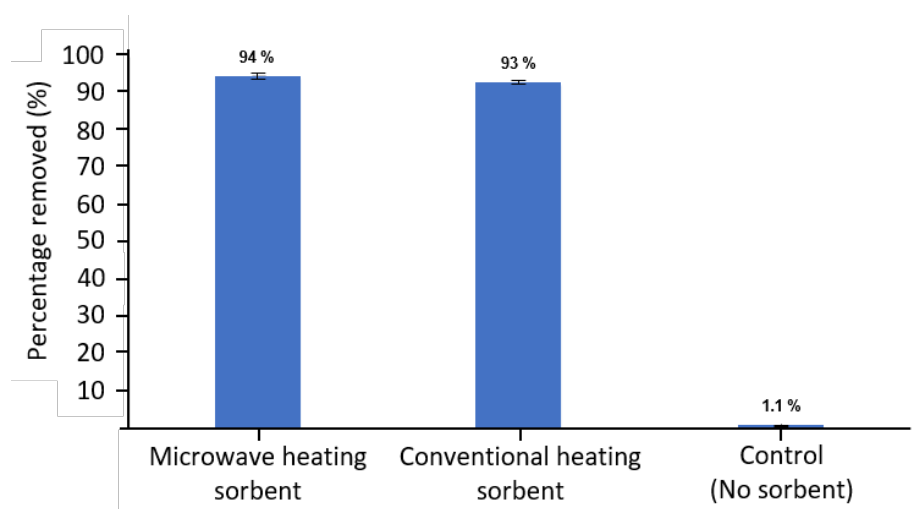


Figure 56 – Results for Fe(III) treatment using porous 50-poly(S-*r*-canola) prepared using microwave irradiation and conventional heating methods.

The sample prepared from microwave irradiation demonstrated equivalent Fe(III) removal efficiency to the sorbent prepared by conventional heating methods. This means although the

material prepared has some differences chemically, it behaves the same for its intended purpose, as a Fe(III) sorbent material. This is important as it not only demonstrated the first instance of using microwave irradiation to initiate inverse vulcanisation, but it makes this sorbent material accessible to areas in which conventional preparation methods aren't available.

2.6 Conclusion

Novel Fe(III) sorbent materials were prepared by inverse vulcanisation of sulfur with canola oil. These sorbents were demonstrated to not only maintain but slightly improve upon elemental sulfur's ability to remove Fe(III) from water whilst also improving its physical properties. A second advantage observed for the polymer particles over elemental sulfur was that they did not cake or adhere to container walls and simply sunk to the bottom of the solution allowing for it to be removed via decantation or simple filtration. The sulfur content of the poly(S-*r*-canola) did not make a significant difference in Fe(III) sorption efficiency and because of this the 50-poly(S-*r*-canola) was chosen as the ideal sorbent material due to it containing less unreacted S₈. This sorbent was demonstrated in Fe(III) removal at industrially relevant concentrations, effectively reducing the Fe(III) concentration below regulation limits. Rapid, scalable, and simple synthesis of the 50-poly(S-*r*-canola) polysulfide material was demonstrated using microwave irradiation. This method is important as it demonstrated a new method for evenly heating the reaction mixture used in the sorbent's synthesis as well as reducing the synthesis time (< 5 mins), process costs and the amount of total heat energy consumed during synthesis. The resulting sorbent material was shown to be just as effective at Fe(III) removal as the sorbents prepared using conventional heating. Finally, waste cooking oil was used in the preparation of the sorbent materials. The resulting sorbents were compared with those prepared from food grade canola oil. The waste cooking oil based 50-poly(S-*r*-canola) sorbent demonstrated a very slight increase in Fe(III) removal efficiency than the one prepared from cooking oil. This was likely due to the cooking oil being hydrolysed during frying resulting in the addition of hydroxyl groups into the structure. The hydroxyl groups would lower the hydrophobicity of the surface, increasing its wetting ability, and in turn increasing its Fe(III) removal efficiency slightly. This demonstrated that effective heavy metal sorbent materials could be prepared entirely from industrial waste, by microwave induced inverse vulcanisation reactions. This is an important advance within the fields of waste valorisation and environmental chemistry.

Figure liscences:

a - "[Aging Cast-iron Water Pipe, Finland / Tubería de agua de hierro fundido, envejecida, Finlandia](#)" by [WATERLAT-GOBACIT](#) licensed under [CC BY-NC 2.0](#), **b** - "[Dry Pipe Supply Main](#)" by [Mr pantswearer](#) licensed under [CC BY-SA 4.0](#). **c** - "[Iron stains in a bucket](#)" by [India Water Portal](#) licenced under [CC BY-NC-SA 2.0](#). **d** - "[Rust from bathtub in Kyiv in water](#)" released into the public domain by its author, [Zweifel](#) at [English Wikipedia](#). **e** - "[faucet-4756043_1920](#)" by [JerzyGorecki](#) free for commercial use under [pixabay liscence](#). **f** - "[Iron Bacteria](#)" by [UGA CAES/Extension](#) licensed under [CC BY-NC 2.0](#). **g** - "[Iron fixing bacteria](#)" by [brewbooks](#) licensed under [CC BY-NC 2.0](#)

APPENDICES

Publications that resulted from the research in this chapter:

1. Lundquist, N. A.; Worthington, M. J. H.; Adamson, N.; Gibson, C. T.; Johnston, M. R.; Ellis, A. V.; Chalker, J. M. "Polysulfides made from re-purposed waste are sustainable materials for removing iron from water" *RSC Adv.* **2018**, 8, 1232-1236.



Cite this: *RSC Adv.*, 2018, 8, 1232

Polysulfides made from re-purposed waste are sustainable materials for removing iron from water†

Nicholas A. Lundquist,^a Max J. H. Worthington,^a Nick Adamson,^{ID ab}
Christopher T. Gibson,^a Martin R. Johnston,^{ID a} Amanda V. Ellis^{ID ab}
and Justin M. Chalker^{ID *a}

Water contaminated with Fe³⁺ is undesirable because it can result in discoloured plumbing fixtures, clogging, and a poor taste and aesthetic profile for drinking water. At high levels, Fe³⁺ can also promote the growth of unwanted bacteria, so environmental agencies and water authorities typically regulate the amount of Fe³⁺ in municipal water and wastewater. Here, polysulfide sorbents—prepared from elemental sulfur and unsaturated cooking oils—are used to remove Fe³⁺ contaminants from water. The sorbent is low-cost and sustainable, as it can be prepared entirely from waste. The preparation of this material using microwave heating and its application in iron capture are two important advances in the growing field of sulfur polymers.

Received 31st October 2017
Accepted 19th December 2017

DOI: 10.1039/c7ra11999b

rsc.li/rsc-advances

The removal of iron from groundwater, potable water and wastewater is an important requirement for water authorities, industry, and environmental agencies.¹ Ferric iron (Fe³⁺) in particular is undesirable because it leads to discolouration of plumbing fixtures^{2,3} and imparts unappealing odour and taste to drinking water.² Additionally, Fe³⁺ promotes the growth of certain bacteria, leading to fouling, clogging of pipes and other undesirable ecological effects.⁴ There are also some indications that adverse health effects in aquatic life may originate from high levels of iron.^{5,6} The control of iron content in water is therefore an important economic and environmental issue, with levels typically regulated by government authorities.^{7,8} There are several methods for removing iron from water including ion exchange,⁹ oxidative precipitation with subsequent flocculation and/or filtration,^{10,11} and adsorption of iron onto activated carbon,¹² among other techniques.¹ However, in scenarios where large volumes of water are treated, these methods may be expensive, low in performance, or both.¹

Our interest in controlling iron content in water stemmed from a recent engagement with an industry partner facing a challenge in meeting regulatory requirements for iron levels in groundwater pumped and discharged from an underground operations centre. A combination of oxidative conversion of Fe²⁺ to Fe³⁺ and separation using flocculants and filters provided

some success in meeting the 3 mg L⁻¹ daily discharge limit, but alternative low-cost methods were desired to facilitate the treatment and discharge of more than 150 000 L per day containing iron levels in the range of 35–60 mg L⁻¹. Our laboratory has recently reported the use of inexpensive polymers made from elemental sulfur and their use in sequestering metals such as palladium and mercury.^{13–15} It was therefore intriguing scientifically, economically and environmentally to determine if these polymers were suitable in the removal of iron from water.

Sulfur polymers, especially those prepared by inverse vulcanisation and related processes,¹⁶ have emerged as versatile materials in diverse areas of science.^{15–20} These studies are motivated, at least in part, by the megaton stores of sulfur available from crude oil desulfurisation.^{21,22} In converting this petroleum by-product into useful polymers, interesting applications have since been reported in power generation^{23,24} and storage,¹⁶ high refractive index and IR transmitting optical devices,^{25–27} dynamic and healable materials,^{26,28} thermal insulation,²⁹ sulfur-doped carbon materials,³⁰ and heavy metal remediation.^{13,14,29–33}

In the case of metal binding, polysulfide polymers have been used primarily to sequester highly toxic mercury salts.^{13,14,31–33} Because these sulfur polymers are simple to prepare in a single chemical step, we hypothesised that even if the affinity of the polysulfide for the harder Fe³⁺ is lower than for the softer Hg²⁺, the polymer may still be useful in removing the former metal from water. This hypothesis is further motivated by Theato's recent discovery that while high-sulfur polymers are excellent at capturing mercury, there is still appreciable binding to Fe³⁺ for an electrospun blend of a poly(sulfur-statistical-diisopropenylbenzene) polysulfide and poly(methyl methacrylate).³²

^aCentre for NanoScale Science and Technology, College of Science and Engineering, Flinders University, Sturt Road, Bedford Park, South Australia, 5042, Australia. E-mail: justin.chalker@flinders.edu.au

^bSchool of Chemical and Biomedical Engineering, University of Melbourne, Parkville, Victoria, 3010, Australia

† Electronic supplementary information (ESI) available: Full experimental details, including polymer synthesis, characterisation and iron binding studies. See DOI: 10.1039/c7ra11999b



We therefore set out to assess the iron-binding properties of a different co-polymer prepared by the direct reaction of elemental sulfur and canola oil. Importantly, this co-polymer is sustainably synthesised using only sulfur and the widely available and renewable canola oil.^{34–36} The resulting material is an elastomeric, high-sulfur factice³⁷ that has previously been studied by Theato as a novel cathode material³⁸ and by our team as a reactive sorbent for mercury pollution.¹⁴ Should this material prove effective in removing Fe^{3+} from water, it would represent a cost-effective method for water treatment through waste valorisation.

As a starting point, the canola oil polysulfide was synthesised by first heating sulfur to 180 °C in order to promote radical ring-opening polymerisation.¹⁴ Canola oil was then added to the polysulfide pre-polymer to cross-link the sulfur chains. The reaction mixture typically reaches its gel point within 20 minutes, at which time the reaction is cooled to provide a rubber-like material. The synthesis was prepared for 50%, 60%, and 70% sulfur by mass. The polymer was then milled into 1.0–2.5 mm diameter particles for subsequent use (Fig. 1 and S4†). Analysis of the polymers by infrared spectroscopy and Raman spectroscopy were consistent with our previous report on the material, in which the key polysulfide structure (S–S bonds) and canola oil backbone groups (e.g. C=O) are evident (S5–S6†).¹⁴ Thermogravimetric analysis and differential scanning calorimetry were also consistent with that previously reported for these materials, with major decompositions initiated over 200 °C. The first of these decompositions corresponds to thermal breakdown of S–S bonds and the second major mass loss above 300 °C corresponds to the decomposition of the remaining canola oil domain of the polymer (S7†). SEM analysis of the polysulfides indicated a smooth polymer surface embedded with high-sulfur micron scale particles (S8–S10†).^{14,38}

With the polymer in hand, we then tested its ability to bind to and remove Fe^{3+} from water. An aqueous solution of FeCl_3 was prepared at a concentration of 50 mg L^{-1} and then equilibrated for 48 hours. The resulting solution (pH 3.0) could be monitored by its absorbance at 306 nm. At this composition, the Fe^{3+} is fully soluble so that any reduction in iron content over time could be attributed to binding to the polymer, rather than precipitation. Accordingly, 2.0 g of the polysulfide was added to a 20 mL sample of the Fe^{3+} solution to benchmark iron removal

efficiency. After 24 hours of incubation with gentle agitation (end over end mixing), the absorbance of the solution at 310 nm was measured to determine the amount of Fe^{3+} captured by the polymer. The concentration of the iron was typically reduced to between 3 and 6 mg L^{-1} for all polymer samples (50, 60 and 70% sulfur, S11–S12†). Subsequent experiments were therefore restricted to the polysulfide prepared at 50% sulfur, 50% canola oil by mass. At this composition, the particles are more elastic and durable; at higher levels of sulfur the particles become more brittle.

The amount of polymer in these initial tests (2.0 g per 20 mL of water) was somewhat arbitrary, but subsequent testing revealed that this mass was indeed required to reduce the iron concentration below 10 mg L^{-1} (S13–S14†). SEM and XRD analysis of the polymer after the water treatment revealed no morphological change (S15–S16†), indicating stability of the polymer structure during the treatment. It should also be noted that relatively low levels of iron are actually bound to the polymer (less than 1 mg Fe^{3+} per 2 g of polymer in these experiments). Nevertheless, the ease at which this polymer can be prepared on relatively large scales allowed a demonstration of a 1 L scale water purification in which the iron concentration was reduced from 50 mg L^{-1} to 1.3 mg L^{-1} , as measured independently by UV-vis analysis and atomic absorption spectroscopy (Fig. 2). Furthermore, exposing the polymer to hydrogen peroxide did not reduce its ability to remove Fe^{3+} from water—an important feature that makes the material compatible with many iron removal processes that rely on the conversion of Fe^{2+} to Fe^{3+} through reaction with hydrogen peroxide (S17–S18†). This demonstration is important because the polymer was not effective in removing Fe^{2+} from water, with no significant reduction in Fe^{2+} , as indicated by AAS (S21†). Another beneficial feature of the polymer (in comparison to elemental sulfur) is that the polymer particles are not prone to caking, which makes filtration a straightforward process (S20†).

Because relatively large amounts of the polysulfide are required to remove Fe^{3+} from water, we anticipated that increasing surface area would improve its performance. Accordingly, a porous version of the polysulfide was prepared by reacting sulfur and canola oil in the presence of a large excess of a sodium chloride porogen (70% of the reaction mixture is sodium chloride). Soaking the resulting product in water

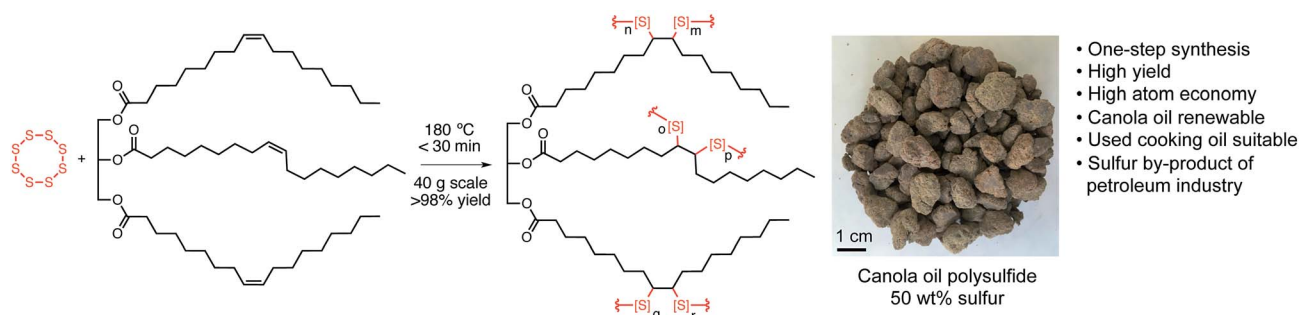


Fig. 1 A canola oil polysulfide was prepared by direct reaction of canola oil and elemental sulfur. The material was prepared with 50, 60, and 70% sulfur by mass for subsequent iron sorption studies (50% sulfur polymer shown). An approximate structure of canola oil is shown, with oleic acid as the major fatty acid in the triglyceride.



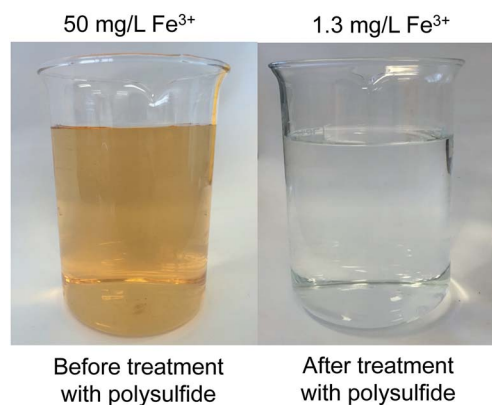


Fig. 2 A 1.0 L solution of Fe^{3+} (50 mg L^{-1}) was treated with 200 g of the non-porous canola oil polysulfide (50% sulfur) for 24 hours at 23°C . The polymer reduced the iron concentration to 1.3 mg L^{-1} , as measured independently by UV-vis spectroscopy and atomic absorption spectroscopy (AAS). After removing the polysulfide by filtration, the treated water appears colourless. See S19† for additional details.

removes the porogen, leaving micron scale pores and channels in the polysulfide material (Fig. 3a and S22†). This material was consistent in its thermal and spectroscopic properties to those previously reported when it was prepared for mercury sorption (S22–S24†).¹⁴ This material was also stable across a wide pH range at 25°C , with minimal decomposition after incubation

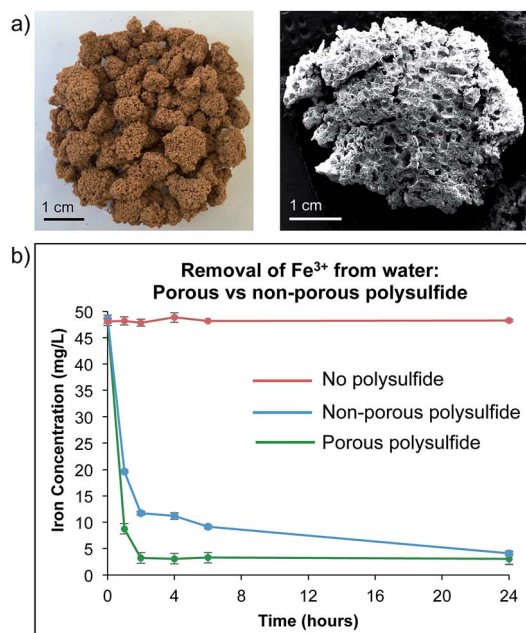


Fig. 3 A porous version of the canola oil polysulfide was prepared by reacting canola oil and sulfur in the presence of a sodium chloride porogen. Sodium chloride was removed from the polymer by washing with water, resulting in a polymer with micron-scale pores. (a) Photograph and SEM micrograph of the porous canola oil polysulfide. (b) Fe^{3+} sorption over time for the porous polysulfide (green plot) and non-porous polysulfide (blue plot). The iron concentration did not change if no polymer was added to the solution (red plot).

for 7 days in water at pH 1, 6 or 13, as indicated by visual inspection and ^1H NMR analysis (S25–S27†).

With the porous canola oil polysulfide in hand, the Fe^{3+} capture experiments were repeated and compared to the non-porous polymer. The porous polymer was superior in the rate of Fe^{3+} removal from water and less polymer was required. For example, 2.0 g of the porous polysulfide was able to reduce the Fe^{3+} concentration in a 20 mL sample from 50 mg L^{-1} to 3 mg L^{-1} in 2 hours (Fig. 3b). It was also demonstrated that only 1.0 g of the polymer was required to reduce the concentration of Fe^{3+} from 50 mg L^{-1} to 3 mg L^{-1} for 20 mL of contaminated water (S28–S30†). Fitting the sorption data to a Langmuir isotherm model indicated a sorption capacity of 0.8 mg g^{-1} (S31†). The reduction of iron concentration was also demonstrated across a pH range of 1 to 10, though precipitation also accounts for the reduction in iron concentration above pH 3.0 (S32†). Even in these cases, the polysulfide is beneficial and serves as a filtration media to prevent caking when removing precipitated iron salts by filtration. Importantly, the polysulfide's ability to remove iron from water was not impacted by the presence of other common ions such as Na^+ , K^+ , Mg^{2+} , Ca^{2+} , and Cl^- , even when all were present at 10 mg L^{-1} in the Fe^{3+} solution (S33–S34†).

If the polymer was re-used in the same iron sorption experiment, the sorption capacity dropped significantly with 95% Fe^{3+} removal on the first run and 62% and 26% on the second and third uses, respectively (S36†). This result suggests that the polymer is best deployed as a single use material in Fe^{3+} binding. Fortunately, when the polymer was prepared from waste cooking oil and sulfur (S37–S39†), it was equally as effective in removing Fe^{3+} from water (S40†). This result means that even though the polymer is best used for a single water treatment, this is a productive example of waste valorisation. We are currently investigating how the polymer-iron complex can be re-purposed yet again as an additive in construction materials and novel composites.

To deploy sulfur polymers for applications in water purification and environmental chemistry, it is useful to have methods to prepare the material rapidly and on-demand. Because sulfur-based polymers are excellent thermal insulators,²⁹ it is difficult to ensure even and reliable heating during the polymerisation. Addressing this issue, we investigated whether microwave irradiation would be practical in the synthesis of the canola oil polysulfide. Because canola oil and unsaturated triglycerides can be heated rapidly with microwave irradiation, we hypothesised that this might be a convenient strategy for heating the reaction mixture. Indeed, both laboratory microwave reactors with precise temperature and power control (S41–S42†) and conventional household microwave ovens (Fig. 4 and S43†) were highly effective for the rapid heating and subsequent co-polymerisation of canola oil and sulfur. For instance, when the polymerisation was carried out in an 1100 W household microwave oven, the polymer was formed within a mere 5 minutes. The spectroscopic, thermal and Fe^{3+} binding properties of the material synthesised in the microwave reactor were no different from the material prepared through the slower conventional heating (S43–S47†). The ability to



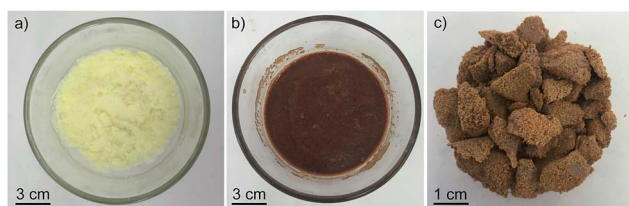


Fig. 4 (a) Reaction mixture to form a porous polysulfide: canola oil (15.0 g), sulfur (15.0 g), and sodium chloride (70.0 g). (b) Product of polymerisation after irradiation in a household microwave (1100 W) for 5 minutes. (c) Porous polysulfide obtained after removing the sodium chloride porogen with a water wash.

prepare these polymers in a conventional microwave may be important in scaling up the synthesis of these polymers because several batches could be prepared in rapid succession or through the use of several inexpensive microwave reactors operating in parallel. This process might also make the polysulfide accessible in areas with limited resources—an important consideration when the polymers will be used to remove heavy metals from water.¹⁴

In summary, a polysulfide material made from canola oil and sulfur was used to remove Fe^{3+} from water. The iron removal was tested at industrially relevant concentrations and purified to levels within the limits of environmental regulatory agencies. A rapid and scalable synthesis of the polysulfide was also executed in a microwave reactor—an important milestone in the synthesis of high-sulfur polymers because of the challenge in reliably and evenly heating these thermally insulating materials. More generally, because the featured polymer can be made entirely from industrial waste, this study is an advance in sustainable chemistry, waste valorisation, and environmental chemistry.

Conflicts of interest

Two authors (M. J. H. W. and J. M. C.) are inventors on a patent associated with the synthesis and applications of the canola oil polysulfide material (Patent No. WO 2017181217).

Acknowledgements

This research was supported financially by Flinders University and the Australian Government National Environmental Science Programme Emerging Priorities Funding. J. M. C. also acknowledges support from the Australian Research Council Discovery Early Career Research Award (DE150101863). We acknowledge the use of the South Australian node of the Australian Microscopy & Microanalysis Research Facility (AMMRF) and Australian National Fabrication Facility (ANFF) at Flinders University. Renata Kucera, Shaun Johns and Melani Dona are thanked for contributing to preliminary experiments. Michael Perkins, Jason Gascooke, David Lewis and Jonathan Campbell are acknowledged for helpful discussions and technical assistance. We thank J. Timothy Jensen of the

Metropolitan Washington Area Transit Authority for insight regarding the treatment and discharge of water contaminated with iron.

Notes and references

- S. Chaturvedi and P. N. Dave, *Desalination*, 2012, **303**, 1–11.
- T. D. Prasad and E. Danso-Amoako, *Procedia Eng.*, 2014, **70**, 1353–1361.
- H. Armand, I. I. Stoianov and N. J. D. Graham, *Urban Water J.*, 2017, **14**, 263–277.
- D. R. Cullimore and A. E. McCann, *The Identification, Cultivation and Control of Iron Bacteria in Ground Water*, Aquatic Microbiology Academic Press, 1978.
- E. I. Ohimain, T. C. N. Angaye and I. R. Inyang, *Am. J. Environ. Prot.*, 2014, **3**, 59–63.
- S. Abdullah, M. Javed and A. Javid, *Int. J. Agric. Biol.*, 2007, **9**, 333–337.
- United States Environmental Protection Agency, Drinking Water Regulations and Contaminants, accessed 26 Oct 2017 from <https://www.epa.gov/dwregdev/drinking-water-regulations-and-contaminants>.
- National Pollutant Discharge Elimination System (NPDES), United States Environmental Protection Agency, accessed 26 Oct 2017 from <https://www.epa.gov/npdes/industrial-wastewater>.
- K. Vaaramaa and J. Lehto, *Desalination*, 2003, **155**, 157–170.
- D. Ellis, C. Bouchard and G. Lantagne, *Desalination*, 2000, **130**, 255–264.
- R. Munter, H. Ojaste and J. Sutt, *J. Environ. Eng.*, 2005, **131**, 1014–1020.
- E. Okoniewska, J. Lach, M. Kacprzak and E. Neczaj, *Desalination*, 2007, **206**, 251–258.
- M. P. Crockett, A. M. Evans, M. J. H. Worthington, I. S. Albuquerque, A. D. Slattery, C. T. Gibson, J. A. Campbell, D. A. Lewis, G. J. L. Bernardes and J. M. Chalker, *Angew. Chem., Int. Ed.*, 2016, **55**, 1714–1718.
- M. J. H. Worthington, R. L. Kucera, I. S. Albuquerque, C. T. Gibson, A. Sibley, A. D. Slattery, J. A. Campbell, S. F. K. Alboaiji, K. A. Muller, J. Young, N. Adamson, J. R. Gascooke, D. Jampaiah, Y. M. Sabri, S. K. Bhargava, S. J. Ippolito, D. A. Lewis, J. S. Quinton, A. V. Ellis, A. Johs, G. J. L. Bernardes and J. M. Chalker, *Chem.–Eur. J.*, 2017, **23**, 16219–16230.
- M. J. H. Worthington, R. L. Kucera and J. M. Chalker, *Green Chem.*, 2017, **19**, 2748–2761.
- W. J. Chung, J. J. Griebel, E. T. Kim, H. Yoon, A. G. Simmonds, H. J. Ji, P. T. Dirlam, R. S. Glass, J. J. Wie, N. A. Nguyen, B. W. Guralnick, J. Park, Á. Somogyi, P. Theato, M. E. Mackay, Y.-E. Sung, K. Char and J. Pyun, *Nat. Chem.*, 2013, **5**, 518–524.
- J. Lim, J. Pyun and K. Char, *Angew. Chem., Int. Ed.*, 2015, **54**, 3249–3258.
- A. Hoefling and P. Theato, *Nachr. Chem.*, 2016, **64**, 9–12.
- J. J. Griebel, R. S. Glass, K. Char and J. Pyun, *Prog. Polym. Sci.*, 2016, **58**, 90–125.



- 20 D. A. Boyd, *Angew. Chem., Int. Ed.*, 2016, **55**, 15486–15502.
- 21 G. Kutney, *Sulfur: History, Technology, Applications & Industry*, ChemTec Publishing, Toronto, 2nd edn, 2013.
- 22 *Mineral Commodity Summaries*, United States Department of the Interior, United States Geological Survey, Sally Jewell (Secretary, U.S. Department of the Interior) and Suzette M. Kimball (Director, U.S. Geological Survey), 2016, pp. 165–166.
- 23 P. Liu, J. M. Gardner and L. Kloo, *Chem. Commun.*, 2015, **51**, 14660–14662.
- 24 S. Zhuo, Y. Huang, C. Liu, H. Wang and B. Zhang, *Chem. Commun.*, 2014, **50**, 11208–11210.
- 25 J. J. Griebel, S. Namnabat, E. T. Kim, R. Himmelhuber, D. H. Moronta, W. J. Chung, A. G. Simmonds, K.-J. Kim, J. van der Laan, N. A. Nguyen, E. L. Dereniak, M. E. Mackay, K. Char, R. S. Glass, R. A. Norwood and J. Pyun, *Adv. Mater.*, 2014, **26**, 3014–3018.
- 26 J. J. Griebel, N. A. Nguyen, S. Namnabat, L. E. Anderson, R. S. Glass, R. A. Norwood, M. E. Mackay, K. Char and J. Pyun, *ACS Macro Lett.*, 2015, **4**, 862–866.
- 27 T. S. Kleine, N. A. Nguyen, L. E. Anderson, S. Namnabat, E. A. LaVilla, S. A. Showghi, P. T. Dirlam, C. B. Arrington, M. S. Manchester, J. Schwiegerling, R. S. Glass, K. Char, R. A. Norwood, M. E. Mackay and J. Pyun, *ACS Macro Lett.*, 2016, **5**, 1152–1156.
- 28 J. J. Griebel, N. A. Nguyen, A. V. Astashkin, R. S. Glass, M. E. MacKay, K. Char and J. Pyun, *ACS Macro Lett.*, 2014, **3**, 1258–1261.
- 29 A. M. Abraham, S. V. Kumar and S. M. Alhassan, *Chem. Eng. J.*, 2018, **332**, 1–7.
- 30 J.-S. M. Lee, D. J. Parker, A. I. Cooper and T. Hasell, *J. Mater. Chem. A*, 2017, **5**, 18603–18609.
- 31 T. Hasell, D. J. Parker, H. A. Jones, T. McAllister and S. M. Howdle, *Chem. Commun.*, 2016, **52**, 5383–5386.
- 32 M. W. Thielke, L. A. Bultema, D. D. Brauer, B. Richter, M. Fischer and P. Theato, *Polymers*, 2016, **8**, 266.
- 33 D. J. Parker, H. A. Jones, S. Petcher, L. Cervini, J. M. Griffin, R. Akhtar and T. Hasell, *J. Mater. Chem. A*, 2017, **5**, 11682–11692.
- 34 M. G. Kulkarni and A. K. Dalai, *Ind. Eng. Chem. Res.*, 2006, **45**, 2901–2913.
- 35 M. A. R. Meier, J. O. Metzger and U. S. Schubert, *Chem. Soc. Rev.*, 2007, **36**, 1788–1802.
- 36 L. Lin, H. Allemekinders, A. Dansby, L. Campbell, S. Durance-Tod, A. Berger and P. J. H. Jones, *Nutr. Rev.*, 2013, **71**, 370–385.
- 37 *Rubber Basics*, ed. R. B. Simpson, Rapra Technology Ltd., Shawbury, UK, 2002, pp. 19–133.
- 38 A. Hoefling, Y. J. Lee and P. Theato, *Macromol. Chem. Phys.*, 2017, **218**, 1600303.



3.0 Powdered activated carbon / 50-Poly(*S-r*-canola) blend

3.1 Acknowledgements

Alfreds Tikoalu for assistance with origin pro software. Salah Alboaji for running the 50-poly(*S-r*-canola) PFOA initial test and the Hemi-micelles analysis under SEM. Kymberley R. Scroggie for running the ¹⁹F NMR analysis. Justin Chalker for guidance and help with experimental design.

3.2 Abstract

Whilst powdered activated carbon (PAC) is efficient at removing many contaminants from solution, it is known to cake and block filters and membranes, making its direct use in both batch and continuous water treatment processes impractical. PAC is also known to generate hazardous dust plumes which are flammable and a respiration hazard making it dangerous to work with. In this chapter, the 50-poly(*S-r*-canola) polymer was demonstrated to act as an efficient support material for PAC immobilising it on the polymer's surface. This immobilisation prevented the generation of the hazardous dust plumes increasing the safety profile for both the storage and use of the PAC. The 50-poly(*S-r*-canola) support material also acted as a hydraulic lubricant facilitating both batch and continuous flow treatment processes without blocking filters or membranes. This sorbent material was demonstrated to be effective for the remediation of persistent micropollutants perfluorooctanoic acid (PFOA) and perfluorooctanesulfonic acid (PFOS). As well as acting as a hydraulic lubricant and immobilization agent for PAC, the 50-poly(*S-r*-canola) also aided in the removal of PFOA. The use of this novel blend to simplify and improve the remediation of PFAS compounds from water is an important advancement in the field of environmental remediation. The first direct proof of the self-assembly of PFOA hemi-micelles on a sorbent surface was demonstrated by SEM imaging. The stabilisation of PAC using its electrostatic attraction towards a support polymer is also a novel concept in the field of environmental sorbent technologies.

3.3 Introduction

3.3.1 50-poly(S-*r*-canola) as an activated carbon support polymer

High sulfur content polymers prepared using inverse vulcanisation have found use directly as sorbent materials for both heavy metal and oil pollution.^{7, 98-103} These are examples of the direct use of sulfur polymers as sorbent materials for environmental remediation; however, they could also potentially be combined with other techniques or sorbent materials to help aid in the remediation efforts of pollutants which have minimal affinity with sulfur polymers. An example of this was demonstrated in chapter 2. The 50-poly(S-*r*-canola) sorbent was not capable of binding with Fe(II) in solution however it was capable of binding with Fe(III). By treating the Fe(II) solution with both the 50-poly(S-*r*-canola) sorbent and H₂O₂ (to oxidise the Fe(II) into Fe(III)) resulted in removal of the Fe(II) pollution from solution. Therefore, by coupling our sorbent method with other techniques, pollutants which weren't previously able to be removed could now be removed from solution. Powdered activated carbon (PAC) is a high-performance sorbent material that typically uses a polymer support for it to be used safely and effectively in large scale water treatment applications. This study will investigate the use of 50-poly(S-*r*-canola) polymer as the support polymer for PAC. Whilst the substantially higher surface area of PAC results in fast removal rates and high sorption capacity, the difficulties associated with its use limit its practical application. The fine PAC particles are known to block filters and membranes making its use in large scale treatment processes impractical. PAC is also known to generate flammable dust plumes during handling making it dangerous to store or handle in large quantities.

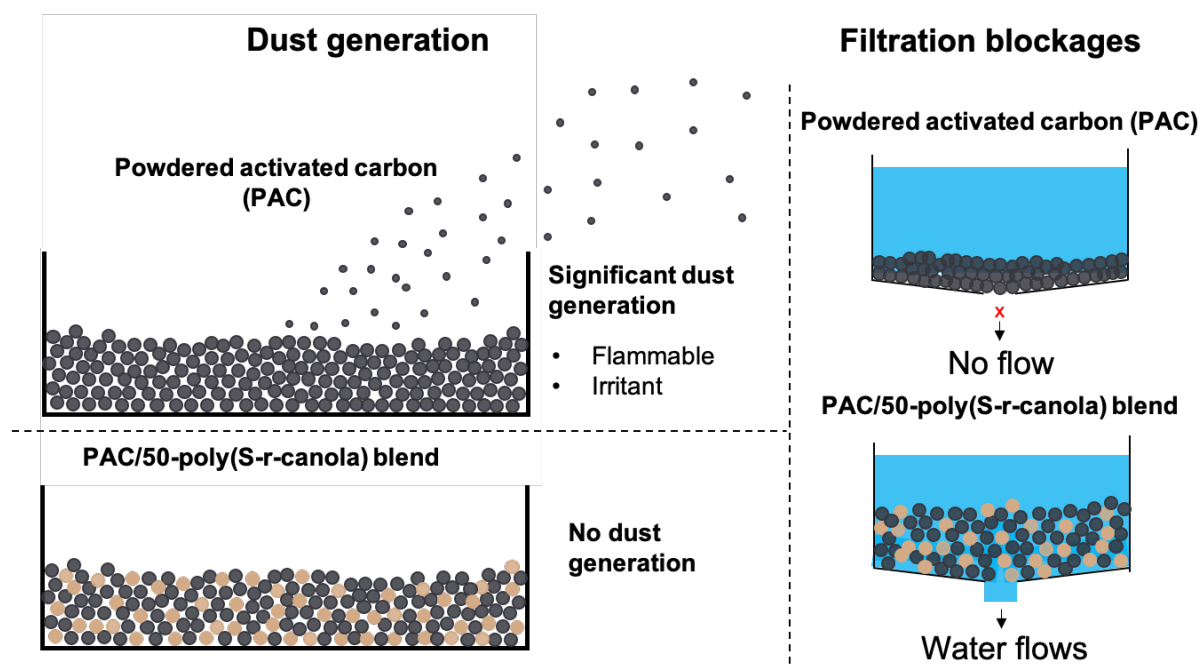


Figure 57 – Image displaying issues associated with PAC and how stabilization with the 50-poly(S-r-canola) polymer results in their elimination.

Although by using the granular form of activated carbon (GAC) these issues are reduced substantially at the beginning, GAC breaks apart under high pressure or flow rate resulting in the formation of fine carbon particles.²²⁴ GAC also has substantially less surface area than PAC resulting in slower removal rates and lower sorption capacities. Therefore, to resolve these issues activated carbon sorbents are typically combined with a polymeric support material. The benefits of stabilisation of PAC using 50-poly(S-r-canola) polymer are shown in Figure 57 above.

3.3.2 PFAS pollution

Perfluoroalkyl substances (PFAS), especially perfluorooctanoic acid (PFOA) and perfluorooctanesulfonic acid (PFOS), have been widely used in protective coatings, lubricants, high-performance fire-fighting foams and in the production of various fluoropolymers such as Teflon. They are typically released into the environment through their use in these applications and through the disposal of PFAS containing products.²²⁵ This results in the contamination of local soil and water sources that are in close proximity to the sources. As a result of the high bond strength of the carbon fluorine bonds in PFAS compounds (130 kcal/mol²²⁶), they are persistent chemicals that do not degrade under environmental conditions.^{227, 228} PFAS compounds have a long biological half-life (~ 4.4 years) suggesting bio-accumulation could occur.²²⁹ This hypothesis was proven when studies found these compounds in the livers,

bladders and blood of humans, fish, birds, and marine mammals around the globe with higher concentrations being found in the species higher in the food chain.²²⁸ It is hypothesised that these properties would result in the transport of PFAS pollution significant distances from its original source location. This hypothesis was supported by surveys into PFAS contamination around the world highlighting the global spread of these pollutants with it appearing in regions where PFAS has not been historically used.²³⁰ This warranted further study into the effects these compounds have on human health and the environment. It was initially believed that PFAS chemicals were inert and low in toxicity, however further studies revealed immunotoxicity and carcinogenicity effects are significantly relevant risks at the exposure levels observed in our environment.²³¹ A lot of the risk evaluations for PFAS assumed that untested effects do not require regulation, resulting in its widespread use and distribution throughout the environment.²³¹ Studies investigating the health effects of PFAS exposure have revealed a statistically significant greater prevalence of angina, myocardial infarction, stroke, chronic bronchitis, shortness of breath on stairs, asthma and other serious health problems for those exposed to these compounds.²²⁹ These studies hypothesised that the conditions were a result of PFOA exposure however it was not directly proven meaning further investigation was needed.²²⁹ Studies on animals found that PFOA was toxic to both rats and rabbits,²²⁸ and further studies have revealed links between PFOA exposure and a variety of human health issues including hepatic²³² and renal²³³ toxicity, thyroid disease^{234, 235} and kidney and testicular cancers.^{233, 236, 237} PFOA has been classified by the United States Environmental Protection Agency (USEPA) as a potential carcinogen.²²⁷ Between 2002 and 2015 all PFAS chemicals were voluntarily phased out of production in the USA and in 2009, both PFOA and PFOS were categorized as persistent organic pollutants.²²⁵ The EPA is still concerned that exposure could still occur from the limited uses of existing PFAS chemical stocks and the importation of polluted goods from countries which still use these substances.²²⁵ Industries still currently using PFAS compounds include fluoropolymer production, the semiconductor industry and chrome plating, mostly based in china.²³⁸ Due to the global spread of PFAS pollution, its environmental persistence, bio-accumulation and potential toxicity, government bodies and environmental protection groups have set regulation limits for PFAS in drinking water. In 2016 the EPA lowered the non-cancer reference dose of both PFOA and PFOS to 20 ng/kg/day with combined drinking water limits of 70 ng/L.²²⁵ This limit was established based on toxicology studies on mice.²²⁵

3.3.2 PFAS remediation

The introduction of these regulation limits created a new challenge for industry and government alike. New methods and materials are needed for efficient removal of these compounds from drinking water to be achieved. Several strategies have been investigated for the removal of PFAS compounds from water. Various methods including microbial reductive dehalogenation and zero valent iron have been previously investigated for PFAS removal by degradation.²³⁸ Whilst these methods show promise in PFAS compound decomposition, they failed to remove the shorter chain PFAS compounds from solution.²³⁹ These methods also showed varying efficiencies for differing PFAS compounds with one study showing significant degradation of PFOA but no degradation of PFOS.²⁴⁰ This demonstrated how different PFAS compounds aren't equally removed using these methods and methods capable of removing a wider range of PFAS compounds must be investigated. The most common strategy successfully implemented to remove both PFOA and PFOS from water on a large scale was adsorption.^{238, 241-243} A number of sorbent materials have previously been investigated including activated carbon, alumina, chitosan²⁴⁴, resin, hydrotalcite²⁴³ and organo-montmorillonite.²³⁸ These sorbent materials have proven useful on laboratory scale but each suffer from issues such as high costs, inability to regenerate and the production of waste eluents on larger scales.²⁴⁵ It is also important that these sorbents have end-of-life recycling strategies to minimize contaminated waste production. It is therefore important for new high performance PFAS sorbent materials to be investigated. This study will demonstrate the use of PAC stabilized with 50-poly(*S-r*-canola) polymer as an advanced PFAS sorption material.

3.4 Experimental

3.4.1 General considerations

3.4.1.1 SEM and EDS

Scanning Electron Microscopy (SEM) R were obtained using an FEI F50 Inspect system, while corresponding EDS spectra were obtained using an EDAX Octane Pro detector.

3.4.1.2 ¹⁹F NMR Spectroscopy

¹⁹F NMR spectra were recorded using a Bruker Ultrashield 600. Deuterium oxide (D₂O/H₂O, 1:9) was used as the solvent and for internal locking. All chemical shifts (δ scale) were

measured in parts per million (ppm) and referenced to the internal standard trifluoroacetic acid ($\delta = -76.55$ ppm).

3.4.1.3 PFAS analysis

Certified PFOA and PFOS analysis was carried out by Envirolab Services Pty Ltd, with accreditation by the National Association of Testing Authorities, Australia (NATA Accreditation Number 2901). The test method was based on EPA/600/R-08/092 Method 537: Determination of Selected Perfluorinated Alkyl Acids In Drinking Water By Solid Phase Extraction and Liquid Chromatography/Tandem Mass Spectrometry (LC/MS/MS). Version 1.1, September 2009.

3.4.2 Material synthesis and characterization

3.4.2.1 50-poly(S-*r*-canola) large-scale synthesis (900.0 gram scale)

Canola oil (450 g) was added to a stainless-steel reaction vessel (4.7 L, 20 cm diameter) that was placed on a hotplate. An overhead stirrer with a stainless-steel impellor, used to stir the reaction mixture, was set to 90 rpm. The hotplate was turned on and the oil was heated to 170 °C. The temperature of the reaction mixture was monitored directly with an internal thermostat probe. Sulfur was then added (450 g) through a funnel over 5-10 minutes ensuring the temperature never dropped below 155 °C. At this point two transparent liquid phases were visible. Over a period of 5-10 minutes the 2 separate layers combine forming an opaque mixture. Then, the thermostat setting for the reaction temperature was increased to 180 °C and the sodium chloride porogen (2100 g, finely ground in a blender) was added through the funnel over approximately 15-20 minutes. Once again, the rate of addition was such that the temperature of the reaction never dropped below 155 °C. At this point the mixture was an orange, opaque, and relatively free flowing liquid. After approximately 10-15 minutes of continuous heating the mixture turns from orange to brown. At this point the viscosity increased with cross-linking. Once the overhead stirrer registered a torque of approximately 40 N•cm, the reaction was stopped. The reaction vessel was removed from the heat plate and placed on a trivet to prevent the flask heating up any further. Due to the potential for H₂S release, this reaction must be carried out inside a fume hood. The polymer was removed from the vessel using a metal spatula and processed using a mechanical grinder to provide particles between 0.5 and 3.0 mm in size. Finally, this polymer was washed with 17 L of water in a 20 L bucket whilst stirring the mixture using the overhead stirrer (200 rpm, 30 min). Finally, the polymer was isolated by filtration through a sieve (0.5 mm cut-off). These washing steps were repeated

three times to ensure that the final product had as much salt as possible removed. The polymer was then dried by passing warm air through the material (5-24 hours, 18 - 42 °C) using a space heater, with further drying in the fume hood until the mass of the material was constant.

3.4.2.2 Preparation of 1.0 kg of a carbon-polysulfide blend (20:80 wt% ratio)

800.0 grams of porous polysulfide was added to a 2.5 L plastic container. Next, 200.0 grams of activated carbon powder (PGW 150 MP, Kuraray) was added. The container's lid was closed, and the container was inverted 20 times to ensure the carbon and polymer mixed sufficiently to create a homogenous blend. The carbon bound to the 50-poly(*S-r*-canola), leaving minimal free-flowing powdered carbon. This blend was then used for subsequent PFOA experiments.

3.4.2.3 Analysis of dust generation for PAC and the carbon-polysulfide blend

A Sensidyne nephelometer was used to quantify dust generated from pouring a 100 mL volume of PAC (Kuraray, PGW 150 MP, 100-200 mesh) or the carbon-polymer blend. This nephelometer uses light scattering to detect airborne particles. Because carbon dust particles are dark, the coal fly ash *k*-factor was used in all experiments. The inlet flow was 1 L/min and total suspended particles were measured. First, a 100 mL dry volume of the carbon-polysulfide blend or the PAC was placed in a plastic scoop and held at a height of 20 cm. The sorbent was then poured in one portion into a cylindrical plastic container (12 cm diameter, 10 cm height). The nephelometer was operated in continuous mode, starting at the same time the PAC or PAC-polysulfide blend was poured. The nephelometer was positioned 50 cm from the center of the container, with the iso-kinetic inlet at a 20 cm height. Measurements of the concentration of airborne particles ($\mu\text{g}/\text{m}^3$) were recorded every second for 2.5 minutes. Background dust (no sorbent poured) was also measured for reference. Each experiment was done in triplicate. The dust generated by the PAC was very high (average maximum $>11,000 \mu\text{g}/\text{m}^3$). The carbon-polysulfide blend (average dust maximum of $159 \pm 21 \mu\text{g}/\text{m}^3$) was no different than background dust at this location (average dust maximum of $161 \pm 16 \mu\text{g}/\text{m}^3$). The average dust concentration over time (average of 3 runs) for both the background and the carbon-polymer blend were plotted separately for clarity.

3.4.2.4 Determination of zero-point charge for powdered activated carbon

50 mL of an aqueous solution of NaCl (0.1 M) was added to each of nine 50 mL centrifuge tubes. The pH of each of these tubes was adjusted by the addition of either a 0.01 M HCl or 0.01 M NaOH solution using a pH meter so that there were two tubes with solutions of pH 2, 3, 4, 5, 6, 7, 8, 9, and 10. Next, 0.15 grams of activated carbon was added into 9 tubes at each

pH. All of the tubes were placed on a rotary mixer and rotated at 25 rpm and 25 °C for 48 hours. After this time, the pH of each solution was measured using the pH meter. The pH point where the $\text{pH}_{\text{initial}} = \text{pH}_{\text{final}}$ was estimated by the point of intersection of the line $y = x$ and a plot of Final vs Initial pH.

3.4.3 PFOA batch sorption studies

3.4.3.1 PFOA sorption using the porous 50-poly(S-*r*-canola)

A PFOA solution (5 mL, 2 mg/mL PFOA in deionized H₂O) was added to a glass vial containing the porous 50-poly(S-*r*-canola) polymer (2.0 g) and incubated without mixing at room temperature. At 5, 10, 60, 120 and 240 minutes, a 600 μL aliquot of the water was sampled and analysed by ¹⁹F NMR spectroscopy. The NMR sample was prepared by adding 60 μL of D₂O spiked with TFA (5.4 mg/ml) to the 600 μL sample of water. The amount of remaining PFOA in the aqueous solution was determined by the relative integration of the CF₃ signals, at δ -76.55 ppm for TFA and at δ -81.85 ppm for PFOA. After 5 minutes, 30% of the PFOA was removed from solution. After 4 hours, 47% of the PFOA was removed from solution.

3.4.3.2 SEM micrographs of PFOA hemi-micelles bound to the 50-poly(S-*r*-canola)

The porous 50-poly(S-*r*-canola) (2.0 grams) was added to a 20 mL glass vial with 5 mL of a (2 mg/mL) PFOA solution. This solution was incubated for 24 hours, after which time the polymer was isolated by filtration and dried in open air. Before SEM analysis, the polymer was coated with a 5 nm platinum coating.

3.4.3.3 PFOA sorption: comparing blend with PAC and GAC

5.0 grams of the PAC/50-poly(S-*r*-canola) blend was added to a 200 mL plastic container along with 100 mL of a PFOA solution (5 ppm PFOA in deionised water). In three separate 200 mL plastic containers, 4.0 grams of 50-poly(S-*r*-canola) polymer, 1.0 gram of powdered activated carbon (Kuraray, PGW 150 MP), or 1.0 gram of granular activated carbon (GC 1200, 0.5- 0.7 mm, Activated Carbon Technologies) were added along with 100 mL of the PFOA solution (5 ppm PFOA in water). The solutions were stirred for 1 hour (250 rpm, 32 × 12 mm stirring bar) and then filtered through a simplepure 0.22 μm PES syringe filter into separate plastic container for further analysis. Each experiment was repeated three times. The PFOA concentrations were determined by Liquid Chromatography Tandem Mass Spectrometry (LC/MS/MS) (negative mode, ESI, see general considerations on page S2). Note: For the polymer control and the blend

treatment only one filter was required. For the activated carbon control, 5 filters were required as they were rapidly blocked with the powdered activated carbon. For the granular carbon control, 4 filters were required as they were also blocked.

3.4.3.4 Comparing filtration ability of the blend, PAC and GAC

100 mL of water was treated with 5.0 grams of the carbon-polymer blend and stirred for 1 hour. After this time, the mixture was transferred repeatedly to a 10 mL syringe and passed through a Simplepure 0.22 μm PES filter at a flow rate of 33 mL/min until all 100 mL was filtered. This process was repeated using 1.0 gram of activated carbon (Kuraray, PGW 150 MP) and again with 1.0 gram of granular activated carbon (GC 1200, 0.5-0.7 mm, Activated Carbon Technologies). The filter was replaced when blocked and the process repeated until all water was filtered. The powdered activated carbon blocked the filter within 28 ± 5 seconds of flow and five filters in total were required to filter all 100 mL of water. The granular activated carbon blocked the filter within 35 ± 3 seconds and a total of four filters were required to process all 100 mL of water. The carbon-polymer blend did not block the filter during the processing of the 100 mL of water.

3.4.3.5 Kinetic study of PFOA sorption using PAC/50-poly(S-*r*-canola) blend

5.0 grams of the carbon-polysulfide blend and 1.0 gram of granular activated carbon (GC 1200, 0.5-0.7 mm, Activated Carbon Technologies) were added into separate 200 mL plastic containers along with 100 mL of a PFOA solution (5000 ppb PFOA in deionised water). The mixture was stirred (250 rpm, 32×12 mm stirring bar) and after 5, 20 and 40 minutes, small aliquots (1 mL) were removed and filtered through a Simplepure 0.22 μm PES syringe filter into separate plastic containers for further analysis. Every sample was prepared in triplicate. The PFOA concentrations were determined by Liquid Chromatography Tandem Mass Spectrometry (LC/MS/MS) (negative mode, ESI, EPA/600/R-08/092 Method 537).

3.4.3.6 Sorption isotherm for PAC/50-poly(S-*r*-canola) blend

Starting from stock solutions of 5000 ppb PFOA, serial dilutions were performed to prepare solutions with concentrations of 5000, 2500, 1000, 500 and 250 ppb. To 15 separate 200 mL containers, 500 mg of the carbon-polymer blend was added (100 mg PAC in blend). To three of these containers 100 mL of 5000 ppb PFOA solution were added along with a 3.2×1.5 cm stir bar and the containers were placed on a stir plate at 100 rpm for 24 hours at 20 °C. The same was done for each of the other concentrations (2500, 1000, 500 and 250 ppb PFOA). After equilibration, 3.0 mL of solution was removed from each container and centrifuged for

2 minutes. The supernatant was then analysed and the PFOA concentrations were determined by Liquid Chromatography Tandem Mass Spectrometry (LC/MS/MS) as described on page S2 (negative mode, ESI, EPA/600/R-08/092 Method 537).

3.4.4 PFOA continuous sorption studies

3.4.4.1 Removal of PFOA from water using a continuous process

A 30 × 1.5 cm glass column was packed with 40.0 grams of the carbon-polymer blend. 100 mL of PFOA solution (5 ppm in deionized water) was added into the top of the column through a funnel and a beaker was used to collect the solution as it exited through the column after gravity elution. This experiment was carried out twice, with the total run times of 20 minutes and 90 minutes, with the flow rate controlled by the column tap. The PFOA concentrations were determined by Liquid Chromatography Tandem Mass Spectrometry (LC/MS/MS) (negative mode, ESI).

3.4.4.2 Removal of suspended solids using 50-poly(*S-r*-canola) polymer

The 50-poly(*S-r*-canola) (20 g) was loaded into a glass column (2 × 30 cm). The contaminated surface water (300 mL) was passed through the column over the course of 1 minute, using gravity elution. The flowthrough was collected, and the total suspended solids were measured by a certified commercial service (Envirolab).

3.4.4.3 Removal of suspended solids using 50-poly(*S-r*-canola) D600 light scattering experiment

5 g of 50-poly(*S-r*-canola) polymer was placed in a 10 mL syringe barrel and then 10 mL of the contaminated surface water was passed through the polymer filled syringe over 30 seconds. This experiment was carried out in triplicate. The optical density of the flowthrough was measured at 600 nm using a spectrophotometer.

3.4.4.4 Removal of PFOS from contaminated surface water using a polymer-carbon blend

A 45 cm vertical glass column (5 cm diameter) was plugged with a cotton ball at the outlet on top of which were added 15.0 g sand (white quartz, 50-70 mesh) and then 40.0 grams of the carbon-polymer blend (80% polymer and 20% PAC). The top of the carbon-polymer blend was topped with an additional 15.0 g of sand to prevent disturbing the sorbent when the water was added. A 1.0 L reservoir was attached to the top of the column and 1.0 L batches of the contaminated surface water were passed through the column over an average period of 5

minutes. The flow rate was maintained using a hand-pressurised bellow. The process was repeated for a total of 10.0 L of the contaminated surface water. All 10.0 L were collected in a high-density polypropylene container. This experiment was repeated in triplicate. The PFOS content of the 10.0 L samples of treated water were measured by a certified commercial service (EPA/600/R-08/092 Method 537).

3.5 Results and discussion

3.5.1 Synthesis and characterization of PAC / 50-poly(S-*r*-canola) blend sorbent

In order for a sorbent to be feasible for large scale treatment processes it must be able to be prepared on a large scale. Using a method previously established⁷, the porous 50-poly(S-*r*-canola) polymer was prepared on a 900 gram scale (450 g S₈, 450 g Canola Oil, 2100 g NaCl).

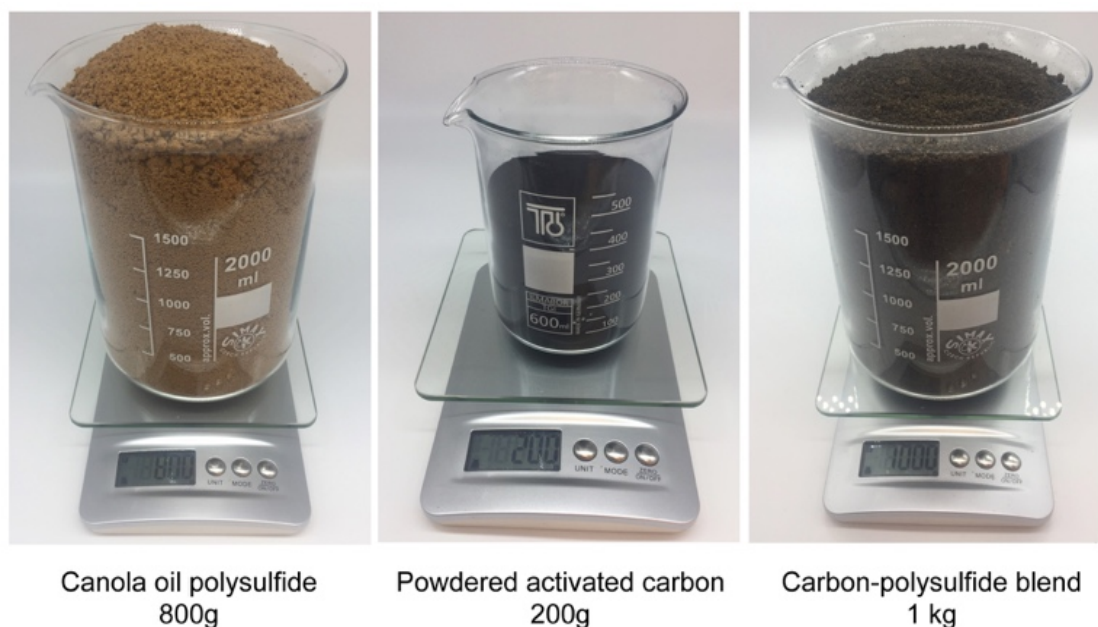


Figure 58 – From left to right: Porous 50-poly(S-*r*-canola) polymer (800 g), powdered activated carbon powder (PGW 150 MP, 200 g) and the PAC/50-poly(S-*r*-canola) blend (1.0 kg) that results from their mixing.

The resulting 1 kg of blend is shown in Figure 58. To characterise this material, SEM / EDX analysis was performed on the blend, the 50-poly(S-*r*-canola) support material, the PAC and the GAC. SEM analysis of the 50-poly(S-*r*-canola), shown in Figure 59, revealed it had a similar surface structure as in previous studies.⁷ Although regions of amorphous polymer and crystalline sulfur particles were both observed on the surface as expected, it seemed as if less free sulfur crystalline particles were present on the surface in comparison to the non-porous 50-poly(S-*r*-canola) polymer.

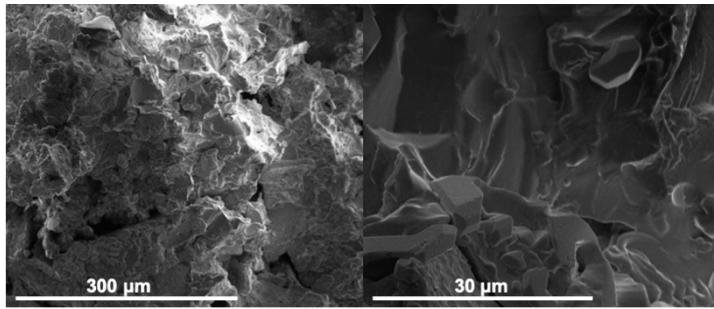


Figure 59 – SEM micrographs of 50-poly(*S-r*-canola) polymer

All activated carbon samples were observed to contain some extent of porous structure as expected. This is shown in Figure 60. It's important to note that these materials may be more porous than they appear if they contain nanoscale porosity below the working resolution of the SEM.

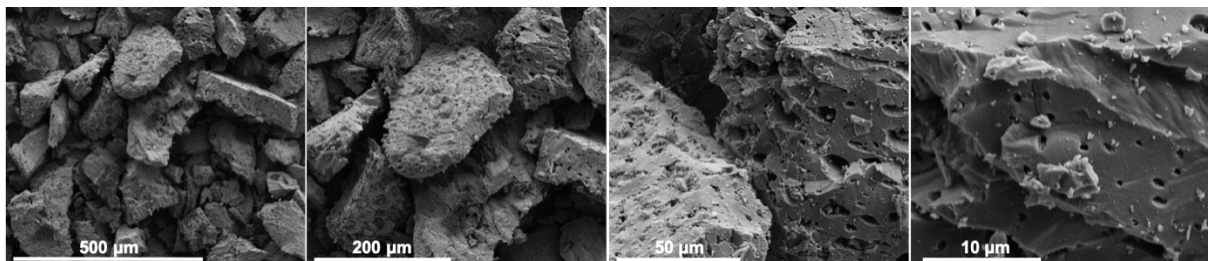


Figure 60 – SEM micrographs of powdered activated carbon (Kuraray, PGW 150 MP).

EDX mapping of the surface (Figure 61) reveals that the major elements present in this PAC where carbon (81%), sulfur (10%), oxygen (2%) and nitrogen (1%). All samples where coated in 10 nm of platinum, accounting for the 6% PtM signal observed.

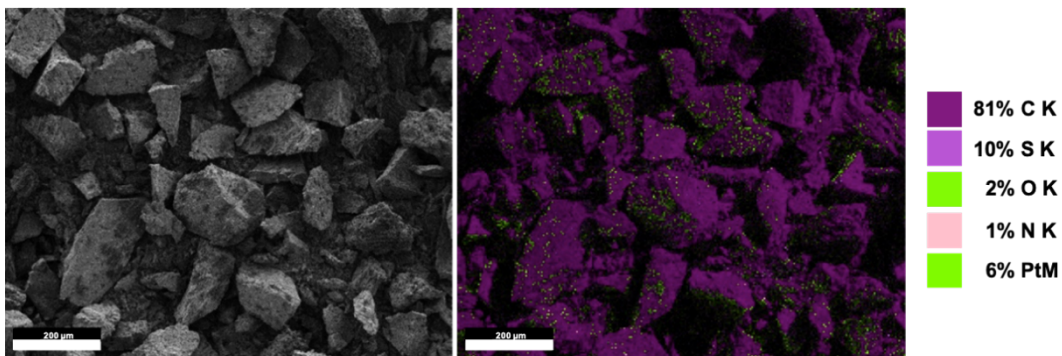


Figure 61 – EDX mapping of powdered activated carbon (Kuraray, PGW 150 MP).

The GAC particles under SEM (Figure 62) did not seem to contain any macro sized pores like the PAC did, however its surface does appear to be coated in nanostructures increasing its surface area substantially.

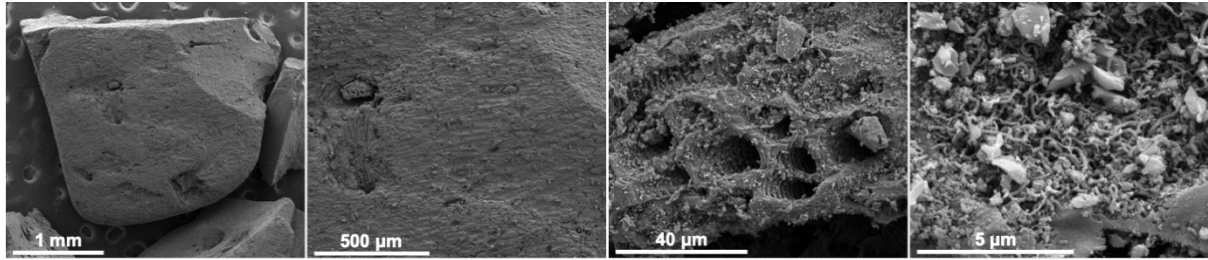


Figure 62 – SEM micrographs of granular activated carbon (GC 1200, 0.5 - 0.7 mm, Activated Carbon Technologies).

EDX analysis (Figure 63) revealed that the granular activated carbon didn't contain any sulfur and consisted of carbon (84%), oxygen (6%) and nitrogen (1%). The platinum signal (8%) was again attributed to the platinum surface coating applied to the sample before analysis.

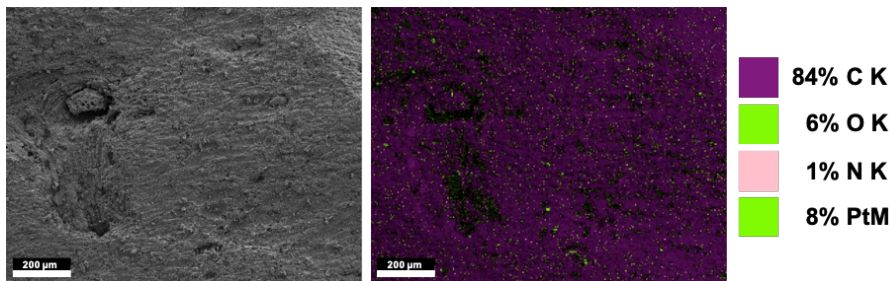


Figure 63 – EDX mapping of granular activated carbon (GC 1200, 0.5-0.7 mm, Activated Carbon Technologies).

Next SEM analysis was performed on the carbon-polymer blend (Figure 64). The surface structures previously observed for both PAC and 50-poly(*S-r*-canola), were both observed.

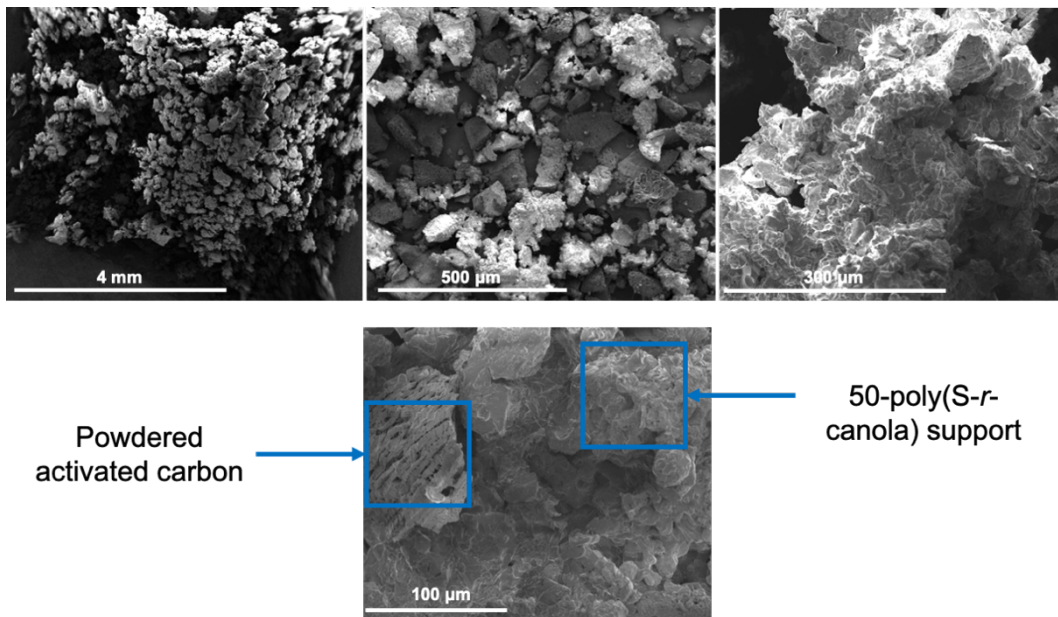


Figure 64 – SEM micrographs of carbon polymer blend (top) and SEM image with PAC and polymer support structures highlighted.

EDX analysis of the PAC revealed it contained carbon (81%), sulfur (10%), oxygen (2%) and nitrogen (1%). PAC is only present in the blend at 20% suggesting that the EDX signals should decrease upon formation of the blend. This however was not the case. EDX analysis of the blend (Figure 65) determined the percentages to be 84% carbon, 10% sulfur and 6% oxygen. This is likely due to the fact that the carbon adheres to the surface of the polymer blocking it from observation. This means that the majority of the signal picked up through EDX was from the PAC on the surface and not the 50-poly(*S-r*-canola) polymer beneath. This explains the observed difference in EDX results.

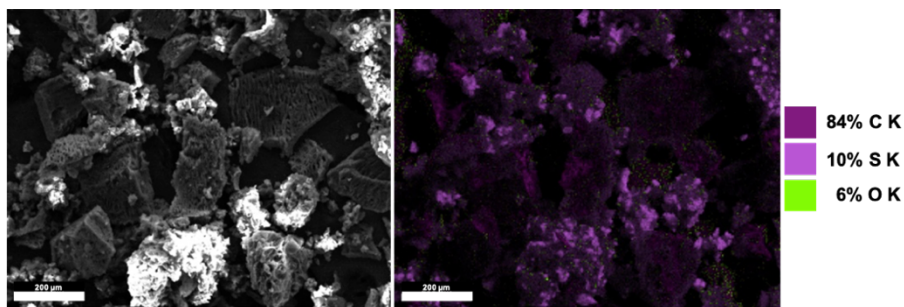


Figure 65 – EDX mapping of carbon / polymer blend (20:80 wt%).

To determine whether the PAC exhibits a surface charge, the point of zero charge was calculated. The point of zero charge (pH_{pzc}) is the pH value by which the surface charges are equal to zero. A low pH_{pzc} value indicates a negative surface charge whilst a high pH_{pzc} value indicates a positive surface charge.

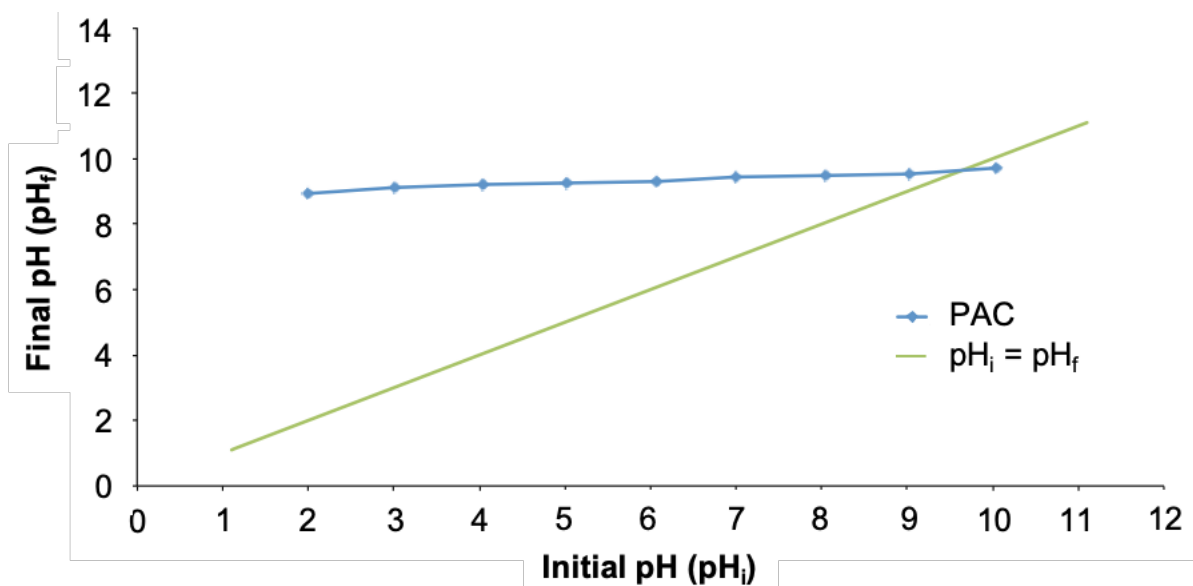


Figure 66 – Graph for point of zero charge (pH_{pzc}) experiment for powdered activated carbon (PAC).

The point of zero charge was calculated from Figure 66 to be $\text{pH}_{\text{pzc}} = 9.6$. This means that the activated carbon possesses a slightly positive surface charge. This result supports the hypothesis that the attraction between the PAC and the 50-poly(*S-r*-canola) is likely electrostatic in nature. Finally, to investigate the effect of 50-poly(*S-r*-canola) polymer stabilization on PAC dust generation, the dust generated from dropping the sample into a container from 20 cm height was measured using a nephelometer for 160 seconds. The results are plotted in Figure 67.

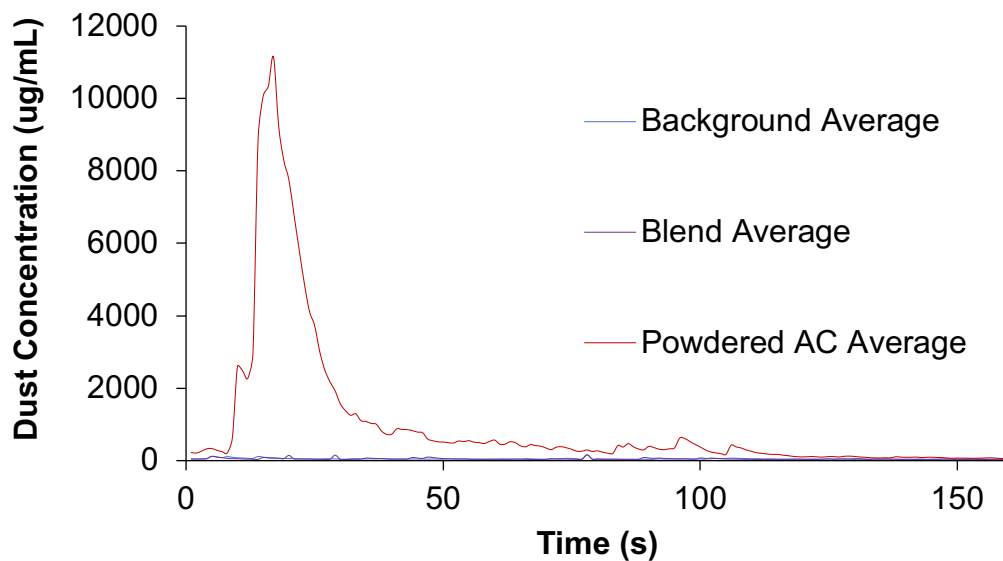


Figure 67 – Dust concentration over time recorded 50 cm away from the samples being dropped from 20 cm.

As seen above, the dust levels generated by the PAC reached 11145 ug/L 17 seconds after it being dropped into the container. In contrast the Blend and the background average were almost identical never reaching values above 160 ug/L. A zoomed in plot of dust concentration against time is shown below to highlight the similarities between the background and blend results.

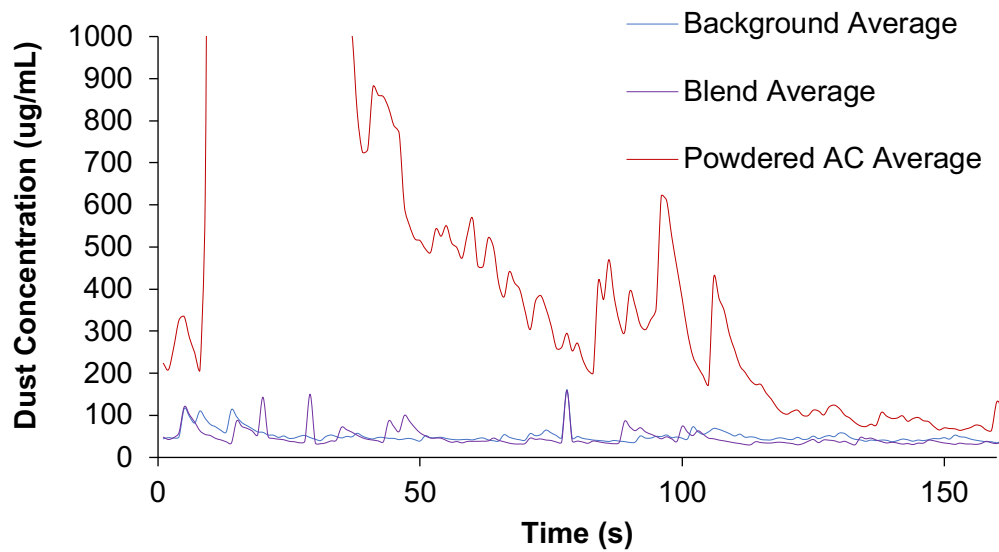


Figure 68 – Close up of dust concentration against time graph highlighting the similarities between the background and blend samples.

This demonstrates how the 50-poly(*S-r*-canola) support material can eliminate dust generation resulting from PAC’s use when mixed in a blend. The maximum average dust concentrations for each sample are shown below in Figure 69.

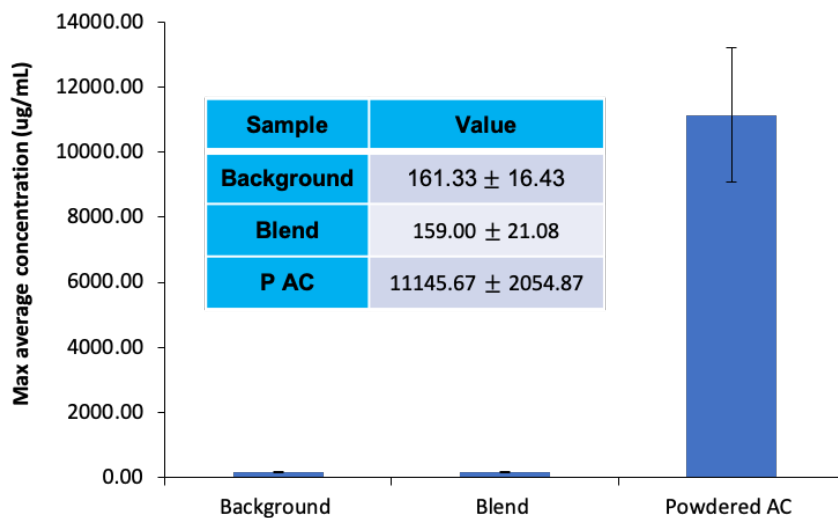


Figure 69 – Max average dust concentrations for dust experiment.

The maximum average dust concentration was identical (within error) for the background and the PAC/50-poly(*S-r*-canola) ($161 \pm 16 \mu\text{g/L}$ and $159 \pm 21 \mu\text{g/L}$ respectively). The PAC however reached $11,145 \pm 2054 \mu\text{g/L}$, 2 orders of magnitude larger than the background and blend. This demonstrates the effectiveness of 50-poly(*S-r*-canola) to suppress the generation of PAC dust plumes and their associated issues.

3.5.2 PFOA treatment using 50-poly(*S-r*-canola) sorbent

The PFOA in solution was monitored using ^{19}F NMR analysis using D_2O as a solvent spiked with trifluoroacetic acid (TFA, 5.4 mg/ml). The TFA was used as an internal standard. The amount of PFOA remaining was determined by the relative integration of the CF_3 signals, at δ -76.55 ppm for TFA and at δ -81.85 ppm for PFOA. The results are shown below in Figure 70.

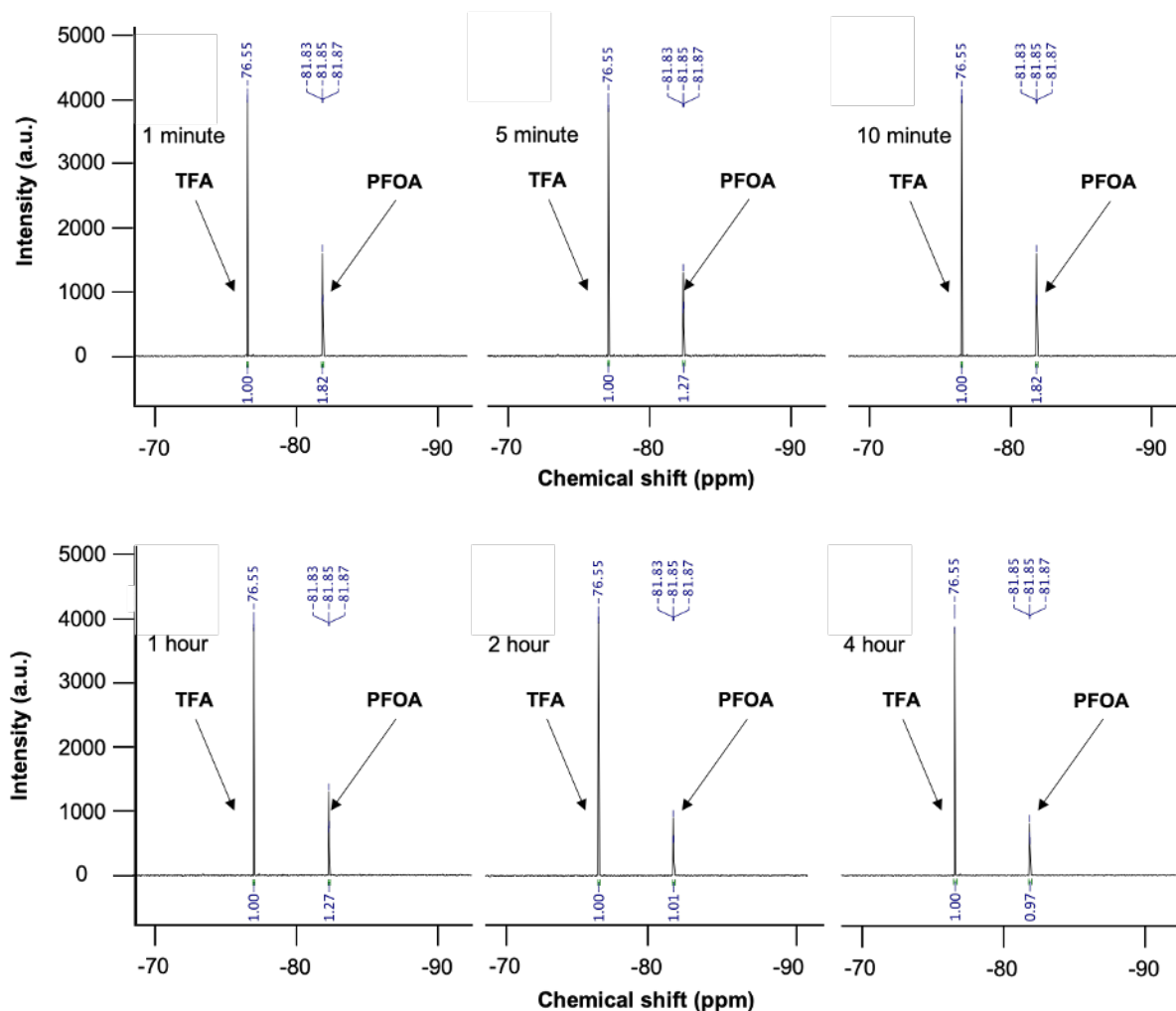


Figure 70 – ^{19}F NMR analysis of PFOA solutions (2.5 mg/mL) after undergoing varying amounts of treatment time with 50-poly(*S-r*-canola) sorbent.

Results indicated that the PFOA was being removed from solution by the 50-poly(*S-r*-canola) sorbent. After 5 minutes, 30% of the PFOA was removed from solution. By 2 hours the PFOA concentration was reduced by 45% (Figure 71).

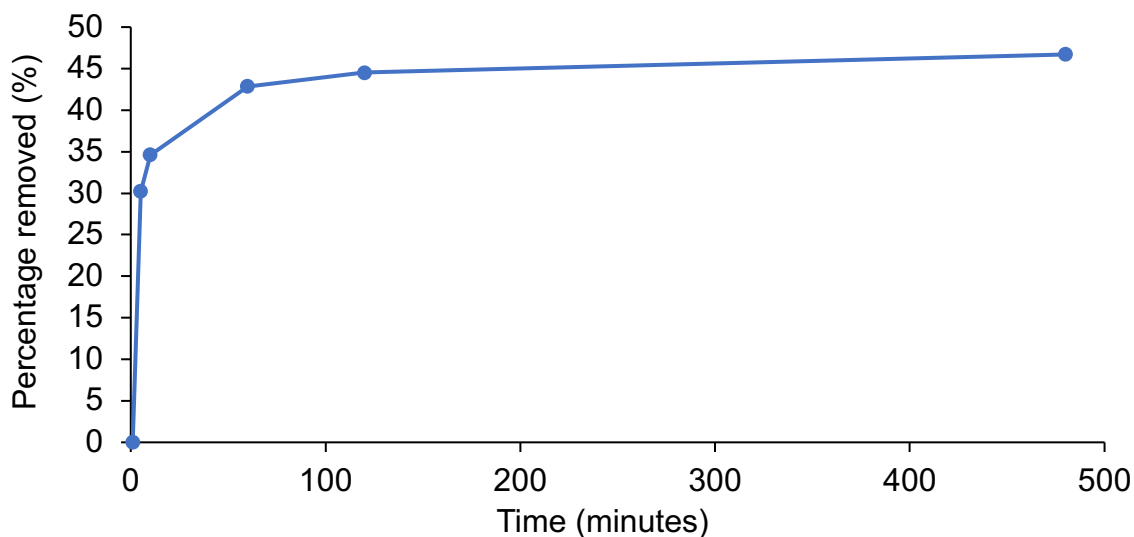
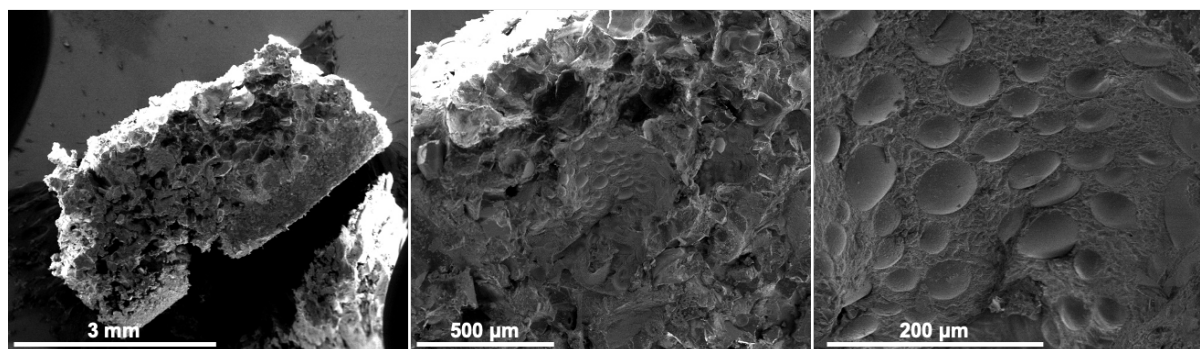


Figure 71 – Plot showing the percentage of PFOA removed from solution over time

After 2 hours only a slight increase in removed PFOA was observed (47% at 4 hours) suggesting that the 50-poly(*S-r*-canola) was reaching its PFOA sorption capacity. As 2.0 grams of 50-poly(*S-r*-canola) sorbent was used to treat 4 mL of 2 mg / mL PFOA solution (8 mg PFOA in 4 mL solution) and 47% of the PFOA was removed (3.76 mg), the sorption capacity for PFOA by 50-poly(*S-r*-canola) sorbent was estimated to be 1.9 mg / g. To investigate the effects of the treatment process on the 50-poly(*S-r*-canola) sorbent, SEM analysis was performed (Figure 72). Hemi-micelles had formed on the surface of the 50-poly(*S-r*-canola) sorbent after treatment. To confirm that these hemi-micelle structures were in fact PFOA hemi-micelles, EDX analysis was performed.



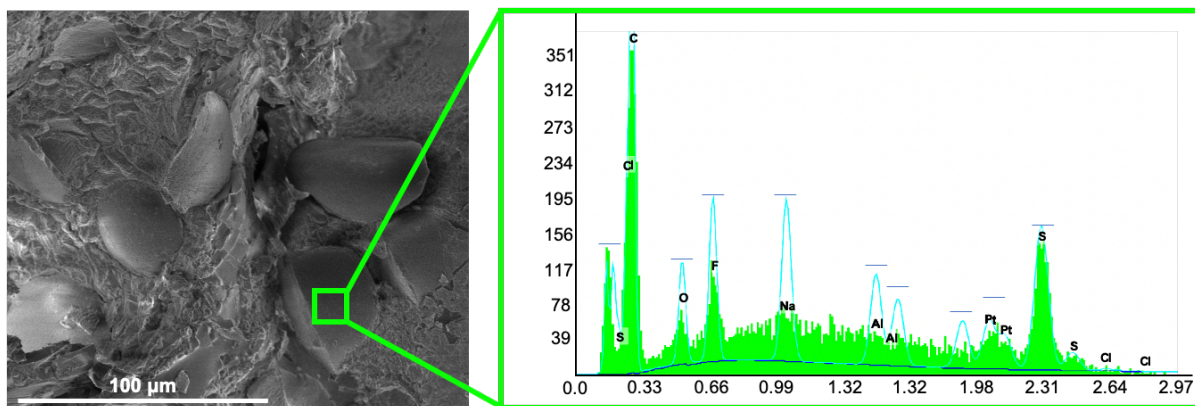


Figure 72 – (Top) SEM images of 50-poly(*S-r*-canola) sorbent material after treatment with PFOA. (Bottom) EDX analysis of PFOA hemimicelles on the surface of the treated 50-poly(*S-r*-canola) sorbent.

EDX revealed a strong presence of both carbon and fluorine within the hemi-micelle structures. This confirmed that treatment of an aqueous solution of PFOA with the 50-poly(*S-r*-canola) polymer resulted in formation of PFOA hemi-micelles on its surface. The formation and adsorption of PFOA hemi-micelles on sorbents surfaces has been hypothesised to occur in literature but never directly proven to occur.²⁴⁵ These results highlight the first direct proof of this hypothesis, improving the understanding of PFOAs adsorption mechanism opens the door for more accurate theoretical models and better ability to design high capacity PFOA sorbent materials.

3.5.3 PFOA treatment using PAC / 50-poly(*S-r*-canola) blend sorbent (batch)

Although the 50-poly(*S-r*-canola) polymer can remove PFOA by itself, its sorption capacity was not very high. Due to powdered activated carbons high PFOA sorption capacity, the carbon-polymer blend was investigated as a PFOA sorbent material. Initially, the carbon-polymer blend was compared with PAC, GAC and the 50-poly(*S-r*-canola) polymer at PFOA sorption.

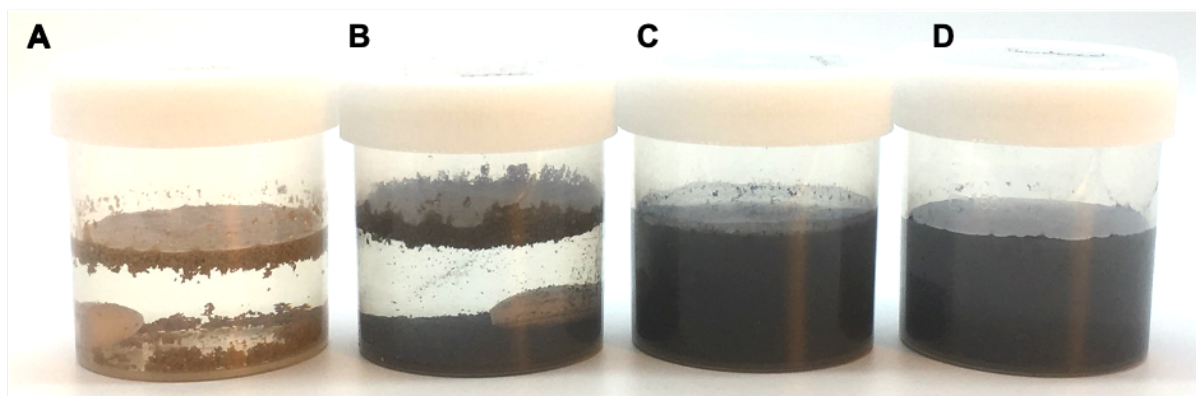


Figure 73 – PFOA treated with **A**) 50-poly(*S-r-canola*) polymer, **B**) PAC/50-poly(*S-r-canola*) blend, **C**) GAC and **D**) PAC.

Shown in Figure 73 both the GAC and PAC formed a suspension of particles upon treatment, whilst the blend and the 50-poly(*S-r-canola*) polymer either sunk to the bottom or floated to the top. To separate the sorbent particles from solution before its analysis, the treated solutions were passed through 0.22 μm syringe filters.

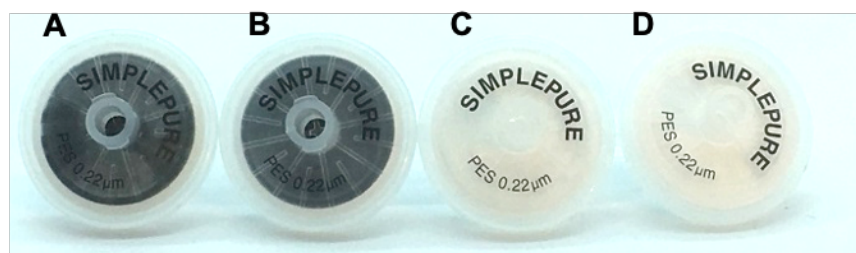


Figure 74 – SimplePure (0.22 μm) syringe filters after filtering mixtures containing: **A**) the blend, **B**) PAC, **C**) GAC and **D**) no solids.

Both the poly(*S-r-canola*) polymer and the carbon polymer blend passed through the filter without issue, however the PAC and GAC samples clogged the filters almost instantly and required multiple syringe filters to be used to achieve a solid free sample for analysis (Figure 74). This result highlights one example of how the use of 50-poly(*S-r-canola*) polymer as a PAC support material eliminates the major issues associated with using PAC and GAC in water treatment processes. The amount of PFAS removed by each sorbent material was determined and is compared below in Table 2.

Sample and remediation method	Final concentration (ppb)	Comments
PFOA in water (100 mL)	5000	Negative control
No treatment		

50-poly(S- <i>r</i> -canola) 4.0 g 1 hour stirring in batch process	4000 ± 340	Polymer support binds to PFOA
Powdered activated carbon 1.0 g 1 hour stirring in batch process	0.30 ± 0.14	High PFOA sorption Severe filter clogging
Granular activated carbon 1.0 g 1 hour stirring in batch process	220 ± 150	Low PFOA sorption Filter clogging
PAC/50-poly(S- <i>r</i> -canola) 1 hour stirring in batch process	30 ± 25	Easy handling Efficient filtering

Table 2 – Results for comparison of PFOA remediation.

The maximum PFOA sorption capacity was determined by performing an isotherm experiment. To do this, 20 mL solutions (V) of different initial PFOA concentrations (C_0) were treated with an equal mass (m) of PAC/50-poly(S-*r*-canola) blend. After treatment the equilibrium PFOA concentration (C_e) was recorded. This data was used to calculate the amount of PFOA adsorbed per gram of sorbent (q_e) using the following equation.

$$q_e = \frac{V(C_0 - C_e)}{m} \quad \text{Equation 4}$$

The results gained for PFOA sorption are shown below in Table 3.

Mass (g)	Volume (L)	C_0 (mg/L)	C_e (mg/L)	q_e (mg/g)
1	0.02	3.75	0.31	0.069
1	0.02	1.83	0.1	0.035
1	0.02	0.72	0.022	0.014
1	0.02	0.082	0.00058	0.0016

Table 3 – PFOA sorption data obtained through PFOA sorption using the PAC/50-poly(S-*r*-canola) blend.

The resulting data was fit to both Langmuir and Freundlich isotherm models. The equations describing these models are shown in Table 4.

Model	Equation	Parameters
Langmuir	$q_e = \frac{q_m^2 k_2 C_{eq}}{1 + q_m k_2 C_{eq}}$	K_L = Langmuir sorption constant (L / mg) q_m = Maximum sorption capacity (mg / g)
Freundlich	$q_e = K_F C_e^{1/n}$	K_F = Freundlich sorption constant (mg/g)(L / mg) ^{1/n} n = Dimensionless constant relating to sorption intensity

Table 4 – Langmuir and Freundlich isotherm model equations with corresponding parameters.⁹⁹

The dimensionless constant (*n*) is related to the sorption intensity. If *n* = 1 its homogenous but if *n* < 1 it is heterogeneous.⁹⁹ Origin pro software was then used to plot the *q_e* values against *C_e* values and fit the data to non-linear Langmuir and Freundlich isotherm models. The resulting plots along with the values for each parameter obtained from the models are shown below in Figure 75.

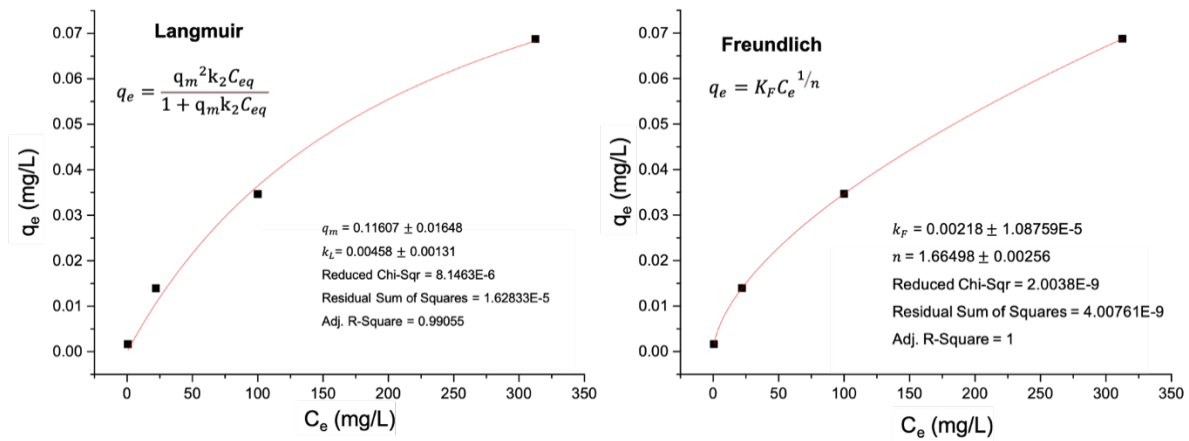


Figure 75 – Langmuir and Freundlich isotherm models fitted to PFOA sorption by PAC/50-poly(*S-r*-canola) blend data.

The Langmuir model fitting resulted in a maximum capacity of 0.12 ± 0.02 mg/g and an affinity constant of 4.58 ± 1.31 L/ μ g. The Sorption constant determined was for 1.0 gram of polymer however only 0.2 grams of PAC was present. Therefore, this would correspond to a PAC sorption capacity of 0.58 mg/g. This value is slightly higher than typically observed for PAC²⁴⁶ suggesting that the 50-poly(*S-r*-canola) support had aided in HgCl₂ removal as expected. The Freundlich model fitting resulted in a Freundlich isotherm constant (*k_F*) of 2.18 ± 0.01 μ g/g and dimensionless constant of 1.67 ± 0.0026 L/mg. The dimensionless constant (*n*) was larger than 1 suggesting that the sorption process was favourable. Now that the Isotherm experiment has been performed the kinetics of PFOA sorption was investigated. The kinetics of PFOA sorption by the carbon / 50-poly(*S-r*-canola) blend was compared to that of granular activated carbon, the current industry standard. The mass of PFOA removed per gram sorbent (*q_t*) was determined using the following equation:

$$q_t = \frac{V(C_0 - C_t)}{m} \quad \text{Equation 5}$$

The q_t value was then plotted against sorption time (t). Two models were used to investigate the kinetics of these adsorption processes: the pseudo-first order and pseudo-second order models. The equations describing these models are shown in Table 5.

Model	Equation	Parameters
Pseudo-First Order ²⁴⁷	$q_t = q_e[1 - e^{-k_1 t}]$	t = Adsorption time (minutes) q_t = Amount of adsorbed solute at time t (mg/g) q_e = Amount of adsorbed solute at equilibrium (mg/g) k_1 = Pseudo-first order rate constant (L/mg)
Pseudo-Second Order ⁴	$q_t = \frac{q_e^2 k_2 t}{1 + q_e k_2 t}$	t = Adsorption time (minutes) q_t = Amount of adsorbed solute at time t (mg/g) q_e = Amount of adsorbed solute at equilibrium (mg/g) k_2 = Pseudo-second order rate constant (g.mg.h)

Table 5 – Pseudo-First and Pseudo-second order kinetics model equations and corresponding parameters.

The q_e values obtained through experiment were then plotted against time and the resulting data was fitted to the first and second order non-linear kinetics models using origin pro software. The results are shown in Figure 76.

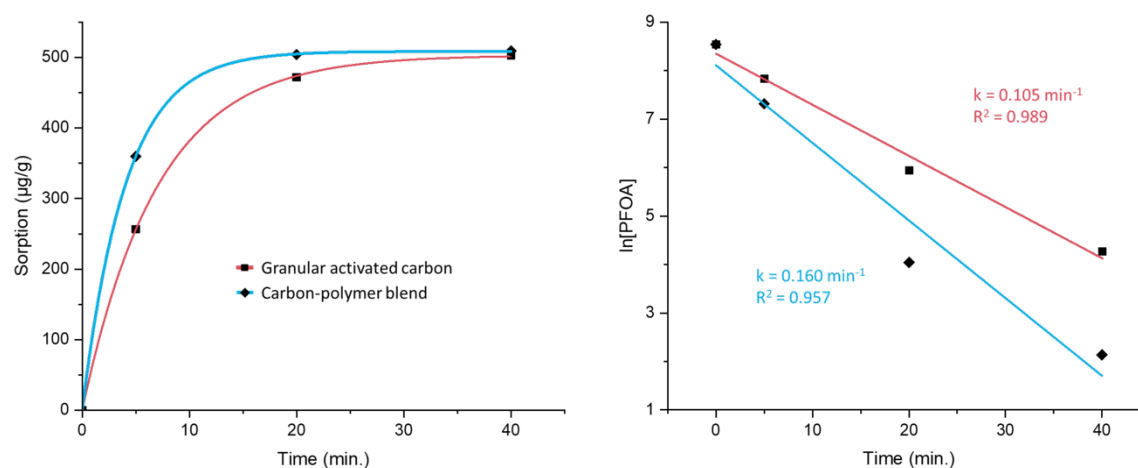


Figure 76 – Data from PFOA isotherm experiments for GAC and the PAC/50-poly(*S-r*-canola) polymer modelled by the pseudo-second order non-linear (left) and linear (right) kinetics

The calculated rate constants are $k_1 = 0.11 \text{ min}^{-1}$ for GAC and $k_1 = 0.16 \text{ min}^{-1}$ for the carbon-polymer blend. This demonstrates how the PAC/50-poly(*S-r*-canola) blend achieves faster removal rates than the current industry standard, GAC.

3.5.4 PFOA treatment using PAC / 50-poly(S-r-canola) blend sorbent (batch process)

To demonstrate the use of the carbon polymer blend in continuous flow PFOA treatment, a cotton wool ball was packed at the bottom of a 30 × 1.5 cm glass column. On top of the cotton wool ball a layer of 15.0 grams of sand was added. The sand was added to ensure that the blend did not wash through the column and acted as a filter. The cotton wool was placed to ensure the sand didn't wash through the column during the treatment process. On top of the sand layer 50.0 grams of PAC/50-(S-r-canola) blend was packed. On top of the blend a second layer of 15.0 grams of sand was added. This second layer of sand ensured that the blend remained in the column upon addition of water and didn't float to the top of the column. This setup is depicted in Figure 77. All continuous flow experiments were performed using this setup.

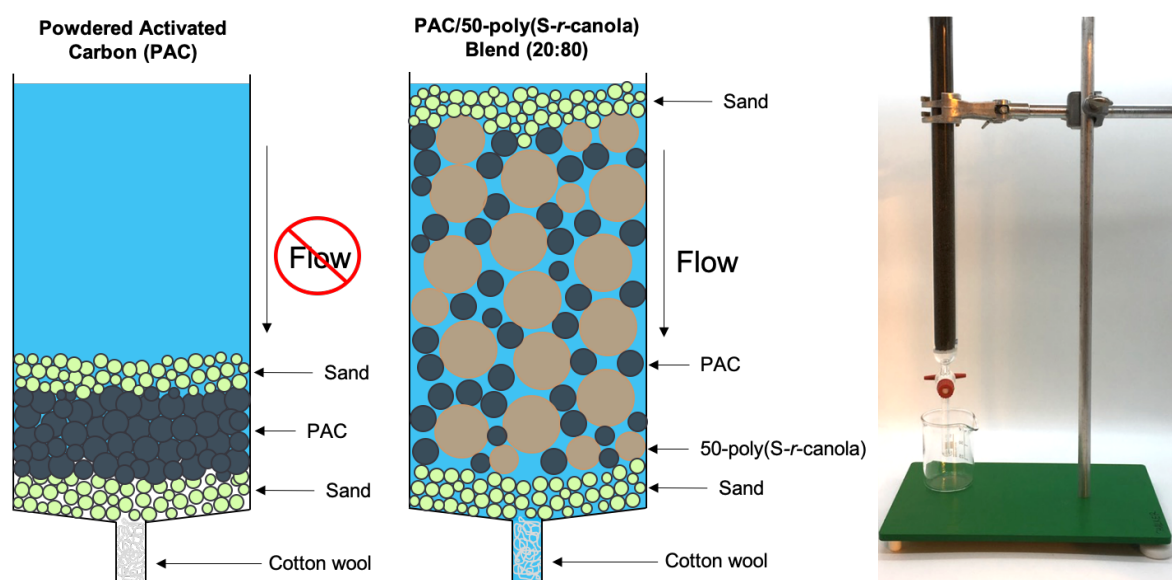


Figure 77 – A) Diagram depicting the setup for continuous flow treatment, B) Image of setup used for continuous flow experiments.

Continuous flow treatment was performed on 5 ppm PFOA solution by pumping the solution through the column at a controlled flow rate using a hand-pressurised bellow. This was performed at two different residence times: 20 and 90 minutes and the results are shown in Table 6.

Sample and remediation details	Final PFOA concentration	Comments
Carbon / 50-poly(S-r-canola) blend (80:20) 30 × 1.5 cm column 20 min residence time	170 ppb	Continuous process No caking

Carbon / 50-poly(<i>S-r</i> -canola) Blend (80:20) 30 × 1.5 cm column 90 min residence time	0.06 ppb	Meets EPA limits Continuous process No caking
---	----------	---

Table 6 – Results for continuous flow PFOA treatment experiments.

The same experiment was performed using PAC however the PAC quickly caked and clogged the column restricting water flow and preventing treatment. For this reason, only the PAC/50-poly(*S-r*-canola) continuous flow treatment results are shown. These results demonstrate that the PAC/50-poly(*S-r*-canola) blend could reduce the PFOA concentration to below regulation limits in a continuous flow process whilst the PAC clogged the filter rendering it incapable of being used under continuous flow. This highlights the advantages of using the 50-poly(*S-r*-canola) polymer as a PAC support material allowing PAC to be used in continuous flow processes. Total suspended solids are another undesired component in wastewater which typically require removal and are known to foul sorbent materials. The 50-poly(*S-r*-canola) support polymer was investigated to determine whether it could remove them from solution. To do this a OD600 Light experiment was used to monitor the suspended solids in solution before and after continuous flow treatment with the 50-poly(*S-r*-canola) polymer. Optical density (OD) measurements measure the absorbance of light in a sample. In bacterial analysis the wavelength of 600nm is frequently used (giving the term OD600). This measurement can be used to determine the concentration of solids in suspension by the amount of light scattering occurring.²⁴⁸

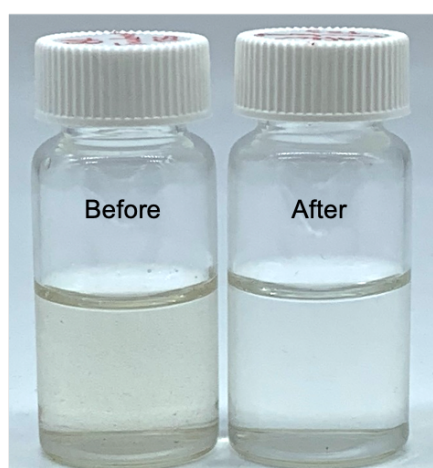


Figure 78 – Image of water containing suspended solids before (left) and after (right) treatment with 50-poly(*S-r*-canola).

Before treatment, the OD₆₀₀ was 0.060 ± 0.004 . After the filtration, the OD₆₀₀ was 0.010 ± 0.001 . This result is consistent with the polymer removing suspended solids. The removal of the suspended solids was observed visually and can be seen in Figure 78. Finally, to demonstrate the use of this blend in the continuous flow treatment of PFAS a field sample of water contaminated with PFAS was treated. The sample was obtained directly from a municipal catchment site using a high-density polypropylene container. This surface water is downstream from an air force base with known PFOS contamination. Certified commercial analysis revealed these field samples had pH 6.28, a conductivity of 163 mS/cm, 3 mg/L of dissolved organic content, 23 mg/L of total suspended solids and 150 ± 20 ng/L of PFOS. Using the same setup as the previous continuous flow experiments, continuous flow treatment of the contaminated field sample was performed. Upon treatment with the blend, the suspended solids were reduced from 23 mg/L to <5 mg/L for triplicate experiments. The PFOS content of the 10 L samples of treated water were measured by a certified commercial service (EPA/600/R-08/092 Method 537). The final PFOS content was 23 ± 5 ng/L, which is an 85% reduction in PFOS and a reduction below the 70 ng/L limit in this jurisdiction for drinking water and irrigation. This demonstrates how the blend can be effectively used in continuous flow treatment processes to reduce PFAS concentrations to below regulation limits. Further investigation needs to be done to determine suitable strategies to recover the PFAS chemicals from the blend sorbent. Combustion has been used previously to both remove and breakdown the PFAS from activated carbon as well as regenerate the activated carbon sorbent.²⁴⁹ These combustion methods would likely work well with the spent blend sorbent however it would result in a loss of the 50-poly(*S-r*-canola) material. To minimize the production of solid waste, future work would focus on new green methods for the regeneration of the blend material. One potential route to investigate is washing the spent sorbent with ethanol (or isopropyl alcohol) with ammonium hydroxide (NH₄OH) additive. This has been shown in a previous study to remove the PFAS from activated carbon sorbents.²⁵⁰ Another point to address in future work is whether binding of PFAS using the blend results in a change to its structure. In this case the PFOA binds mainly with the PAC within the blend and the interaction of PFAS with activated carbon have been investigated previously. One study showed that when the activated carbon contaminated with PFAS was treated with ethanol (or isopropyl alcohol) and ammonium hydroxide (NH₄OH) additive, the PFAS was recovered and its structure unchanged.²⁵⁰ This suggests that the structure of PFOA would likely remain unchanged after sorption by the blend.

3.6 Conclusion

The 50-poly(*S-r*-canola) polymer was shown to be an effective support material for PAC, eliminating the generation of hazardous dust and facilitating continuous flow processing by acting as a hydraulic lubricant preventing the caking and blockages typically observed with PAC. This blend was demonstrated to be an effective sorbent material for PFAS remediation outperforming granular activated carbon (GAC), the current industry standard. The maximum sorption capacity was determined to be 0.12 ± 0.017 mg/g of blend or 0.58 mg/g of PAC in the blend. The Freundlich sorption model fit the experimental data best suggesting multilayer sorption. The kinetics for PFOA sorption was best modelled by the pseudo-first order kinetics model with $k_1 = 0.16 \text{ min}^{-1}$. The 50-poly(*S-r*-canola) polymer was also observed to remove PFOA from solution, however this was only noticed at higher concentrations. Another important discovery was PFOA hemi-micelle formation on a sorbent's surface, whereby SEM imaging was used to capture the first direct proof of their formation in literature.

APPENDICES

Publications that resulted from the research in this chapter:

1. Lundquist, N. A., *et al.* "Polymer Supported Carbon for Safe and Effective Remediation of PFOA- and PFOS-Contaminated Water." *ACS Sustain. Chem. Eng.* **2019**, 7, 11044-11049.

Polymer Supported Carbon for Safe and Effective Remediation of PFOA- and PFOS-Contaminated Water

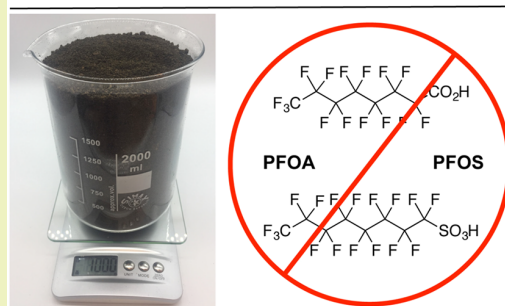
Nicholas A. Lundquist,[†] Martin J. Sweetman,^{‡,§,||} Kimberley R. Scroggie,[†] Max J. H. Worthington,[†] Louisa J. Esdaile,[†] Salah F. K. Alboaiji,^{†,⊥} Sally E. Plush,^{*,§,||} John D. Hayball,^{*,‡,§,#} and Justin M. Chalker^{*,†,Ⓜ}[†]Institute for NanoScale Science and Technology, College of Science and Engineering, Flinders University, Sturt Road, Bedford Park, South Australia 5042, Australia[‡]Experimental Therapeutics Laboratory, Cancer Research Institute, University of South Australia, North Terrace, Adelaide, South Australia 5000, Australia[§]School of Pharmacy and Medical Sciences, University of South Australia, North Terrace, Adelaide, South Australia 5000, Australia^{||}Future Industries Institute, University of South Australia, Mawson Lakes Boulevard, Mawson Lakes, South Australia 5095, Australia[⊥]Department of Chemical Engineering and Process Technology, Jubail Industrial College, 6 Al Huwaylate, Al Khalij, Jubail Industrial City 35718, Saudi Arabia[#]Robinson Research Institute and Adelaide Medical School, University of Adelaide, 55 King William Road, Adelaide, South Australia 5005, Australia

Supporting Information

ABSTRACT: Powdered activated carbon (PAC) is an economical sorbent for removing micropollutants from water, but it generates hazardous dust that is flammable and a respiration hazard. Additionally, the fine particles of PAC can cake and block filters and membranes, complicating its use in continuous processes. In this study, we present a sulfur polymer support for PAC that overcomes these problems. The blend of the sulfur polymer and PAC generates low dust and it does not block filters. The utility of the sorbent is demonstrated in the remediation of water contaminated with perfluorooctanoic acid (PFOA) and perfluorooctanesulfonic acid (PFOS), persistent micropollutants that currently threaten water safety worldwide. Fundamental discoveries of PFOA self-assembly are also reported, as well as testing on a field sample of contaminated surface water.

KEYWORDS: Activated carbon, Dust control, Inverse vulcanization, PFAS, PFOA, PFOS, Sulfur polymer, Water purification

Polymer supported carbon for water purification



INTRODUCTION

Per- and polyfluorinated alkyl substances (PFAS) have been used for decades in the production of fluoropolymers such as polytetrafluoroethylene (PTFE), protective coatings, lubricants, and high-performance fire fighting foams.¹ In the early 2000s, PFAS such as perfluorooctanoic acid (PFOA) and perfluorooctanesulfonic acid (PFOS) (Figure 1) were found to

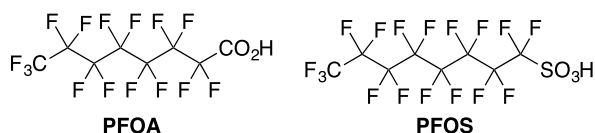


Figure 1. Perfluorooctanoic acid (PFOA) and perfluorooctanesulfonic acid (PFOS) belong to the class of persistent micropollutants collectively referred to as per- and polyfluorinated alkyl substances (PFAS).

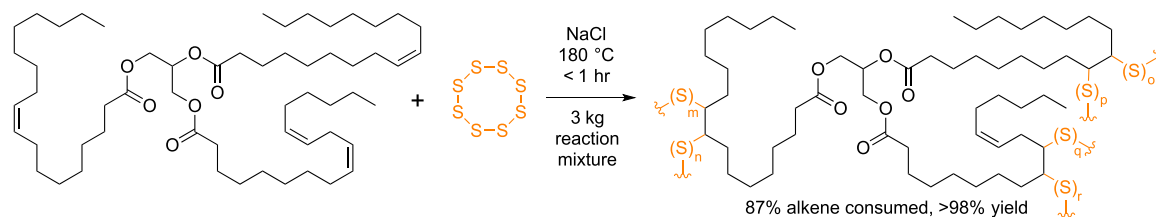
be distributed widely in the environment and in humans,^{2,3} prompting evaluations of their toxicity.¹ While a full assessment of the public health burden requires additional epidemiological studies,⁴ PFOA and PFOS exposure has been implicated in a variety of health issues⁵ including hepatic⁶ and renal⁷ toxicity, thyroid disease^{8,9} and kidney and testicular cancers.^{5,7,10} Accordingly, governments have issued regulations on emissions and exposure limits for these compounds.^{11,12} The United States Environmental Protection Agency, for instance, has issued an advisory limit of 70 ng/L (0.070 ppb) for PFOA in drinking water, based on toxicological studies in mice.^{13,14}

To meet these limits, it is critical to have efficient, scalable and cost-effective technologies to remove PFASs from

Received: March 30, 2019

Revised: May 19, 2019

Published: June 3, 2019

Scheme 1. Polysulfide Polymer Prepared by the Reaction of Sulfur and Canola Oil^a

^aThe sodium chloride porogen, used to increase surface area, is removed with water. This scheme and synthesis was adapted from our previous report and was reproduced under a Creative Commons License.¹⁹

water.^{12,15} Activated carbon is an attractive sorbent because of its low cost and scalability. Indeed, remediation using granular activated carbon (GAC) filters is the most common method for purifying water contaminated with PFOA, though there are some reports of reverse osmosis, membrane filtration, and ion exchange treatment at industrial and municipal facilities.^{12,16,17} Powdered activated carbon (PAC) is also used in removing micropollutants from water, including PFOA.¹² PAC benefits from a higher surface area and faster uptake of PFAS, relative to GAC,¹² but it is used less frequently because of challenges filtering fine particles and the hazardous dust it generates during handling.

In this study, we report a new strategy for deploying PAC and its application in removing PFOA and PFOS from water. The featured sorbent is a blend of PAC and a polysulfide polymer made by inverse vulcanization of canola oil.^{18,19} The polymer provides a support for the carbon that prevents caking during filtration, overcoming a common challenge using PAC. The carbon powder adheres to the polymer, so the blend does not produce plumes of fine carbon particles during handling, lowering the risk of spontaneous combustion, fire, and respiratory harm from inhalation. Both the polymer and the activated carbon contribute to PFAS binding, so the polymer is more than just a solid support and hydraulic lubricant. Batch and continuous water purification is demonstrated, including remediation of a field sample of contaminated surface water. These sorption experiments span the range of concentrations of PFOA and PFOS encountered in the environment including low concentrations in ground, surface, and tap water downstream from pollution sources (50 ppt to 2 ppb),²⁰ as well as the far higher concentrations (100 ppb to >10 000 ppb) found in groundwater plumes, wastewater ponds, and spills at the locations where PFAS-containing aviation fire-fighting foams were used.^{21–25}

We recently reported the synthesis of a polysulfide polymer made by direct reaction of equal masses of sulfur and canola oil (Scheme 1 and S3–S5).^{18,19} When the polymer is prepared in the presence of a sodium chloride porogen to increase surface area, the salt can be removed with a simple water wash.¹⁸ Because millions of tons of excess sulfur are produced each year by the petroleum industry and used unsaturated cooking oils are suitable in the synthesis, the raw materials are inexpensive and sustainably sourced. The polymer is scalable and can be routinely prepared on a 1 kg scale in the laboratory, with the high atom economy further contributing to sustainability metrics.¹⁹ These polysulfides and related polymers prepared by inverse vulcanization²⁶ have been explored in a variety of applications including cathode materials for lithium–sulfur batteries,^{26,27} lenses for infrared imaging,²⁸ sorbents for heavy metal remediation^{18,29–36} and

oil-spill cleanup,¹⁹ and components of slow-release fertilizers.³⁷ The affinity of our canola oil polysulfide for hydrophobic materials like crude oil and other hydrocarbon pollution¹⁹ prompted us to test its affinity for the perfluorinated backbone of PFAS.

RESULTS AND DISCUSSION

As a first test, PFOA was prepared as a 2 mg/mL solution in water and then 2.0 g of the polysulfide was added to 5 mL of this solution. The concentration of PFOA was monitored by ¹⁹F NMR spectroscopy using trifluoroacetic acid as an internal standard to quantify the amount of PFOA in solution (S11–S12). After 4 h of static incubation, the polymer had removed 47% of the PFOA. While the concentrations of PFOA used in this experiment were quite high, we were encouraged that the polymer had some affinity for PFOA. To confirm that PFOA could indeed bind to the polymer, the sorbent was analyzed by scanning electron microscopy (SEM) and energy dispersive X-ray (EDX) spectroscopy (Figure 2 and S13–S14), revealing

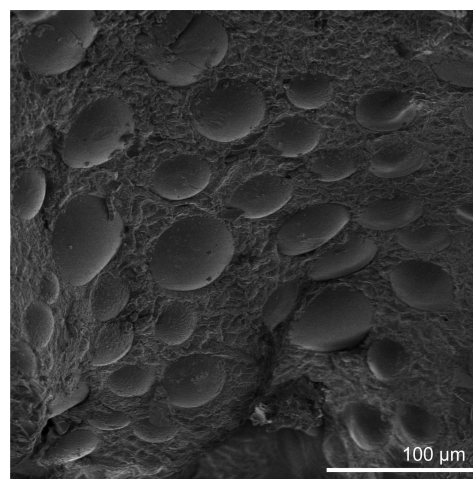


Figure 2. At high concentrations in aqueous solution (2 mg/mL), PFOA forms hemimicelles ($41 \pm 16 \mu\text{m}$) on the surface of the canola oil polysulfide polymer.

hemimicelles of PFOA on the polymer surface. While the formation of PFOA hemimicelles on surfaces has been proposed in the literature,³⁸ this is the first direct imaging of this phenomenon and an important milestone in understanding the fundamental chemical behavior and self-assembly of PFOA.

To improve the rate of PFOA uptake and sorption capacity, we blended the polymer with PAC (Kuraray, PGW 150 MP,

100–200 mesh, point of zero charge: $\text{pH}_{(\text{pzc})} = 9.6$, see S20 for details). In the event, 800 g of the polysulfide and 200 g of PAC were sealed in a 2 L plastic tub and inverted 20 times. The powdered carbon and the polymer were highly attracted to each other, likely due to a combination of electrostatic and hydrophobic forces, and formed a homogeneous blend (Figure 3 and S6). Using more than 20% carbon by mass in the blend

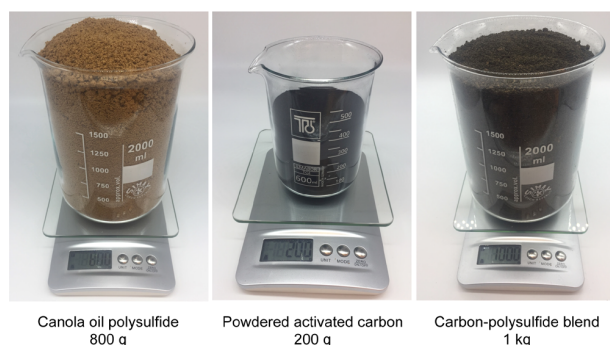


Figure 3. When the canola oil polysulfide is blended with powdered activated carbon, the carbon particles adhere to the surface of the polymer. The preparation of this blend is routinely carried out on a kilogram scale.

led to unbound carbon. (See S7–S9 for SEM and EDX micrographs of the carbon and the carbon-polymer blend.) This blend has several benefits over the PAC alone. First, the blend is easy to handle and generates far less dust than the powdered carbon (Supplementary Video S1), an important safety aspect with respect to inhalation and flammability risks of PAC. Additionally, the carbon-polymer blend is easier to remove from water by filtration than the PAC alone (see below), overcoming this common problem with PAC.³⁹

The dust generation was quantified using a nephelometer (Figure 4 and S10). In the event, a 100 mL dry volume of the PAC or the carbon-polysulfide blend was poured into one portion from a 20 cm height into a cylindrical plastic container (12 cm diameter \times 10 cm height). The dust generated was monitored at fixed position 50 cm from center of the dish at a height of 20 cm. Measurements were recorded every second for 2.5 min. The PAC manipulation generated significant amounts of dust, with an average maximum concentration of suspended particles $>11\,000\ \mu\text{g}/\text{m}^3$. In contrast, the manipulation of the carbon-polysulfide blend generated no more dust than what was detected in the background measurements (Figure 4). The carbon-polysulfide blend is therefore superior to PAC in terms of respiratory risks and other dangers associated with suspended dust particles.

To test the carbon-polymer blend in PFOA sorption, 5.0 g of the blend (4.0 g polymer, 1.0 g PAC) was added to 100 mL of a 5000 ppb aqueous stock solution of PFOA and stirred for 1 h. For comparison, three additional control experiments were carried out using only the polysulfide polymer (4.0 g) and either PAC (1.0 g) or GAC (1.0 g) (page S15). All experiments were run in triplicate. After 1 h of treatment, the water was filtered through a $0.22\ \mu\text{m}$ poly(ether sulfone) (PES) syringe filter. The PFOA was then quantified by a certified commercial laboratory using solid phase extraction followed by LC-MS-MS analysis of eluted PFOA (EPA/600/R-08/092 Method 537).⁴⁰ (Table 1, Entries 1–5). The polymer alone reduced the PFOA concentration to an average

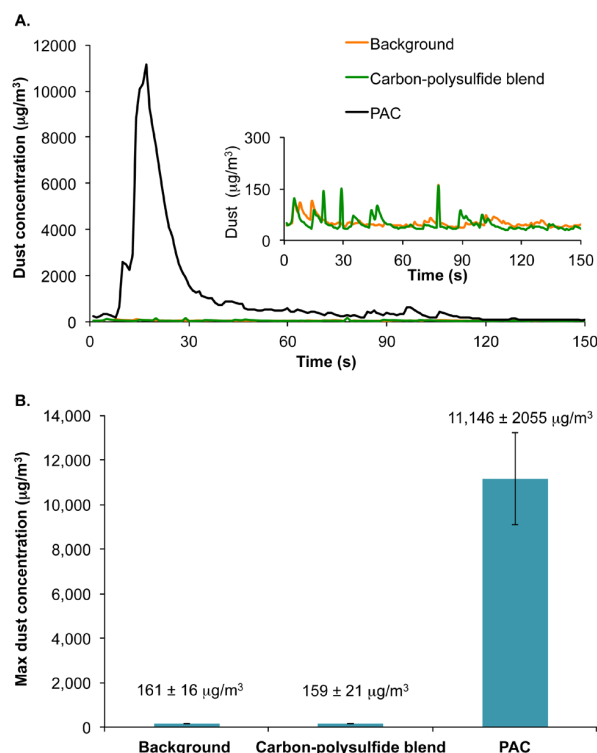


Figure 4. (A) Dust generation over 2.5 min at 50 cm distance from where a 100 mL volume of PAC or carbon-polysulfide blend was poured into a container. At $t = 0$, all of the sorbent has been poured and the nephelometer operation commences. All values are the average of triplicate experiments. The inset is a magnified display showing background dust and the dust generated from the carbon-polysulfide blend. (B) The average maximum dust detected in the experiment (average of triplicate experiments).

of 4000 ppb over the hour treatment. GAC reduced the PFOA concentration to an average of 220 ppb, which is still well above the 0.070 ppb US EPA Lifetime Health Advisory limit. The powdered activated carbon and the carbon-polymer blend, in contrast, were more effective at removing the PFOA, reducing the concentration from 5000 to 0.30 and 30 ppb, respectively.

These results imply that the PFOA sorption improves by an order of magnitude over this time period if GAC is replaced with the carbon-polymer blend. Free PAC did perform better than the blend in this experiment, but we note that the fine particles of the PAC remained suspended in the water and blocked the syringe filters. Testing this blocking in repeated filtrations, it was found that PAC blocked the filter within 28 ± 5 s for a filtration at 33 mL/min flow rate (Figure 5 and S16), making it tedious, costly, and impractical to remove the PAC from water. In fact, five syringe filters were required for just 100 mL of solution. Even the granular activated carbon led to filter clogging after 35 ± 3 s of filtration at a 33 mL/min flow rate. In this case, four syringe filters were required to remove the GAC from 100 mL of water. In contrast, the carbon-polymer blend did not block over the 100 mL filtration, a promising lead for a continuous remediation process. To that end, the carbon-polymer blend (40 g) was packed into a glass column and water containing 5000 ppb of PFOA was passed through the column (Table 2 and S17). With a 20 min elution time, the PFOA concentration was reduced to 170 ppb. With a

Table 1. PFOA Batch Sorption Studies Comparing the Polysulfide Polymer, GAC, PAC, and the Carbon-Polysulfide Blend^a

Entry	Method	Final PFOA concentration	Comments
1	PFOA in water No treatment	5000 ppb	Negative control
2	Polysulfide polymer 4.0 g, 1 h stirring, batch process	4000 ± 340 ppb	Polymer support binds measurably to PFOA
3	GAC ^b 1.0 g, 1 h stirring, batch process	220 ± 150 ppb	Low PFOA sorption Filter clogging
4	PAC ^c 1.0 g, 1 h stirring, batch process	0.30 ± 0.14 ppb	High PFOA sorption Severe filter clogging
5	Carbon-polysulfide blend 4.0 g polymer, 1.0 g carbon, 1 h stirring, batch process	30 ± 25 ppb	Easy handling Efficient filtering

^aAll entries employ 100 mL of water with 5000 ppb PFOA. Triplicate experiments were carried out where averages and standard deviations are reported. ^bGC 1200, 0.5–0.7 mm, Activated Carbon Technologies. ^cKuraray, PGW 150 MP.



Figure 5. Carbon-polymer blend is easier to remove from water by filtration than either PAC or GAC. Left to right: syringe filter clogged with GAC (GC 1200, 0.5–0.7 mm, Activated Carbon Technologies), syringe filter clogged with PAC (Kuraray, PGW 150 MP), syringe filter used to filter the carbon-polymer blend (no clogging), and an unused syringe filter.

Table 2. Continuous Removal of PFOA from Water Using the Carbon-Polymer Blend^a

Entry	Method	Final PFOA concentration	Comments
1	Carbon-polysulfide blend 32.0 g polymer, 8.0 g carbon, 30 × 1.5 cm column Continuous process, 20 min elution time	170 ppb	Continuous process No caking
2	Carbon-polysulfide blend 32.0 g polymer, 8.0 g carbon, 30 × 1.5 cm column Continuous process, 90 min elution time	0.06 ppb	Below US EPA Lifetime Health Advisory levels for drinking water Continuous process No caking

^a100 mL, initial concentration of 5000 ppb PFOA.

90 min elution time, the PFOA concentration was reduced to 0.06 ppb or 60 ng/L, which is below the US EPA Lifetime Health Advisory levels for drinking water.¹¹

Investigating the rate of sorption, the PFOA uptake was measured as a function of time over 40 min, using 5.0 g of the carbon-polysulfide blend in 100 mL of deionized water containing 5000 ppb PFOA (Figure 6 and S18). The rate of uptake was compared to granular activated carbon, the most common form of carbon used in PFAS remediation, using the same process. In both experiments the amount of carbon is normalized (1.0 g of carbon). As shown in Figure 6, the carbon-PAC blend is superior in the rate of uptake. Fast sorption is critical in continuous processes that can limit the contact time of the contaminated water and the sorbent, so this

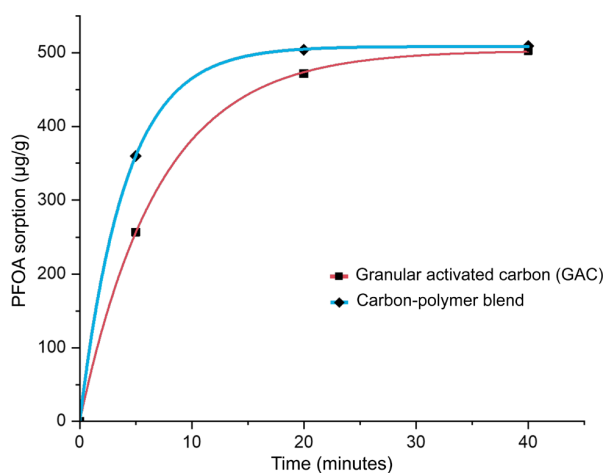


Figure 6. The carbon-polymer blend has a higher rate of PFOA sorption than granular activated carbon. The carbon-polymer blend (5.0 g) or the granular activated carbon (1.0 g) were added to a 100 mL solution of PFOA (4000 ppb) and the PFOA concentration was measured after 5, 20, and 40 min. The experiments were carried out in triplicate, and the average PFOA uptake ($\mu\text{g PFOA/g carbon}$ in sorbent) was plotted. Note that the amount of carbon for GAC and the carbon-polymer blend is the same for each experiment (1.0 g) and sorption is normalized for carbon content. Fitting this data to a pseudo-first-order kinetic model revealed a rate constant of $k_1 = 0.105 \text{ min}^{-1}$ for GAC and $k_1 = 0.160 \text{ min}^{-1}$ for the carbon-polymer blend.

is an important result. Fitting the data to a pseudo-first-order sorption process revealed rate constants of $k_1 = 0.105 \text{ min}^{-1}$ for GAC and $k_1 = 0.160 \text{ min}^{-1}$ for the carbon-polymer blend. Assessing the binding capacity of the carbon-polysulfide blend, a sorption isotherm was determined for the carbon-polymer blend. Fitting the data to a Langmuir–Freundlich isotherm model revealed a regressed maximum sorption capacity of 355 $\mu\text{g PFOA/g carbon}$ in the blend (S19).

A final test of the carbon-polymer blend was carried out on a field sample surface water contaminated with low concentrations of PFAS. This water was obtained from a catchment downstream from an air force base contaminated with PFAS-based fire-fighting foams. The major contaminant was PFOS, measured at $150 \pm 20 \text{ ppt}$ for three samples, a level that makes this water currently unusable in its jurisdiction, even for irrigation. The pH of the water was 6.28 with a conductivity of 163 mS/cm. Dissolved organic content was 3 mg/L and total suspended solids were 23 mg/L (S21). It was discovered that by simply filtering the water through a column of the canola oil

polysulfide polymer, the suspended solids could be reduced by >80%, suggesting that the polymer could serve a role in clarifying contaminated water before contact with the carbon (S21). To demonstrate PFOS removal with the carbon-polysulfide blend, 10 L of the contaminated surface water was passed through a column containing 40 g of the sorbent at an average flow rate of 200 mL/min (S22). For triplicate experiments, the PFOS content was measured by a certified commercial lab (EPA/600/R-08/092 Method 537). PFOS was reduced by 85% to 23 ± 5 ppt, which is below the recommended 70 ppt limits in this jurisdiction for drinking water and irrigation. This preliminary demonstration has motivated future field trials at larger scale and flow rates, which will be reported in due course.

CONCLUSIONS

In summary, we have developed a new sorbent made from a blend of a sustainable sulfur polymer and powdered activated carbon. We have directly observed, for the first time, the assembly of hemimicelles of PFOA on the sulfur polymer surface, revealing fundamental information about PFOA self-assembly and binding. The sorbent blend is easy to handle and generates low dust. The blend is superior to GAC with respect to caking and rate of PFOA uptake. We also note that activated carbon⁴¹ and the polymer^{18,19,32,42} in this sorbent blend can, in principle, be made entirely from industrial waste and repurposed biomass, which merges our interests in using sustainable carbon^{43,44} and sulfur polymers^{18,19,29,31,32} for purifying water. The blend is scalable and we have prepared more than 25 kg in our laboratory. In future work, we will evaluate the sorption of other types of poly- and perfluorinated micropollutants,^{45,46} and methods for regenerating the sorbent (S23–S24). Field studies are also underway to validate the use of this sorbent on industrial scales.

ASSOCIATED CONTENT

Supporting Information

The Supporting Information is available free of charge on the ACS Publications website at DOI: [10.1021/acssuschemeng.9b01793](https://doi.org/10.1021/acssuschemeng.9b01793).

Full experimental details and characterization data (PDF)

Video S1 (ZIP)

AUTHOR INFORMATION

Corresponding Authors

*S. Plush. E-mail: Sally.Plush@unisa.edu.au.

*J. D. Hayball. E-mail: john.hayball@unisa.edu.au.

*J. M. Chalker. E-mail: justin.chalker@flinders.edu.au.

ORCID

Justin M. Chalker: [0000-0002-7504-5508](https://orcid.org/0000-0002-7504-5508)

Notes

The authors declare the following competing financial interest(s): Five authors are inventors on patents and patent applications related to this research. J.M.C. and M.J.H.W. are inventors on a patent describing the synthesis and uses of the sulfur polymer featured in this research (WO 2017181217. Priority Application AU 2016-901470, April 20 2016). M.J.S., S.E.P., J.D.H., and J.M.C. are inventors on a provisional patent application describing the carbon-polymer blends and their

applications, including PFOA sorption (Application AU 2018-902544, July 13 2018).

ACKNOWLEDGMENTS

This research was funded by the South Australian Defence Innovation Partnership (M.J.S., S.E.P., J.D.H., J.M.C.) and the Australian Government National Environmental Science Programme Emerging Priorities Funding (J.M.C.). We acknowledge the support of the Australian Microscopy and Microanalysis Research Facility at Flinders University and that this work was performed in part at the South Australian node of the Australian National Fabrication Facility. We acknowledge Kuraray for generously providing samples of activated carbon.

REFERENCES

- (1) Lindstrom, A. B.; Strynar, M. J.; Libelo, E. L. Polyfluorinated Compounds: Past, Present, and Future. *Environ. Sci. Technol.* **2011**, *45*, 7954–7961.
- (2) Giesy, J. P.; Kannan, K. Global Distribution of Perfluorooctane Sulfonate in Wildlife. *Environ. Sci. Technol.* **2001**, *35*, 1339–1342.
- (3) Kannan, K.; Corsolini, S.; Falandysz, J.; Fillmann, G.; Kumar, K. S.; Loganathan, B. G.; Mohd, M. A.; Olivero, J.; van Wouwe, N.; Yang, J. H.; Aldous, K. M. Perfluorooctanesulfonate and Related Fluorochemicals in Human Blood from Several Countries. *Environ. Sci. Technol.* **2004**, *38*, 4489–4495.
- (4) Steenland, K.; Fletcher, T.; Savitz, D. A. Epidemiologic Evidence on the Health Effects of Perfluorooctanoic Acid (PFOA). *Environ. Health Perspect.* **2010**, *118*, 1100–1108.
- (5) Li, K.; Gao, P.; Xiang, P.; Zhang, X.; Cui, X.; Ma, L. Q. Molecular mechanisms of PFOA-induced toxicity in animals and humans: Implications for health risks. *Environ. Int.* **2017**, *99*, 43–54.
- (6) Gallo, V.; Leonardi, G.; Genser, B.; Lopez-Espinosa, M.-J.; Frisbee, S. J.; Karlsson, L.; Ducatman, A. M.; Fletcher, T. Serum Perfluorooctanoate (PFOA) and Perfluorooctane Sulfonate (PFOS) Concentrations and Liver Function Biomarkers in a Population with Elevated PFOA Exposure. *Environ. Health Perspect.* **2012**, *120*, 655–660.
- (7) Barry, V.; Winquist, A.; Steenland, K. Perfluorooctanoic Acid (PFOA) Exposures and Incident Cancers among Adults Living Near a Chemical Plant. *Environ. Health Perspect.* **2013**, *121*, 1313–1318.
- (8) Melzer, D.; Rice, N.; Depledge, M. H.; Henley, W. E.; Galloway, T. S. Association between Serum Perfluorooctanoic Acid (PFOA) and Thyroid Disease in the U.S. National Health and Nutrition Examination Survey. *Environ. Health Perspect.* **2010**, *118*, 686–692.
- (9) Lopez-Espinosa, M.-J.; Mondal, D.; Armstrong, B.; Bloom, M. S.; Fletcher, T. Thyroid Function and Perfluoroalkyl Acids in Children Living Near a Chemical Plant. *Environ. Health Perspect.* **2012**, *120*, 1036–1041.
- (10) Morrissey Donohue, J.; Moore Duke, T.; Wambaugh, J. *Health Effects Support Document for Perfluorooctanoic Acid (PFOA)*; EPA 822-R-16-003; United States Environmental Protection Agency: Washington, DC, 2016.
- (11) Zushi, Y.; Hogarh, J. N.; Masunaga, S. Progress and perspective of perfluorinated compound risk assessment and management in various countries and institutes. *Clean Technol. Environ. Policy* **2012**, *14*, 9–20.
- (12) Rahman, M. F.; Peldszus, S.; Anderson, W. B. Behaviour and fate of perfluoroalkyl and polyfluoroalkyl substances (PFASs) in drinking water treatment: A review. *Water Res.* **2014**, *50*, 318–340.
- (13) *Drinking Water Health Advisory for Perfluorooctanoic Acid (PFOA)*; EPA 822-R-16-005; United States Environmental Protection Agency: Washington, DC, 2016.
- (14) *Technical Fact Sheet - Perfluorooctane Sulfonate (PFOS) and Perfluorooctanoic acid (PFOA)*; EPA 505-F-17-001; United States Environmental Protection Agency: Washington, DC, 2017.

- (15) Post, G. B.; Cohn, P. D.; Cooper, K. R. Perfluorooctanoic acid (PFOA), an emerging drinking water contaminant: A critical review of recent literature. *Environ. Res.* **2012**, *116*, 93–117.
- (16) Du, Z.; Deng, S.; Bei, Y.; Huang, Q.; Wang, B.; Huang, J.; Yu, G. Adsorption behavior and mechanism of perfluorinated compounds on various adsorbents—A review. *J. Hazard. Mater.* **2014**, *274*, 443–454.
- (17) Ross, I.; McDonough, J.; Miles, J.; Storch, P.; Kochunaryanan, P. T.; Kalve, E.; Hurst, J.; Dasgupta, S. S.; Burdick, J. A review of emerging technologies for remediation of PFASs. *Remediation* **2018**, *28*, 101–126.
- (18) Worthington, M. J. H.; Kucera, R. L.; Albuquerque, I. S.; Gibson, C. T.; Sibley, A.; Slattery, A. D.; Campbell, J. A.; Alboaiji, S. F. K.; Muller, K. A.; Young, J.; Adamson, N.; Gascooke, J. R.; Jampaiah, D.; Sabri, Y. M.; Bhargava, S. K.; Ippolito, S. J.; Lewis, D. A.; Quinton, J. S.; Ellis, A. V.; Johs, A.; Bernardes, G. J. L.; Chalker, J. M. Laying Waste to Mercury: Inexpensive Sorbents Made from Sulfur and Recycled Cooking Oils. *Chem. - Eur. J.* **2017**, *23*, 16219–16230.
- (19) Worthington, M. J. H.; Shearer, C. J.; Esdaile, L. J.; Campbell, J. A.; Gibson, C. T.; Legg, S. K.; Yin, Y.; Lundquist, N. A.; Gascooke, J. R.; Albuquerque, I. S.; Shapter, J. G.; Andersson, G. G.; Lewis, D. A.; Bernardes, G. J. L.; Chalker, J. M. Sustainable Polysulfides for Oil Spill Remediation: Repurposing Industrial Waste for Environmental Benefit. *Adv. Sustainable Syst.* **2018**, *2*, 1800024.
- (20) Hu, X. C.; Andrews, D. Q.; Lindstrom, A. B.; Bruton, T. A.; Schaidler, L. A.; Grandjean, P.; Lohmann, R.; Carignan, C. C.; Blum, A.; Balan, S. A.; Higgins, C. P.; Sunderland, E. M. Detection of Poly- and Perfluoroalkyl Substances (PFASs) in U.S. Drinking Water Linked to Industrial Sites, Military Fire Training Areas, and Wastewater Treatment Plants. *Environ. Sci. Technol. Lett.* **2016**, *3*, 344–350.
- (21) Moody, C. A.; Field, J. A. Determination of Perfluorocarboxylates in Groundwater Impacted by Fire-Fighting Activity. *Environ. Sci. Technol.* **1999**, *33*, 2800–2806.
- (22) Moody, C. A.; Martin, J. W.; Kwan, W. C.; Muir, D. C. G.; Mabury, S. A. Monitoring Perfluorinated Surfactants in Biota and Surface Water Samples Following an Accidental Release of Fire-Fighting Foam into Etobicoke Creek. *Environ. Sci. Technol.* **2002**, *36*, 545–551.
- (23) Arias, V. A.; Mallavarapu, M.; Naidu, R. Identification of the source of PFOS and PFOA contamination at a military air base site. *Environ. Monit. Assess.* **2015**, *187*, 4111.
- (24) Hutton, J.; Holton, C.; DiGiuseppi, B. Occurrence and behavior of per- and polyfluoroalkyl substances from aqueous film-forming foam in groundwater systems. *Remediation* **2018**, *28*, 89–99.
- (25) Sullivan, M. *Addressing Perfluorooctane Sulfonate (PFOS) and Perfluorooctanoic Acid (PFOA). Official Response to United States House of Representatives Report 115-200*; United States Department of Defense, March 2018.
- (26) Chung, W. J.; Griebel, J. J.; Kim, E. T.; Yoon, H.; Simmonds, A. G.; Ji, H. J.; Dirlam, P. T.; Glass, R. S.; Wie, J. J.; Nguyen, N. A.; Guralnick, B. W.; Park, J.; Somogyi, A.; Theato, P.; Mackay, M. E.; Sung, Y.-E.; Char, K.; Pyun, J. The use of elemental sulfur as an alternative feedstock for polymeric materials. *Nat. Chem.* **2013**, *5*, 518–524.
- (27) Hoefling, A.; Lee, Y. J.; Theato, P. Sulfur-Based Polymer Composites from Vegetable Oils and Elemental Sulfur: A Sustainable Active Material for Li–S Batteries. *Macromol. Chem. Phys.* **2017**, *218*, 1600303.
- (28) Griebel, J. J.; Glass, R. S.; Char, K.; Pyun, J. Polymerizations with elemental sulfur: A novel route to high sulfur content polymers for sustainability, energy and defense. *Prog. Polym. Sci.* **2016**, *58*, 90–125.
- (29) Crockett, M. P.; Evans, A. M.; Worthington, M. J. H.; Albuquerque, I. S.; Slattery, A. D.; Gibson, C. T.; Campbell, J. A.; Lewis, D. A.; Bernardes, G. J. L.; Chalker, J. M. Sulfur-Limonene Polysulfide: A Material Synthesized Entirely from Industrial By-Products and Its Use in Removing Toxic Metals from Water and Soil. *Angew. Chem., Int. Ed.* **2016**, *55*, 1714–1718.
- (30) Esdaile, L. J.; Chalker, J. M. The Mercury Problem in Artisanal and Small-Scale Gold Mining. *Chem. - Eur. J.* **2018**, *24*, 6905–6916.
- (31) Worthington, M. J. H.; Kucera, R. L.; Chalker, J. M. Green chemistry and polymers made from sulfur. *Green Chem.* **2017**, *19*, 2748–2761.
- (32) Lundquist, N. A.; Worthington, M. J. H.; Adamson, N.; Gibson, C. T.; Johnston, M. R.; Ellis, A. V.; Chalker, J. M. Polysulfides made from re-purposed waste are sustainable materials for removing iron from water. *RSC Adv.* **2018**, *8*, 1232–1236.
- (33) Hasell, T.; Parker, D. J.; Jones, H. A.; McAllister, T.; Howdle, S. M. Porous inverse vulcanised polymers for mercury capture. *Chem. Commun.* **2016**, *52*, 5383–5386.
- (34) Parker, D. J.; Jones, H. A.; Petcher, S.; Cervini, L.; Griffin, J. M.; Akhtar, R.; Hasell, T. Low cost and renewable sulfur-polymers by inverse vulcanisation, and their potential for mercury capture. *J. Mater. Chem. A* **2017**, *5*, 11682–11692.
- (35) Thielke, M. W.; Bultema, L. A.; Brauer, D. D.; Richter, B.; Fischer, M.; Theato, P. Rapid Mercury(II) Removal by Electrospun Sulfur Copolymers. *Polymers* **2016**, *8*, 266.
- (36) Abraham, A. M.; Kumar, S. V.; Alhassan, S. M. Porous sulphur copolymer for gas-phase mercury removal and thermal insulation. *Chem. Eng. J.* **2018**, *332*, 1–7.
- (37) Mann, M.; Kruger, J. E.; Andari, F.; McErlean, J.; Gascooke, J. R.; Smith, J. A.; Worthington, M. J. H.; McKinley, C. C. C.; Campbell, J. A.; Lewis, D. A.; Hasell, T.; Perkins, M. V.; Chalker, J. M. Sulfur Polymer Composites as Controlled-Release Fertilisers. *Org. Biomol. Chem.* **2019**, *17*, 1929–1936.
- (38) Yu, Q.; Zhang, R.; Deng, S.; Huang, J.; Yu, G. Sorption of perfluorooctane sulfonate and perfluorooctanoate on activated carbons and resin: Kinetic and isotherm study. *Water Res.* **2009**, *43*, 1150–1158.
- (39) Chen, W.; Zhang, X.; Mamadiev, M.; Wang, Z. Sorption of perfluorooctane sulfonate and perfluorooctanoate on polyacrylonitrile fiber-derived activated carbon fibers: in comparison with activated carbon. *RSC Adv.* **2017**, *7*, 927–938.
- (40) Shoemaker, J. A.; Grimmett, P. E.; Boutin, B. K. *Determination of Selected Perfluorinated Alkyl Acids in Drinking Water by Solid Phase Extraction and Liquid Chromatography/Tandem Mass Spectrometry (LC/MS/MS)*; EPA/600/R-08/092; United States Environmental Protection Agency: Washington, DC, 2009.
- (41) Jain, A.; Balasubramanian, R.; Srinivasan, M. P. Hydrothermal conversion of biomass waste to activated carbon with high porosity: A review. *Chem. Eng. J.* **2016**, *283*, 789–805.
- (42) Meier, M. A. R.; Metzger, J. O.; Schubert, U. S. Plant oil renewable resources as green alternatives in polymer science. *Chem. Soc. Rev.* **2007**, *36*, 1788–1802.
- (43) Sweetman, M. J.; May, S.; Mebberson, N.; Pendleton, P.; Vasilev, K.; Plush, S. E.; Hayball, J. D. Activated Carbon, Carbon Nanotubes and Graphene: Materials and Composites for Advanced Water Purification. *C* **2017**, *3*, 18.
- (44) Sweetman, M. J.; Sebben, D.; Noll, B. D.; Wang, W. H.; May, S.; Mebberson, N.; Plush, S. E.; Hayball, J. D. A rapid technique to determine performance and efficiency of activated carbon water filters. *Water Sci. Technol.: Water Supply* **2018**, *18*, 371–382.
- (45) Wang, Z.; DeWitt, J. C.; Higgins, C. P.; Cousins, I. T. A Never-Ending Story of Per- and Polyfluoroalkyl Substances (PFASs)? *Environ. Sci. Technol.* **2017**, *51*, 2508–2518.
- (46) Xiao, F. Emerging poly- and perfluoroalkyl substances in the aquatic environment: A review of current literature. *Water Res.* **2017**, *124*, 482–495.

4.0 Reactive compression moulding

4.1 Acknowledgements

Alfrets Tikoalu for assistance with composite synthesis and compression testing. Sam Tonkin for running three-point bending tests on composites. Dr. Max Worthington for running ^1H NMR samples. Christopher Gibson for Raman spectroscopy. Louisa Esdaile for developing and optimising the up scaling of polymer synthesis. Jonathan Campbell for DMA analysis and instrument training. Dr. Filip Stojcevski and Prof. Luke C. Henderson for supplying waste carbon fibre for composite synthesis, running nano-indentation analysis as well as contact angle experiments on carbon fibre composites. Dr. Amir Karton for calculating BDE's using high level ab initio methods for $\text{Me-S}_n\text{-Me}$ species of varying n .

4.2 Abstract

Sulfur polymers prepared by inverse vulcanisation have found use in a number of important applications including energy storage, infrared optics, repairable materials, environmental remediation, and fertilizers.⁵⁶ Despite this large number of applications, efficient methods for recycling and repurposing these polymers must still be established. This study will investigate the use of a new process, termed reactive compression moulding, to recycle and repurpose sulfur polymers prepared using inverse vulcanisation. Reactive compression moulding involves bringing the polysulfides reactive interfaces into direct contact through mechanical compression whilst applying heat to initiate S-S exchange. This process was shown to occur at temperatures as low as 70 °C. Mechanically sound polysulfide mats and bricks were formed rapidly (10 minutes) under compression at 100 °C. Previous studies used inverse vulcanised polymers capable of melt processing. As these processes aren't compatible with thermoset sulfur polymers new strategies must be investigated. Reactive compression moulding is unique in that it facilitates the recycling of thermoset sulfur polymers through the solid phase. Heat or compression alone were not capable of facilitating the recycling and reforming of these materials making this a novel concept in the field of sulfur polymer manipulation. Experimental results were complimented by high-level ab initio calculations which revealed a linear decrease of the weakest S-S bonds energy as the sulfur rank of the polysulfide increased from 2-4. The bond energy remained relatively constant ($\sim 100 \text{ kJ mol}^{-1}$) for polysulfides of higher sulfur ranks. This information is vital for engineering sulfur polymers for S-S metathesis. Using this information, the repair, recycling, and repurposing of sulfur polymers into new composite was demonstrated.

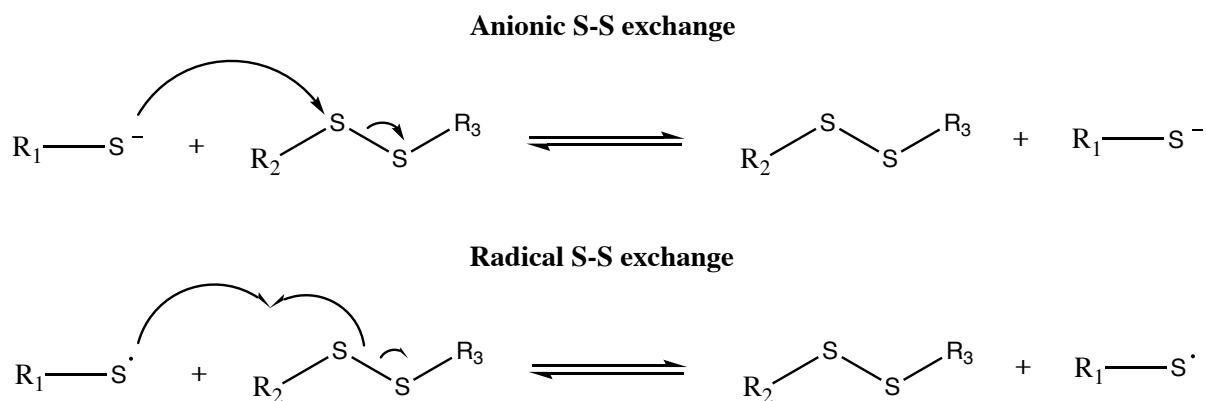
4.3 Introduction

4.3.1 Recycling of thermoset polymers

Whilst the preparation of materials from sustainable resources is important, designing efficient recycling, reforming and re-use strategies is equally as important to achieve maximum sustainability. Polymeric materials can be categorised as either thermoplastic or thermoset polymers. Thermoplastics can undergo melt processing to be recycled, reformed and re-used in new applications. Thermoset polymers are not capable of melting and therefore cannot be recycled, reformed or re-used using melt processing techniques. This means they are typically not recycled and at the end of their life they are subjected to chemical degradation, incineration or combined with another material to form a new composite.²⁵¹⁻²⁵³ Thermoset polymers are typically disposed of in landfills due to the lack of practical repurposing or recycling strategies available. Poly(*S-r*-canola) polymers are thermoset polymeric materials that are insoluble in most organic solvents. This means typical melt and solvent processing methods are non-applicable. This chapter will investigate methods to facilitate the moulding of poly(*S-r*-canola) particles into new materials.

4.3.2 Exchangeable cross-linkers

Encouraging advances in the repair, recycling and reforming of waste polymeric materials have been facilitated by chemically reversible or exchangeable cross-linkers.²⁵⁴ Sulfide or sulfur exchange is a reaction whereby disulfide bonds react with other disulfide bonds resulting in an exchange of chemical bonds.^{255, 256} Due to the low costs and useful chemical properties of sulfur, this reaction is of particular interest.²⁵⁴ Sulfur exchange can occur via both anionic exchange and radical exchange mechanisms (Figure 79) and has been extensively studied for healing applications of materials containing disulfide bonds. Anionic sulfur exchange must be initiated by attack from a thiolate ion, which was generated through treatment with a base or addition of a catalyst.²⁵⁷ The radical sulfur exchange is initiated by the homolytic cleavage of a S-S bonds followed by radical transfer and crossover reactions.²⁵⁷



Where R_1, R_2, R_3 = Alkyl, Aryl and H groups

Figure 79 - Mechanisms of sulfur exchange in disulfides

The cleavage is typically induced by radical initiators, heat or as a photochemical response to light. This process has been reported to occur without initiators at room temperature for aromatic disulfides.¹⁶⁸ Odriozola *et al.* investigated the use of bis(4-aminophenyl) disulfide as a dynamic cross-linker for poly(urea-urethane) elastomers demonstrating significant self-healing capabilities at room temperature without the addition of a catalyst or heat.¹⁶⁸ Simple contact for 2 hours between two cut pieces of this material resulted in self-healing and after 24 hours the mechanical properties were equivalent to the unbroken counterpart.¹⁶⁸ Room temperature healing by the application of pressure is useful however this has only been demonstrated with aromatic disulfides and not higher sulfur rank polymers. Many of these room temperature self-healing materials rely on a secondary interaction to aid or template the healing process such as hydrogen bonding. UV light radiation,^{173, 258} chemical initiators¹⁶⁹⁻¹⁷¹ and heat²⁵⁹ have been investigated for inducing sulfur exchange in S-S containing materials. For a polymeric material to be recycled on a large scale, the process must be fast, simple, low cost and be capable of reforming the material into new shapes and sizes. UV radiation becomes difficult to use when the material needs to be reformed at the same time. In this case, the set up used to mould the material would have to be transparent to UV light. Once compressed the light will also have difficulty reaching the inner bulk material leading to the sulfur exchange reaction only occurring on the surface exposed to the light and not in the bulk material. Radical initiators are also not ideal for recycling purposes as they must be separated from the final product reducing simplicity and increasing process time. Thermal initiation is the favoured method for reforming and recycling applications due to its simplicity, speed, and compatibility with simple compression methods. With the recent advent of inverse vulcanisation high sulfur content polymers are beginning to find use in a wide variety of applications. These materials

contain high percentages of S-S bonds suggesting that sulfur exchange could be utilized to repair and heal them. Some studies have investigated this potential, as discussed next.^{32, 88, 164, 177, 180, 181, 260, 261}

4.3.3 Use of sulfur exchange reaction in polymers made via inverse vulcanization

Various applications involving sulfur exchange in polymers prepared by inverse vulcanisation have been investigated.^{32, 88, 164, 167, 177, 180, 181, 260-263} Applications investigated include methods to facilitate the repair and recycling of sulfur polymers,^{88, 164, 177, 180, 181, 260, 261} the insertion of different monomers into the backbone of sulfur pre-polymers,²⁶² delayed curing systems²⁶³ and new adhesive materials.¹⁶⁷ Most of these studies used heat to initiate the exchange reaction however chemical initiators have also been investigated.¹⁶⁷ Recycling and repair strategies are important for increasing the lifetime of a material and its effective use within an application. Griebel *et al.* used inverse vulcanisation to prepare thermally healable optical polymers for mid-IR range thermal imaging applications. This allowed for surface defects and scratches to be repaired through thermal treatment allowing for their IR imaging performance to be restored after damage.⁸⁸ This combined with the unique optical properties of S-S bonds give these polymers a unique advantage over current germanium or chalcogenide optical lenses making them a viable alternative.⁸⁸ Thermally initiated S-S exchange has also been investigated in the recycling, self-healing and re-forming of inverse vulcanised polymers prepared from polybenzoxazines,²⁶⁴ poly(4-allyloxystyrene),¹⁷⁷ oleic acid (with zinc oxide),¹⁷⁸ MMA-POSS,¹⁷⁶ span 80 (further crosslinked with diphenyl- methane 4, 4'-diisocyanate (MDI))²⁶⁵ and polybenzoxazines/polybutadiene/sulfur copolymers.²⁶⁶ In each case, higher sulfur content tended to impart the best repair qualities. This suggests that the average sulfur rank plays an important role in the ability of these materials to be recycled using thermal annealing. Whilst these thermal methods are effective, they also require high temperatures to facilitate the process. To initiate the repair at room temperature Tonkin *et al.* used phosphine or amine catalysts as chemical initiators.¹⁶⁷ They demonstrated that chemical initiation of sulfur exchange at room temperature only occurred for sulfur rank of 2 or higher, and that weakly nucleophilic catalysts such as triethylamine and pyridine required a sulfur rank of 3 or higher.¹⁶⁷ Composite materials prepared from sulfur polymers have also been investigated for self-healing materials. Zhang *et al.* demonstrated that a composite consisting of sulfur polymer and liquid metal is capable of healing itself at room temperature. However the mechanism behind this repair is due to attractive interaction between the metal and the polymer and not S-S bond exchange.²⁶⁷ The dynamic S-S bonds have also been recognised as a potential route to achieving more complex

properties in these materials. For instance, some studies have utilized the dynamic sulfur exchange reaction to insert new monomers into the polysulfide backbone to create a new terpolymer material.^{262, 268} This strategy has several benefits to it including the ability to include monomers that were incapable of undergoing inverse vulcanisation due to thermal degradation at the higher temperatures.^{262, 268} Whilst these studies are important steps in creating repairable and healable materials, these processes are typically only applicable to thermoplastics or composites and don't provide practical examples whereby these processes could be implemented for the recycling of thermoset sulfur polymers. One example of such a polymer is the 50-poly(S-*r*-canola) thermoset polymer. Whilst it has found several important applications, a sufficient strategy for recycling it after use has yet to be determined. To ensure maximum viability of the recycling process, thermal methods of initiating sulfur exchange were investigated with the intent to design a sustainable method for recycling sulfur polymers after use.

4.3.4 Reactive compression moulding

To enhance the sustainability of thermoset sulfur polymers, new innovative recycling/repair strategies must be investigated. Earlier chapters have focused on the synthesis and environmental remediation applications of 50-poly(S-*r*-canola). To further extend the lifetime of this material and increase its sustainability, a new method of thermal recycling was investigated. Previous recycling methods used for sulfur polymers proceed through a molten state.¹⁸⁰ This strategy is not applicable to thermoset polysulfides such as 50-poly(S-*r*-canola) due to their inability to melt. We hypothesized that the high S-S bond content would facilitate a polysulfide exchange reaction between neighboring polysulfide chains upon heating. By applying compression, 50-poly(S-*r*-canola) particle surfaces are forced into direct contact. The application of heat would then facilitate a sulfur exchange reaction between the surfaces of neighboring particles effectively annealing them together. This process is termed reactive compression moulding and is depicted in Figure 80 below.

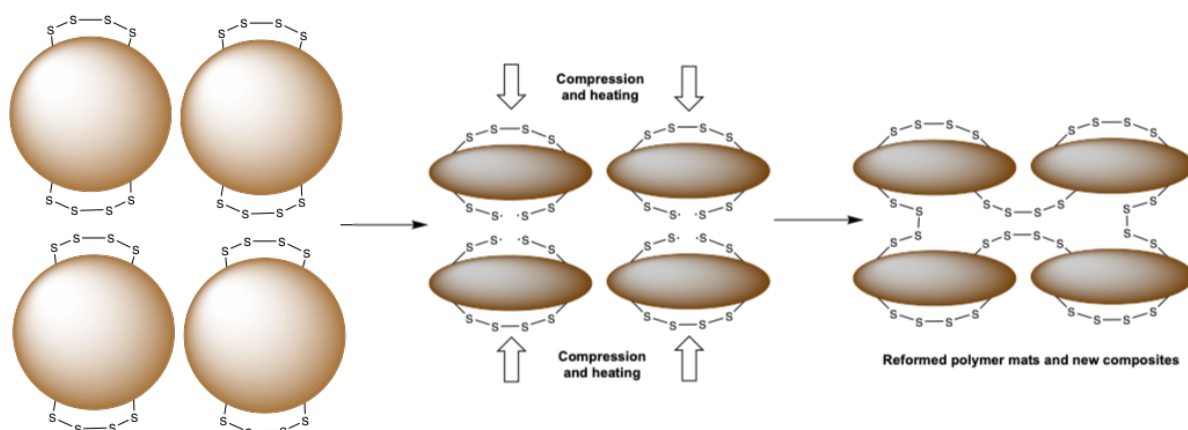


Figure 80 – Figure showing the reactive compression moulding process

Compression moulding has been used to mould waste into forms suitable for use in construction.^{269, 270} Reactive compression moulding was investigated as a potential method by which waste 50-poly(*S-r*-canola) could be recycled into bricks, mats and useful composite materials. Reactive compression moulding differs from traditional compression methods as it would result in chemical bonding and not simply physical reshaping the material. It was also suspected that the process would occur at temperatures lower than required for its synthesis due to sulfur bonds being weaker in polysulfides than in elemental sulfur.²⁷¹

4.3.5 Composite preparation using reactive compression moulding

The unique properties of sulfur polymers have resulted in a wide variety of potential applications. Whilst these polymers have interesting chemical properties, their use in most applications could be significantly improved if the mechanical properties were better controlled.¹⁹³ Sulfur polymers have been investigated previously for their use in the formation of composite materials. Most studies investigating sulfur polymer composite materials revolved around improving their efficiency in lithium sulfur batteries. These studies typically combine sulfur polymers with carbon materials, such as single- and multi-wall carbon nanotubes,²⁷²⁻²⁷⁵ porous carbon nanobelts,²⁷⁶ porous carbon spheres,^{55, 56} graphene²⁷⁷ and carbon nano-fibres.²⁷⁸ These composites were mostly prepared with the intention to reduce the negative impact of lithium polysulfide shuttling on cathode efficiency. The addition of carbon not only helps to reduce the shuttling effect, but it also increases the cathodes conductivity. Another strategy used to counteract the low conductivities of the sulfur polymers was to prepare composite materials with other conductive polymers. Examples of conductive polymers that have been investigated in sulfur polymer composites include polypyrrole, PEDOT:PSS, polyaniline and dehydrogenated polyacrylonitrile.^{275, 279-282} Sulfur polymers have also been utilised in the formation of composite materials with nanoparticles including Au,

InP/ZnS quantum dots, Fe₃O₄, CoO and PbS nanoparticles.¹¹¹ Another intriguing application of sulfur polymer composites was demonstrated by Mann *et al.* It was shown that by encapsulating NPK fertilizer inside 50-poly(S-*r*-canola) polymer, a composite material was formed which demonstrated effective use as a slow release fertilizer.⁹⁷ One typical application of composite materials is as sustainable construction materials. This application has not been studied extensively for sulfur polymer composites, but the similarity to sulfur cement portends to the use of sulfur polymers in construction in the future.²⁸³ Other uses for sulfur in construction materials include as a mortar to produce prefabricated brick panels²⁸⁴ and in foamed sulfur-gypsum mixtures to produce a stronger lightweight wallboard material.²⁸⁴ Whilst all these examples demonstrate sulfur composites in construction the composites are all prepared by addition of filler particles during the synthesis of the polymer. This effectively encapsulates the filler material within the sulfur polymer. However, this approach has several limitations. Firstly, it requires high temperatures (140-180 °C) restricting the possible filler materials to those that can withstand these high temperatures. Secondly these composites can only be made during the synthesis of the sulfur polymer. To repurpose waste sulfur polymer into composite materials for construction, the composite preparation must be able to occur post-synthesis. Therefore, a new method must be established to facilitate an efficient recycling process for used sulfur polymers. Reactive compression moulding, discussed above, could facilitate the preparation of composite materials directly from high sulfur content polymers and the desired filler material. This method would have several benefits including lower temperatures than what was used in the original polymers synthesis, no solvents or catalysts would be required, and the composite preparation could be achieved, potentially, in a matter of minutes. Another important benefit of this process is that filler materials that degrade at the high synthesis temperatures can still be incorporated into the material. Due to the 50-poly(S-*r*-canola) polymers ability to undergo reactive compression moulding its use in the preparation of composite materials with varying filler materials was investigated. 50-Poly(S-*r*-canola) has been investigated, both directly as a sorbent and indirectly as a sorbent support material, for the remediation of several different pollutants. To enhance the sorbent materials sustainability, the ability to potentially lock the contaminated material inside larger blocks of material using reactive compression moulding was also investigated. This would serve to prevent leaching of the pollutant during both storage and transport of the contaminated waste. It would also make the final product safer for handling. Therefore on-top of facilitating a simple method by which sulfur polymers can be recycled, re-used and reformed, reactive compression moulding can

also be used to lock pollutants into blocks preventing further contamination during transport and storage.

4.4 Experimental

4.4.1 General considerations

4.4.1.1 UV/Vis Spectroscopy analysis

UV/Vis spectroscopy was performed using an Agilent Technologies Cary 60 UV-Vis spectrometer. Disposable 2 mL cuvettes were used for each measurement. A sample size of 2 ml was used for each measurement. All measurements were initially referenced to pure water before sample measurement. Fe(III) concentration was monitored at 306 nm.

4.4.1.2 SEM and EDX analysis

Scanning Electron Microscopy (SEM) images were obtained using an FEI F50 Inspect system, while corresponding EDS spectra were obtained using an EDAX Octane Pro detector. All samples were coated with 10 nm of platinum before imaging.

4.4.1.3 ¹H NMR analysis

Proton nuclear magnetic resonance (¹H NMR) were recorded on a 600 MHz spectrometer. All chemical shifts are quoted on the δ scale in ppm using residual solvent as the internal standard (¹H NMR: CDCl₃ δ = 7.26, C₅D₅N δ = 7.22, 7.58, 8.74). Max Worthington assisted with all ¹H NMR analysis.

4.4.1.4 STA analysis

Thermogravimetric analysis (TGA) and differential scanning calorimetry (DSC) were carried out on a 449 F5 Jupiter simultaneous thermal analyser. A sample size between 4-5 mg was used in each run. The furnace was purged at 20 mL/min with nitrogen and equilibrated for 1 minute at 30 °C before each run. Heating was carried out up to 600 °C using a 20 °C/min heating rate. The temperature was held isothermally at 600 °C at the end of each experiment to oxidize remaining organic matter.

4.4.1.5 DMA analysis

For compression testing, samples were loaded onto the compression clamp on a Q800 dynamic mechanical analyser, and the measurement was carried out in triplicate at room temperature (\pm 20 °C) with the ramp force at 3 N/min to 18 N. Compressive stress (σ) was obtained by dividing applied force (F_S) by a cross sectional area (A) of the composites. All 3-point bending tests were performed on a TA Q800 dynamic mechanical analyser using a 60 mm wide 3-point bending clamp. The DMA controlled force module was used with a force ramp rate of 0.2 N/

min to a maximum of 18 N. Temperature control was not used, with polymer composites maintained at room temperature (approximately 20 °C). Each composite was tested in triplicate along with a control of a polymer mat with no filler. These measurements were performed together with Alfrets Tikoalu, a masters student in our lab.

4.4.2 First generation reactive compression moulding

4.4.2.1 Reactive compression moulding of 50-poly(S-*r*-canola)

PTFE sheets were placed on top of two 14.5 × 14.5 cm aluminium sheets to prevent the polymer from sticking to the metal. 20.0 grams of 50-poly(S-*r*-canola) was added in between the PTFE sheets and C-clamps were used to create pressure on the polymer particles and force the reactive faces together. The initial volume of the polysulfide before compression was ~160 cm³. This system was then added into an oven at 110 °C for 24 hours. After 24 hours the system was removed from the oven and left to cool back to room temperature in a fume hood. Once cool, the C-clamps were loosened, and the polymer mat was removed.

4.4.2.2 Heat treated 50-poly(S-*r*-canola) with no compression

30.0 grams of canola oil polysulfide were added to a 100 mL beaker. This beaker was added to the oven and left to sit for 24 hours at a temperature of 110 °C. After 24 hours the beaker was removed from the oven and left to cool to room temperature.

4.4.2.3 Reactive compression moulding of 50-poly(S-*r*-canola) at varying temperatures

A PTFE sheet was placed on top of a 14.5 × 14.5 cm square metal plate followed by 20.5 grams of 50-poly(S-*r*-canola). A second PTFE baking sheet was placed on top the canola oil polysulfide before another 14.5 × 14.5 cm metal plate was used to sandwich the polysulfide between it and the first metal sheet. C-clamps were then applied to the four corners of these sheets to create pressure on the polysulfide between them. This entire setup was then placed into an oven at 110 °C for 24 hours. After which time the setup was removed from the oven and left to cool to room temperature. Once at room temperature the C-clamps were removed, and the metal sheets separated revealing the canola oil polysulfide mat that resulted. This process was repeated at temperatures of 80, 90 and 100 °C.

4.4.3 Second generation reactive compression moulding

4.4.3.1 Reactive compression moulding varying reaction times (100 °C, 30 MPa, 1-360 minutes)

A 10 × 10 cm PTFE sheet was added to the aluminium mould shown below. On top of the PTFE sheet, 5.0 grams of canola oil polysulfide was added, followed by a second PTFE sheet. The lid for the mould was added and the whole system was placed into the S15 Devil Press 10-ton hydraulic heated press pre-heated to 100 °C. The heat plates were pressed until they were in contact with the mould without applying any pressure. Once the temperature stabilized at 100 °C the pressure was increased to 30 MPa. This pressure was maintained for 1 minute before being released and the resulting polysulfide mat then removed from the mould. This process was repeated using times of 5 minutes, 10 minutes, 30 minutes, 60 minutes, 120 minutes, 240 minutes, and 360 minutes.

4.4.3.2 Reactive compression moulding at 100 °C for 10 minutes varying pressure

A 10 × 10 cm PTFE sheet was added to the mould followed by 5.0 grams of 50-poly(*S-r*-canola) polymer and another PTFE sheet. The lid for the mould was added and the whole system was placed into the S15 Devil Press 10-ton hydraulic heated press pre-heated to 100 °C. The heat plates were pressed until they were in contact with the mould without applying any pressure. Once the temperature stabilized at 100 °C the pressure was increased up to 10 MPa. This pressure was maintained for 10 minutes before being released and the resulting polysulfide mat then removed from the mould. This process was repeated using pressures of 0, 20, 30 and 40 MPa. For the 0 MPa sample, the mould was placed in an oven preheated to 100 °C so there was no added pressure other than the lid of the mould.

4.4.3.3 Reactive compression moulding at 90 °C for 10 minutes varying pressure

A 10 × 10 cm PTFE sheet was added to the mould followed by 5.0 grams of 50-poly(*S-r*-canola) polymer and another PTFE sheet. The lid for the mould was added and the whole system was placed into the S15 Devil Press 10-ton hydraulic heated press pre-heated to 90 °C. The hot plates were pressed until they were in contact with the mould without applying any pressure. Once the temperature stabilized at 90 °C the pressure was increased up to 10 MPa. This pressure was maintained for 10 minutes before being released and the resulting polysulfide mat then removed from the mould. This process was repeated using pressures of 20, 30 and 40 MPa.

4.4.3.4 Reactive compression moulding at 40 MPa for 10 minutes varying temperature

A 10 × 10 cm PTFE sheet was added to the mould, followed by 5.0 grams of 50-poly(*S-r*-canola) and then another PTFE sheet. The lid for the mould was added and the whole system was placed into the S15 Devils Press 10-ton hydraulic heated press pre-heated to 100 °C. The heat plates were pressed until they were in contact with the mould without applying any pressure. Once the temperature stabilized at 100 °C the pressure was increased to 40 MPa. This pressure was maintained for 10 minutes before being released and the resulting polysulfide mat then removed from the mould. This process was repeated using temperatures of 70, 80 and 90 °C.

4.4.4 Effect of free sulfur and formation of high sulfur content surface layer

4.4.4.1 Free sulfur calibration curve using quantitative DSC

The area between 100 °C and 150 °C in the DSC of elemental sulfur correspond to the specific phase transitions for sulfur allotropes (rhombic and monoclinic phase). The first endothermic peak at ~104 °C corresponds to the phase transition from rhombic to monoclinic while the second endothermic peak at ~118 °C corresponds to the melting of those phases into liquid sulfur. The area of these peaks increases linearly with sulfur mass. Within the range tested, on average 1 mg of elemental sulfur had a heat flow value of 50 J/g. This allows a calibration curve to be constructed for the estimation of free sulfur content in the polymers.

4.4.4.2 Reactive compression moulding for 30-poly(*S-r*-canola) and comparison to 50-poly(*S-r*-canola)

A 10 × 10 cm PTFE sheet was added to the mould, followed by 5.0 g of either 30-poly(*S-r*-canola) or 50-poly(*S-r*-canola). Another PTFE sheet was added along with the mould lid. The whole system was placed into the S15 Devil Press pre-heated to 100 °C. The hot plates were pressed until they were in contact with the mould without applying any pressure. Once the temperature stabilized at 100 °C the pressure was increased up to 40 MPa. This pressure was maintained for 20 minutes before releasing and removing and the polymer mat.

4.4.4.3 Negative control: Reactive compression moulding of sulfur and canola oil at optimized conditions

A 10 × 10 cm PTFE sheet was added to the mould, followed by 2.5 grams of canola oil and 2.5 grams of sulfur. Another PTFE sheet was added and then the lid was placed on the mould. The whole system was placed into the S15 Devil Press, pre-heated to 100 °C. The hot plates were

brought into contact with the mould. Once the temperature stabilized at 100 °C, the pressure was increased to 40 MPa. This pressure was maintained for 10 minutes before removing the mould.

4.4.5 Recycling, reforming and re-use facilitated by reactive compression moulding

4.4.5.1 Recycling by reactive compression moulding

A polymer mat was made from 50-poly(*S-r*-canola) using the optimized reactive compression moulding procedure (4.3.4.2). The resulting mat was then ground up into small pieces and then added back into the mould between two PTFE sheets. The reactive compression moulding was then repeated to provide a new mat.

4.4.5.2 Treatment of FeCl_{3(aq)} solution with 50-poly(*S-r*-canola) polymer

A FeCl₃ solution was prepared by dissolving 50 mg of anhydrous FeCl₃ in 1.0 L of distilled water. A 2.0 mL aliquot of this sample was transferred into a plastic cuvette for analysis using UV / Vis spectroscopy at 306 nm. After analysis this solution was returned to the bulk solution. To this 1 L solution, 250 g of 50-poly(*S-r*-canola) was added along with a 40 × 15 mm magnetic stir bar. This mixture was placed onto a magnetic stir plate and stirred at 500 rpm for 24 hours. After 24 hours the 50-poly(*S-r*-canola) was filtered using a water aspirator and left to dry overnight in the fume hood. A 2 mL sample of the remaining solution was transferred into a plastic cuvette and analysed using UV / Vis spectroscopy at 306 nm. The concentration of the iron was calculated using a calibration curve prepared in chapter 2.

4.4.5.3 Repurposing spent 50-poly(*S-r*-canola) contaminated with Fe(III)

The recovered and dried polymer from 4.3.5.2 was processed into a mat by reactive compression moulding. The polymer was placed in the mould between two PTFE sheets. The lid for the mould was added and the whole system was placed into the S15 Devil Press, preheated to 100 °C. The hot plates were pressed until they were in contact with the mould without applying any pressure. Once the temperature stabilized at 100 °C the pressure was increased up to 40 MPa. This pressure was maintained for 10 minutes before removing the polymer mat from the mould.

4.4.5.4 Reactive compression moulding of 50-poly(*S-r*-canola) on a 15.0 g scale

15.0 g of 50-poly(*S-r*-canola) was placed into the mould between two PTFE sheets. The mould was then placed in the S15 Devil Press, preheated to 100 °C. The hot plates were pressed until they were in contact with the mould without applying any pressure. Once the temperature

stabilized at 100 °C the pressure was increased up to 40 MPa. The pressure dropped initially to below 30 MPa (due to compression of material) and was instantly increased back up to 40 MPa. This pressure was maintained for 20 minutes before removing the polymer mat from the mould.

4.4.5.5 Nano-indentation testing on 15.0 gram 50-poly(S-*r*-canola) mat

Nano-indentation testing was conducted using a Bruker Ti-950 Triboindenter. Of these points only 8 provided valid data measurements thereby providing a 40% test success rate. During testing it was noted that the high porosity and inhomogeneous nature of the material caused differences in depth penetration to occur. Depth penetration was stopped when the needle tip reached a maximum compressive force of 98 (± 0.08) μN . These measurements were recorded by Dr. Filip Stojcevski in Prof. Luke C. Henderson's lab at the institute of frontier materials at Deakin University.

4.4.6 Composite material preparation facilitated by reactive compression moulding

4.4.6.1 Preparation of composites made from 50-poly(S-*r*-canola) and coconut coir, sand, and polyvinylchloride (PVC) waste

First, the 50-poly(S-*r*-canola) (particle size diameter ≤ 2.5 mm) and the filler were mixed in plastic container. For coconut coir composite, the total wt% of the coconut coir was 50, 60 or 70%, with the remaining mass the 50-poly(S-*r*-canola). For PVC, the total wt% was 50, 60, 70, or 80% of PVC shavings, with the remaining mass the 50-poly(S-*r*-canola). To form the composite mats, the 50-poly(S-*r*-canola) and filler mixtures were placed between two PTFE sheets in the mould and processed as described in previously. These composites were prepared together with Alfrets Tikoalu, a masters student in our lab.

4.4.6.2 Additive assembly of composite mats

Three coconut coir composites mats made from 50 wt% coconut coir and 50 wt% 50-poly(S-*r*-canola) were prepared as described above. Next these mats were bonded together by a second reactive compression moulding process where powdered 50-poly(S-*r*-canola) was used as a binder for the mats. Accordingly, 100 mg of powdered 50-poly(S-*r*-canola) was placed between each mat and then the entire stack was placed in the mould between two PTFE sheets. Reactive compression moulding was then carried out as in 4.3.6.1. All three mats were bonded together in the process. The mould was removed from the press and the resulting mat was separated from the PTFE sheets. These composites were prepared together with Alfrets Tikoalu, a masters student in our lab.

4.4.6.3 Young's Modulus for compression measurements

50-Poly(*S-r*-canola) mats and the composites were cut into squares (~1 cm²). The composite samples were then loaded onto the compression clamp in a Dynamic Mechanical Analyzer Q800 machine, and the measurements were carried out in triplicate at room temperature (± 20 °C) with the ramp force at 3 N/min to 18 N. Compressive stress (σ) was obtained by dividing applied force (F_s) by a cross sectional area (A) of the composites (equation 6). Strain (ε) is a unit less number obtained from the change of length (dL) over the initial length (L_0) of the tested composite (Equation 2). As shown in Equation 3, the Young's modulus for compression can be calculated by dividing the stress (σ) by strain (ε). These measurements were prepared together with Alfrets Tikoalu, a master's student in our lab.

$$\sigma = \frac{F_s}{A} \quad \text{Equation 6}$$

$$\varepsilon = \frac{dL}{L_0} \quad \text{Equation 7}$$

$$E = \frac{\sigma}{\varepsilon} \quad \text{Equation 8}$$

4.4.6.4 Three-point bending test

Polymer composites were cut with a sharp scalpel into 70 mm \times 10 mm pieces. Three pieces were cut from distinct parts of each mat. The 50-poly(*S-r*-canola) composites tested were PVC (50-80 wt%), coconut coir (50-70 wt%) and sand (70-80 wt%). All 3-point bending tests were performed on a TA Q800 dynamic mechanical analyser using a 60 mm wide 3-point bending clamp. The DMA controlled force module was used with a force ramp rate of 0.2 N/ min to a maximum of 18 N. Temperature control was not used, with polymer composites maintained at room temperature (approximately 20 °C). Each composite was tested in triplicate along with a control sample consisting of a 50-poly(*S-r*-canola) polymer mat with no filler. These measurements were prepared together with Sam Tonkin, an honors student in our lab.

4.4.6.5 Preparation of 50-poly(*S-r*-canola) composites using waste carbon fibre

4.5 grams of powdered carbon fibre waste was combined with 11.5 grams of powdered 50-poly(*S-r*-canola) polymer in a plastic container. The container was inverted 10 times to mix the two materials. This mixture was added to the 10 cm \times 10 cm stainless steel mould in between 2 PTFE sheets. The mould was added to the press and preheated to 100 °C. Once the temperature stabilized, the pressure was increased to 40 MPa and the system was left to react for 20 minutes. After 20 minutes the pressure was relieved, and the mould was removed from

the press. The resulting composite mat was then removed from the mould and separated from the PTFE sheets.

4.4.6.6 Contact angle testing on 50-poly(*S-r*-canola) and composites made using carbon fibre powder

Contact angle testing was conducted using an Attension Contact Angle Theta unit. Deionized water ($\gamma_L=72.8$ mN/m, $\gamma_L^D=22$ mN/m, $\gamma_L^P=50.7$ mN/m), glycerol ($\gamma_L=63.4$ mN/m, $\gamma_L^D=37$ mN/m, $\gamma_L^P=26.4$ mN/m) and ethanol ($\gamma_L=21.4$ mN/m, $\gamma_L^D=18.8$ mN/m, $\gamma_L^P=2.6$ mN/m) were used with droplet sizes of 3.5 μ L to determine the effects of varying surface energy polarities on the polymer or composite surface. These measurements were recorded by Dr. Filip Stojcevski in Prof. Luke C. Henderson's lab at the institute of frontier materials at Deakin University.

4.4.7 Confining spent pollution sorbents in a safe medium

4.4.7.1 Lead sorption using the polymer-carbon blend

A solution of Pb^{2+} was prepared by adding 250 mg of $Pb(NO_3)_2$ to a 500 mL volumetric flask and dissolving in deionized water. After diluting to the 500 mL mark, an aliquot of the solution was filtered (25 μ m nylon syringe filter), and the concentration was measured to be 560 ppm by ICP-MS by Envirolab Services Pty Ltd., with accreditation by the National Association of Testing Authorities, Australia (NATA Accreditation Number 2901). 250 mL of the Pb^{2+} solution was added to a 1.0 L plastic container along with 20 g of the polymer-carbon blend. The mixture was stirred for 1 hour at 20 °C. After 1 hour, 10 mL of the treated solution was transferred, through a syringe filter (25 μ m, nylon), into a glass storage container for analysis. The carbon-polymer blend was isolated by filtration and left to dry in a fume hood for 24 hours.

4.4.7.2 Lead sorption using 50-poly(*S-r*-canola) polymer

100 mL of the Pb^{2+} solution (above) was added to a 1 L plastic container along with 6.4 g of 50-poly(*S-r*-canola). The mixture was stirred for 1 hour at 20 °C. After 1 hour, 10 mL of the treated solution was transferred, through a syringe filter (25 μ m, nylon), into a glass storage container for analysis. The carbon-polymer blend was isolated by filtration and left to dry in a fume hood for 24 hours. The final lead concentration was measured by ICP-MS using a certified commercial service as described above.

4.4.7.3 Confinement via reactive compression moulding

Polymer mats were prepared from 50-poly(*S-r*-canola) by reactive compression moulding, as previously described in 4.4.4.2. In short, 5.0 g of the powdered 50-poly(*S-r*-canola) was placed between two PTFE sheets in a 10 × 10 cm mould. The mould was placed in a pressure controlled heated press then processed at 100 °C and 40 MPa for 10 min. The resulting polymer mats were then used as a barrier in which the spent polymer-carbon sorbent could be contained. To encapsulate the spent sorbent, one of the pre-formed polymer mats was placed on a PTFE sheet in the mould. Next, the polymer-carbon blend (5.0 g of the spent sorbent bound to lead) was placed in the center of one of the pre-formed polymer mats. Then, 2.0 g of powdered 50-poly(*S-r*-canola) was added around the perimeter of the mat. Next, the top polymer mat was added, followed by another PTFE sheet. The mould was placed in the heat- and pressure-controlled press and then processed at 100 °C and 40 MPa for 10 min. After cooling to room temperature, the polymer-encapsulated sorbent was removed from the mould and tested in leaching experiments.

4.4.7.4 Leaching experiment on spent sorbent

All leaching tests were carried out in triplicate. A 1.0 g sample of the spent polymer-carbon blend (with bound Pb²⁺) was added to a 50 mL plastic centrifuge tube along with 50 mL of deionized water. The sealed tubes were mixed at 20 °C using an end-over-end mixer operating at 25 rpm. After 1 week, the water was filtered (25 µm nylon syringe filter) determination of the lead concentration by ICP-MS.

4.4.7.5 Leaching experiment on encapsulated blend sorbent

All leaching tests were carried out in triplicate. The polymer mats encapsulating the spent sorbent were submerged in 250 mL of water in a 500 mL plastic container. The sealed container was placed on a rocker table at 20 °C for 8 weeks. The water was sampled and filtered (25 µm nylon syringe filter) at 1 and 8 weeks followed by determination of lead concentration by ICP-MS.

4.5 Results and discussion

4.5.1 First-generation reactive compression moulding

To facilitate the moulding of 50-poly(*S-r*-canola) polysulfide particles the effects of heat was investigated. Firstly 20 g of the 50-poly(*S-r*-canola) polymer was placed in a beaker and incubated in an oven at 110 °C for 24 hours. The resulting powder had darkened in color however it remained in powdered form suggesting that no melting process occurred under these conditions (Figure 81). It was noted that there were some small aggregates of powder particles that formed, however even these aggregates were not bound together strongly and fell apart back into a free-flowing powder when handled. This illustrated the need for more than high temperatures to facilitate the moulding and recycling of these materials.



Figure 81 – Images showing 50-poly(*S-r*-canola) before (left) and after (right) being heated for 24 hours at 110 °C.

It was hypothesized that the reactive S-S groups on the polymer surface were not in sufficient contact to undergo S-S exchange. This experiment was repeated with compression to force the reactive surfaces into direct contact to gain maximum binding between particles. In this experiment, 20 g of powdered 50-poly(*S-r*-canola) was compressed between two metal plates using C-clamps (Figure 82B). To prevent adhesion to the metal plates, PTFE sheets were placed between the polymer and the metal plates. The polymer, now compressed between the two metal plates, was placed into an oven at 110 °C for 24 hours. This time the individual polymer particles had bound together to form the flexible rubber mat shown in Figure 82D.



Figure 82 – **A)** 50-poly(*S-r*-canola) particles on a metal sheet separated by PTFE paper. **B)** Compression system used to compress the 50-poly(*S-r*-canola) particles into direct contact. **C)** Section of mat prepared using reactive compression moulding. **D)** Image demonstrating the flexibility of the mats.

^1H NMR analysis (Figure 83) was undertaken to investigate any chemical changes which may have occurred throughout moulding. Assignment of peaks is shown in Figure 84.⁷ Pyridine- d_5 was used as a solvent for the ^1H NMR analysis of the 50-poly(*S-r*-canola) polymer samples. Pyridine has been shown to trigger sulfur-sulfur exchange in polymers prepared through inverse vulcanisation.¹⁶⁷ This reaction results in the cleavage of the S-S bonds in the polymer, which allow it to be dissolved. The ^1H NMR spectrum is actually the products that result from the cleavage of the S-S cross-links in 50-poly(*S-r*-canola).¹⁶⁷

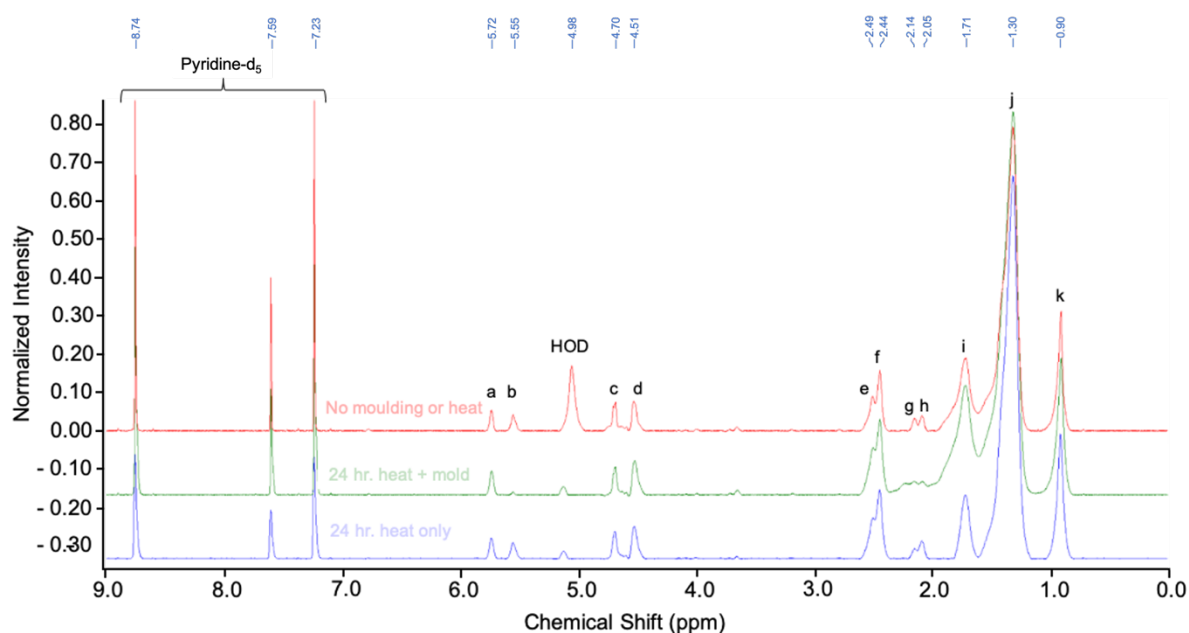


Figure 83 – ^1H NMR spectrum for 50-poly(*S-r*-canola) before and after moulding at $110\text{ }^\circ\text{C}$ for 24 hours (600 MHz, pyridine- d_5): $\delta = 8.74, 7.59, 7.23$ (**pyridine- d_5**), 5.72 (**a**), 5.55 (**b**), 4.98 (**HOD**), 4.70 (**c**), 4.51 (**d**), 2.50 (**e**), 2.44 (**f**), 2.14 (**g**), 2.05 (**h**), 1.71 (**i**), 1.30 (**j**), 0.90 (**k**).

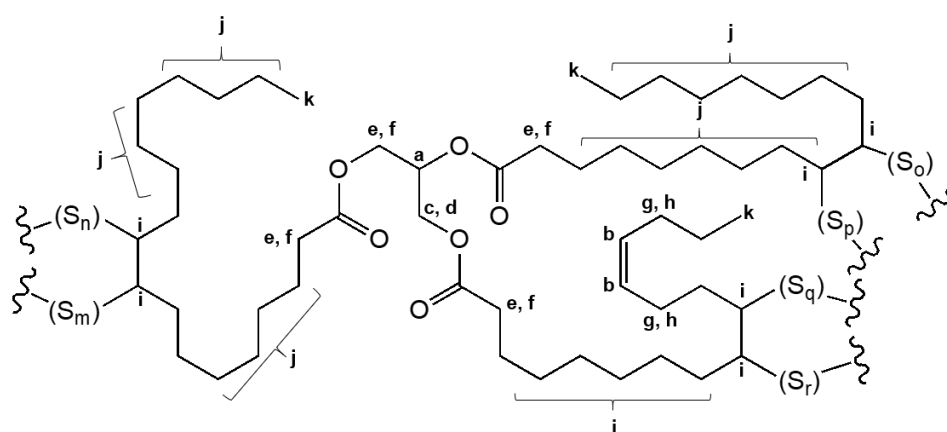


Figure 84 – Peak assignments for poly(*S-r*-canola)⁷

Analysis revealed that after 24 hours the peak occurring at 5.55 ppm (**a**) and the twin peaks occurring at 2.14 ppm (**g**) and 2.05 ppm (**h**) have practically disappeared. These peaks

correspond to the hydrogens bound to unreacted alkene groups remaining in the 50-poly(*S-r*-canola) material. The sulfur exchange reaction initiated by heat and pressure not only allows for moulding of these materials, but it also facilitated the full consumption of remaining alkenes. This is consistent with the hypothesis that heat would induce homolytic cleavage of the S-S bonds forming sulfur radicals that recombine or react further with unreacted alkene comonomers. It should also be noted that the alkene peaks were not consumed when the polymer was incubated in a beaker for 24 hours at 110 °C without undergoing compression. This suggests that the major reaction is sulfur exchange, but the addition of the thiyl radical to any remaining alkenes can also occur. The compression acts to facilitate direct contact with reactive interfaces resulting in a higher percentage of active reaction sites. This suggests that the compression has a large effect on the rate of both sulfur exchange and sulfur-alkene reactions. To test the effects of temperature, this procedure was repeated using the simple C-clamp compression method at 80, 90 and 100 °C for 24 hours. Images of the resulting mats are shown in Figure 85 below.

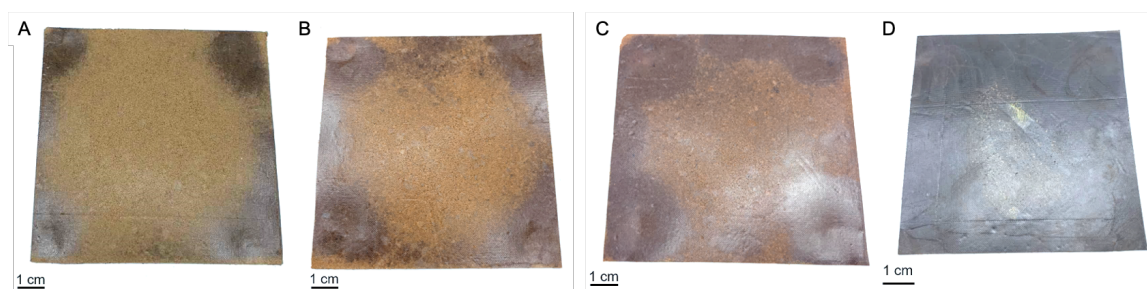


Figure 85 – 50-poly(*S-r*-canola) sheet after 24 hours of reactive compression moulding at **A)** 80 °C, **B)** 90 °C, **C)** 100 °C, **D)** 110 °C.

Reactive compression moulding occurred at all temperatures investigated however a clear difference in reaction rates was observed with the 100 °C sample showing the highest extent of reaction. This reactivity was observed by the darkened color of the mat and higher tensile strength of the material in that area. It was observed that the highest extent of reaction was occurring for all samples directly under the location in which the c-clamps were applying direct pressure to the system. This is highlighted in Figure 86.

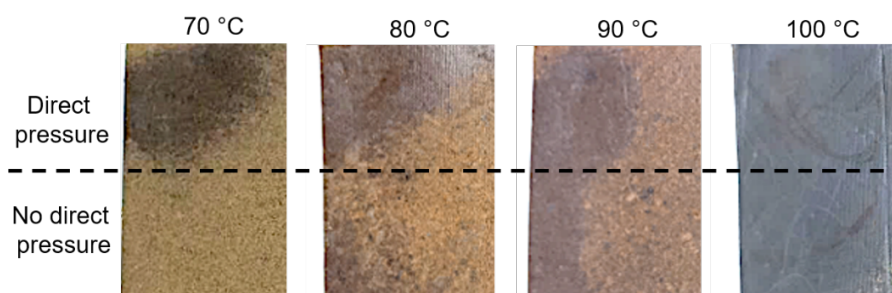


Figure 86 – Figure showing zoomed in sections of mats formed at varying temperatures, highlighting the regions where pressure was and wasn't applied directly.

This further suggests that the pressure plays an important role in both controlling the reaction rate of the process as well as producing a uniform final material.

4.5.2 Second-generation reactive compression moulding

Discovering the importance of controlling the pressure, a S15 Devil Press Hydraulic 10-ton dual heating plates rosin press wax extractor was used for subsequent experiments (Figure 87). This system allowed for control of applied pressure (0 - 60 MPa), uniform pressure application and temperature control.

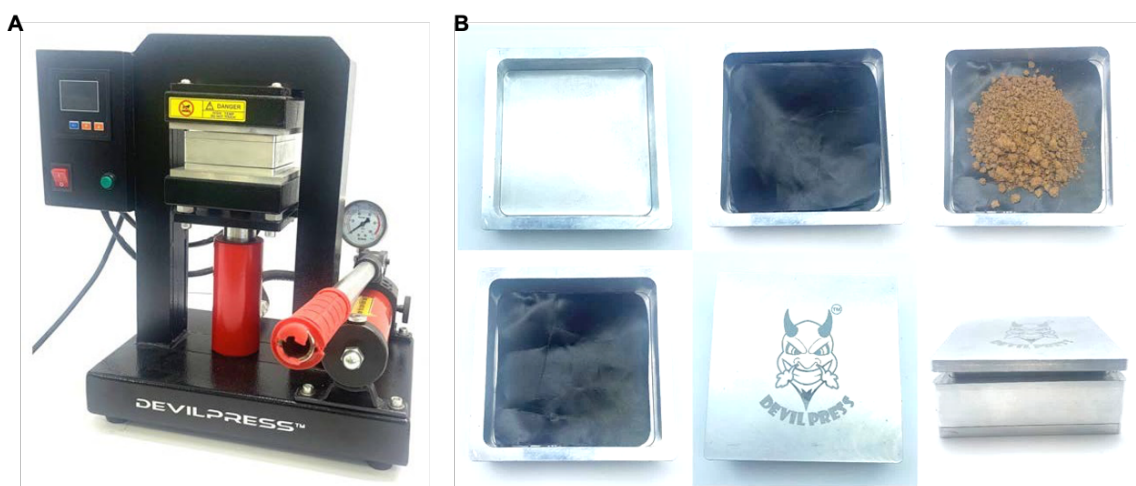


Figure 87 – A) S15 Devil Press Hydraulic 10-ton dual heating plates rosin press wax extractor used for reactive compression moulding. B) Images demonstrating the process of placing the 50-poly(S-*r*-canola) into the mould separated from direct contact by PTFE sheets.

A stainless-steel mould (10 cm × 10 cm) was lined with PTFE sheets before addition of 5.0 g of 50-poly(S-*r*-canola). The mould, now containing the 50-poly(S-*r*-canola) particles was added into the S15 Devils press which was pre-heated to 100 °C. The system was left to equilibrate until the mould became isothermal at 100 °C. The pressure was increased to 10 MPa and the system was left for 10 minutes. After ten minutes the mould was removed from the heated press, the mould was opened, and the product was removed and separated from the

PTFE sheets. It was observed that the individual particles had been effectively moulded into a flexible rubber 50-poly(*S-r*-canola) mat (Figure 88).



Figure 88 – Image showing 50-poly(*S-r*-canola) before and after moulding for 10 minutes at 10 MPa, 100 °C.

4.5.3 Optimizing reaction conditions

To optimize the process, the pressure, temperature, and reaction time were all varied. Initially, the effect of pressure was investigated by performing the process over 10 minutes at 100 °C. The resulting mats are shown in Figure 89.

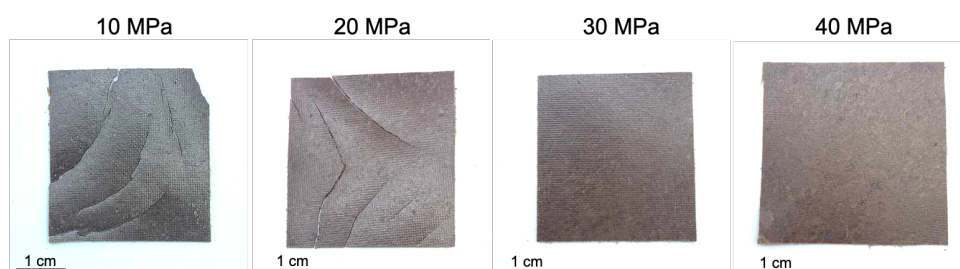


Figure 89 – Images of mats formed at varying pressures at 100 °C.

In agreement with initial experiments, the sample with zero applied pressure did not change visually and remained a powder. Application of at least 10 MPa of pressure led to the formation of a relatively uniform polymer mat. Although the mats prepared at 10, 20 and 30 MPa pressure still formed they typically contained small cracks or defects. Only those formed under 40 MPa pressure consistently formed mats without cracks or mechanical defects. It's important to note that whilst the reactive compression moulding process works at the lower pressures, the emphasis in this study is on optimizing the time required to form a stable mat consistently.

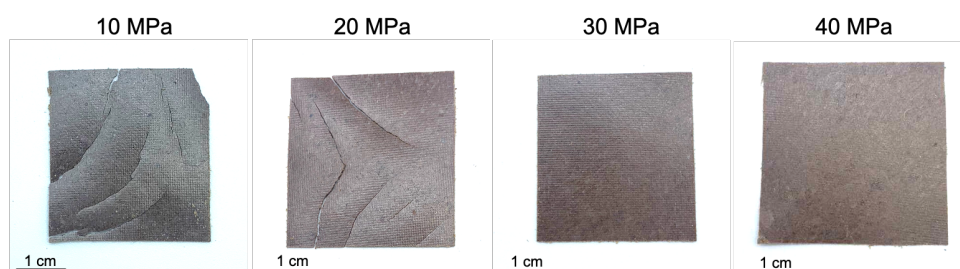


Figure 90 – Images of mats prepared using varying the pressure at 90 °C.

This process was repeated using a reaction temperature of 90 °C (Figure 90). As was the case at 100 °C, the extent of binding and the mechanical stability of the resulting mat seemed to increase with pressure. It was observed that both the 10 and 20 MPa mats formed however large cracks and structural defects were observed. This jeopardized the mechanical stability of the mat and made it undesirable for practical use. The sample prepared at 30 MPa had very small barely visible cracks however the mat produced at 40 MPa did not have any major structural defects or cracks observable. To further investigate the effect of temperature on forming mechanically sound 50-poly(*S-r*-canola) mats, the moulding process was repeated varying the temperature between 70 – 100 °C (Figure 91).

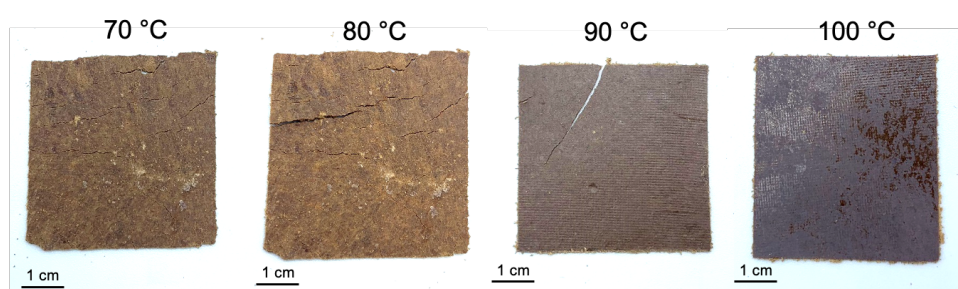
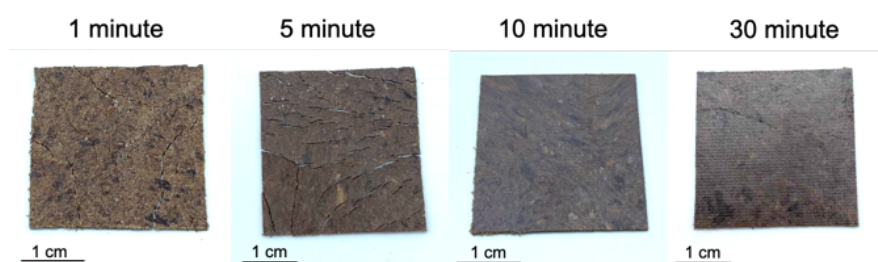


Figure 91 - Images of mats prepared varying the reaction temperature.

Binding of polymer particles was observed to occur under compression at temperatures as low as 70 °C. Although a mat was formed at all temperatures, those formed under 90 °C contained significant cracks and defects. The mat formed at 90 °C didn't contain any cracks upon opening the mould however the mat wasn't as strong and cracked upon removal of the PTFE sheet. For use in practical applications, limited cracking and structural defects must be present. Therefore, for consistency in producing mechanical sound defect free mats, a temperature of 100 °C is required. Another key point to raise is that whilst it is likely that 70 °C is enough to form a crack/defect free mat over long reaction times, to increase the viability of the final product the time required to prepare the mat was minimized. It's also important to note that the sulfur exchange reaction occurred at temperatures as low as 70 °C, far lower than temperatures previously reported for sulfur exchange in materials under compression.¹⁸⁶ Finally the reaction time was varied and the resulting mats are shown in Figure 92.



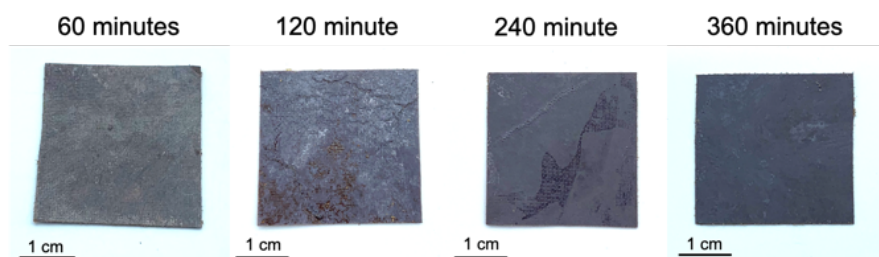


Figure 92 – Images of mats prepared varying the reaction time.

After 1 minute of moulding, it was clear that binding of the polymer particles had occurred however the resulting mat was neither continuous nor uniform. By performing the process for just 10 minutes the resulting mat is mechanically sound with no noticeable defects or cracks. This suggests that 10 minutes heating is enough to form a stable polymer mat under these conditions. To better observe the surfaces of these mats, scanning electron microscopy (SEM) analysis was performed. SEM analysis (Figure 93) revealed the presence of three distinct features across the surface: amorphous polysulfide regions, microtextured crystalline particles and a crystalline surface layer. The amorphous polysulfide regions and the microtextured crystalline particles are typically observed by SEM / EDX analysis of these materials. These crystalline particles have previously been determined to be unreacted sulfur particles.¹⁰⁰ The surface layer, however, was not typically observed under SEM analysis of un-moulded 50-poly(*S-r*-canola) particles. The regions where a surface layer has formed appear visually like the free-sulfur particles also observed. This suggests that the surface layer could potentially be aggregates of free-sulfur particles combining to form a layer on the surface.

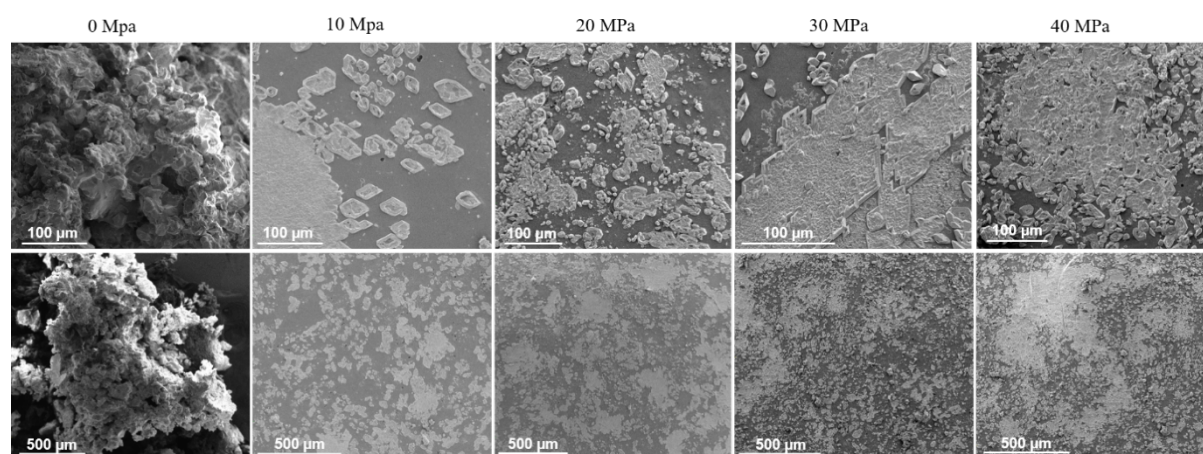


Figure 93 – SEM images at 100 μm and 500 μm for mats formed at 100 °C varying the pressure

The mats formed at 100 °C varying the pressure showed very little difference under SEM (Figure 93). It does appear that the higher pressures resulted in higher surface layer coverage than lower pressures. The sample heated at 0 MPa looked identical to typical 50-poly(*S-r*-canola) particles under SEM.

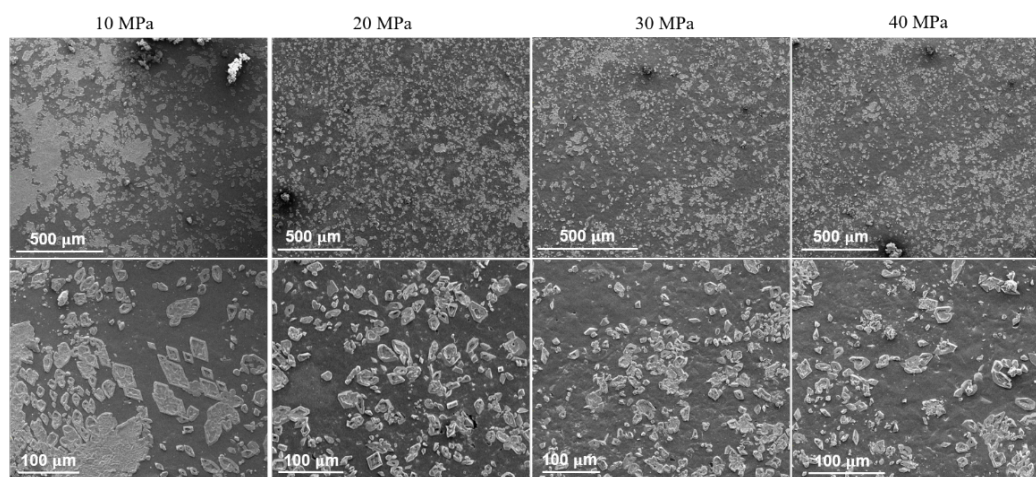


Figure 94 – SEM images at 100 μm and 500 μm for mats formed at 90 $^{\circ}\text{C}$ varying the pressure.

For the same mats formed at 90 $^{\circ}\text{C}$, although some had formed, very little surface coating was observed with a larger extent of free sulfur particles present instead (Figure 94). This suggests that the temperature plays an important role in the surface chemistry resulting from this process.

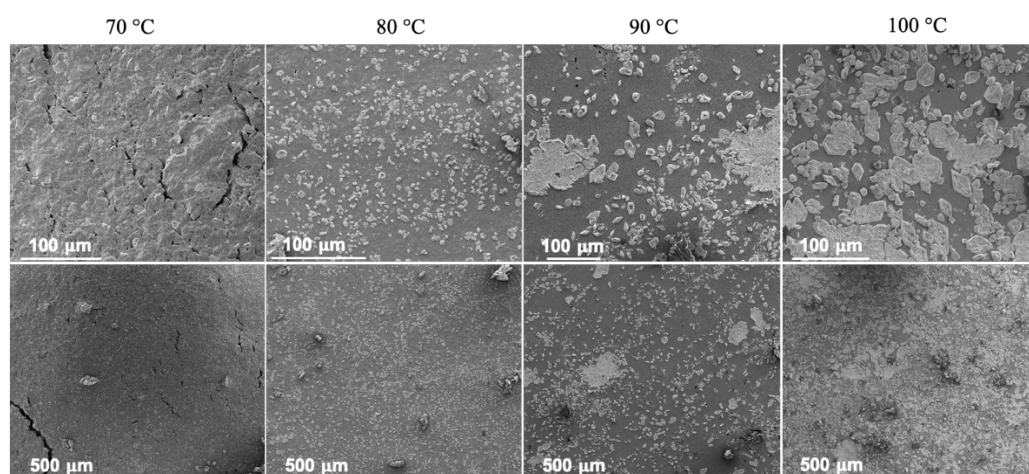


Figure 95 – SEM images at 100 μm and 500 μm for mats formed at varying temperature.

Further evidence for this is given in the SEM images of mats formed at different reaction temperatures (Figure 95). The 70 $^{\circ}\text{C}$ sample shows small crystals of free sulfur embedded in the material with very few on the materials surface. This is similar to the starting material. As the temperature is increased to 80 $^{\circ}\text{C}$ the number of free sulfur particles on the surface increases and small areas of surface coating start forming. By 90 $^{\circ}\text{C}$, larger patches of surface coating start appearing and by 100 $^{\circ}\text{C}$ the surface is largely covered by portions of this coating. Finally SEM analysis of the surface of the mats formed at varying reaction times is shown in Figure 96.

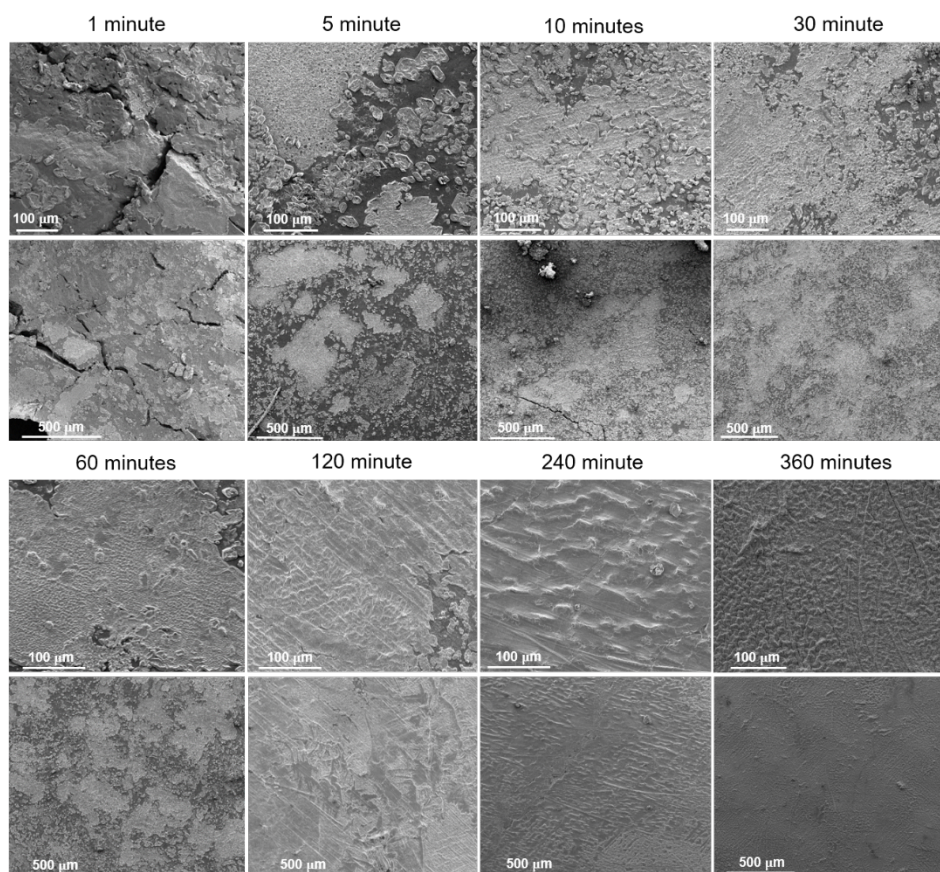


Figure 96 – SEM images at 100 μm and 500 μm for mats formed at varying reaction times.

This suggest that during the reaction, free sulfur particles migrate to the surface of the polymer and overtime combine to form a free sulfur layer on the surface of the material. Next, STA analysis (TGA and DSC) was performed on all samples.

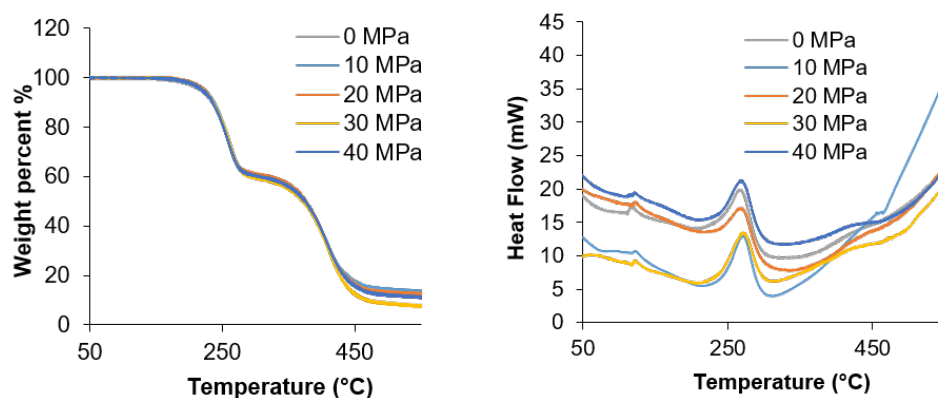


Figure 97 – STA analysis of mats formed when varying pressure at 100 $^{\circ}\text{C}$.

No observable difference was observed between the mats formed at different pressures under TGA and DSC (Figure 97). The difference in heat flow observed for the 10 and 30 MPa samples compared to the rest is likely due to the particle size of the samples. As the poly(*S-r*-canola) materials are thermally insulating, they retain heat. The bulkier the sample the more heat it will

retain, and the less heat energy is required to heat the sample up to the required temperature. This results in a lower heat flow for bulkier samples and is most likely the reason for the observed difference in Figure 98.

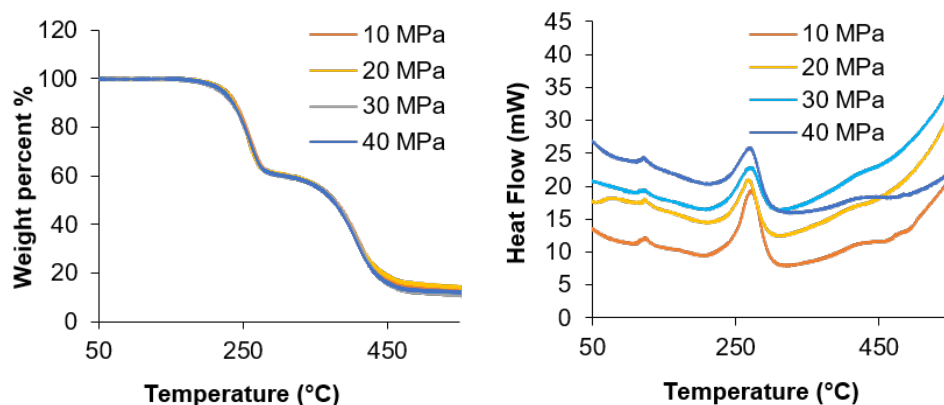


Figure 98 - STA analysis of mats formed when varying reaction pressure at 90 °C.

Matching the results at 100 °C, the pressure had no noticeable effect on the thermal degradation of the materials. The heat flow intensity seems to increase with pressure used. As the 50-poly(*S-r*-canola) material is thermally insulating the particle size and the density are important factors effecting the heat flow intensity. As all samples were roughly the same particle size, this trend could be due to the higher pressure forming higher density mats. The higher the density, the higher the heat flow, as shown above.

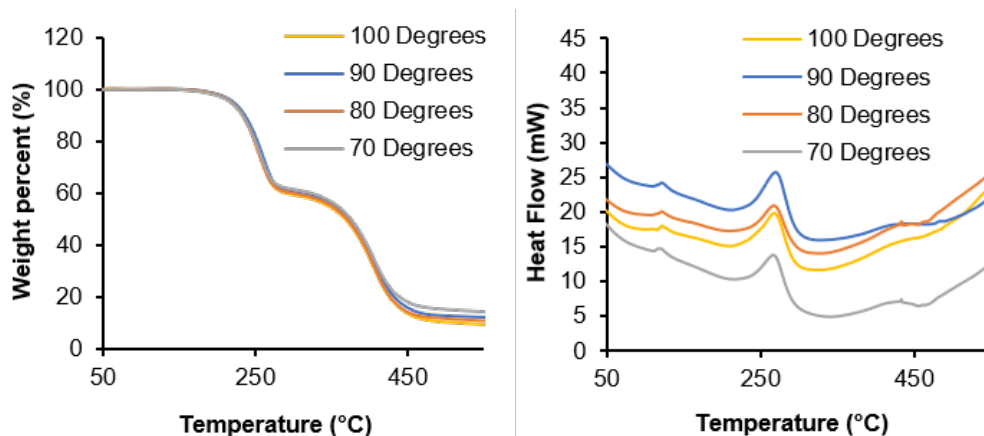


Figure 99 – STA analysis of mats formed when varying reaction temperature.

The temperature of the reaction did not demonstrate any significant effect on the thermal properties of the material (Figure 99). A clear difference was however observed during visual inspection of the mats. As no change is occurring in the thermal properties of the material it suggests that the reaction taking place results in re-formation of the same material. This offers further evidence that S-S exchange is the dominant reaction facilitating the reactive

compression moulding process. Finally, STA analysis of the mats formed under varying reaction times was performed (Figure 100).

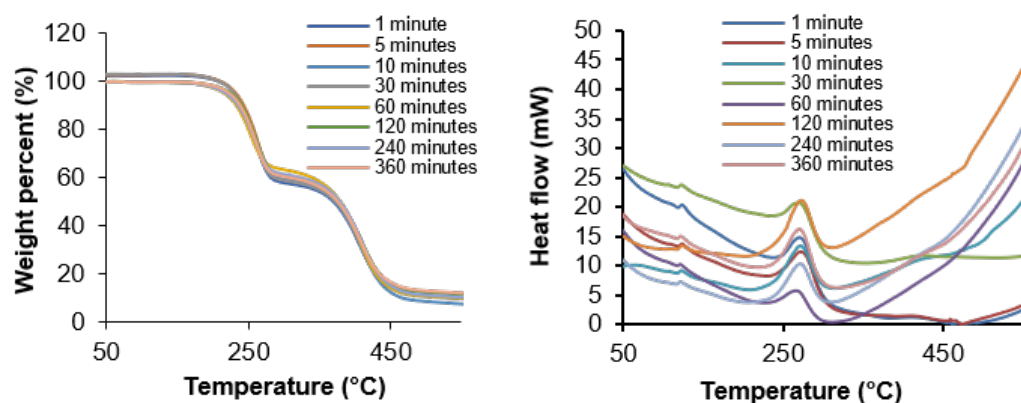


Figure 100 – STA analysis of mats formed when varying the reaction time.

Once again, no significant difference in the TGA plots were observed. All DSC plots demonstrated the same peaks and significant features with the only differences between samples being the heat flow intensity. In general, when altering the moulding conditions, all samples demonstrated almost identical TGA and DSC profiles. The DSC curves for all samples showed the same major features; the endothermic peaks at approximately 120 °C and 230 °C and the gradual increase in heat flow after 330 °C. The two peaks correspond to the melting of unreacted ‘free sulfur’ and the first degradation peak occurring due to the loss of sulfur from S-S bond breaking. The final rise in heat flow corresponds with the beginning of the second major mass loss shown in the TGA. This is likely due to the decomposition of the remaining organic material. The major difference observed between DSC curves was the variation in heat flow intensity. This likely resulted from differences in both sample particles size and density effecting the thermal conductivity of the sample and therefore the heat flow required to heat the sample to the desired temperature. The reactive compression moulding process therefore produces materials with roughly equivalent thermal properties. This observation is due to the sulfur exchange reaction which does not result in an overall change in sulfur rank. Therefore, to first approximation, the structure before and after reactive compression moulding are highly similar. Next to further probe the chemical structure of the resulting products, ^1H NMR analysis was performed, and the results are shown in Figure 101. It revealed that all samples displayed the characteristic peaks of the starting material, 50-poly(S-*r*-canola). The peaks occurring in all samples at 7.22, 7.58 and 8.74 ppm are the peaks characteristic for pyridine- d_5 . The peak that occurs in some samples around 4.96-4.98 ppm are due to HOD. Although no water is present the pyridine- d_5 is anhydrous and likely adsorbed a small amount of water from the

atmosphere upon use. The intensity of this peak likely corresponds to the exposure time the pyridine-d₅ had with the atmosphere before the sample was run.

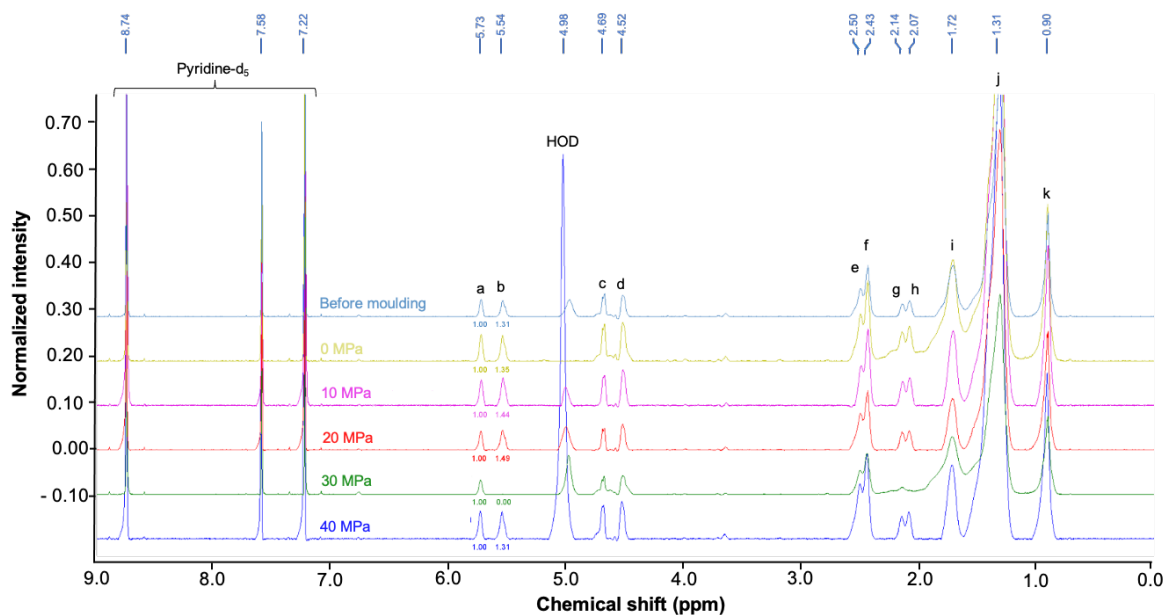


Figure 101 – A) ¹H NMR of samples where pressure was varied at 100 °C. (600 MHz, pyridine-d₅): δ = 8.74, 7.58, 7.22 (**pyridine-d₅**), 5.73 (**a**), 5.54 (**b**), 4.98 (**HOD**), 4.69 (**c**), 4.52 (**d**), 2.50 (**e**), 2.43 (**f**), 2.14 (**g**), 2.07 (**h**), 1.72 (**i**), 1.31 (**j**), 0.9 (**k**).

In the samples prepared at 100 °C and varied pressure, the 30 MPa sample shows some deviation from the rest of the samples with both the twin peaks occurring at 2.1 and 2.3 ppm and the alkene peak at 5.55 ppm are not observed in the 30 MPa sample. This suggest that there are less unreacted alkene groups in this sample than others. This is likely due to the use of a different batch of starting material in which the alkenes had already been consumed. No observable change was seen under ¹H NMR analysis before and after moulding at any pressure. ¹H NMR analysis of the samples prepared at 90 °C and varied pressure is shown below in Figure 102.

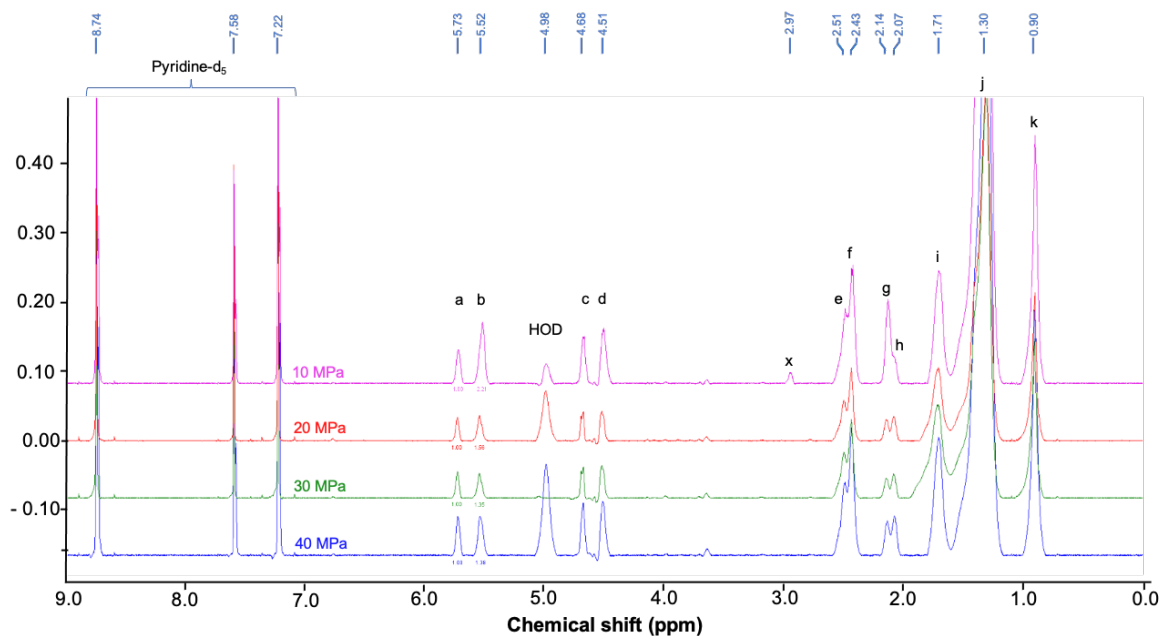


Figure 102 – ^1H NMR of samples where pressure was varied at $90\text{ }^\circ\text{C}$. (600 MHz, pyridine- d_5): $\delta = 8.74, 7.58, 7.22$ (pyridine- d_5), 5.73 (a), 5.52 (b), 4.98 (HOD), 4.68 (c), 4.51 (d), 2.97 (x), 2.51 (e), 2.43 (f), 2.14 (g), 2.07 (h), 1.71 (i), 1.3 (j), 0.9 (k).

Again, when the pressure was adjusted at $90\text{ }^\circ\text{C}$, no significant differences were observed between samples. The 10 MPa sample contained an extra peak (x) at 2.97 ppm. This peak is at a similar chemical shift to the peak seen in the canola oil ^1H NMR corresponding to a CH_2 hydrogen bound to two alkene groups.²⁸⁵ As canola oil contains 12% α -linolenic acid, the presence of this peak as well as an increase in signal b, suggests the extent of reaction between sulfur radicals and alkene groups was lower in this sample than the rest. This could be due to the lower pressure (10 MPa) and temperature ($90\text{ }^\circ\text{C}$) used however the ^1H NMR of starting material and the one formed at 0 MPa do not contain this peak. This suggest that this starting material used to prepare this mat had reacted to a lesser extent and its unlikely that the moulding conditions resulted in this difference. ^1H NMR analysis of the samples prepared at 40 MPa for 10 minutes varying the moulding temperature from $70\text{ }^\circ\text{C}$ to $100\text{ }^\circ\text{C}$ is shown below in Figure 103.

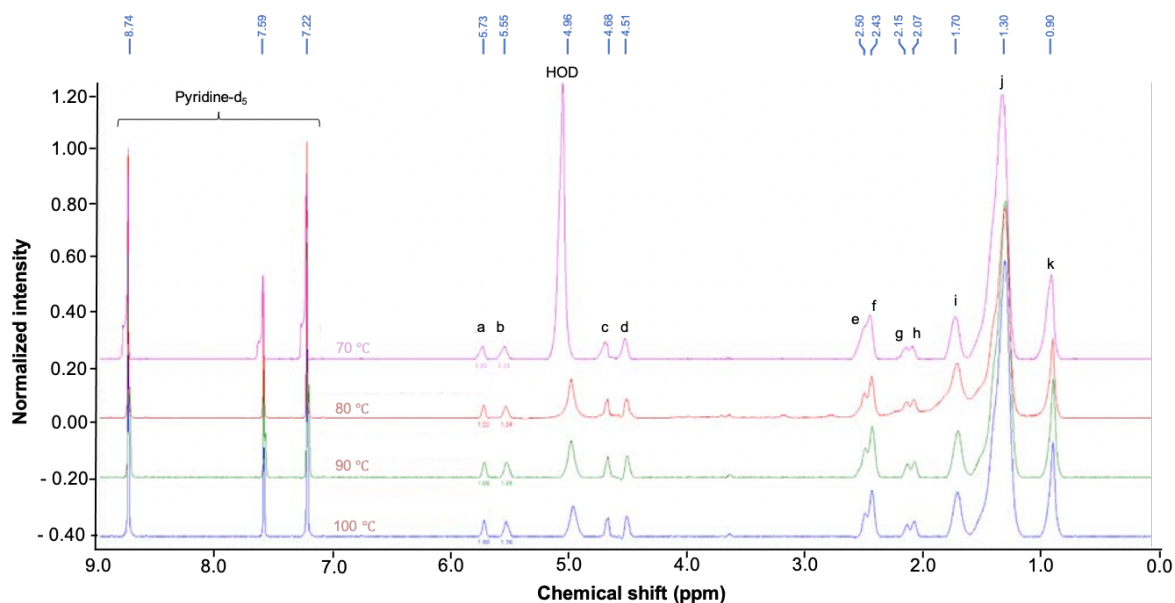


Figure 103 – ¹H NMR of samples where temperature was varied. (600 MHz, pyridine-d₅): δ = 8.74, 7.58, 7.22 (**pyridine-d₅**), 5.73 (**a**), 5.55 (**b**), 4.96 (**HOD**), 4.68 (**c**), 4.51 (**d**), 2.50 (**e**), 2.43 (**f**), 2.15 (**g**), 2.07 (**h**), 1.70 (**i**), 1.30 (**j**), 0.90 (**k**).

No significant difference was observed between the samples prepared at varying temperature. This suggests that within the temperature range investigated the chemical structures of the final product remain the same. ¹H NMR analysis of the samples prepared at 40 MPa and 100 °C varying the moulding reaction time from 1 – 360 minutes is shown below in Figure 104. Over ten minutes moulding time, the reaction temperature was not shown to have a significant effect on the chemical structure of the product. As a reaction must have occurred to bind the mats

together and no difference is observable under ^1H NMR analysis, it suggests that the dominant mechanism involved in the reactive compression moulding process is sulfide exchange.

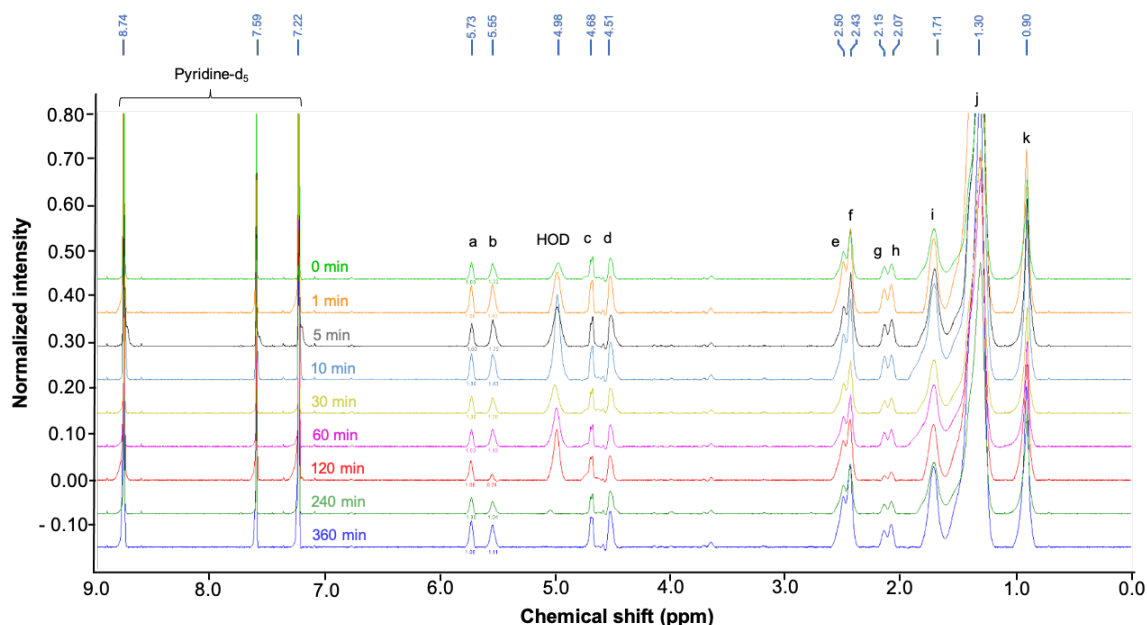


Figure 104 – ^1H NMR of samples where reaction time was varied. (600 MHz, pyridine- d_5): δ = 8.74, 7.59, 7.22 (pyridine- d_5), 5.73 (a), 5.55 (b), 4.98 (HOD), 4.68 (c), 4.51 (d), 2.50 (e), 2.43 (f), 2.15 (g), 2.07 (h), 1.71 (i), 1.3 (j), 0.9 (k).

In general, no significant changes were observed between samples when changing the experimental conditions. These results suggest no further reaction with the unreacted alkenes is occurring, in contrast to when the process was conducted at 110 °C for 24 hours. This offers further evidence that sulfur exchange is the dominant mechanism by which reactive compression moulding occurs. The small differences observed between the spectra are mainly in the alkene related peaks (b, g and h) and the HOD peak. From the information obtained through SEM, STA and ^1H NMR analysis, the optimized reaction condition, with respect to time, was determined to be 10 minutes moulding at 100 °C and 40 MPa. Using these conditions, a mechanically stable mat was able to be formed consistently.

4.5.4 Sulfur surface layer

SEM analysis revealed the formation of a surface layer forming over the course of the moulding process. By 6 hours the coating was observed to uniformly cover the entire surface of the mat. To further characterize this surface layer; Raman spectroscopy, SEM imaging and EDX analysis were performed on the surface and cross-section of the mat formed after reactive compression moulding for 6 hours (Figure 105).

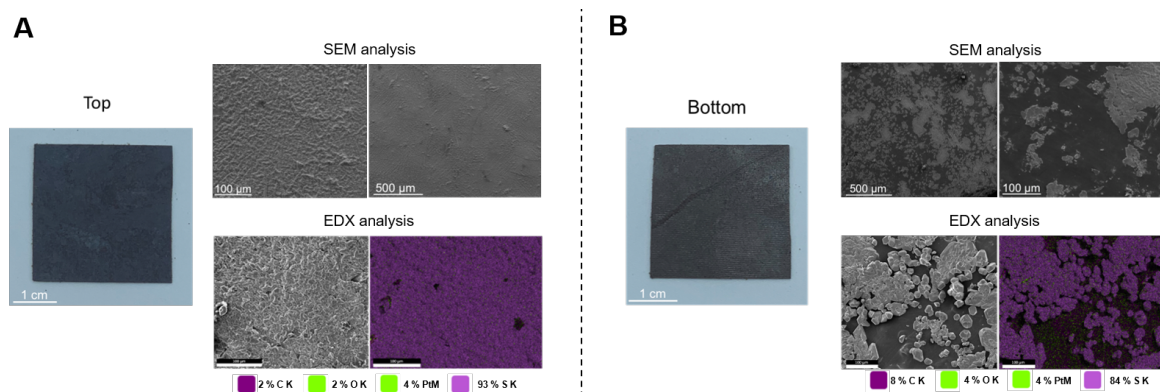


Figure 105 – **A)** Images of the top side of the mat (left), SEM images of surface of mat (right, top), EDX analysis of surface of mat (right, bottom). **B)** Images of the bottom side of the mat (left), SEM images of surface of mat (right, top), EDX analysis of surface of mat (right, bottom).

SEM analysis clearly shows the presence of a uniform surface layer having formed on the mat. It was noted that the surface coverage by this layer is far more uniform for the top side of the mat in comparison to the bottom face. The bottom face of the mat still demonstrated large portions of layer formation however the area covered was significantly less. EDX mapping shows a strong signal for sulfur in the areas where the surface layer had formed and where the free particles were located. The areas in which the free particles and layer are not located, the signals are a combination of carbon, oxygen, and sulfur. This suggests that the surface layer consists entirely of free sulfur particles that overtime combine to form a surface layer. This was supported by Raman analysis (Figure 106) that showed the top surface consisted primarily of elemental sulfur whilst the bottom surface displayed characteristic peaks for both elemental sulfur and 50-poly(*S-r*-canola).

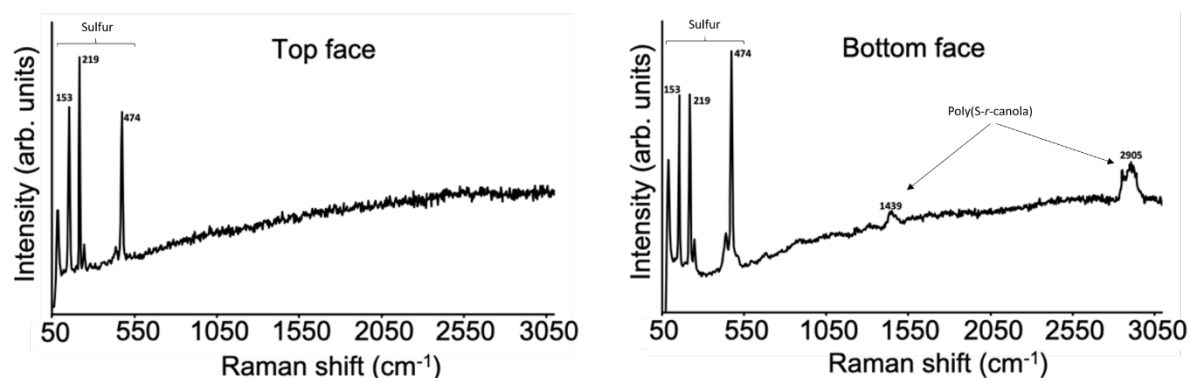


Figure 106 – Raman analysis of top and bottom surface of the polysulfide mat.

This was consistent with the SEM and EDX results. The preferential formation of the free sulfur layer on the top surface of the polymer is evidence towards sublimation potentially being the mechanism driving the migration of free sulfur particles to the top surface of the mat to

form the layer. SEM and EDX analysis of the cross section (Figure 107) revealed a layer thickness of approximately 0.19 μm . It also revealed that free sulfur particles are still present in the bulk of the material.

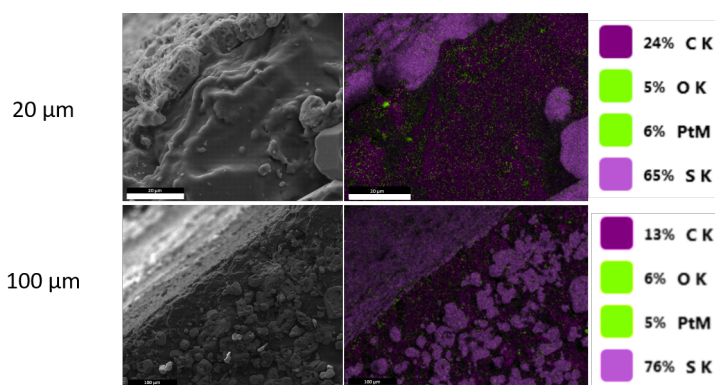


Figure 107 – SEM (left) and EDX (right) analysis of the cross section of 50-poly(*S-r*-canola) mat after reactive compression moulding for 6 hours.

The question then becomes, if this process occurs during moulding, does the free sulfur effect the reactive compression moulding process. To assess this possibility, the process was repeated, under the optimized conditions with 30-poly(*S-r*-canola) polysulfide which has negligible free sulfur content.

4.5.5 Effect of free sulfur on the moulding process

Due to the presence of free sulfur in 50-poly(*S-r*-canola), the effect of its presence on the reactive compression moulding process was investigated. 30-poly(*S-r*-canola) has been previously shown to contain less than 4 % free sulfur content.¹⁰⁰ Therefore, to see whether the reactive compression moulding process effected by the free sulfur content, the process was performed on both 30- and 50-poly(*S-r*-canola) polymers and the resulting mats were analyzed using SEM (Figure 108), STA (Figure 109) and ¹H NMR (Figure 110).

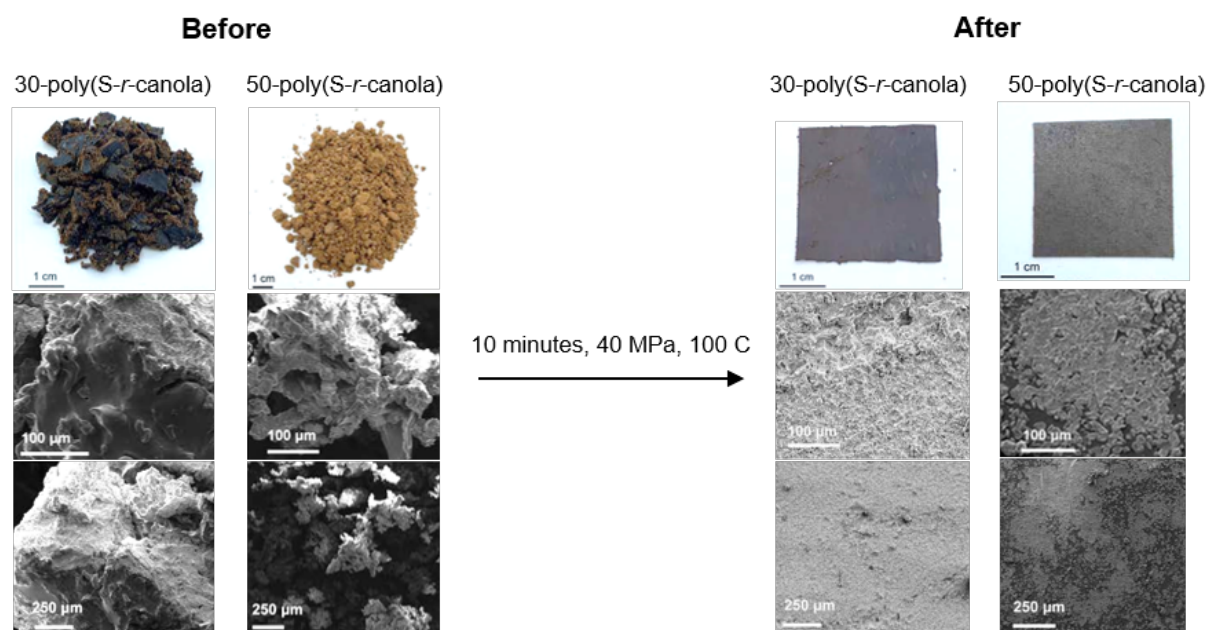


Figure 108 – Images of 30- and 50-poly(S-*r*-canola) before and after moulding at 40 MPa, 100 °C for 10 minutes.

The 30-poly(S-*r*-canola) was shown to undergo the reactive compression moulding process under the same conditions as 50-poly(S-*r*-canola) without an issue. This suggests that the free sulfur doesn't engage in the sulfur exchange reaction used to facilitate the reactive compression moulding process or at very least elemental sulfur is not required for reactive compression moulding. This was expected due to the reaction temperature (100 °C) being far lower than the floor temperature for S₈ (159 °C). The surface of the 30-poly(S-*r*-canola) mat was noted to be far more-sticky than the 50-poly(S-*r*-canola) mats surface, weakly adhering to objects it touched. This could potentially be due to the free sulfur particles on the surface of the 50-poly(S-*r*-canola) polysulfide effectively eliminating the adhesive properties of the 30-poly(S-*r*-canola) mat or it could simply be due to the higher canola oil content altering the surface adhesion properties.

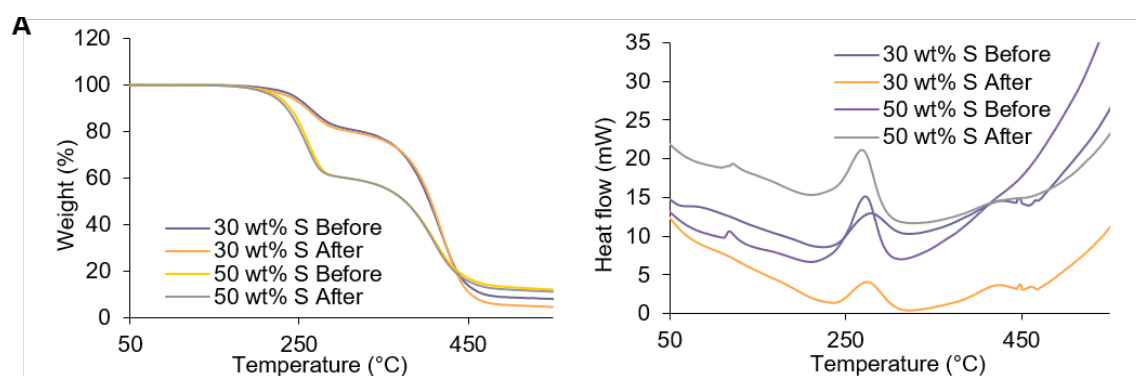


Figure 109 – A) TGA (left) and DSC (right) curves for 30- and 50-poly(S-*r*-canola) polymers before and after moulding,

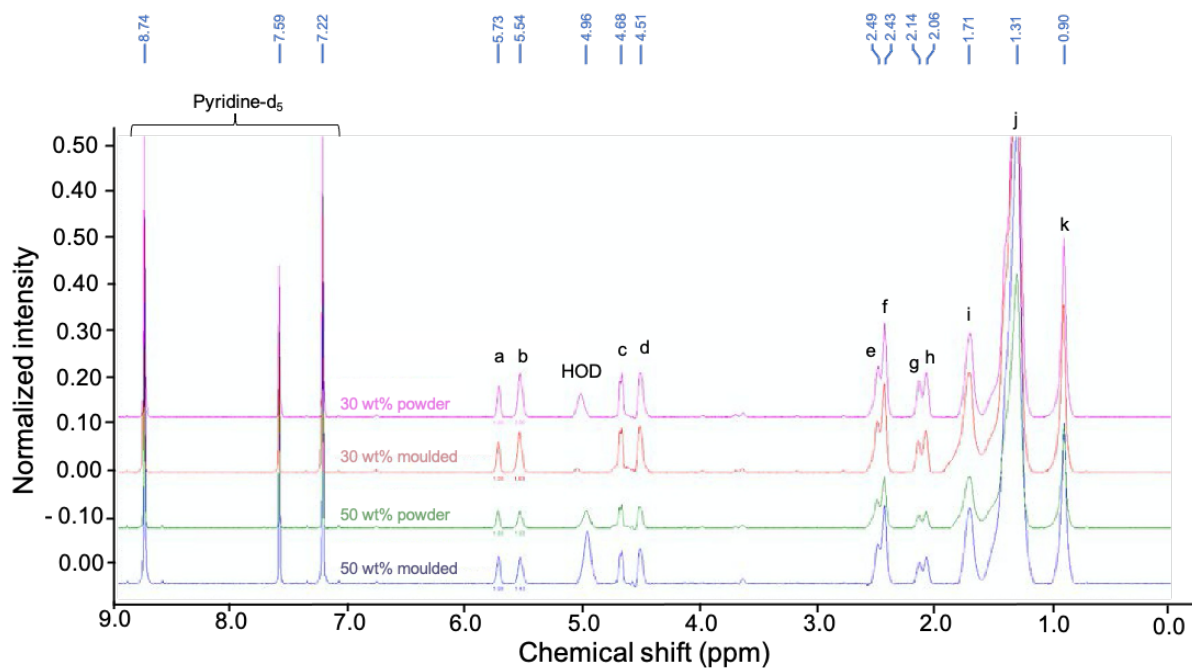


Figure 110 – ^1H NMR spectra for 30- and 50-poly(*S-r*-canola) polymers before and after moulding (600 MHz, pyridine- d_5): δ = 8.74, 7.59, 7.22 (pyridine- d_5), 5.73 (a), 5.54 (b), 4.96 (HOD), 4.68 (c), 4.51 (d), 2.49 (e), 2.43 (f), 2.14 (g), 2.06 (h), 1.71 (i), 1.31 (j), 0.9 (k).

STA analysis was performed on all samples before and after moulding. Both the 30- and the 50-poly(*S-r*-canola) polysulfides demonstrate the same thermal properties before and after moulding. The endothermic peak in the DSC at approximately 120 °C is only present in the 50-poly(*S-r*-canola) polymers. This peak represents the melting transition of S_8 and corresponds to the amount of free sulfur in the material. The lack of this peak in the 30-poly(*S-r*-canola) suggest that the sample contains no free sulfur. The presence of the peak in the 50-poly(*S-r*-canola) samples showed that free sulfur was present in the polymer before and after moulding with no significant change. These results indicate that the free sulfur content isn't affecting the efficiency of the reactive compression moulding process.

4.5.6 Free sulfur content analysis

^1H NMR and STA analysis revealed that radical addition of polysulfide radicals to alkene groups is not the dominant reaction facilitating the moulding process. Although the process was shown to occur effectively without S_8 present, it could still participate or form during the reaction. To determine if the free sulfur content is affected by the reactive compression moulding process, a calibration curve (Figure 111) for sulfur was created in the DSC by integrating the endotherm between 100 and 150 °C for different masses of sulfur. This endotherm, shown in Figure 111, corresponds to the transition of sulfur from an orthorhombic

to monoclinic crystalline state followed by its melting. The free sulfur content of all 50-poly(*S-r*-canola) mats was then determined by integrating this peak in their DSC traces.

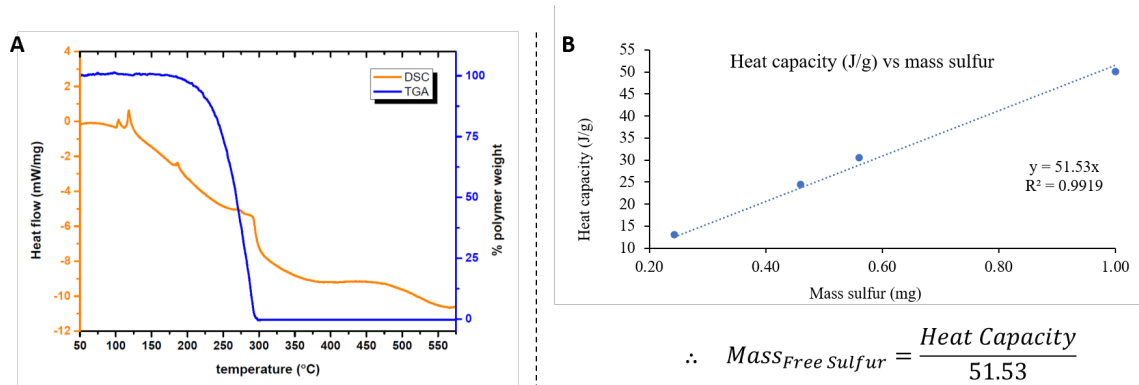


Figure 111 – A) TGA (blue) and DSC (orange) traces for the elemental sulfur. **B)** Calibration curve created using STA for free sulfur content in polysulfide

DSC analysis indicated that the amount of free sulfur in the materials (Figure 113) did not change significantly, suggesting that the elemental sulfur did not partake in the sulfur exchange reaction itself. It's important to note that the location and size of the sample being analyzed can affect the free sulfur content being measured. Previous results suggest that the free sulfur particles migrate towards the surface of the material over time forming a sulfur layer on the surface. This sulfur layer is not uniform and forms to a greater extent on the top surface compared to the bottom. This means the sample will demonstrate a different free-sulfur content depending on whether it was sourced from the top surface, bottom surface, or bulk of the material. As the sulfur layer isn't uniform, the sulfur content can also change significantly at different locations on the surface of the mat.

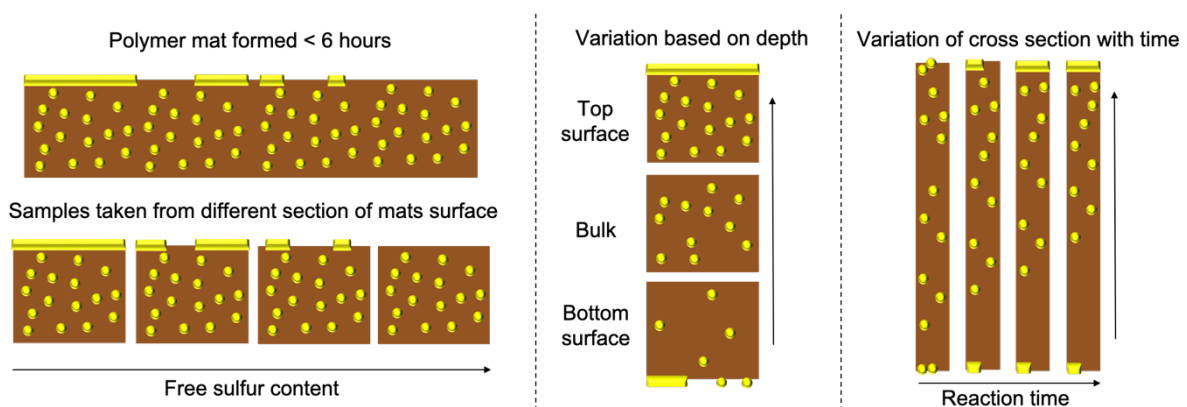


Figure 112 – Figure showing the variation in free sulfur content for samples taken at; different locations on surface (left), different depths in the mat (middle) and cross sections of mats over the course of sulfur migration (right).

Therefore, to obtain the most accurate results samples were taken, when possible, from thin

mats, which included the top surface, bottom surface, and the bulk in one piece. This is shown in Figure 112. As the sulfur layer is formed from sulfur migrating to the surface, the cross section (including both top and bottom surfaces) would contain approximately the same amount of free sulfur regardless of conditions as it hasn't been lost its just moved towards the top surface of the mat. This sample preparation issue and the non-uniform displacement of sulfur within the mats is likely the cause for the small variations observed in the results. It's also important to note, if the free sulfur content isn't affected, it suggests that the free sulfur isn't playing a role in the exchange reaction providing more evidence to suggest sublimation as the mechanism of sulfur migration to the surface. The free sulfur levels for each sample are shown below in Figure 113.

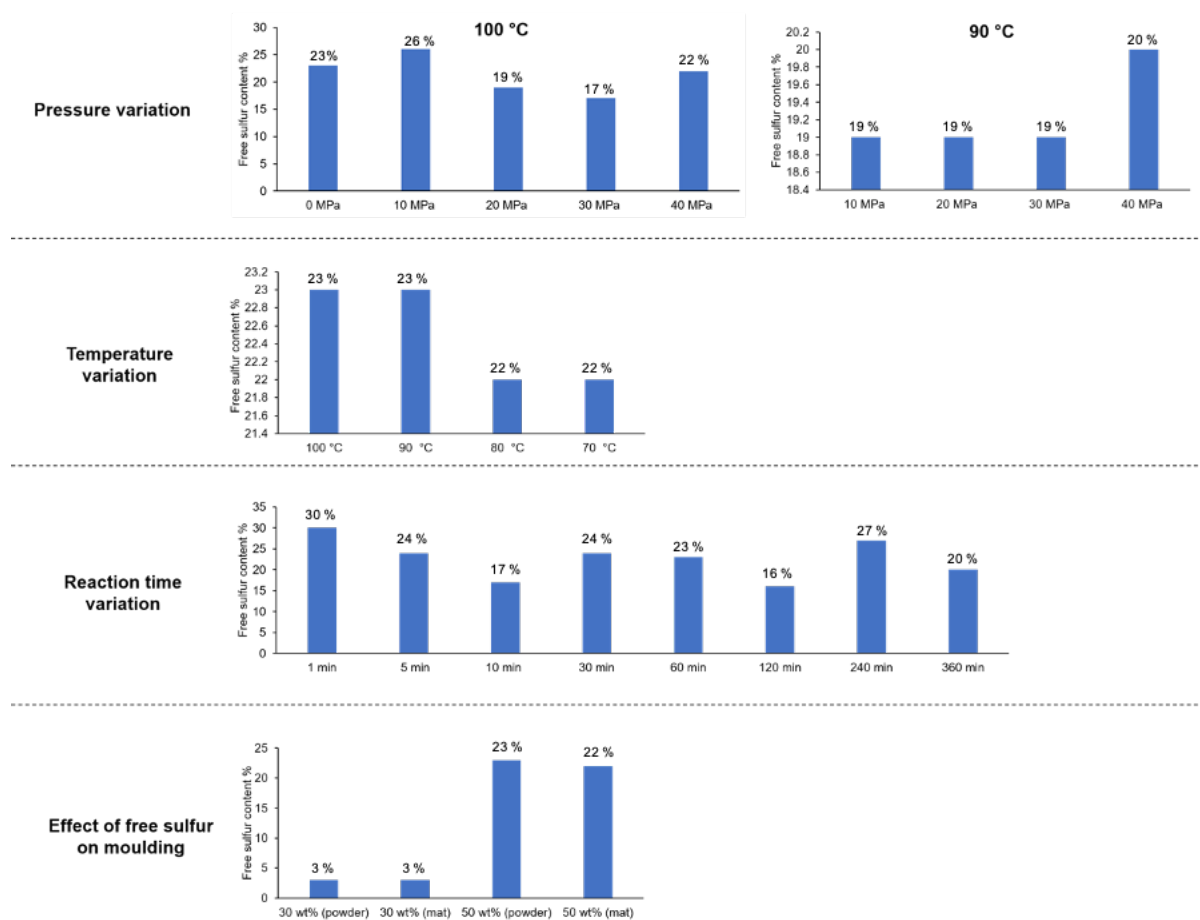


Figure 113 – Free sulfur content for poly(*S-r*-canola) polymer before and after moulding under different conditions (top three) and a comparison of 30- and 50-poly(*S-r*-canola) polymers (bottom).

Although cross-section samples taken from thin mats increased the accuracy of free sulfur content determination, variation still exists. Another possible cause of variation is the batch of starting material used. Samples from the same synthesis can contain varying amounts of free

sulfur and this could also translate to the observed variations after moulding. This variation in starting material is supported by earlier ^1H NMR analysis revealing differences in the 50-poly(*S-r*-canola) mats which did not occur throughout the moulding process.

4.5.7 Reactive compression moulding of canola oil and elemental sulfur – a control

The temperature required for reactive compression moulding ($\sim 100\text{ }^\circ\text{C}$) is far lower than the materials synthesis temperature ($180\text{ }^\circ\text{C}$). We attribute this phenomenon to the S-S bonds in the polymer being weaker than those in elemental sulfur. To illustrate this difference, a control experiment was run in the press in which 2.5 g of sulfur and 2.5 g of canola oil were pressed at 40 MPa at $100\text{ }^\circ\text{C}$ for 10 minutes. Only unreacted sulfur and canola oil were recovered (Figure 114).

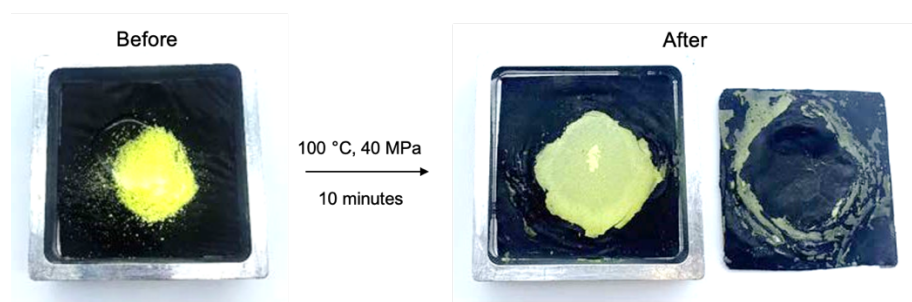


Figure 114 – A) Sulfur + canola oil in mould before moulding at optimized conditions.

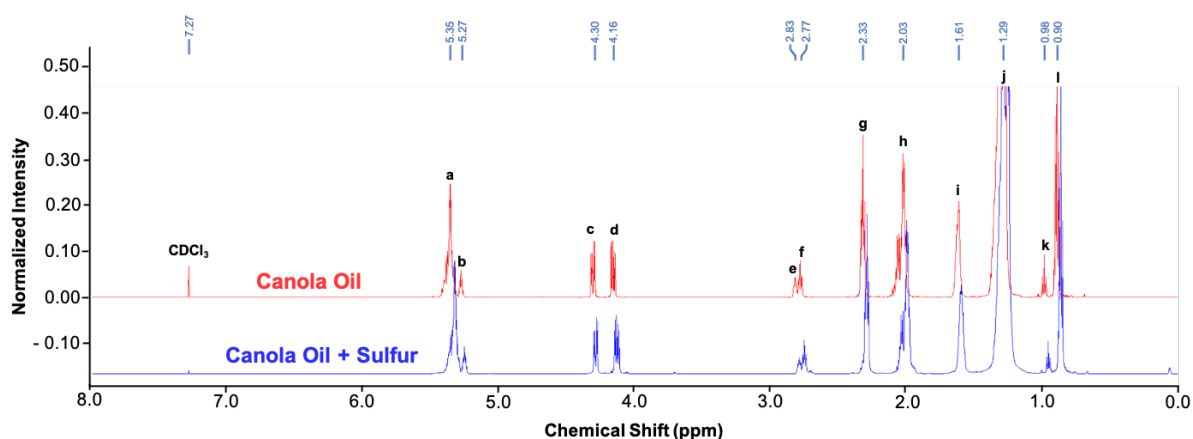


Figure 115 – ^1H NMR analysis of canola oil before and after being moulded with sulfur (600 MHz, CDCl_3): $\delta = 7.23$ (CDCl_3), 5.35 (a), 5.27 (b), 4.30 (c), 4.16 (d), 2.83 (e), 2.77 (f), 2.33 (g), 2.03 (h), 1.61 (i), 1.29 (j), 0.98 (k), 0.90 (l).

Assignment of ^1H NMR signals to canola oils structure is shown below in Figure 116.²⁸⁵

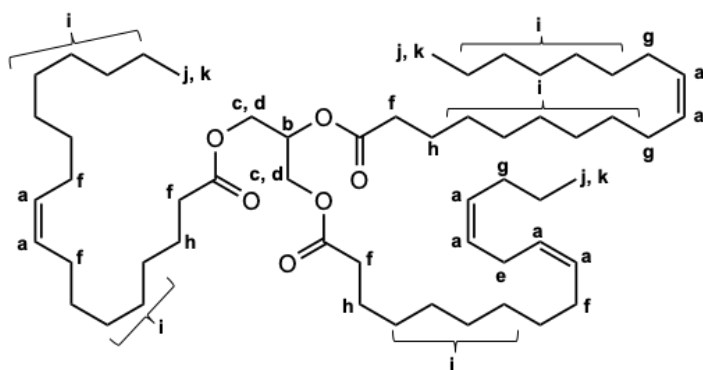


Figure 116 – Peak assignments for ^1H NMR analysis of canola oil before and after reactive compression moulding with sulfur.²⁸⁵

^1H NMR analysis (Figure 115) showed that the alkene peaks (**a**, **g** and **e**) were not consumed under these conditions. This demonstrates that the sulfur exchange reaction, initiated by homolytic S-S bond cleavage, can be initiated at a lower temperature for 50-poly(S-*r*-canola) polysulfide than S_8 . This is an interesting discovery as it suggests that the S-S bond strength is lower in polysulfides than in S_8 .

4.5.8 Theoretical considerations regarding S-S metathesis of organic polysulfides

To better understand the mechanisms behind this process, Dr. Amir Karton (A collaborator from the School of Molecular Sciences at the University of Western Australia) performed high-level ab initio calculations using the Gaussian-4 (G4) thermochemical protocol to determine the S-S bond strengths in sulfur chains of ranks 1-7. The average sulfur rank for 50-poly(S-*r*-canola) was previously calculated to be 5.7 for 50-poly(S-*r*-canola) and 4.5 for 30-poly(S-*r*-canola). As the materials sulfur rank may influence the S-S bond strength, and therefore the temperature by which the process is initiated, it's important to understand this relationship. The Gaussian-4 (G4) thermochemical protocol produces bond dissociation energies (BDEs) with chemical accuracy (arbitrarily defined as $\sim 4 \text{ kJ mol}^{-1}$). The B3LYP/6-31G(2df,p) optimized geometries for each sulfur species were calculated and verified to have all real harmonic frequencies. Only the homolytic BDEs ($\Delta G_{298\text{K}}$) of the S-S bonds in model dimethyl polysulfides (MeS_nMe , where $n = 2, 3, 4, 5, 6,$ and 7) were investigated.

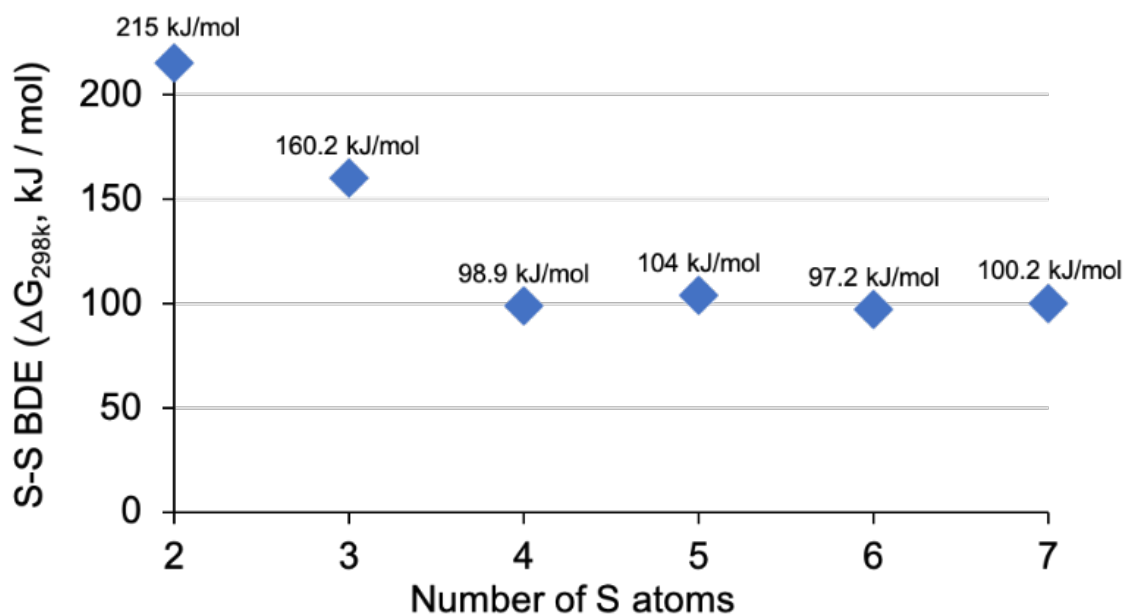


Figure 117 – Graph showing weakest S-S BDE verse number of S in MeS_nMe (n = 2-7).

The weakest S-S bond was determined to be the one which, upon breaking, forms a dithiyl radical. For a polysulfide chain of N sulfur atoms, this would correspond to the bond between S₂ and S_{N-2} sulfur atoms, depicted as Me-S₂-S_{N-2}-Me. A plot of the Gibbs-free BDEs for the weakest S-S bond in each of the Me-S_n-Me chains (n = 2–7) is shown in Figure 117. The S-S bond energy is reduced linearly for chains of 2, 3, and 4 sulfur atoms, with Gibbs-free BDEs of 215.0 (MeS₂Me), 160.2 (MeS₃Me), and 98.9 (MeS₄Me) kJ mol⁻¹. However, for chains with four or more sulfur atoms the S-S bond energy remains approximately constant at ~100 kJ mol⁻¹. This information demonstrated that the ideal target sulfur rank for initiating sulfur exchange is 4 and that polymers of higher sulfur rank do not provide weaker S-S bonds. It also suggests that if more stable polymers are required, a sulfur rank of below 3 should be targeted. Reports in literature have suggested that the difference in S-S bond strength could account for the variations in these materials' rheological properties,¹⁶⁴ but the results in Figure 117 are the first to rigorously characterize the S-S bond strength in these polysulfides. The bond energy for S-S bonds in elemental sulfur (S₈) is 169.452 kJ/mol and sulfur exchange occurs at 159 °C.³⁹ When elemental sulfur (S₈) is converted into 50-poly(S-r-canola) through inverse vulcanisation it results in the formation of polysulfide chains (-S_n-) where n = 1 - 7. As shown in Figure 117, the S-S bond strength reduces to ~98.9 kJ for chains where n > 4. This decrease in bond energy likely accounts for the significant reduction in the temperature required to initiate sulfur exchange. The bond energy decreased by 41.6%. If the initiation temperature (159 °C) decreased by the same amount (41.6%) then the temperature expected to initiate sulfur

exchange for $n \geq 4$ would be ~ 66.1 °C. This supports the results observed previously whereby sulfur exchange was initiated with a temperature as low as 70 °C. The compression simply facilitated the direct contact of the reactive interfaces increasing the rate of reaction.

4.5.9 Reactive compression moulding for recycling and repurposing

Now that the optimized protocol (with respect for time) and a sound understanding of the theoretical considerations behind the sulfur exchange reaction had been determined, potential applications of this chemistry were investigated. The ability to mould materials into desired shapes and sizes is important, however the ability to perform this process repeatedly opens the possibility for the material to be continuously re-formed and re-purposed for new uses. To test this, a mat was first formed using the optimized reactive compression moulding conditions. The resulting mat was then ground back up into a powder and a new mat was reformed using the same reaction conditions. To characterize any differences between the mat before and after re-forming; TGA, DSC, ^1H NMR and SEM analysis were performed.

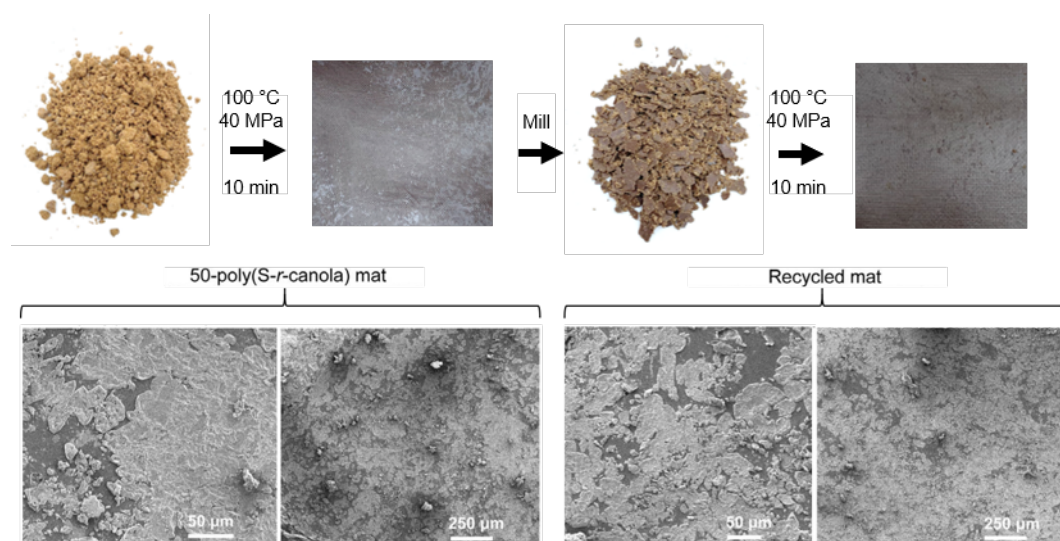


Figure 118 – Outline of successful recycling experiment using reactive compression moulding (top) and SEM images of the surface of 50-poly(S-r-canola) before and after recycling.

The recycled mat appeared visually the same as the first mat. SEM analysis (Figure 118) revealed no significant difference in the mats before and after being recycled.

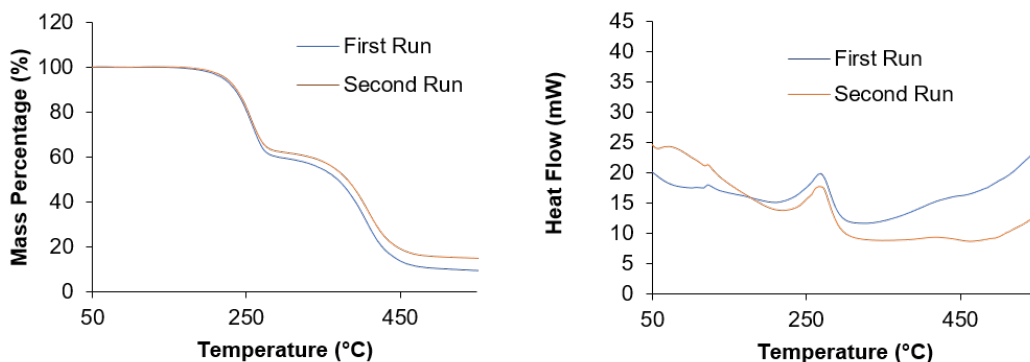


Figure 119 – TGA (top) and DSC (bottom) analysis of 50-poly(S-*r*-canola) mat before and after recycling.

No significant difference for samples before and after recycling was observed under TGA and DSC analysis (Figure 119). The sulfur-sulfur exchange reaction was suggested to initiate at ~ 66 °C, only slightly after the beginning of the DSC runs (50 °C). In all DSC curves a small change in heat flow is observable around 60-70 °C. This change could potentially be due to the onset of sulfur-sulfur exchange.

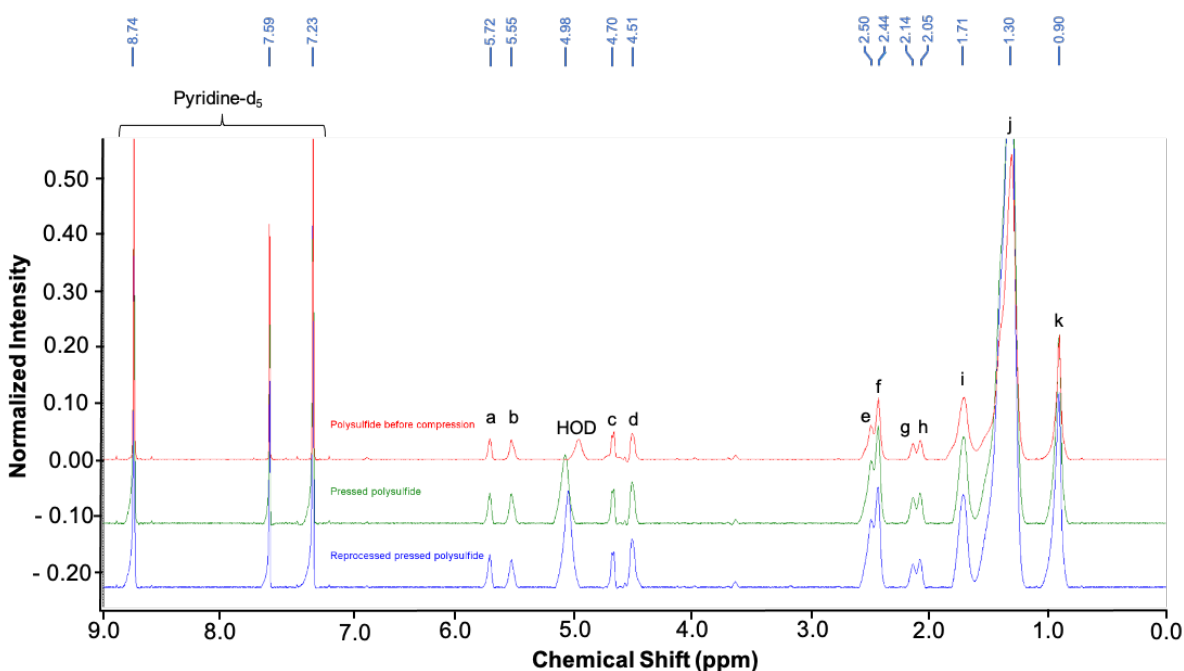


Figure 120 – ^1H NMR analysis of 50-poly(S-*r*-canola) before and after moulding and recycling. (600 MHz, pyridine- d_5): $\delta = 8.74, 7.59, 7.23$ (pyridine- d_5), 5.72 (a), 5.55 (b), 4.98 (HOD), 4.70 (c), 4.51 (d), 2.50 (e), 2.44 (f), 2.14 (g), 2.05 (h), 1.71 (i), 1.3 (j), 0.9 (k).

The re-formed material was almost identical under ^1H NMR analysis (Figure 120) with the only observable difference being the position and intensity of the HOD peak. This is likely due to the different levels of contamination of pyridine- d_5 over time by moisture in the air. All the

results conclude that no significant change in chemical structure occurs after recycling the material using reactive compression moulding. This adds further evidence to support the idea that sulfur exchange is the dominant mechanism by which the reactive compression moulding process occurs. This new process therefore offers a potential route for the recycling of polysulfides prepared by inverse vulcanization. Now that the ability to re-form and re-use 50-poly(*S-r*-canola) materials has been demonstrated, the ability to use this process to recycle 50-poly(*S-r*-canola) after Fe(III) remediation was investigated. 50-poly(*S-r*-canola) was investigated previously for the removal of Fe³⁺ from water to decolorize it and prevent biofouling induced by iron. It was shown that large quantities of 50-poly(*S-r*-canola) were required to reduce the iron concentration to below the regulation limits. This means a sustainable recycling and repurposing strategy must be developed for the sorbent if it is to be a viable option for iron remediation. It was hypothesized that reactive compression moulding could be used to repurpose spent sorbent as components in building and construction materials. To test this possibility, 250 g of 50-poly(*S-r*-canola) was added to a 1.0 L solution of FeCl₃ (50 mg/L). After 24 hours, >90% of the Fe(III) was removed and the water was clear (Figure 121 A, B). The 50-poly(*S-r*-canola) particles (now with bound iron) were isolated by filtration, dried in a fume hood, and subjected to reactive compression moulding. The resulting mat appeared no different than the mat formed from untreated 50-poly(*S-r*-canola) (Figure 121 C). The iron bound to the polymer did not seem to interfere with the S-S metathesis reaction during the moulding process. To investigate this further SEM, EDX, STA and ¹H NMR analysis were performed on all samples.

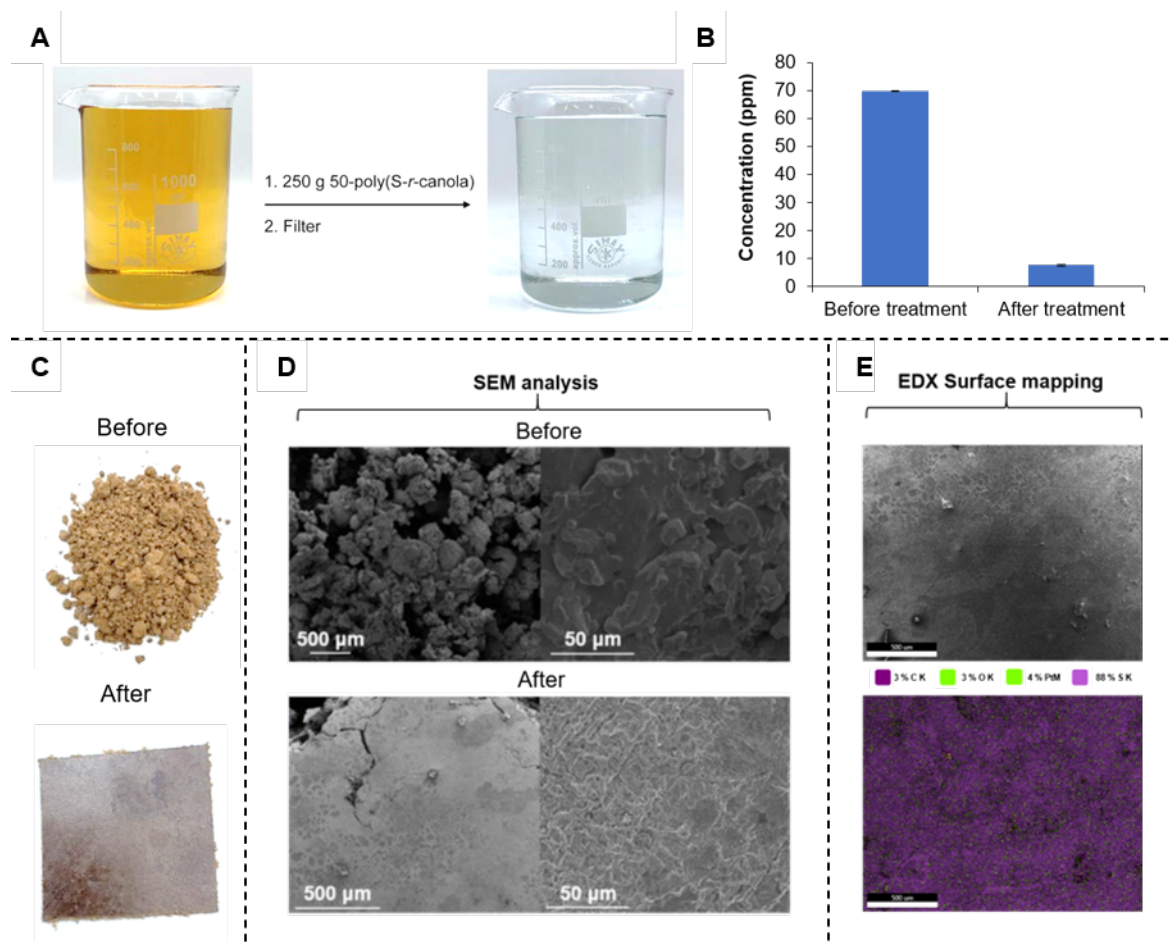


Figure 121 – **A**) Image showing iron solution before and after treatment, **B**) Fe(III) concentration before and after treatment, **C**) Visual images of Fe(III) treated 50-poly(*S-r*-canola) before and after moulding, **D**) SEM analysis at 50 and 500 μm before and after moulding, **E**) EDX mapping of the surface of the mat formed from Fe(III) treated 50-poly(*S-r*-canola).

SEM analysis (Figure 121 D) revealed no significant difference between the mat formed from 50-poly(*S-r*-canola) without and without previous treatment with Fe(III). No Fe(III) signal was observed under EDX mapping of the surface(Figure 121 E). This was likely due to the formation of the high sulfur content layer on the surface.

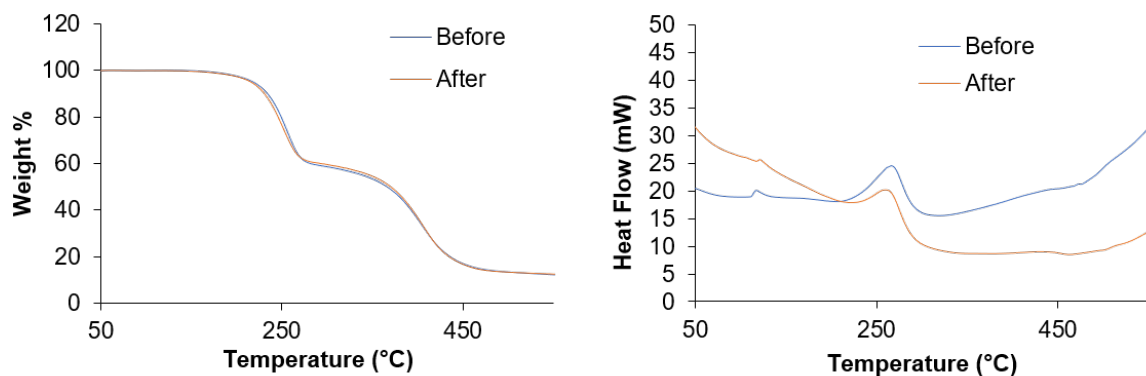


Figure 122 – A) TGA (left) and DSC (right) curves for Fe(III) treated 50-poly(*S-r*-canola) before and after moulding.

TGA and DSC traces (Figure 122) show no significant differences with both displaying the expected peaks. The difference in heat flow intensity is likely due to the difference in thermal conductivities of the materials when in bulk or powder form.

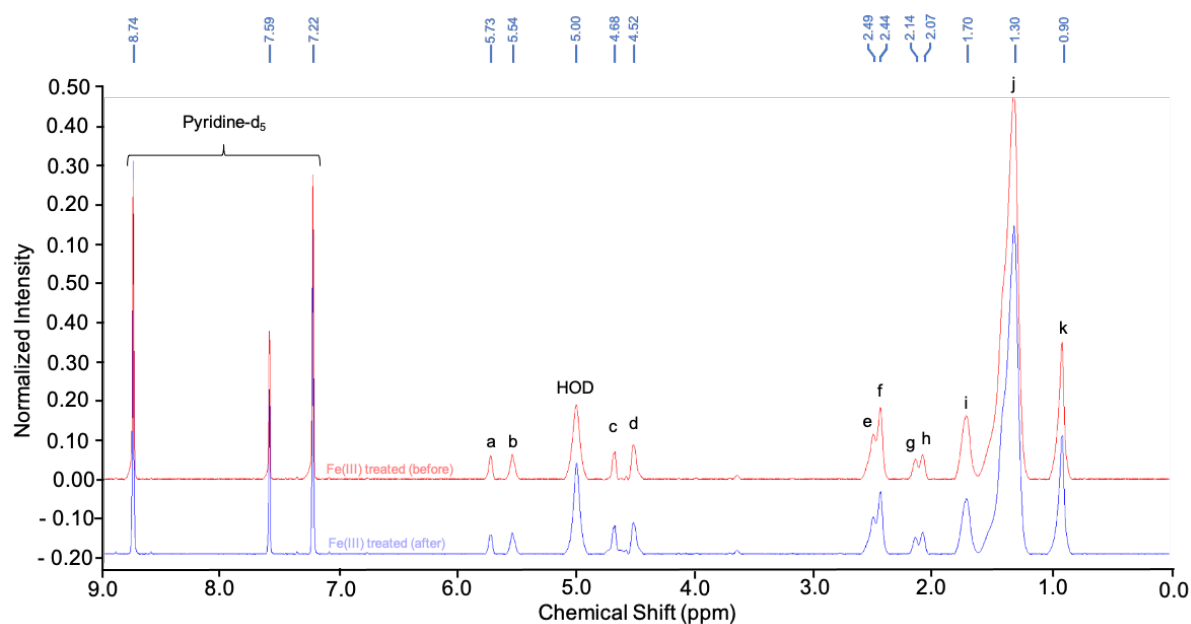


Figure 123 – ¹H NMR analysis of Fe(III) treated 50-poly(*S-r*-canola) before and after moulding. (600 MHz, pyridine-*d*₅): δ = 8.74, 7.59, 7.22 (pyridine-*d*₅), 5.73 (a), 5.54 (b), 5.00 (HOD), 4.68 (c), 4.52 (d), 2.49 (e), 2.44 (f), 2.14 (g), 2.07 (h), 1.70 (i), 1.30 (j), 0.90 (k).

Analysis using ¹H NMR (Figure 123) shows that the Fe(III) treated 50-poly(*S-r*-canola) material was chemically identical before and after moulding suggesting that the Fe(III) did not interfere in the chemistry of the moulding process. This demonstrated that the bound Fe(III) did not impact the moulding process in any noticeable way. This was also a direct demonstration of repurposing the 50-poly(*S-r*-canola) after its use in one of the many remediation applications already demonstrated previously in this thesis.

4.5.10 Reactive compression moulding on a 15.0 gram scale

The optimized process was repeated on a larger scale to produce a 15 gram mat. This mat was compared with the smaller scale mats to examine any differences observed.

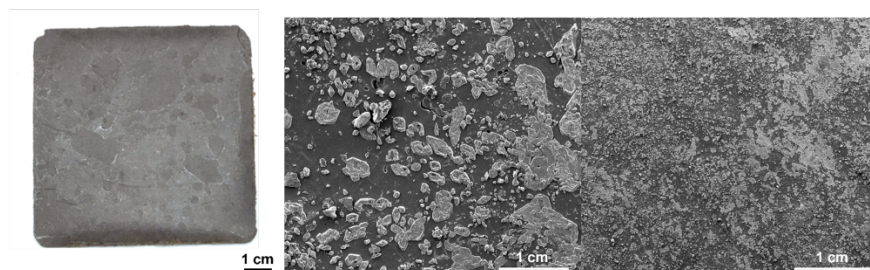


Figure 124 – Image of 15.0-gram mat (left) and SEM images of the mats surface at 100 μm (middle) and 500 μm (right).

The 15.0 g mat appeared visually the same as those produced at 5.0 grams. The surface of the 15.0 gram mat demonstrated the same free sulfur particles and surface coatings as the mats prepared on 5.0 gram scale (Figure 124).

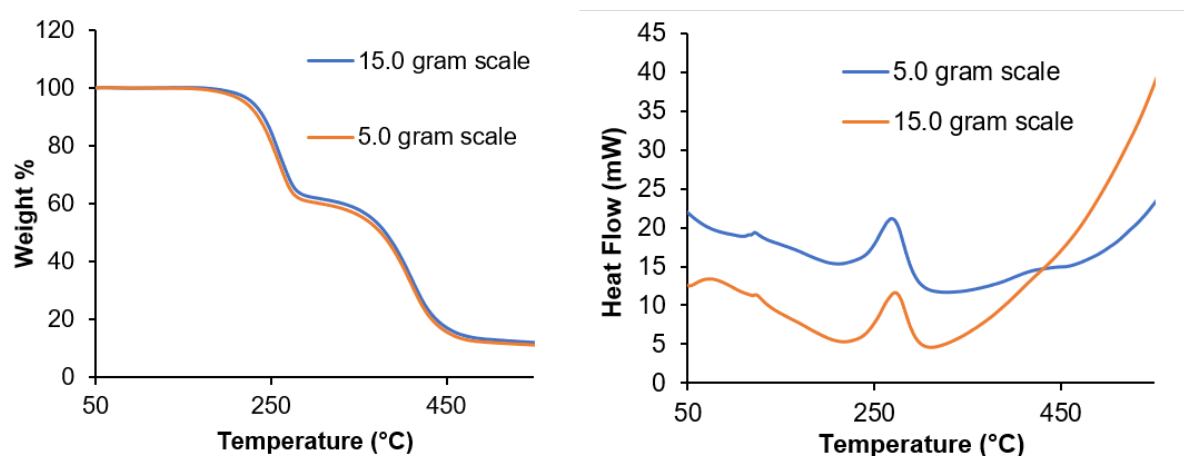


Figure 125 – TGA (left) and DSC (right) traces, obtained by STA, comparing the mats formed using 5.0 and 15.0 grams of 50-poly(*S-r*-canola).

No significant differences were observed under TGA or DSC curves (Figure 125). The small difference in average heat flow intensity is likely due to the thermal conductivities of the material. The 50-poly(*S-r*-canola) is thermally insulating and therefore retains heat. The more sample that is present the less heat energy is required to maintain the same temperature and therefore a difference in heat flow is observed.

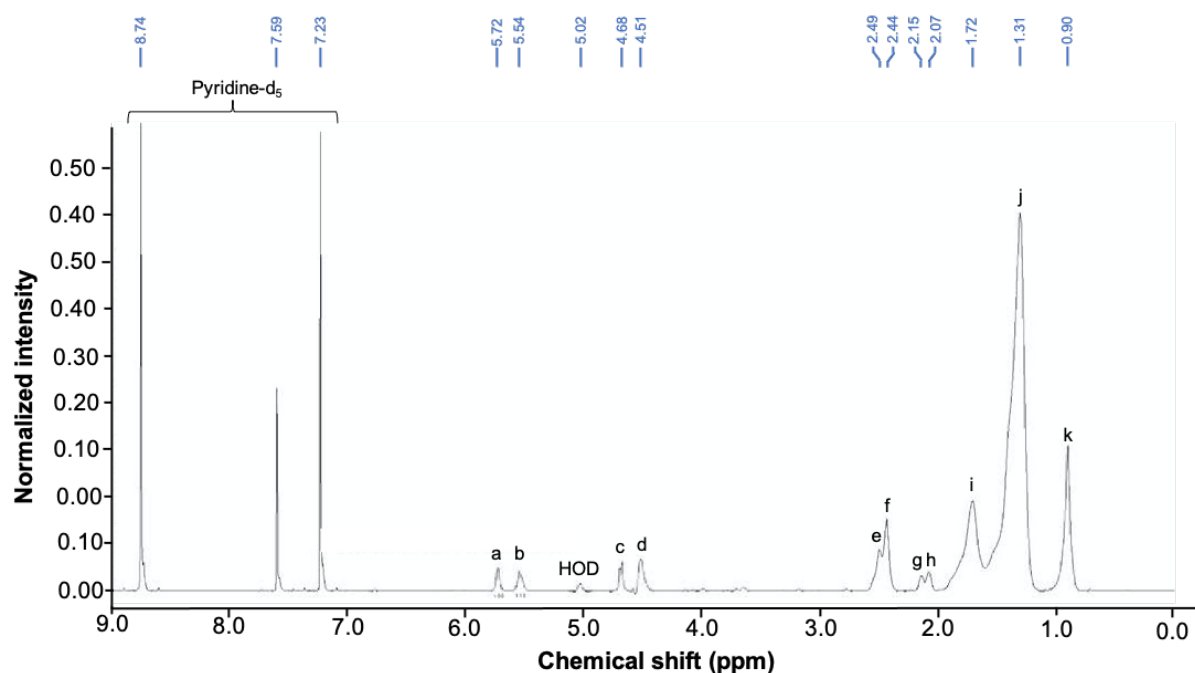


Figure 126 – ^1H NMR analysis of 15.0 gram mat. (600 MHz, pyridine- d_5): $\delta = 8.74, 7.59, 7.23$ (pyridine- d_5), 5.72 (a), 5.54 (b), 5.02 (HOD), 4.68 (c), 4.51 (d), 2.49 (e), 2.44 (f), 2.15 (g), 2.07 (h), 1.72 (i), 1.31 (j), 0.9 (k).

No difference was observed in the ^1H NMR spectra (Figure 126) suggesting the material remains chemically identical to the material made on a 5.0 gram scale. Next, to probe the mechanical properties of the 50-poly(*S-r*-canola) material nano-indentation analysis was performed. Figure 127 below provides the average values of hardness, stiffness and reduced elastic modulus for the nano-indentation samples. Results are presented for all data points ($n=8$) and with soft and hard outliers removed ($n=5$).

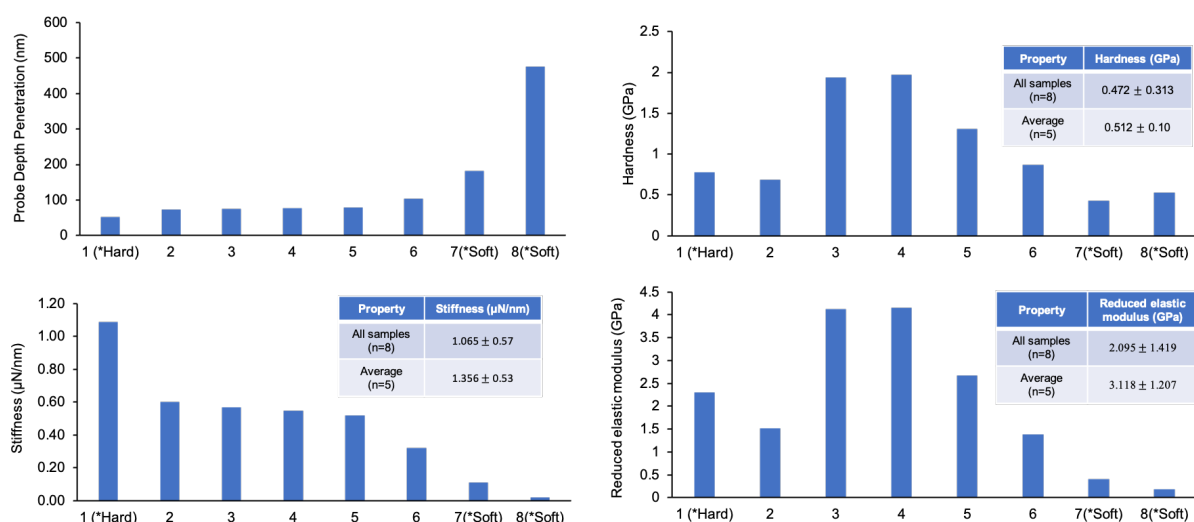


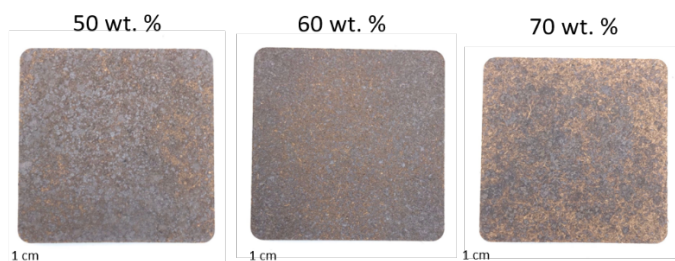
Figure 127 – Results for nano-indentation experiments

Three distinct areas, labeled as ‘soft’, ‘average’ and ‘hard’ were identified. A needle penetration depth below 70 nm were labeled ‘hard’, between 70 nm to 110 nm labeled as ‘average’ and a depth of above 110 nm was classified as ‘soft’. The most observed penetration depths were in the ‘average’ range (63% of usable data sets). This is likely due to penetration of the 50-poly(*S-r*-canola) surface where no surface sulfur layer is present. The hard punctures correspond to areas in which the sulfur surface layer was present. The soft signals are found due to areas in which the probe compressed an area with an air pocket directly below the surface thereby offering little resistance. Analysis of results revealed that the 50-poly(*S-r*-canola) mat had a surface hardness of 0.5 ± 0.1 GPa, a stiffness of 1.4 ± 0.5 $\mu\text{N}/\text{nm}$, and a reduced elastic modulus of 3 ± 1 GPa. These results highlight the soft and flexible mechanical properties of the mats formed.

4.5.11 Preparation of composite materials using reactive compression moulding

Whilst the soft and flexible properties are useful for some applications, altering the mechanical properties for use in a wider range of applications is important. To do this, reactive compression moulding was used to prepare composites with sustainable reinforcement materials. To do this 50-poly(*S-r*-canola) was investigated as a reactive resin material that would bind together and encapsulate other filler materials to prepare composites. Filler materials investigated included coconut coir, sand, PVC, and powdered carbon fibre. These filler materials were picked because they are either agricultural waste (coco-fibre),²⁰ construction waste (PVC shavings) or they are materials already used for composite materials in construction (sand). Out of all of the potential construction waste materials to pick from, PVC was chosen because there are currently few options for its recycling.²² Composite formation was achieved by simply mixing the 50-poly(*S-r*-canola) with the filler material and then performing reactive compression moulding on the mixture. Composites of coco-fibre and waste PVC were prepared with filler content between 50 and 80 wt%. The coco-fibre composites were only prepared up to 70 wt% coco-fibre content as the fibres were light weight and high volume meaning the 80 wt% coco-fibre mixture was too high in volume to fit in the 10×10 mould.

A Coco-fiber composites



B Waste PVC

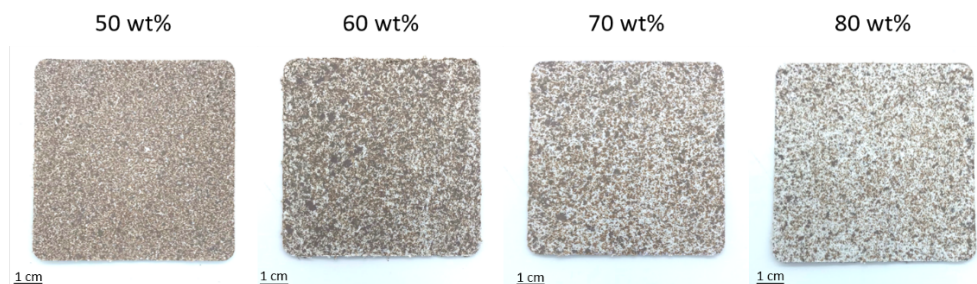
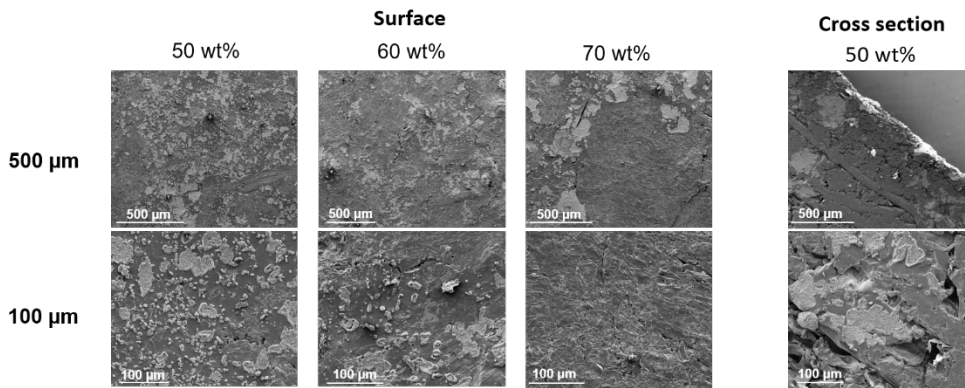


Figure 128 – A) Images of 50-70 wt% coco-fibre composites, **B)** Images of 50-80 wt% waste PVC composites.

Figure 128 shows the coco-fibre and PVC composite mats formed using reactive compression moulding. The mats appeared more rigid and strong upon simple physical inspection. Under SEM analysis (Figure 129) the surface of the PVC mats looked identical to mats made from the starting material with increasing amounts of the filler material present. The sample at 80 wt% appears more like a PVC mat with 50-poly(*S-r*-canola) polymer embedded within and bound to the surface. The coco-fibres are more difficult to differentiate from the 50-poly(*S-r*-canola) surface under SEM. Although coco-fibres are present they conveniently blended in with the surface features of the typical polymer resin. In the 50 and 60 wt% coco-fibre composites, fibres are observable on the surface however they are difficult to observe. Once the concentration of fibres reaches 70 wt%, their presence under SEM is more clearly observable. Analysis of the cross section show that the PVC and coco-fibre are not localised to the surface and are distributed throughout the bulk of the polymer.

A Coco – fiber composites



B Waste PVC composites

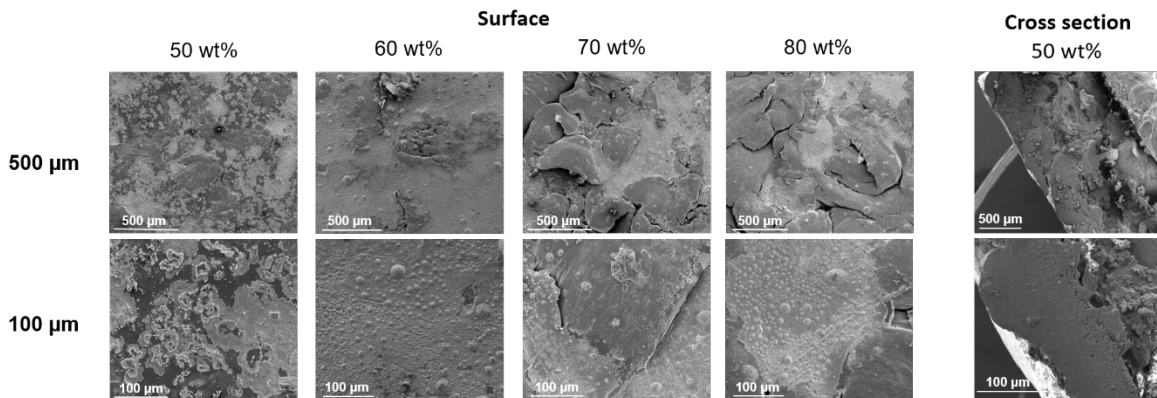


Figure 129 – A) SEM images of the surface and cross section of coco-fiber composites, **B)** SEM images of the surface and cross section of waste PVC composites.

Unlike the coco-fiber and PVC, the sand, and the 50-poly(*S-r-canola*) didn't mix well resulting in mechanically unstable mats being formed upon compression. Therefore, to prepare a composite material from sand and 50-poly(*S-r-canola*) a different method had to be established. This method is highlighted in Figure 130.

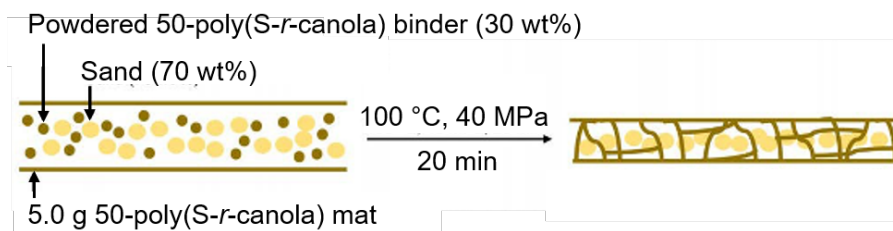


Figure 130 – Diagram describing the method used to prepare sand composites



Figure 131 – Images showing step-by-step process to prepare the sand composites using the method described above.

This process (Figure 131) involved firstly preparing two 5.0 gram 50-poly(*S-r*-canola) mats. A mixture of the desired sand/50-poly(*S-r*-canola) composition is then sandwiched between the two premade mats using reactive compression moulding for 20 minutes at 40 MPa and 100 °C. Preparing a composite with 90 wt% sand was attempted using this method however it did not form a mechanically sound mat. SEM analysis was performed on all sand composites (Figure 132).

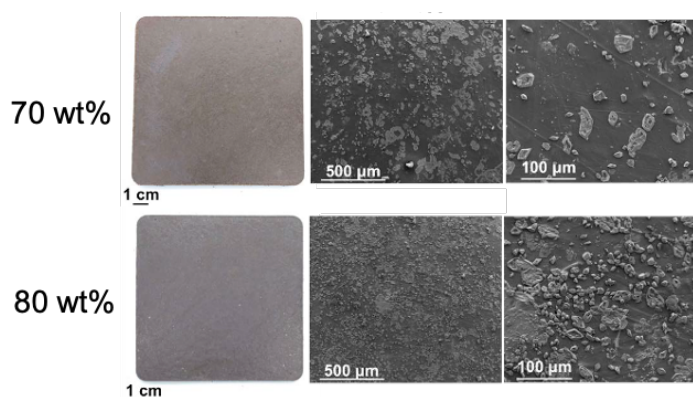


Figure 132 – Images of 70 and 80 wt% sand composites (left), SEM images of the surface of the 70 and 80 wt% sand composites at 500 μm and 100 μm magnifications.

Due to the surfaces containing no sand and only 50-poly(*S-r*-canola) mats before moulding, the surfaces after moulding looked identical to typical 100 wt% 50-poly(*S-r*-canola) mats formed under the same conditions.

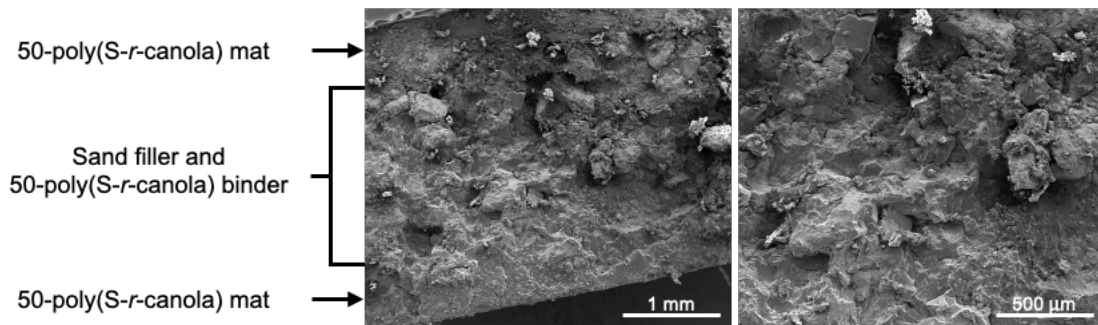


Figure 133 – SEM analysis of cross section of the 70 wt% sand composites.

SEM analysis (Figure 133) of the cross section (70 wt% sand composite) revealed that both sand and 50-poly(S-*r*-canola) are observed in the middle section of the mats however a thin layer (0.5-1 mm) on the top and bottom surface of the mat appear to consist entirely of 50-poly(S-*r*-canola). As multiple 50-poly(S-*r*-canola) mats can be combined, additive manufacturing of composites mats was investigated whereby multiple pre-formed mats are adhered together to form a single larger mat. This was done using the 50-coco-poly(S-*r*-canola) samples (Figure 134).

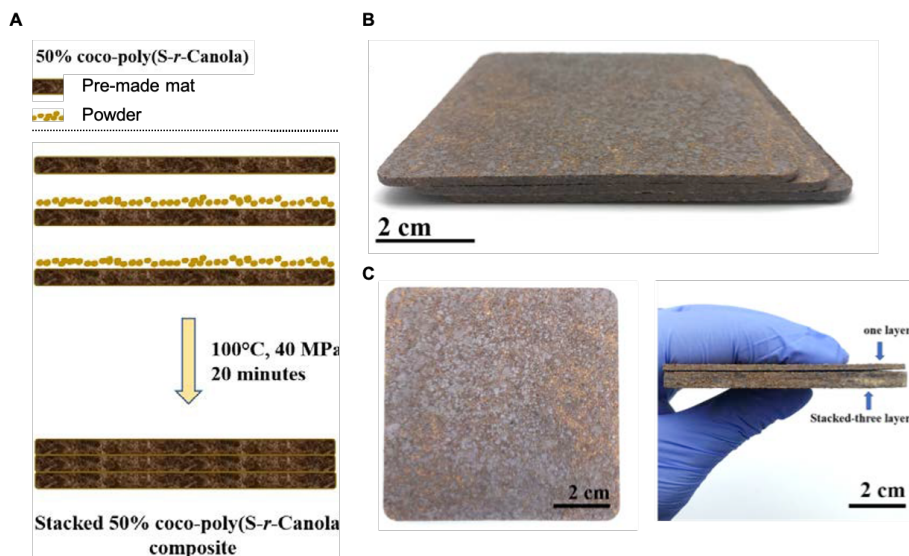


Figure 134 – **A**) Image demonstrating the process of additive reactive compression moulding. **B**) Three individual 50-poly(S-*r*-canola) / coco-fiber composite mats, **B**) Mat formed from additive reactive compression moulding of mats shown in **A** (left) and image showing thickness of the mat formed from additive reactive compression moulding of mats in **A** in comparison to an individual mat (right).

Three mats were successfully bound into one larger mat. This process is useful for creating larger structures than the mould would initially allow as well as creating new more complex shapes and structures not typically achieved using compression moulding. The effect of filler amount and composition on the mechanical properties of the resultant composite material was

investigated next. Compression testing was performed on all composite samples using the compression clamp setup on the Q800 dynamic mechanical analyzer. The modulus of compression for each sample was determined and the results are shown in Figure 135.

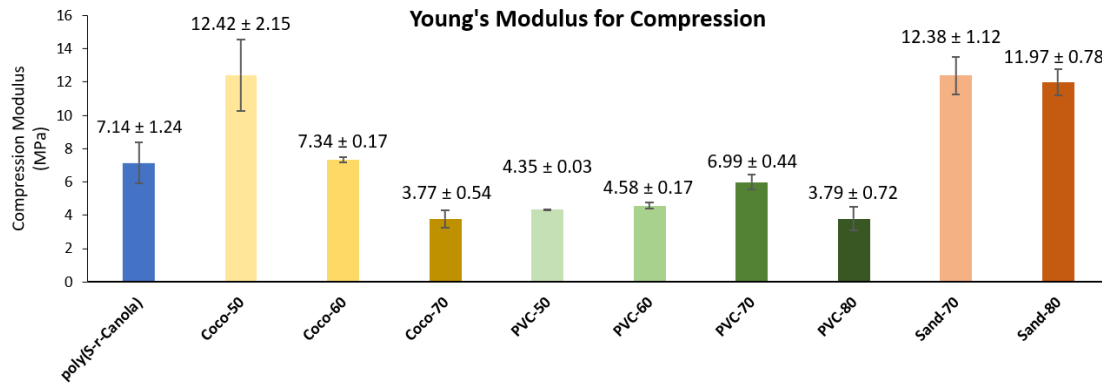


Figure 135 – Young's modulus for compression (modulus of elasticity) of the composites prepared from 50-poly(S-r-canola) and different fillers: coconut fibre, sand, and PVC plastic waste.

The modulus of elasticity (compression modulus) was determined for all the samples using the compression clamp setup on the Q800 dynamic mechanical analyzer. Therefore, by altering the filler amount and composition it's possible to alter the compression modulus of the material. Since PVC typically has a T_g around 70-100 °C it was hypothesised that the PVC composite would also contain a secondary T_g .²⁸⁶ DSC analysis was performed revealing the presence of a T_g at 84.3 °C. This allows the composites shape to be adjusted by heating to 85.0 °C.

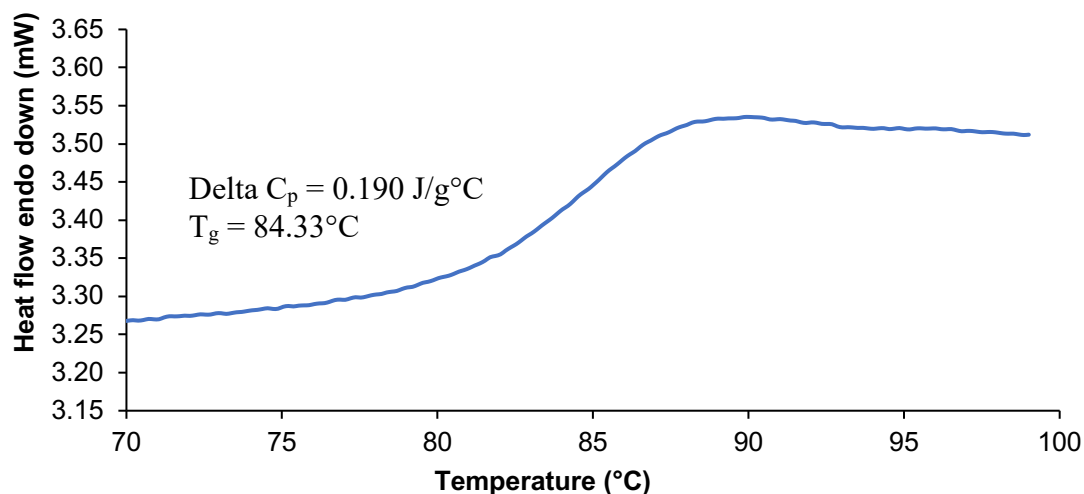


Figure 136 – T_g analysis of the PVC plastic waste. The T_g measurement was carried out using Perkin Elmer DSC8000. The sample size was 6 mg.

Three-point bend testing was also performed on all samples. The set up for this test is shown below in Figure 137.

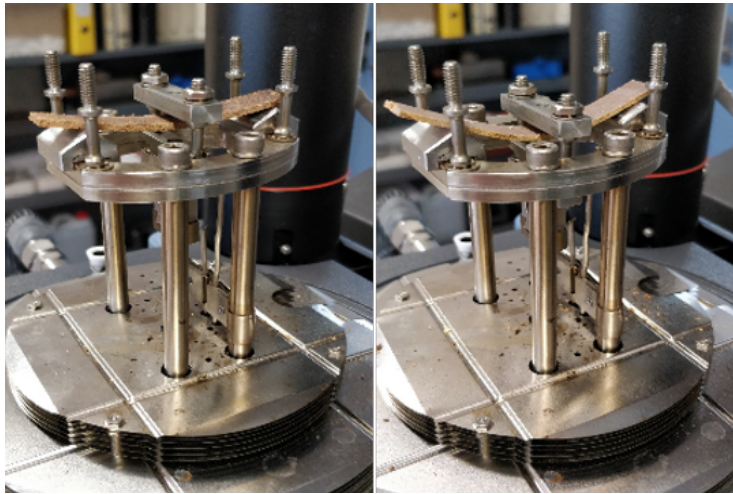


Figure 137 – Images of the three-point bend attachment on the DMA directly before (left) and after (right) analysing the 50 wt% coco-fibre composite

The modulus of elasticity (Figure 138) and rupture (Figure 139) were both insignificant for the 50-poly(*S-r*-canola) sample. This is not an accurate value due to the highly flexible nature of these mats; the force that's applied by the three-point bend test simply bends the sample until it hits the force limit with very little if any resistance. Therefore, the value for 50-poly(*S-r*-canola) appears to be very low but its true value would be significantly larger than all other samples shown.

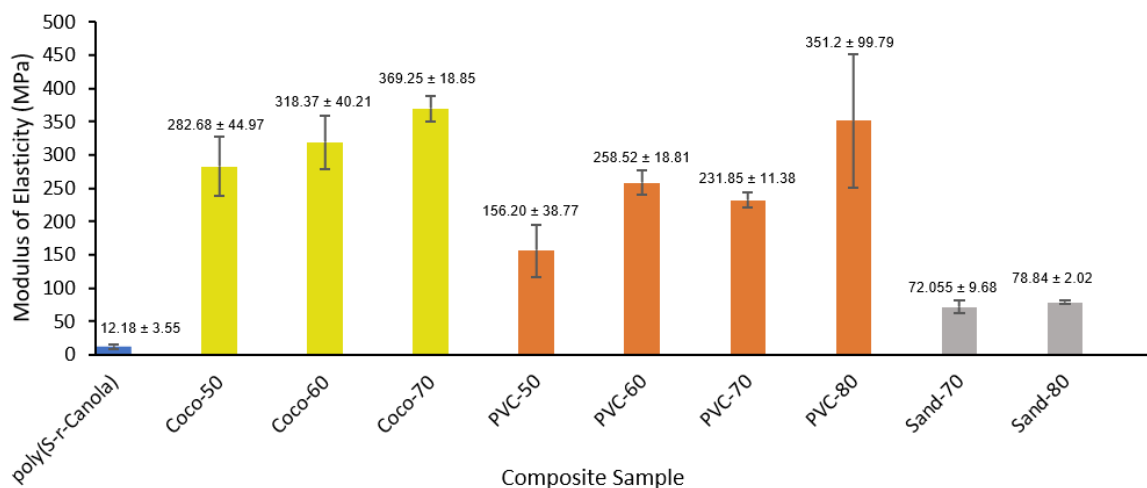


Figure 138 – Modulus of elasticity of all composite samples found using three-point bend test.

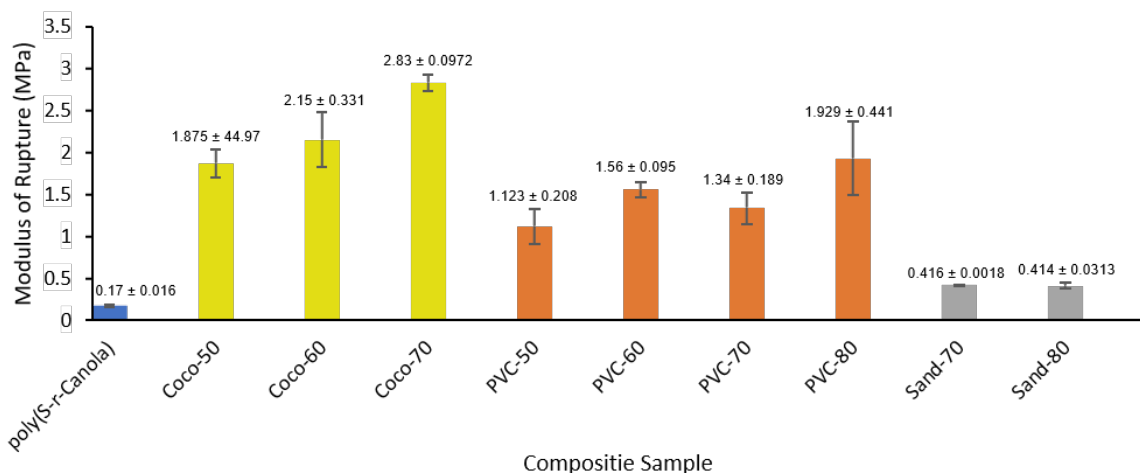


Figure 139 – Modulus of Rupture of all composite samples found using three-point bend test.

Testing revealed that in all cases addition of filler material effected the modulus of elasticity and rupture. By increasing the amount of filler material from 50 to 80 both modulus values were shown to increase. This information is important for the design of these composite allowing for their mechanical properties to be tailored for use in specific applications.

4.5.12 Encapsulation of spent sorbent for safer handling, transport, and storage

Reactive compression moulding has been demonstrated as an effective method for recycling and re-using poly(S-r-canola) materials. As these materials have been heavily used in pollution remediation strategies, we decided to investigate weather reactive compression moulding could be utilised to encapsulate spent sorbent materials, eliminating the issues associated with contaminant leaching and enhancing the safe handling, storage, and transport of the spent sorbent after use. The proposed method of encapsulation is shown in Figure 140.

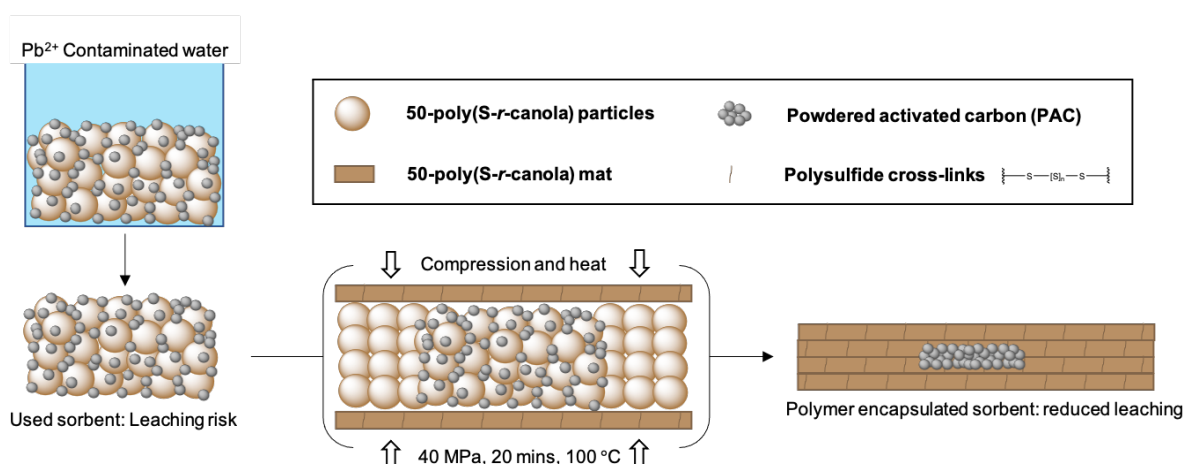


Figure 140 – Figure describing the lead treatment followed by encapsulation of sorbent material.

To do this a concentrated lead solution (560 ppm Pb^{2+}) was initially treated with the 50-poly(*S-r*-canola) polymer. An average of 0.2 mg of lead was bound per gram of polymer in triplicate experiments. This was repeated at the same lead concentration using the carbon polymer blend from chapter 3. After 1 hour of exposure time the polymer carbon blend (20.0 grams) had approximately 10 mg of lead bound to it based on the decrease of lead in solution, as measured by ICP-MS. This result indicates that the lead removal for the polymer carbon blend is due primarily the activated carbon (1.8 mg / g AC), though the polymer is also a minor contributor to lead binding (0.2 mg / g 50-poly(*S-r*-canola)). These treatment experiments were not optimized for remediation as the experiment was aimed at testing whether or not reactive compression moulding could be used to encapsulate the spent sorbent and stop leaching. The spent sorbent was filtered and dried before undergoing leaching experiments. The spent blend material was added to water in a centrifuge tube (1.0 g per 50 mL) and left to mix for 1 week on a rotary mixer. The water was then filtered and analyzed by ICP-MS. The blend without being encapsulated was shown to leach the adsorbed lead back into solution over 1 week (2.3 μ g of the 500 μ g bound). This level of leached lead is above the standard regulation limits for lead in water, so it is significant.²⁸⁷ To tackle the leaching issue, the spent sorbent was completely encapsulated in 50-poly(*S-r*-canola) using reactive compression moulding. To do this 5.0 g of the sorbent (bound to lead) was placed between two pre-formed 5.0 g 50-poly(*S-r*-canola) mats. To ensure complete encapsulation 2.0 grams of powdered 50-poly(*S-r*-canola) was added to the perimeter of the spent sorbent. This process is shown in Figure 141.

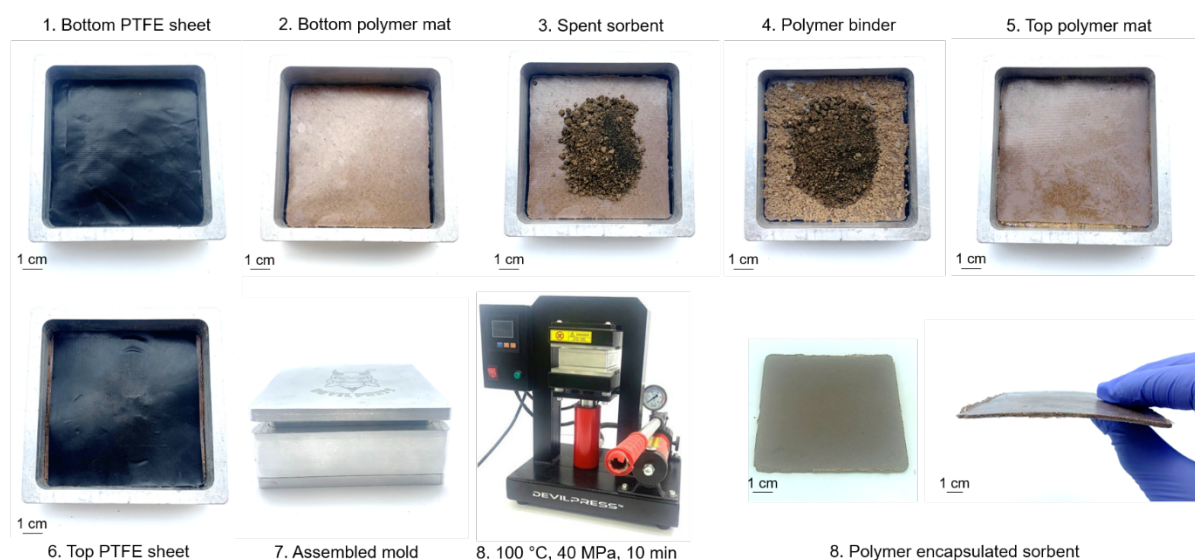


Figure 141 – Images from 1 - 9 showing the process used to encapsulate the spent sorbent materials within 50-poly(*S-r*-canola) using reactive compression moulding.

The blend material consists of 80 wt% 50-poly(*S-r*-canola), the same material being used for encapsulation and will therefore chemically react with the preformed 50-poly(*S-r*-canola) mats and the 2.0 grams added around its perimeter, locking it into the middle of the formed mat / block. Leaching experiments were performed on the mats with encapsulated lead treated sorbent. It was demonstrated that no observable leaching occurred (detection limit 0.030 mg/L) from the spent lead sorbent after encapsulation. This method was therefore shown to be effective in encapsulating spent 50-poly(*S-r*-canola) based sorbent materials eliminating leaching and increasing safe handling, transport, and storage. This method could also be applied to a range of other pollutants including PFAS and mercury.

4.6 Conclusions

Reactive compression moulding was demonstrated to be an effective method by which high-sulfur content polymers prepared by inverse vulcanization could be rapidly moulded into new shapes and forms by the application of heat and pressure. Processing temperatures are significantly lower than the materials synthesis temperature and the underlying S-S metathesis reaction at the center of this process was also studied computationally. This revealed that the weakest S-S bond in a polysulfide chain decreases as the sulfur rank increases from 1 to 4 but remains relatively steady above 4 sulfur atoms. After validating the technique, it was utilized to effectively remould 50-poly(S-*r*-canola) multiple times as well as repurpose the 50-poly(S-*r*-canola) that had been used previously in water remediation experiments. This was an important achievement as most cross-linked thermoset polymers are unrecyclable. Reactive compression moulding was also demonstrated as an effective method to prepare composite materials from polymers prepared by inverse vulcanization. By forming composites, the mechanical properties of the resulting mats could be altered by changing the composition and ratio of filler material to polymer. Finally, the ability to encapsulate the spent carbon / polymer sorbent material (used for lead treatment) inside 50-poly(S-*r*-canola) was demonstrated. This eliminated the issues associated with contaminant leaching, increasing the safe handling, transport, and storage of the waste sorbent material. This could also be used to repurpose the spent sorbent inside bricks and mats of 50-poly(S-*r*-canola) to be used in construction applications.

APPENDICES

Publications that resulted from the research in this chapter:

1. Lundquist, N. A.; Tikoalu, A. D.; Worthington, M. J. H.; Shapter, R.; Tonkin, S. J.; Stojcevski, F.; Mann, M.; Gibson, C. T.; Gascooke, J. R.; Karton, A.; Henderson, L. C.; Esdaile, L. J.; Chalker, J. M. "Reactive compression moulding Post-Inverse vulcanization: A Method To Assemble, Recycle, and Repurpose Sulfur Polymers and Composites" *Chem. Eur. J.* **2020**, 26, 10035-10044.
2. Lundquist, N. A.; Chalker, J. M. "Confining a spent lead sorbent in a polymer made by inverse vulcanisation prevents leaching," *Sustain. Mater. Technol.* **2020**, 26, e00222.

 Sustainable Chemistry | *Very Important Paper*



Reactive Compression Molding Post-Inverse Vulcanization: A Method to Assemble, Recycle, and Repurpose Sulfur Polymers and Composites

Nicholas A. Lundquist,^[a] Alfrets D. Tikoalu,^[a] Max J. H. Worthington,^[a] Ryan Shapter,^[a] Samuel J. Tonkin,^[a] Filip Stojcevski,^[b] Maximilian Mann,^[a] Christopher T. Gibson,^[c] Jason R. Gascooke,^[a] Amir Karton,^[d] Luke C. Henderson,^[b] Louisa J. Esdaile,^{*[a]} and Justin M. Chalker^{*[a]}

Abstract: Inverse vulcanization provides dynamic and responsive materials made from elemental sulfur and unsaturated cross-linkers. These polymers have been used in a variety of applications such as energy storage, infrared optics, repairable materials, environmental remediation, and precision fertilizers. In spite of these advances, there is a need for methods to recycle and reprocess these polymers. In this study, polymers prepared by inverse vulcanization are shown to undergo reactive compression molding. In this process, the reactive interfaces of sulfur polymers are brought into contact by mechanical compression. Upon heating these molds at relatively low temperatures ($\approx 100^\circ\text{C}$), chemical bonding occurs at the polymer interfaces by S–S metathesis. This method of processing is distinct

from previous studies on inverse vulcanization because the polymers examined in this study do not form a liquid phase when heated. Neither compression nor heating alone was sufficient to mold these polymers into new architectures, so this is a new concept in the manipulation of sulfur polymers. Additionally, high-level ab initio calculations revealed that the weakest S–S bond in organic polysulfides decreases linearly in strength from a sulfur rank of 2 to 4, but then remains constant at about 100 kJ mol^{-1} for higher sulfur rank. This is critical information in engineering these polymers for S–S metathesis. Guided by this insight, polymer repair, recycling, and repurposing into new composites was demonstrated.

Introduction

New efforts in the design of materials that can be generally recycled and integrated into a circular economy are necessary to overcome the burden of polymer waste on the environment.^[1] Currently, there is an unfortunate reliance on landfills and incineration of polymer waste.^[2] Where polymers are recycled, these materials are typically reprocessed mechanically into new resins or melt-processed to form new goods. In the case of melt-processing, the elevated temperatures lead to chemical degradation of the polymer which can limit the durability and value of the recycled material.^[2a] In the case of thermoset poly-

mers, these cross-linked materials cannot be reprocessed or reformed and so they are not typically recycled.^[2,3] To generalize the recyclability of polymeric materials, there is a need for methods to break down polymers into constituent components (monomers or smaller building blocks) so that they can be re-used in synthesis.^[3] Encouraging advances in vitrimer technology have been reported to address this challenge where polymer repair, recycling and reforming is made possible by chemically reversible or exchangeable cross-links.^[3] Among these cross-links, S–S bonds are of particular interest,^[3] especially with the advent of synthetic methods, such as inverse vulcanization, that provide straightforward access to

[a] N. A. Lundquist, A. D. Tikoalu, Dr. M. J. H. Worthington, R. Shapter, S. J. Tonkin, M. Mann, Dr. J. R. Gascooke, Dr. L. J. Esdaile, Dr. J. M. Chalker
Institute for Nanoscale Science and Technology
College of Science and Engineering, Flinders University
Sturt Road, Bedford Park, Adelaide, South Australia, 5042 (Australia)
E-mail: louisa.esdaile@flinders.edu.au
justin.chalker@flinders.edu.au

[b] Dr. F. Stojcevski, Prof. Dr. L. C. Henderson
Institute for Frontier Materials, Deakin University
Pigdons Road, Waurn Ponds Campus
Geelong, Victoria, 3216 (Australia)

[c] Dr. C. T. Gibson
Flinders Microscopy and Microanalysis, College of Science and Engineering,
Flinders University
Bedford Park, Adelaide, South Australia 5042 (Australia)

[d] Dr. A. Karton
School of Molecular Sciences, University of Western Australia
Perth, Western Australia 6009 (Australia)

 Supporting information and the ORCID identification number(s) for the author(s) of this article can be found under:
<https://doi.org/10.1002/chem.202001841>.

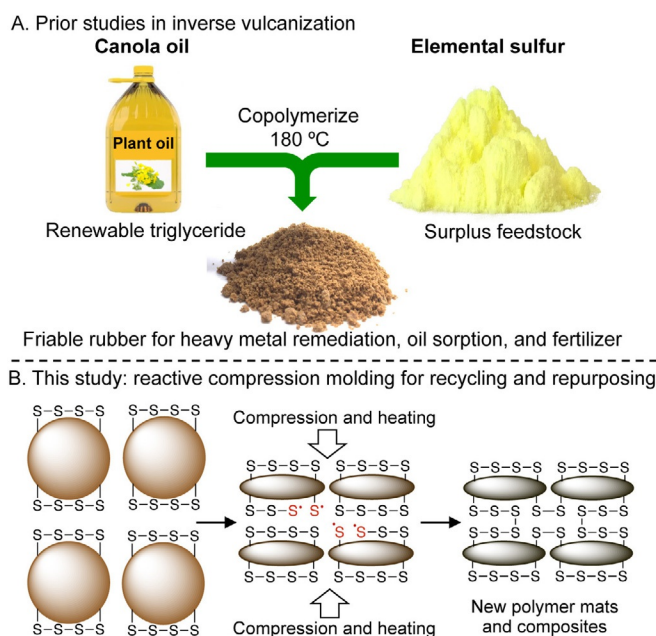
 Part of a Special Collection to commemorate young and emerging scientists. To view the complete collection, visit: [Young Chemists 2020](https://www.chemistry-europe.com/young-chemists-2020).

polysulfide-containing polymers.^[4] In this reaction, introduced by Pyun and collaborators in 2013, elemental sulfur is co-polymerized at a high feed ratio with an unsaturated organic cross-linker (usually an organic polyene), providing materials with sulfur content of typically 50–80% by mass.^[4] These materials have been explored as cathodes for Li-S batteries;^[4] optics equipment for infrared imaging;^[5] sorbents for oil spills;^[6] metals,^[7] and organic micropollution;^[8] components of slow release fertilizers;^[9] antimicrobial materials,^[10] and several other emerging applications.^[11] Another intriguing property of polymers prepared by inverse vulcanization is that the S-S bonds in the backbone of the polymer are dynamic and can be exchanged by heating to repair and recycle these materials.^[12] In this study, we report an investigation into the recycling and repurposing of a polymer made by the inverse vulcanization of canola oil—referred to here as 50-poly(S-*r*-canola), where 50 is the wt% sulfur and *r* designates a random co-polymerization. This friable rubber is sustainable, as it is prepared by the direct reaction of elemental sulfur (a surplus co-product of petroleum refining) with renewable plant oils such as canola oil, sunflower oil, olive oil, castor oil, or rice bran oil.^[7b,d] We have previously shown that this material can even be made from used cooking oil—a capability that aligns with our interests in waste valorization and green chemistry.^[6,7b,c] It is important to point out that 50-poly(S-*r*-canola) is a network polymer that is highly insoluble and only dissolves in the presence of reagents that cleave S–S bonds, such as amines or phosphines.^[7b,d] Therefore solvent-free methods of processing post-polymerization are required, a capability that would facilitate processing, recycling, and repurposing of 50-poly(S-*r*-canola). To this end, thermal processing under compressive force was investigated. Unlike some previous examples of sulfur polymer recycling or melt-processing which proceed through a molten state during the thermal treatment,^[4,12b,c] it was found that 50-poly(S-*r*-canola) can be reformed only if the reactive surfaces are mechanically forced into contact while heating and no liquid phase was formed. We demonstrate that this reactive compression molding allows the assembly, recycling, and repurposing of this polymer. And while the study of S–S metathesis reactions in the rubber industry has a rich history,^[13] we note that these polymers are not made from renewable materials, such as unsaturated triglycerides. Furthermore, we demonstrate reactive compression molding in new applications for this class of polymers such as repurposing into composite materials. From a fundamental chemistry perspective, we also show that these specific polymers, with an average sulfur rank between 4 and 6, have a much lower S–S bond strength compared to most disulfide linked polymeric systems. The concept of reactive compression molding is illustrated in Scheme 1.

Results and Discussion

Polymer synthesis

50-Poly(S-*r*-canola) was prepared by the inverse vulcanization of an equal mass of canola oil and elemental sulfur (S₈), as previously described by our laboratory (Scheme 1 A and Support-



Scheme 1. A) Inverse vulcanization: the co-polymerization of canola oil and sulfur provides high sulfur-content materials useful in diverse applications. B) Reactive compression molding is proposed as a new concept in the assembly, recycling, and repurposing of these polymers. In the proposed process, thermally induced homolytic cleavage of S–S bonds leads to rapid S–S metathesis at the polymer interfaces. Compression ensures sufficient contact with these reactive surfaces.

ing Information, page S4).^[6,7b] Briefly, the canola oil (450.0 g) was heated up to 170 °C in a stainless-steel reaction vessel (4.7 L, 20 cm diameter). Stirring was implemented at 90 rpm using an overhead stirrer with a stainless-steel impeller. An equal mass of sulfur (450.0 g) was added to the heated canola oil over 10–15 minutes ensuring that the temperature never dropped below the floor temperature of sulfur (159 °C). Upon

Louisa J. Esdaile earned a Bachelor of Applied Science in Chemistry at Queensland University of Technology (QUT) in 2002. Under the supervision of Prof. D. Arnold at QUT, she completed her Ph.D. in Organic Chemistry in 2007, developing innovative methods in porphyrin synthesis. From 2007 to 2009, Louisa worked as a post-doctoral researcher with Prof. H. Anderson at the University of Oxford, where she studied porphyrin based molecular wires. Louisa then moved to Northwestern University to take up a second post-doctoral research position in the group of Prof. Sir J. F. Stoddart. There, she contributed to the design and synthesis of molecular knots, dendrimers and other molecules with interesting topology. After two years at Dow Electronic Materials and one year of teaching at The University of Tulsa, Louisa moved to Flinders University in Adelaide, where she is an Associate Lecturer. Louisa also has interests in the intersection of science and public policy, earning a Masters of Public Administration (Policy) from Flinders University in 2017. In 2019, she took up a joint-appointment as a Project Manager with Clean Earth Technologies, where she leads research projects on sustainable materials and environmental remediation technology and services.



completion of the sulfur addition, the two-phase reaction typically appears to form one phase. At this point the temperature of the reaction mixture was increased to 180 °C and over the next 20 minutes sodium chloride (2100 g, finely ground) was slowly added ensuring the temperature remained above 159 °C. At this point the mixture was light brown, opaque, and a free flowing liquid. Over 15–20 minutes the viscosity of the reaction mixture increases. Once the overhead stirrer registered a torque of approximately 40 Ncm, the reaction vessel was removed from the hotplate and the product was removed from the reactor and ground into a powder. The final product was washed repeatedly with water to remove the sodium chloride porogen. After drying in air, the product is a soft, brown rubber. This same procedure was adapted in the preparation of poly(*S-r*-canola) with less sulfur (30% sulfur by mass). We subsequently refer to this material as 30-poly(*S-r*-canola). NMR, TGA, SEM and EDX analysis of the polymer were consistent with that previously reported and selected characterization data is provided in the Supporting Information.^[6] Based on lipid analysis of the canola oil used in this polymerization, the average number of alkenes per molecule of canola oil used in this study is 3.4 and the average molecular weight of the canola oil triglyceride was 882.6 g mol⁻¹.^[7d] Alkene conversion for 50-poly(*S-r*-canola) was 86%, consistent with our previous reports of this reaction.^[6,7d] The amount of unreacted sulfur for 50-poly(*S-r*-canola) was approximately 20 wt%, as determined by quantitative DSC analysis (Supporting Information, page S43). For the preparation of 30-poly(*S-r*-canola), the alkene conversion was slightly lower at 75% and the free elemental sulfur in the product was 2.6 wt% (Supporting Information, page S43). At these conversions and feed ratios, the aver-

age sulfur rank of 50-poly(*S-r*-canola) is 5.7 and the average sulfur rank of 30-poly(*S-r*-canola) is 4.5. The sulfur rank is important as this is the average number of S atoms in the polysulfide cross-links between each alkene. The length of this polysulfide cross-link is related to the S–S bond strengths in the polymer and therefore a critical parameter in processing polymers made by inverse vulcanization (*vide infra*).

First-generation reactive compression molding

It was observed in a control experiment that when 20 g of the 50-poly(*S-r*-canola) polymer was placed in a beaker and incubated in an oven at 110 °C for 24 hours, the material darkened in color, but it did not liquefy (Figure 1 A). And while the material did appear to form small aggregates, the sample was not bound together strongly and still behaved as a free-flowing powder. This control experiment illustrated how this polymer is distinct from other polymers made by inverse vulcanization that liquefy upon heating.^[4,12c,14] Suspecting that the reactive S–S groups on the polymer surface were not in sufficient contact to undergo exchange and bond to each other, the experiment was repeated with compression to force together the reactive surfaces. Accordingly, 20 g of powdered 50-poly(*S-r*-canola) was compressed between two metal plates using C-clamps (Figure 1 B and Supporting Information, pages S5 and S6). Poly(tetrafluoroethylene) (PTFE) sheets were used to prevent adhesion to the metal plates. The compressed polymer was incubated in an oven at 110 °C for 24 hours. After this time, the polymer was converted into a flexible rubber mat (Figure 1 B). The ¹H NMR spectra before and after the compression molding differed slightly, with molded polymer showing a

A. 50-poly(*S-r*-canola) (20 g, 110 °C, 24 h, *no compression*)



B. Reactive compression molding of 50-poly(*S-r*-canola) (20 g, 110 °C, 24 h, *compression*)



Figure 1. A) Heating 20 g of 50-poly(*S-r*-canola) in a beaker at 110 °C for 24 hours in an oven does not result in melting and the polymer is recovered as a slightly darkened powder. B) Heating 20 g of polymer between two PTFE sheets and metal plates, with pressure applied from C-clamps, results in the formation of a monolithic and flexible rubber mat (110 °C, 24 h, oven).

reduced integration of the alkene peaks (Supporting Information, page S7). This result is consistent with homolytic cleavage of the S–S bonds and reaction with alkene remaining after the original polymerization (it was later found that the reaction at the alkene only occurs with prolonged heating and the mat can be formed in shorter times where S–S metathesis is dominant mechanism of reaction, *vide infra*). It should also be noted that the alkene peaks were *not* consumed when the polymer was incubated in a beaker for 24 hours at 110 °C without compression (Supporting Information, page S6). This result means that the reaction does indeed require compression to force the reactive interfaces of the polymer powder into contact. The reactive compression molding was then repeated using this simple apparatus at 80, 90 and 100 °C for 24 hours (Supporting Information, page S8). While all of these experiments resulted in a mat, it was clear that 110 °C resulted in a

more uniform appearance and durability—especially in the areas of the mat directly compressed by the clamps (Supporting Information, page S8). This observation prompted us to study the reactive compression molding in a hot press in which the pressure could be controlled and applied more uniformly across the surface of the polymer mat.

Second-generation reactive compression molding

In order to control both the temperature and pressure in the reactive compression molding, we employed a 10-ton hydraulic rosin press with digitally controlled heated steel plates. A stainless steel mold (10 cm × 10 cm) was lined with PTFE sheets and 5.0 g of 50-poly(S-*r*-canola) was added to mold (Figure 2A and Supporting Information, page S9). In optimizing the process, the pressure, temperature and time were all varied. Initial-

A. Second-generation reactive compression molding process



B. Pressure variation (10 min at 100 °C)



0 MPa



10 MPa



20 MPa



30 MPa



40 MPa

C. Temperature variation (10 min at 40 MPa)



70 °C



80 °C



90 °C



100 °C

D. Reaction time variation (100 °C, 30 MPa)



1 min



5 min



10 min



30 min



60 min

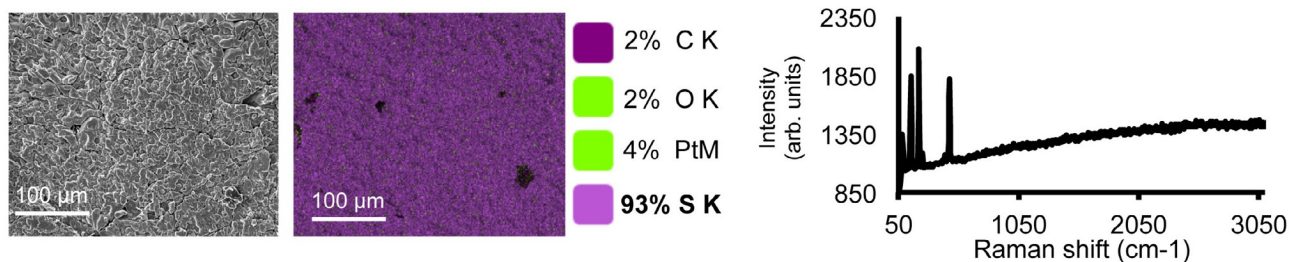
Figure 2. A) Second-generation reactive compression molding of 5.0 g of 50-poly(S-*r*-canola) into a rubber mat. A stainless steel mold and heated hydraulic press were used to control the temperature and pressure. B) Compression of the polymer is required to obtain a uniform mat of 50-poly(S-*r*-canola). Shown is the effect of pressure for a 10 minute reaction at 100 °C. C. At 40 MPa, 90 °C or higher is required to provide a uniform 5.0 g 50-poly(S-*r*-canola) polymer mat within 10 minutes. D. At 30 MPa and 100 °C a polymer mat made of 50-poly(S-*r*-canola) is formed within 10 minutes. Continued reaction provides a continually darker and more uniform surface.

ly, the reactive compression molding was tested in a short 10 minute process at 100 °C. Without any pressure, the polymer did not change by visual inspection and was recovered as powdered particles (Figure 2B). However, simply applying 10 MPa of pressure at 100 °C for 10 minutes led to the formation of a relatively uniform mat. Repeating the experiment at 20, 30 and 40 MPa lead to increasingly homogenous mats with fewer cracks and defects (Figure 2B and Supporting Information, pages S16–S18). Similar results were observed at 90 °C at these pressures (Supporting Information, pages S19–S21). These results are striking in that they show the reactive compression molding occurs very rapidly (within minutes) under at least 10 MPa pressure. To determine the lowest temperature for this process, the compression reaction was run at 40 MPa for 10 minutes at 70, 80, and 90 °C. While a mat formed in all cases, 90 °C was required otherwise significant cracks and defects were observed (Figure 2C and Supporting Information, pages S22–S24). Notably this is a far lower processing temperature than other recent S-S metathesis reactions in materials under compression.^[15] In examining the time required to provoke reactive compression molding, the mold was placed under 30 MPa of pressure and then heated to 100 °C. The reaction time was varied from 1 minute at 100 °C to 1 hour at 100 °C (see Supporting Information, page S10 for more examples). The resulting polymer mats are shown in Figure 2D. Even after 1 minute, it was clear that the polymer was reacting, though the mat was neither continuous nor uniform. However, with additional time the mat becomes more uniform and durable (Figure 2D). ¹H NMR analysis of the product mat showed little or no change in the integration of the alkene peaks in

the original polymer, so we attribute the bonding in the mat to S–S metathesis reactions at the surface of the compressed polymer (Supporting Information, page S14). Interestingly, a layer of elemental sulfur formed on the surface of the mat over the course of the reactive compression molding, as indicated by both Raman spectroscopy and EDX analysis of the surface and cross-section of the mat (Figure 3 and Supporting Information, pages S11–S13). DSC analysis indicated that the amount of free sulfur in the material did not change (Supporting Information, page S15), so we attribute the formation of this sulfur film to the sublimation of free sulfur during the molding procedure. If the free sulfur is unwanted, 30-poly(*S-r*-canola) contains only 2.6 wt% residual elemental sulfur. This polymer provided a very similar polymer mat after reactive compression molding, but no layer of free sulfur. This experiment also indicates that free sulfur is not required for the reactive compression molding (Supporting Information, pages S25–S27). Regarding the potential utility of the sulfur film on the top surface of the 50-poly(*S-r*-canola) polymer mat, we note it could be of interest in modulating the surface chemistry, imparting chemical resistance, or even antibacterial effects to the mat surface.

It is noteworthy that the temperature required for reactive compression molding (≈ 100 °C) is far lower than the temperature of the original inverse vulcanization (180 °C). We attribute this phenomenon to the S–S bonds in the polymer that are weaker than those in elemental sulfur. To illustrate this difference, a control experiment was run in the press in which 2.5 g of sulfur and 2.5 g of canola oil were pressed at 40 MPa at 100 °C for 10 minutes. Only unreacted sulfur and canola oil

A. Top surface of 50-poly(*S-r*-canola) mat (SEM, EDX, Raman)



B. Cross section of mat

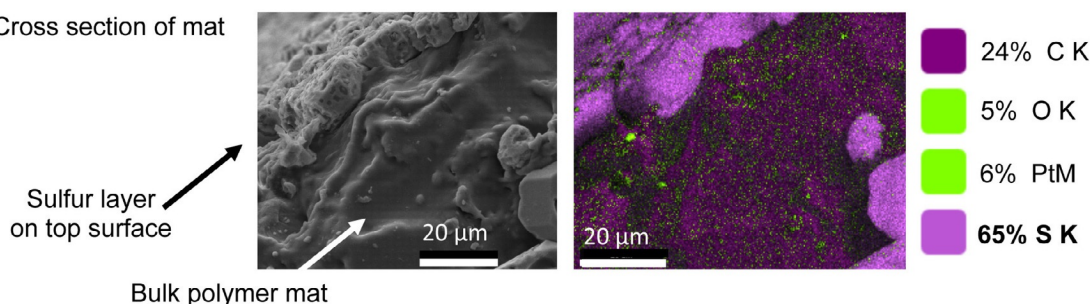


Figure 3. Reactive compression molding of 50-poly(*S-r*-canola) provides a mat in which the free elemental sulfur coats the top surface. This sulfur layer is likely formed by sublimation. For this sample, the reactive compression molding was carried out for extended time to further accentuate the formation of this layer (360 min, 30 MPa, 100 °C). A) EDX and Raman spectroscopy of the top surface are consistent with elemental sulfur (see Supporting Information, page S11–S13 for additional details). B) A cross-section of the mat also reveals the sulfur layer on the top surface.

were recovered (Supporting Information, page S28). This result shows how the polymer made by inverse vulcanization can be reacted and manipulated in ways not possible with the original sulfur and canola oil monomers.

Theoretical considerations regarding S-S metathesis of organic polysulfides

The facile manipulation of poly(*S-r*-canola) by reactive compression molding was attributed to S–S bonds that can be thermally cleaved and reformed in a metathesis process (Scheme 1B). As mentioned previously, the average sulfur rank for poly(*S-r*-canola) was calculated to be 5.7 for 50-poly(*S-r*-canola) and 4.5 for 30-poly(*S-r*-canola). As this sulfur rank might influence the S–S bond strength, and therefore the temperature at which reactive compression molding is possible, it is important to understand this relationship. Therefore, we examined the S–S bond strength of a series of dimethyl polysulfides (MeS_{*n*}Me) computationally.

Accordingly, high-level ab initio calculations (with the ab initio Gaussian-4 (G4) thermochemical protocol)^[16] were performed to probe the strength of the S–S bonds in polysulfide chains. The G4 protocol is an efficient composite procedure for approximating the CCSD(T) energy (coupled cluster with singles, doubles, and quasiperturbative triple excitations) in conjunction with a large triple- ζ -quality basis set and has been found to produce bond dissociation energies (BDEs) and other thermochemical properties with chemical accuracy (arbitrarily defined as ≈ 4 kJ mol⁻¹).^[16–17] We considered the homolytic BDEs of the S–S bonds in model dimethyl polysulfides (MeS_{*n*}Me, in which *n* = 2, 3, 4, 5, 6, and 7). The BDEs of the S–S bonds on the enthalpic (ΔH_{298}) and Gibbs free (ΔG_{298}) potential energy surfaces (PESs) at 298 K are tabulated in the Supporting Information (pages S29–S32). Inspection of these BDEs reveals that for MeS_{*n*}Me chains with more than two sulfur atoms, the weakest S–S bond is the MeS₂–S_{*n-2*}Me bond. A plot of the Gibbs-free BDEs for the weakest S–S bond in each of the MeS_{*n*}Me chains (*n* = 2–7) is shown in Figure 4. This plot shows that the S–S bond energy is reduced linearly for chains of 2, 3, and 4 sulfur atoms, with Gibbs-free BDEs of 215.0 (MeS₂Me), 160.2 (MeS₃Me), and 98.9 (MeS₄Me) kJ mol⁻¹. However, for chains with four or more sulfur atoms the S–S bond energy remains fairly constant at ≈ 100 kJ mol⁻¹, with Gibbs-free BDEs of 104.0 (MeS₅Me), 97.2 (MeS₆Me), and 100.2 (MeS₇Me) kJ mol⁻¹.

The results in Figure 4 are consistent with classic experimental observations of Tobolsky in the thermal decomposition of dimethyl polysulfides^[18] and provide important insight into the processability of polysulfide polymers. For instance, in the design of polymers made by inverse vulcanization, a sulfur rank of at least 4 should be targeted if S–S lability is desired. These weak S–S bonds (compared to materials with sulfur ranks of 2 or 3) would allow thermally promoted S-S metathesis at a lower temperature. Additionally, the data in Figure 4 suggests that a polymer made by inverse vulcanization with a sulfur rank > 4 would not provide a system with weaker S–S bonds. This is an important consideration as S–S bond strength in these polymers has been invoked previously in the

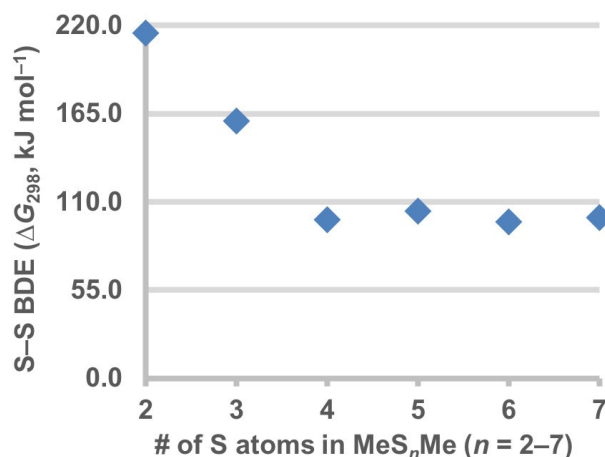


Figure 4. Gibbs-free bond dissociation energies (BDEs) at 298 K (ΔG_{298} , G4 theory, kJ mol⁻¹) for the weakest S–S bond in dimethyl polysulfides (MeS_{*n*}Me) containing 2–7 sulfur atoms.

literature to account for the variation in rheological properties of polysulfide polymers with different sulfur ranks.^[12a] For the polymer system in Figure 2, the calculated S–S bond strengths are consistent with the proposed S–S metathesis that occurs rapidly at temperatures even below 100 °C. These results are also consistent with a study by Jenkins in which S–S bond cleavage in polymers made by inverse vulcanization occurred at temperatures as low as 90 °C.^[19]

Reactive compression molding for recycling and repurposing 50-poly(*S-r*-canola)

With optimized protocols for reactive compression molding in hand, as well as a sound theoretical understanding of the thermally initiated S-S metathesis reaction, we next investigated applications of this chemistry. The first application of reactive compression molding tested was recycling of a 50-poly(*S-r*-canola) mat (Figure 5A). The original mat was first prepared by reacting 5.0 g of the poly(*S-r*-canola) powder at 100 °C for 10 minutes at 40 MPa. The resulting mat was then cut up and then ground into a powder. A small portion (500 mg) of this polymer was saved for analysis and the remaining material was returned to the hot press and re-subjected to the reactive compression molding process. The recycled mat appeared the same as the first mat and there was no difference observed by TGA, DSC, ¹H NMR and SEM analysis (Supporting Information, pages S33–S35). This process demonstrates that a cross-linked polymer prepared by inverse vulcanization can be recycled through reactive compression molding. This is distinct from other cross-linked rubbers that are rarely recycled because heating these materials leads to thermal degradation.^[20] In contrast, the 50-poly(*S-r*-canola) material can be reformed and recycled at a relatively low temperature.

The recycling concept validated in Figure 5A was then extended to polymer re-purposing. Poly(*S-r*-canola) has previously been explored in removing Fe³⁺ from water to decolorize and prevent bio-fouling induced by iron.^[7c] However, in this process

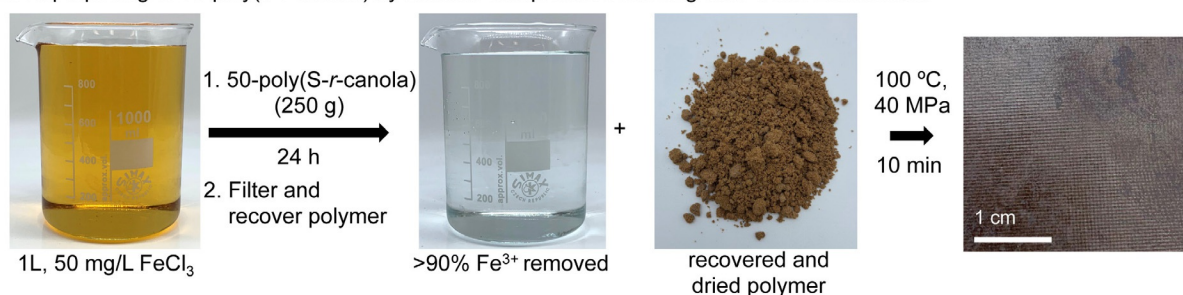
A. Recycling of 5.0 g of 50-poly(*S-r*-canola) by reactive compression moldingB. Repurposing of 50-poly(*S-r*-canola) by reactive compression molding after water remediation

Figure 5. A) Reactive compression molding can be used to recycle the 50-poly(*S-r*-canola) mat. B) 50-poly(*S-r*-canola) can be used to remove Fe^{3+} from water and then repurposed to a new architecture via reactive compression molding. At these levels, the bound iron did not affect the reactive compression molding.

it was found that large quantities of polymer were required to remove the iron. In such cases, a plan for repurposing the polymer would be required. We considered that reactive compression molding might be useful in converting the powdered polymer sorbent into a rubber mat after use in the remediation process. In this way, the polymer might be useful as a component of building materials or other composites. To test this possibility, 250 g of poly(*S-r*-canola) was added to a 1 L solution of FeCl_3 (50 mg L^{-1}). After 24 hours, $>90\%$ of the iron was removed and the water was clear. The polymer (with bound iron) was then isolated by filtration, dried in a fume hood, and subjected to reactive compression molding (100°C , 40 MPa, 10 min, 5.0 g of the recovered polymer). The resulting mat (Figure 5B) appeared no different than the mat formed from pristine poly(*S-r*-canola) and was indistinguishable by ^1H NMR, SEM, TGA, and DSC analysis (Supporting Information, pages S36–S39). This experiment demonstrates that the iron bound to the polymer did not interfere with the S–S metathesis reaction during the reactive compression molding. More generally, this process illustrates a strategy for repurposing the poly(*S-r*-canola) after the many remediation applications already demonstrated in our laboratory.^[6,7b-d,8]

Reactive compression molding to access composite materials with tunable mechanical properties

A mat made by reactive compression molding of 50-poly(*S-r*-canola) (100 MPa, 100°C , 20 min) was analyzed by nanoindentation (Supporting Information, page S40). Averaging over five samples revealed a hardness of $0.5 \pm 0.1 \text{ GPa}$, a stiffness of $1.4 \pm 0.5 \mu\text{N nm}^{-1}$, and a reduced elastic modulus of $3 \pm 1 \text{ GPa}$.

These values reflect the soft and flexible nature of the rubber mat resulting from the reactive compression molding. And while this material might be directly useful in applications in which a soft and flexible rubber mat is required, we next considered ways in which the mechanical properties of the mat could be altered. We therefore next examined the 50-poly(*S-r*-canola) as a “reactive mortar” to bind together other fillers in the preparation of composite materials. Coconut coir, sand, PVC, and powdered carbon fiber were all used to explore this concept. Coconut coir can be considered agricultural waste,^[21] sand, sand-surrogates and gravel-like substances are important fillers in construction,^[22] and there are limited options for PVC recycling.^[23] In forming the composites, 50-poly(*S-r*-canola) was simply blended with the filler (50–80 wt% filler) and then subjected to reactive compression molding (100°C , 40 MPa, 20 min) (Figure 6A and Supporting Information, pages S44–S53). The resulting composites could be further reacted in an additive fashion, producing laminate type materials through reactive compression molding (Figure 6B and Supporting Information, pages S46–S49). The composites were then subjected to mechanical testing. It was found that the compression modulus and flexibility of the composites were indeed different than the parent polymer mat. For instance, the sand composites and the composite made from 50 wt% coconut coir have compression moduli of $\approx 12 \text{ MPa}$, nearly double that of the polymer mat alone (Supporting Information, pages S50–S51). In a three-point bend test, all of the composites were stiffer and had a higher elastic modulus than the polymer control (Figure 6A and C, Supporting Information, pages S52 and S53). An interesting feature of the PVC composite is that because the T_g of the PVC is 84°C (Supporting Information, page S51),

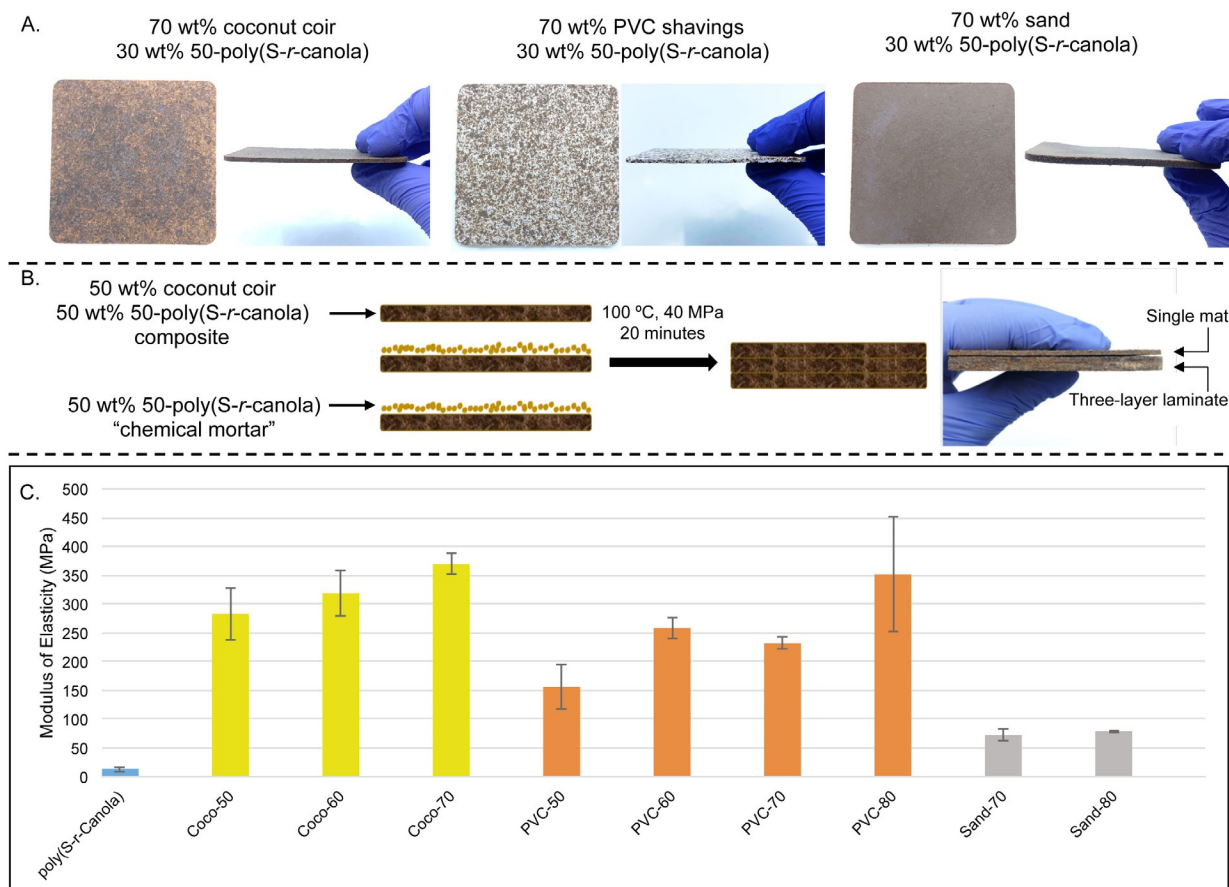


Figure 6. A) Representative composites prepared by the reactive compression molding of the powdered 50-poly(S-r-canola) and varying amounts of coconut coir, PVC shavings, and sand. B) A composite mat made by reactive compression molding can be reacted further in an additive process, using additional powdered 50-poly(S-r-canola) at the interface as a "chemical mortar". C. Three-point bend test of composites prepared by reactive compression molding show the filler material leads to a composite that is stiffer than a polymer mat made without filler.

the composite is flexible when it is removed from the 100 °C mold and it can therefore be further re-shaped (for instance into a curved mat) before the composite cools and sets. We note that the composites made from either coconut coir or PVC have a relatively high variability in the measured modulus of elasticity. This is likely due to the non-uniform size of the filler particles and the resulting inhomogeneity of the composite. In contrast, the sand filler is more uniform, which leads to less variability in these measurements. Despite this variability, the reactive compression molding method is a rapid and simple way to incorporate the coconut coir and PVC waste into new composite materials.

Next, a composite made from powdered carbon fiber and 50-poly(S-r-canola) was prepared. Composites of 10, 20 and 30 wt% carbon were then made through reactive compression molding with poly(S-r-canola) (100 °C, 40 MPa, 20 min), providing black composite mats. At higher levels of carbon, free carbon was observed to flake off of the composite. Rather than test the mechanical properties of this composite, we instead assessed how the contact angle of solvents (water, ethanol and glycerol) changed with carbon fiber (Figure 7 and Supporting Information, page S54). While the variation of the contact angle was not uniform, it is clear that the surface energy

and interaction of the polymer and composites can be modulated. This capability might find use in developing new applications of these composites in which solvent interaction or repel-

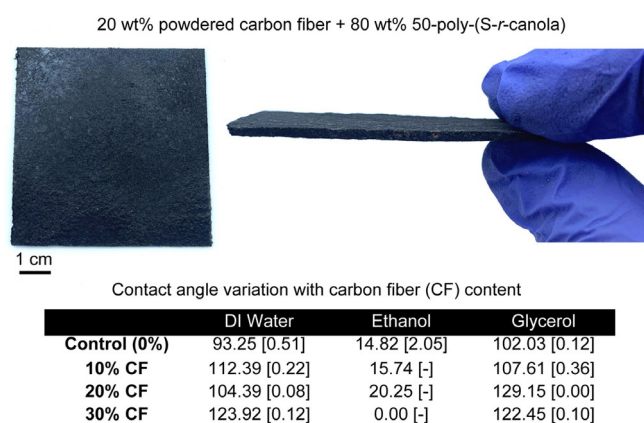


Figure 7. A composite mat made from powdered carbon fiber (CF, 10, 20, and 30 wt%, 20 wt% shown) and 50-poly(S-r-canola) (90, 80, and 70 wt%, 80 wt% shown). The mat was prepared by reactive compression molding (100 MPa, 100 °C, 20 min). The carbon fiber was found to modulate the contact angle for water, ethanol and glycerol. Standard deviations are indicated in brackets.

lency is important. As carbon fiber is increasingly incorporated into machinery and other commercial products, new processes are required to recycle and repurpose this material.^[24] We demonstrate one strategy for such a process in this study and will report additional integration of this composite into new construction materials and other applications in due course.

Conclusions

Reactive compression molding was introduced as a new processing method for rubber-like materials made by inverse vulcanization. This process is rapid and technically simple, requiring only a simple hot press to force the reactive faces of the polymer together. Notably, the processing temperatures ($\approx 100^\circ\text{C}$) are far lower than the original polymerization. The S–S metathesis reaction at the center of this process was also studied computationally, revealing that the weakest S–S bond in an organic polysulfide decreases from di- to tri- to tetrasulfides, but then levels off for higher sulfur rank. This information is critical in the design of polymers amenable to reactive compression molding because the rate of the process will be directly related to the sulfur rank. The reactive compression molding of poly(S-*r*-canola) was then validated in the recycling and repurposing of this material, which is an important milestone in managing the life cycle of cross-linked polymers—most of which are currently unrecyclable. Finally, we demonstrate that reactive compression molding can be integrated into the synthesis of composite materials with a range of useful and tunable mechanical properties. We anticipate that these findings will impact efforts in sustainable materials and their use in a number of applications.

Acknowledgements

The authors acknowledge financial support from the Australian Research Council (DP200100090), The AMP Tomorrow Fund and the Flinders University Impact Seed Funding for Early Career Researchers (J.M.C.). The authors also acknowledge the support of the Microscopy Australia research facility at Flinders University. This work was performed in part at the South Australian node of the Australian National Fabrication Facility under the National Collaborative Research Infrastructure Strategy to provide nano and microfabrication facilities for Australia's researchers. This research was also undertaken with the assistance of resources from the National Computational Infrastructure (NCI), which is supported by the Australian Government. A.K. gratefully acknowledges an Australian Research Council Future Fellowship (FT170100373). L.C.H. and F.S. acknowledge funds from the circular economy initiative within the IFM at Deakin University, and thank the ARC (IIC160100032) and Office of Naval Research Global (N62909-18-1-2024) for additional funding. We thank Dr. Jonathan Campbell and Prof. David Lewis for helpful discussions and technical assistance.

Conflict of interest

Three authors (M.J.H.W., M.M., and J.M.C.) are inventors on patents and patent applications assigned to Clean Earth Technologies (WO2017181217 and AUS/2019901135). These patents include the synthesis and applications of polymers made by the copolymerization of alkenes and sulfur, including the polymers featured in this study.

Keywords: composites · inverse vulcanization · recycling · sulfur · sulfur polymer

- [1] a) J. R. Jambeck, R. Geyer, C. Wilcox, T. R. Siegler, M. Perryman, A. Andrad, R. Narayan, K. Lavender Law, *Science* **2015**, *347*, 768–771; b) B. A. Helms, T. P. Russell, *Chem* **2016**, *1*, 816–819.
- [2] a) A. Rahimi, J. M. Garcia, *Nat. Rev. Chem.* **2017**, *1*, 0046; b) J. Hopewell, R. Dvorak, E. Kosior, *Phil. Trans. R. Soc. B* **2009**, *364*, 2115–2126.
- [3] D. J. Fortman, J. P. Brutman, G. X. De Hoe, R. L. Snyder, W. R. Dichtel, M. A. Hillmyer, *ACS Sustainable Chem. Eng.* **2018**, *6*, 11145–11159.
- [4] W. J. Chung, J. J. Griebel, E. T. Kim, H. Yoon, A. G. Simmonds, H. J. Ji, P. T. Dirlam, R. S. Glass, J. J. Wie, N. A. Nguyen, B. W. Guralnick, J. Park, A. Somogyi, P. Theato, M. E. Mackay, Y.-E. Sung, K. Char, J. Pyun, *Nat. Chem.* **2013**, *5*, 518–524.
- [5] J. J. Griebel, S. Namnabat, E. T. Kim, R. Himmelhuber, D. H. Moronta, W. J. Chung, A. G. Simmonds, K.-J. Kim, J. van der Laan, N. A. Nguyen, E. L. Dereniak, M. E. MacKay, K. Char, R. S. Glass, R. A. Norwood, J. Pyun, *Adv. Mater.* **2014**, *26*, 3014–3018.
- [6] M. J. H. Worthington, C. J. Shearer, L. J. Esdaile, J. A. Campbell, C. T. Gibson, S. K. Legg, Y. Yin, N. A. Lundquist, J. R. Gascooke, I. S. Albuquerque, J. G. Shapter, G. G. Andersson, D. A. Lewis, G. J. L. Bernardes, J. M. Chalker, *Adv. Sustainable Syst.* **2018**, *2*, 1800024.
- [7] a) M. P. Crockett, A. M. Evans, M. J. H. Worthington, I. S. Albuquerque, A. D. Slattery, C. T. Gibson, J. A. Campbell, D. A. Lewis, G. J. L. Bernardes, J. M. Chalker, *Angew. Chem. Int. Ed.* **2016**, *55*, 1714–1718; *Angew. Chem.* **2016**, *128*, 1746–1750; b) M. J. H. Worthington, R. L. Kucera, I. S. Albuquerque, C. T. Gibson, A. Sibley, A. D. Slattery, J. A. Campbell, S. F. K. Alboaiji, K. A. Muller, J. Young, N. Adamson, J. R. Gascooke, D. Jampaiah, Y. M. Sabri, S. K. Bhargava, S. J. Ippolito, D. A. Lewis, J. S. Quinton, A. V. Ellis, A. Johs, G. J. L. Bernardes, J. M. Chalker, *Chem. Eur. J.* **2017**, *23*, 16219–16230; c) N. A. Lundquist, M. J. H. Worthington, N. Adamson, C. T. Gibson, M. R. Johnston, A. V. Ellis, J. M. Chalker, *RSC Adv.* **2018**, *8*, 1232–1236; d) A. D. Tikoalu, N. A. Lundquist, J. M. Chalker, *Adv. Sustainable Syst.* **2020**, *4*, 1900111.
- [8] N. A. Lundquist, M. J. Sweetman, K. R. Scroggie, M. J. H. Worthington, L. J. Esdaile, S. F. K. Alboaiji, S. E. Plush, J. D. Hayball, J. M. Chalker, *ACS Sustainable Chem. Eng.* **2019**, *7*, 11044–11049.
- [9] M. Mann, J. E. Kruger, F. Andari, J. McErlean, J. R. Gascooke, J. A. Smith, M. J. H. Worthington, C. C. C. McKinley, J. A. Campbell, D. A. Lewis, T. Hasell, M. V. Perkins, J. M. Chalker, *Org. Biomol. Chem.* **2019**, *17*, 1929–1936.
- [10] a) Z. Deng, A. Hoefling, P. Theato, K. Lienkamp, *Macromol. Chem. Phys.* **2018**, *219*, 1700497; b) J. A. Smith, R. Mulhall, S. Goodman, G. Fleming, H. Allison, R. Raval, T. Hasell, *ACS Omega* **2020**, *5*, 5229–5234; c) V. S. Wadi, K. K. Jena, K. Halique, S. M. Alhassan, *ACS Appl. Polym. Mater.* **2020**, *2*, 198–208.
- [11] a) J. J. Griebel, R. S. Glass, K. Char, J. Pyun, *Prog. Polym. Sci.* **2016**, *58*, 90–125; b) D. A. Boyd, *Angew. Chem. Int. Ed.* **2016**, *55*, 15486–15502; *Angew. Chem.* **2016**, *128*, 15712–15729; c) M. J. H. Worthington, R. L. Kucera, J. M. Chalker, *Green Chem.* **2017**, *19*, 2748–2761; d) J. M. Chalker, M. J. H. Worthington, N. A. Lundquist, L. J. Esdaile, *Top. Curr. Chem.* **2019**, *377*, 16; e) Y. Zhang, R. S. Glass, K. Char, J. Pyun, *Polym. Chem.* **2019**, *10*, 4078–4105; f) J. A. Smith, S. J. Green, S. Petcher, D. J. Parker, B. Zhang, M. J. H. Worthington, X. Wu, C. A. Kelly, T. Baker, C. T. Gibson, J. A. Campbell, D. A. Lewis, M. J. Jenkins, H. Willcock, J. M. Chalker, T. Hasell, *Chem. Eur. J.* **2019**, *25*, 10433–10440.
- [12] a) J. J. Griebel, N. A. Nguyen, A. V. Astashkin, R. S. Glass, M. E. MacKay, K. Char, J. Pyun, *ACS Macro Lett.* **2014**, *3*, 1258–1261; b) J. J. Griebel, N. A.

- Nguyen, S. Namnabat, L. E. Anderson, R. S. Glass, R. A. Norwood, M. E. MacKay, K. Char, J. Pyun, *ACS Macro Lett.* **2015**, *4*, 862–866; c) D. J. Parker, S. T. Chong, T. Hasell, *RSC Adv.* **2018**, *8*, 27892–27899; d) M. Arslan, B. Kiskan, Y. Yagci, *Sci. Rep.* **2017**, *7*, 5207; e) T. Thiounn, M. K. Lauer, M. S. Bedford, R. C. Smith, A. G. Tennyson, *RSC Adv.* **2018**, *8*, 39074–39082; f) M. S. Karunarathna, M. K. Lauer, T. Thiounn, R. C. Smith, A. G. Tennyson, *J. Mater. Chem. A* **2019**, *7*, 15683–15690; g) M. K. Lauer, T. A. Estrada-Mendoza, C. D. McMillen, G. Chumanov, A. G. Tennyson, R. C. Smith, *Adv. Sustainable Syst.* **2019**, *3*, 1900062; h) A. D. Smith, T. Thiounn, E. W. Lyles, E. K. Kibler, R. C. Smith, A. G. Tennyson, *J. Polym. Sci. Part A* **2019**, *57*, 1704–1710.
- [13] M. D. Stern, A. V. Tobolsky, *J. Chem. Phys.* **1946**, *14*, 93–100.
- [14] B. Zhang, S. Petcher, T. Hasell, *Chem. Commun.* **2019**, *55*, 10681–10684.
- [15] S. Zhang, L. Pan, L. Xia, Y. Sun, X. Liu, *React. Funct. Polym.* **2017**, *121*, 8–14.
- [16] a) L. A. Curtiss, P. C. Redfern, K. Raghavachari, *J. Chem. Phys.* **2007**, *127*, 124105; b) L. A. Curtiss, P. C. Redfern, K. Raghavachari, *WIREs Comput. Mol. Sci.* **2011**, *1*, 810–825.
- [17] a) A. Karton, N. Sylvetsky, J. M. L. Martin, *J. Comput. Chem.* **2017**, *38*, 2063–2075; b) R. J. O'Reilly, A. Karton, *Int. J. Quantum Chem.* **2016**, *116*, 52–60; c) R. J. O'Reilly, A. Karton, L. Radom, *Int. J. Quantum Chem.* **2012**, *112*, 1862–1878; d) B. Chan, L. Radom, *J. Phys. Chem. A* **2012**, *116*, 4975–4986.
- [18] T. L. Pickering, K. J. Saunders, A. V. Tobolsky, *J. Am. Chem. Soc.* **1967**, *89*, 2364–2367.
- [19] C. R. Westerman, C. L. Jenkins, *Macromolecules* **2018**, *51*, 7233–7238.
- [20] S. Bandyopadhyay, S. L. Agrawal, R. Ameta, S. Dasgupta, R. Mukhopadhyay, A. S. Deuri, S. C. Ameta, R. Ameta, *Prog. Rubber Plast. Re.* **2008**, *24*, 73–112.
- [21] M. V. Madurwar, R. V. Ralegaonkar, S. A. Mandavgane, *Constr. Build. Mater.* **2013**, *38*, 872–878.
- [22] B. Bhardwaj, P. Kumar, *Constr. Build. Mater.* **2017**, *156*, 661–674.
- [23] N. Singh, D. Hui, R. Singh, I. P. S. Ahuja, L. Feo, F. Fraternali, *Composites Part B* **2017**, *115*, 409–422.
- [24] S. R. Naqvi, H. Mysore Prabhakara, E. A. Bramer, W. Dierkes, R. Akkerman, G. Brem, *Resour. Conserv. Recycl.* **2018**, *136*, 118–129.

Manuscript received: April 16, 2020

Revised manuscript received: May 9, 2020

Accepted manuscript online: May 19, 2020

Version of record online: June 18, 2020



Confining a spent lead sorbent in a polymer made by inverse vulcanization prevents leaching

Nicholas A. Lundquist, Justin M. Chalker*

Flinders University, Institute for Nanoscale Science and Technology, Bedford Park, South Australia 5042, Australia



ARTICLE INFO

Article history:

Received 3 July 2020

Received in revised form 6 August 2020

Accepted 10 September 2020

Keywords:

Activated carbon

Inverse vulcanization

Leaching

Lead

Polysulfide

Reactive compression molding

ABSTRACT

The capture of heavy metal pollution in water is important for ensuring environmental and public health. In this study, a sorbent comprised of powdered activated carbon and a sustainable polysulfide polymer made by inverse vulcanization was used to remove lead from water. The dynamic S—S bonds in the polysulfide polymer were then used to form a composite block by reactive compression molding: a process that confines the pollution and prevents leaching. Leaching was prevented when the composite was submerged in water for 1 week. The reactive compression molding technique is a simple method for preventing leaching during the transport and storage of spent sorbents.

© 2020 Published by Elsevier B.V.

1. Introduction

The remediation of water contaminated with heavy metals is essential for public and environmental health. Lead pollution poses a substantial health risk, with harm to child development an ongoing concern [1–3]. Activated carbon is a common sorbent to remove Pb^{2+} from water [4], but there have been few reports on the full life cycle management of the spent sorbents. For persistent pollution such as heavy metals, there is a need for strategies to prevent leaching and contamination during the transport and storage of spent sorbents. In this study, we report a simple and effective method to confine lead to a powdered activated carbon sorbent. The method involves using a surface-reactive polymer to form a barrier around the spent carbon. The key polymer was made by inverse vulcanization—a copolymerization of sulfur and polyenes that provides organic polysulfides [5–7]. We have previously shown that this polymer, when blended with powdered activated carbon (PAC), reduced dust plumes of the finely powdered carbon, making PAC safer to handle [8]. The polysulfide support also prevented PAC from caking and blocking filters in continuous purification of water contaminated with *per*- and polyfluoroalkyl substances (PFAS) [8]. In this study, we report a new capability of the polymer support that takes advantage of the reactive S—S bonds contained in the material. Specifically, the polymer could be used as a barrier to contain

lead-contaminated PAC. The barrier is formed by dynamic exchange of the S—S bonds in the polymer that convert it from a powder to a monolithic block. This process is referred to as *reactive compression molding*, a technique recently reported as a method to make a variety of composite materials [9]. Here, this processing technology was applied to the confinement of a spent carbon sorbent to prevent leaching. The concept is illustrated in Fig. 1. The key polymer used in the reactive compression molding is also sustainable because it is made from renewable canola oil and elemental sulfur (a byproduct of petroleum refining). The barrier of the poly(*S-r*-canola) polymer was found to prevent lead leaching from the sorbent when submerged in water for one week.

2. Materials and methods

2.1. Poly(*S-r*-canola) synthesis

The polymer was prepared as previously described by the copolymerization of sulfur and canola oil [10]. Briefly, canola oil (450.0 g) was added to a 4.7 L, 20 cm diameter stainless steel reactor and heated to 170 °C. The canola oil was stirred with an overhead stirrer equipped with a stainless steel impeller and the oil temperature was monitored using a thermocouple placed directly in the reaction mixture. Sulfur (450.0 g) was then added over a period of 10 min. Care was taken so that the reaction temperature remained at least 155 °C. After the sulfur addition was complete, the thermostat of the reaction vessel was set to 180 °C and sodium chloride (2.10 kg) was added

* Corresponding author.

E-mail address: justin.chalker@flinders.edu.au (J.M. Chalker).

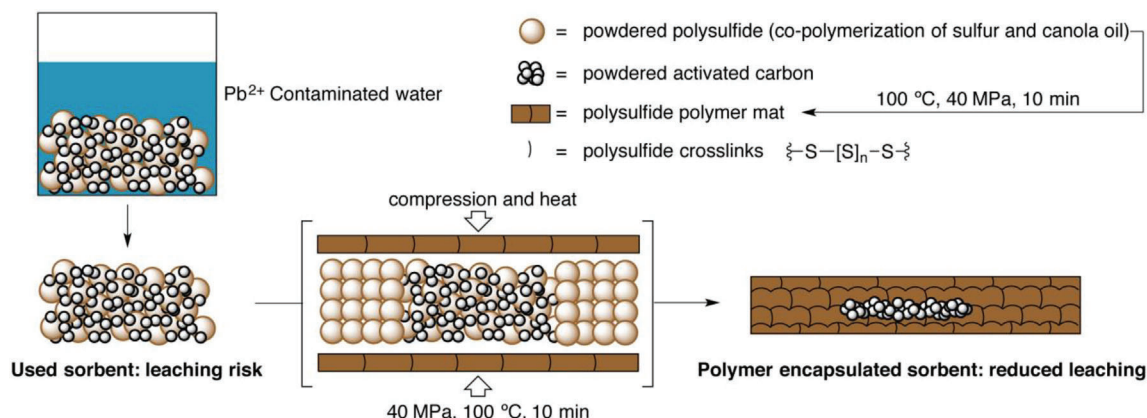


Fig. 1. Reactive compression molding [9] was used to encapsulate a spent sorbent and prevent leaching of captured lead. The sorbent was made from a blend of a polysulfide polymer and powdered activated carbon (PAC). The polymer reduces dust plumes by binding to the PAC, rendering it safer to handle [8]. The polymer in the sorbent has a reactive surface that becomes the mortar that allows adhesion to the final polymer casing. The adhesion occurs through metathesis of the S–S bonds in the polysulfide polymer [9].

over the course of 15 min. The reaction was heated for an additional 10–15 min with continuous stirring until the torque meter on the overhead stirrer registered 40 N·cm. At that stage, the stirring was stopped and the reactor was removed from the hot plate and cooled on a trivet. The polymer was removed from the reactor and mechanically ground to particles <3 mm in size. The sodium chloride porogen was then removed by stirring the ground polymer in 17 L of water. The polymer was isolated by filtration and washed twice more with water in the same manner. The washed polymer was dried in a fume hood, providing 850–900 g of poly(S-*r*-canola) product. All characterization data including thermal analysis (DSC and TGA) and spectroscopic analysis (IR and NMR) were fully consistent with that previously reported for this polymer [11–13].

2.2. Polymer-carbon sorbent preparation

The sorbent was made as previously described [8]. Briefly, 800 g of the poly(S-*r*-canola) polymer and 200 g powdered activated carbon (PGW 150 MP, Kuraray) were added to a plastic container and inverted repeatedly. The powdered activated carbon adheres to the polymer, forming a homogeneous and free-flowing blend. This sorbent was used for all lead sorption experiments.

2.3. Lead concentration measurements

Lead concentrations in water were measured by ICP-MS by Envirolab Services Pty Ltd., with accreditation by the National Association of Testing Authorities, Australia (NATA Accreditation Number 2901).

2.4. Lead sorption using the polymer-carbon blend

A solution of Pb²⁺ was prepared by adding 250 mg of Pb(NO₃)₂ to a 500 mL volumetric flask and dissolving in deionized water. After diluting to the 500 mL mark, an aliquot of the solution was filtered (25 μm nylon syringe filter), and the concentration was measured to be 560 ppm by ICP-MS using a certified commercial service as described above. In the sorption experiment, 250 mL of the Pb²⁺ solution was added to a 1 L plastic container along with 20 g of the polymer-carbon blend. The mixture was stirred for 1 h at 20 °C before isolating the carbon-polymer blend by filtration. The Pb²⁺ concentration of the filtrate was measured after an additional filtration through a syringe filter (25 μm, nylon). The carbon-polymer blend (with bound lead) was dried in a fume hood for 24 h before proceeding to the leaching experiments.

2.5. Control experiment using only polymer as a lead sorbent

An aqueous solution of Pb(NO₃)₂ prepared at a concentration of 560 ppm as described above, with the concentration verified by ICP-MS. Next, a 100 mL aliquot of this solution was added to a 500 mL plastic container along with 6.4 g of the poly(S-*r*-canola) polymer. This experiment was performed in triplicate and no carbon was used. The mixture was stirred for 1 h at 20 °C before isolating the polymer by filtration. The Pb²⁺ concentration of the filtrate was measured after an additional filtration through a syringe filter (25 μm, nylon). The final lead concentration was measured by ICP-MS using a certified commercial service as described above.

2.6. Reactive compression molding to confine the spent sorbent

Polymer mats were prepared from poly(S-*r*-canola) by reactive compression molding, as previously described [9]. Briefly, 5.0 g of the powdered poly(S-*r*-canola) was placed between two poly(tetrafluoroethylene) (PTFE) sheets in a 10 × 10 cm mold. The mold was placed in a heat- and pressure-controlled press and then processed at 100 °C and 40 MPa for 10 min. The resulting polymer mats were then used as a barrier in which the spent polymer-carbon sorbent could be contained. To encapsulate the spent sorbent, one of the pre-formed polymer mats was placed on a PTFE sheet in the mold. Next, the polymer-carbon blend (5.0 g of the spent sorbent bound to lead) was placed in the center of one of the pre-formed polymer mats. Then, 2.0 g of powdered poly(S-*r*-canola) was added around the perimeter of the mat. Next, the top polymer mat was added, followed by another PTFE sheet. The mold was placed in the heat- and pressure-controlled press and then processed at 100 °C and 40 MPa for 10 min. After cooling to room temperature, the polymer-encapsulated sorbent was removed from the mold and tested in leaching experiments.

2.6.1. Leaching of lead from the spent polymer-carbon blend

All leaching tests were carried out in triplicate. A 1.0 g sample of the spent polymer-carbon blend (with bound Pb²⁺) was added to a 50 mL plastic centrifuge tube along with 50 mL of deionized water. The sealed tubes were mixed at 20 °C using an end-over-end mixer operating at 25 rpm. After 1 week, the water was filtered (25 μm nylon syringe filter) and then the concentration of lead was determined by ICP-MS.

2.6.2. Leaching lead from the polymer encapsulated sorbent

All leaching tests were carried out in triplicate. The polymer mats encapsulating the spent sorbent were submerged in 250 mL of water in a 500 mL plastic container. The sealed container was placed on a rocker

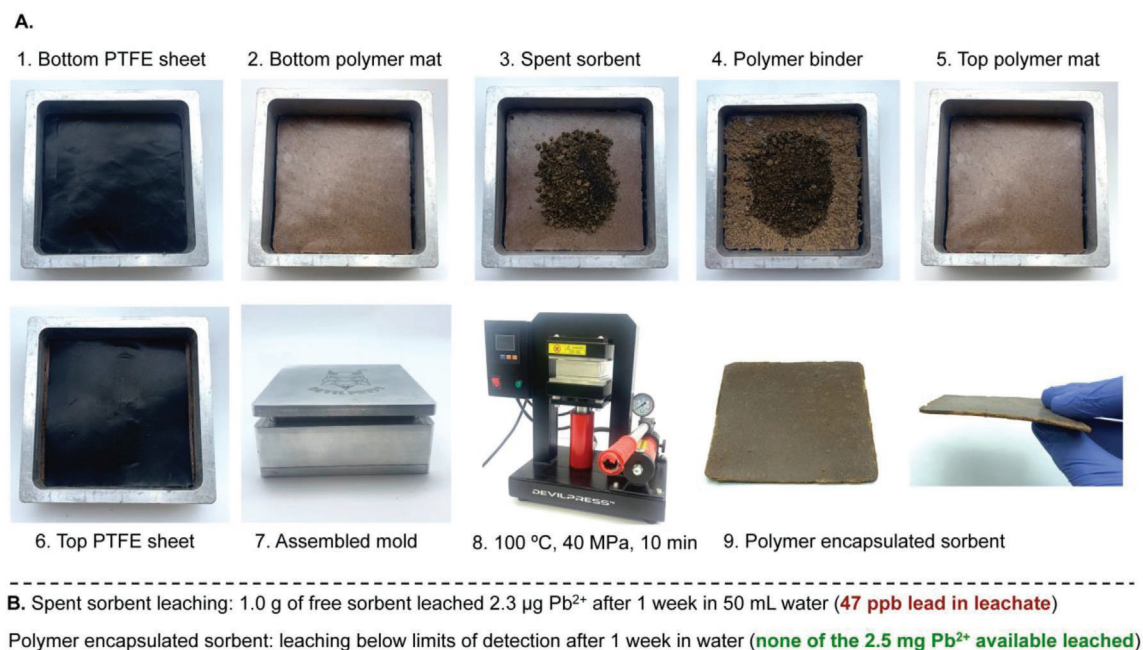


Fig. 2. A. Reactive compression molding allows a spent lead sorbent to be encapsulated in a polymer barrier. The mold is 10 × 10 cm. B. The polymer barrier prevents lead leaching after submerging in water for 1 week.

table at 20 °C for 8 weeks. The water was sampled and filtered (25 µm nylon syringe filter) after 1 week and 8 weeks and the concentration of lead was determined by ICP-MS.

3. Results and discussion

An excess of a concentrated lead solution (560 ppm Pb²⁺) was used so that lead could be rapidly bound to the carbon-polymer blend for the purpose of generating a spent sorbent. After 1 h of exposure of the polymer-carbon blend (16.0 g polymer and 4.0 g PAC) to the aqueous solution of lead (250 mL), it was found that 10 mg of Pb²⁺ was bound to the sorbent based on the reduction of lead in solution, as measured by ICP-MS. In a control experiment in which only polymer was used in the lead sorption experiment, an average of 0.2 mg of lead was bound per gram of polymer in triplicate experiments at the same lead concentration. This result indicates that the lead removal for the polymer-carbon blend is due primarily the activated carbon (1.8 mg of lead bound per g activated carbon), though the polymer is also a minor contributor to lead binding. The amount of sorbent and type of carbon was not optimized as the goal of this study was to focus on preventing leaching rather than the water remediation step. After isolating the spent sorbent by filtration, it was air-dried in a fume hood for 24 h before proceeding to leaching experiments.

To test leaching of the spent sorbent, 1.0 g of the carbon-polymer blend was placed in 50 mL of deionized water in a plastic centrifuge tube. This experiment was carried out in triplicate. After rotating for 1 week, the water was filtered and analyzed by ICP-MS. The lead concentration due to leaching was 46.7 ± 0.5 ppb. While this corresponds to leaching of only 2.3 µg of the 500 µg bound to the 1.0 g of sorbent, the concentration of leached lead is well above acceptable concentrations for drinking water. In Canada, for instance, the maximum acceptable concentration of lead in water is 5 ppb [14]. Therefore, exposure of the spent sorbent to water results in sufficient leaching to pose a health risk.

To prevent this leaching, the spent sorbent was encapsulated in a barrier of the poly(*S-r*-canola) polymer (the same polymer used to support the PAC in the sorbent). The polymer barrier was made through reactive compression molding—a process in which pressure is applied

with mild heating to provoke S–S metathesis and covalent bonding between the polymer pieces [9]. The poly(*S-r*-canola) polymer used for this purpose is unique in that it does not form a liquid phase during reactive compression molding. Rather, the flexible polymer is compressed and the reactive faces are forced into contact and bond via S–S metathesis. To completely encapsulate the spent sorbent, 5.0 g of the sorbent (bound to lead) was placed between two 5.0 g poly(*S-r*-canola) polymer mats (made by reactive compression molding). An additional 2.0 g of powdered poly(*S-r*-canola) was added to the perimeter of the spent sorbent and used as chemical mortar to bind together the two mats. The polymer from the sorbent mats was also designed to facilitate covalent bonding to the top and bottom mats. The encapsulated sorbent was then placed in a mold between two PTFE sheets and compressed at 40 MPa and 100 °C for 10 min. After this time, the spent sorbent was completely confined to the inside of the polymer block (Fig. 2).

To determine if the polymer barrier could prevent leaching, the encapsulated sorbent mat from Fig. 2 was placed in 250 mL of deionized water and placed on a rocking table for 8 weeks. The water was sampled and measured for lead content by ICP-MS after 1 week and 8 weeks. After 1 week, the levels of lead were below the limits of detection. After 8 weeks completely submerged in water, the concentration of leached lead was a mere 1.5 ppb. This result indicates that only 0.38 µg of lead was leached from a possible 2500 µg of lead in the 5.0 g of spent sorbent bound in the polymer mat. This is a promising finding that illustrates how reactive compression molding can effectively confine spent sorbents containing toxic heavy metals and prevent leaching. It should also be noted that for storage and transport, the polymer encapsulated sorbent would likely not be stored in water so leaching would very likely be negligible in such a situation.

4. Conclusions

Reactive compression molding was used to create a polymer barrier around a spent sorbent bound to lead. The barrier greatly reduced the amount of lead leached from the sorbent when it was completely submerged in water. The reactive compression molding takes advantage of the reactive S–S bonds on the poly(*S-r*-canola) surface, which allows the formation of a polymer mat or block via S–S metathesis. The

polymer is multifunctional in this strategy of water remediation: it is a support for the carbon sorbent that lowers dust and serves as a hydraulic lubricant [8], the polymer can also bind to pollutants such as hydrocarbons [10] and mercury [11,13], and it has a reactive surface that enables reactive compression molding [9] to confine the spent sorbent. This is yet another environmentally beneficial application of the unique polysulfide polymers made by inverse vulcanization [15–18]. The encapsulation and stabilization of toxic heavy metals is of increasing interest as the use and trade of these substances becomes more restricted and regulated [19]. Confining these contaminated materials in polysulfide polymers is a promising option to address this challenge.

Declaration of Competing Interest

The authors declare the following financial interests/personal relationships which may be considered as potential competing interests.

The materials and techniques in this study are subject to the following patent applications: WO2017181217, WO2020010407, and AU2020901215. The commercial rights for the synthesis, processing, and applications of the polysulfide polymer in this study are owned by Clean Earth Technologies.

Acknowledgements

The authors thank the Australian Research Council for financial support (DP200100090).

References

- [1] H.L. Needleman, The current status of childhood low-level lead toxicity, *Neurotoxicology* 14 (1993) 161–166.
- [2] A. Evens, D. Hryhorczuk, B.P. Lanphear, K.M. Rankin, D.A. Lewis, L. Forst, D. Rosenberg, The impact of low-level lead toxicity on school performance among children in the Chicago public schools: a population-based retrospective cohort study, *Environ. Health* 14 (2015) 1–9.
- [3] S. Zahran, S.P. McElmurry, R.C. Sadler, Four phases of the flint water crisis: evidence from blood lead levels in children, *Environ. Res.* 157 (2017) 160–172.
- [4] E.A. Deliyanni, G.Z. Kyzas, K.S. Triantafyllidis, K.A. Matis, Activated carbons for the removal of heavy metal ions: a systematic review of recent literature focused on lead and arsenic ions, *Open Chem.* 13 (2015) 699–708.
- [5] W.J. Chung, J.J. Griebel, E.T. Kim, H. Yoon, A.G. Simmonds, H.J. Ji, P.T. Dirlam, R.S. Glass, J.J. Wie, N.A. Nguyen, B.W. Guralnick, et al., The use of elemental sulfur as an alternative feedstock for polymeric materials, *Nat. Chem.* 5 (2013) 518–524.
- [6] J.J. Griebel, R.S. Glass, K. Char, J. Pyun, Polymerizations with elemental sulfur: a novel route to high sulfur content polymers for sustainability, energy and defense, *Prog. Polym. Sci.* 58 (2016) 90–125.
- [7] Y. Zhang, R.S. Glass, K. Char, J. Pyun, Recent advances in the polymerization of elemental Sulphur, inverse vulcanization and methods to obtain functional chalcogenide hybrid inorganic/organic polymers (chips), *Polym. Chem.* 10 (2019) 4078–4105.
- [8] N.A. Lundquist, M.J. Sweetman, K.R. Scroggie, M.J.H. Worthington, L.J. Esdaile, S.F.K. Alboaiji, S.E. Plush, J.D. Hayball, J.M. Chalker, Polymer supported carbon for safe and effective remediation of PFOA- and PFOS-contaminated water, *ACS Sustain. Chem. Eng.* 7 (2019) 11044–11049.
- [9] N.A. Lundquist, A.D. Tikoalu, M.J.H. Worthington, R. Shapter, S.J. Tonkin, F. Stojcevski, M. Mann, C.T. Gibson, J.R. Gascooke, A. Karton, L.C. Henderson, et al., Reactive compression molding post-inverse vulcanization: a method to assemble, recycle, and re-purpose sulfur polymers and composites, *Chem. Eur. J.* (2020) <https://doi.org/10.1002/chem.202001841> In press.
- [10] M.J.H. Worthington, C.J. Shearer, L.J. Esdaile, J.A. Campbell, C.T. Gibson, S.K. Legg, Y. Yin, Nicholas A. Lundquist, J.R. Gascooke, I.S. Albuquerque, J.G. Shapter, et al., Sustainable polysulfides for oil spill remediation: repurposing industrial waste for environmental benefit, *Adv. Sustain. Syst.* 2 (2018), 1800024.
- [11] M.J.H. Worthington, R.L. Kucera, I.S. Albuquerque, C.T. Gibson, A. Sibley, A.D. Slattery, J.A. Campbell, S.F.K. Alboaiji, K.A. Muller, J. Young, N. Adamson, et al., Laying waste to mercury: inexpensive sorbents made from sulfur and recycled cooking oils, *Chem. Eur. J.* 23 (2017) 16219–16230.
- [12] N.A. Lundquist, M.J.H. Worthington, N. Adamson, C.T. Gibson, M.R. Johnston, A.V. Ellis, J.M. Chalker, Polysulfides made from re-purposed waste are sustainable materials for removing iron from water, *RSC Adv.* 8 (2018) 1232–1236.
- [13] A.D. Tikoalu, N.A. Lundquist, J.M. Chalker, Mercury sorbents made by inverse vulcanization of sustainable triglycerides: the plant oil structure influences the rate of mercury removal from water, *Adv. Sustain. Syst.* 4 (2020), 1900111.
- [14] Guidelines for Canadian Drinking Water Quality: Guideline Technical Document – Lead, Health Canada, Ottawa, Canada, 2019. <https://www.canada.ca/en/health-canada/services/publications/healthy-living/guidelines-canadian-drinking-water-quality-guideline-technical-document-lead.html>.
- [15] J.M. Chalker, M.J.H. Worthington, N.A. Lundquist, L.J. Esdaile, Synthesis and applications of polymers made by inverse vulcanization, *Top. Curr. Chem.* 377 (2019) 16.
- [16] M.J.H. Worthington, R.L. Kucera, J.M. Chalker, Green chemistry and polymers made from sulfur, *Green Chem.* 19 (2017) 2748–2761.
- [17] D.J. Parker, H.A. Jones, S. Petcher, L. Cervini, J.M. Griffin, R. Akhtar, T. Hasell, Low cost and renewable sulfur-polymers by inverse vulcanization, and their potential for mercury capture, *J. Mater. Chem. A* 5 (2017) 11682–11692.
- [18] M.S. Karunarathna, M.K. Lauer, T. Thiounn, R.C. Smith, A.G. Tennyson, Valorisation of waste to yield recyclable composites of elemental sulfur and lignin, *J. Mater. Chem. A* 7 (2019) 15683–15690.
- [19] F.A. López, A. López-Delgado, I. Padilla, H. Tayibi, F.J. Alguacil, Formation of metacinnabar by milling of liquid mercury and elemental sulfur for long term mercury storage, *Sci. Total Environ.* 408 (2010) 4341–4345.

5.0 Multi-functional 50-poly(*S-r-canola*) / Fe₂O₃ composites

5.1 Acknowledgements

Dr Yanting Yin for XPS characterisation of all composite samples. Associate Professor Justin Chalker for help with experimental design. Israa Bu Najmah for assistance with thermal conductivity measurements for the 50-poly(*S-r-canola*) polymer.

5.2 Abstract

A sustainable multifunctional magnetic composite material is prepared directly from 50-poly(*S-r-canola*) polymer and γ -Fe₂O₃ nanoparticles using a process called reactive compression moulding. This involves blending 50-poly(*S-r-canola*) polymer with γ -Fe₂O₃ nanoparticles then placing the mixture in a hot press at 40 MPa at 100 °C for 20 minutes. The composite material was shown to retain the 50-poly(*S-r-canola*) polymers chemical reactivity towards HgCl₂ whilst the incorporation of the γ -Fe₂O₃ nanoparticles facilitated magnetic filtration further simplifying the remediation process whilst reducing solid waste production. The magnetic properties of the nanoparticles also facilitate rapid heating of the composite by microwave irradiation. The rate of heating of the composite was shown to be directly proportional to the γ -Fe₂O₃ content of the composite which allowed determination of the irradiation time required to heat a composite of given γ -Fe₂O₃ content to a desired temperature. Rapid reactive compression moulding was demonstrated using microwave irradiation. This shortened the length of moulding time substantially and facilitated a method by which the composites could be quickly remoulded into different shapes and sizes. Finally, a 75% composite cylinder was prepared and its use as the active magnetic component of a solenoid valve was investigated. The solenoid valve was shown to function in a pump reducing the component weight by a factor of ten. This demonstrates just one of the possible applications this sustainable composite material could be utilised for within the fields of electronics, mechanics, and soft robotics.

5.3 Introduction

5.3.1 Composite materials from reactive compression moulding

The need to create sustainable materials, manufacturing methods and recycling processes has increased substantially in the last decade. New multifunctional materials are being developed to fulfil the demand for sustainable and more efficient chemical and mechanical systems. In this study a multifunctional magnetic composite material was prepared directly from 50-poly(*S-r*-canola) polymer and γ -Fe₂O₃ nanoparticles using the process developed in chapter 4, reactive compression moulding. This process used mild pressure (10-40 MPa) and heat (≤ 100 °C) to initiate a sulfur-sulfur exchange reaction between polymer particles binding them together and moulding them into a desired shape.²¹⁹ This process was investigated in chapter 4 for recycling and re-use purposes in order to increase the sustainability of the material however was also shown to be an efficient strategy for preparing composite materials from 50-poly(*S-r*-canola) polymer particles and a desired filler material. By changing the filler material, it was possible to impart different physical properties to the resulting mats facilitating a method by which the properties of the material could be tailored and optimised for use in specific applications.²¹⁹ By incorporating the γ -Fe₂O₃ nanoparticles in with the polymer before moulding, the process would encapsulate the nanoparticles within the polymer matrix forming a magnetic composite material that combines the chemical and mechanical properties of the polymer with the magnetic properties of the nanoparticles. This process is depicted below in Figure 142.

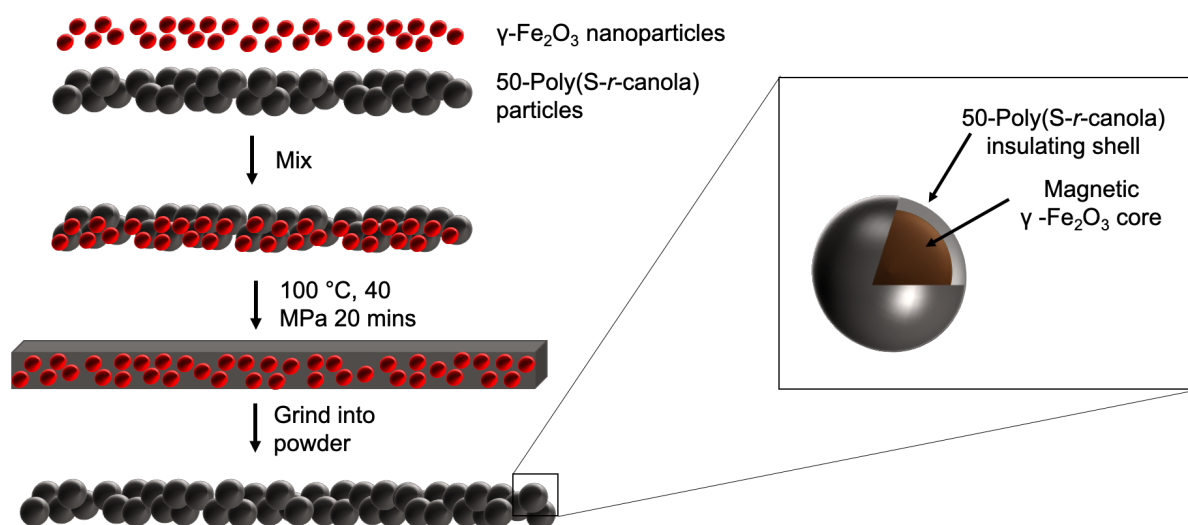


Figure 142 -Diagram depicting the process suggested to prepare the magnetic composite material.

The 50-poly(*S-r*-canola) material is inexpensive, easy to process into various shapes and sizes, can be produced on a large scale and has shown to have several important applications due to its chemical reactivity and physical properties. The useful properties displayed by different inverse vulcanized sulfur polymers has resulted in their use in a number of useful applications including heavy metal absorption,^{99, 156, 159, 288, 289} oil spill remediation,⁷ self-healing applications,^{88, 219} Li-S batteries,⁵⁸⁻⁸⁶ IR lenses^{87, 88, 290} and slow release fertilizers.⁹⁷ The 50-poly(*S-r*-canola) polymer has specifically found use in heavy metal remediation^{99, 100}, oil spill remediation⁷ and slow release fertilizers.⁹⁷ We hypothesised that by combining the magnetic properties of the γ -Fe₂O₃ nanoparticles and the chemical and physical properties of the 50-poly(*S-r*-canola) polymer, a multifunctional magnetic composite material would be formed with practical utility in a number of important applications. The 50-poly(*S-r*-canola) polymer has been shown in previous studies to remove Fe(III) from water and several compounds consisting only of iron and sulfur have been observed to exist under environmental conditions.^{156, 213} The γ -Fe₂O₃ nanoparticles could potentially bind with the sulfur within the 50-poly(*S-r*-canola) polysulfide forming a Fe-S bond during composite synthesis. This hypothesis will also be investigated throughout the study.

5.3.2 Magnetic materials and composites

Magnetic materials can be classified as either hard or soft magnets. One clear distinction between hard and soft magnetic materials can be observed in their magnetic hysteresis curves (B(H)).²⁹¹ Hard magnetic materials are also known as permanent magnets. These materials are typically used in applications including small motors, loudspeakers, electronic tubes, and other mechanical work based devices.²⁹² Unlike in soft magnetic materials (SMM), high amounts of magnetic hysteresis are desired in hard magnetic materials. Permanent magnets require a higher magnetic anisotropy than soft magnets in order to keep their magnetization in a specific direction.²⁹³ Useful features of hard magnetic materials include their coercive force, remnant magnetization and the energy product (BH)_{max}.²⁹² The energy product (BH)_{max} is the most common quantity used to merit a specific hard magnetic material.²⁹² Soft magnetic materials generally display high permeability, low hysteresis loss as well as low eddy current and anomalous losses.²⁹² Soft magnetic materials are characterised by a very low anisotropy to both maximise the permeability and minimize the hysteretic losses.²⁹² Materials which display intermediate anisotropies are typically used as magnetic recording media.²⁹³ SMM's are effective at higher frequencies and are currently being investigated for use in application requiring these higher frequencies.²⁹⁴ Current SMM's being used in electrical applications

includes ferrites (Fe-Ni, Fe-Ni-Mo & Fe-Si), permalloys, supermalloys as well as bulk SMM's such as amorphous, silicon steel and nanocrystalline strips.²⁹⁴ These materials typically display high permeabilities, high saturation magnetic induction, low coercivity as well as low power losses.¹⁸⁵ Eddy current loss is undesirable for most practical applications of SMM's. One method used to reduce or eliminate eddy current losses is to coat the magnetic powder particles in an insulating material. The insulating layers used to coat the magnetic cores can be classified into two different categories; resin based organic layers (I.e. Polyimides,²⁹⁵⁻²⁹⁸ Parylene,²⁹⁹ Phenolic,³⁰⁰⁻³⁰² Epoxy^{299, 303, 304} and Silicon resins³⁰⁵⁻³²⁰) and inorganic layers (I.e. SiO₂,³²¹⁻³²⁶ Al₂O₃,³²⁷⁻³²⁹ TiO₂,³³⁰⁻³³³ MgO,³³⁴⁻³³⁶ Fe₃O₄ and Fe₃(PO₄)₂).

5.3.3 Magnetic composites in filtration and separation

One application of magnetic composites is magnetic filtration and separation. Research into magnetic filtration has gained traction in recent years, especially in the fields of biotechnology³³⁷⁻³³⁹ and large-scale industrial separation processes.^{340, 341} Magnetic filtration is the process of separating a material from a mixture using a permanent magnet.³⁴² This method has the advantage of being able to separate magnetic materials from both liquid and solid contaminants. The general process is shown below in Figure 143. The 50-poly(*S-r*-canola) polysulfide has been investigated extensively in heavy metal remediation.^{99, 100} These remediation processes require the polymer to be physically filtered out of solution after treatment. Whilst this process is effective at removing the pollutants, the physical filtration method means that the polymer sorbent can't be separated from any solids in the mixture. By utilizing a sorbent that responds to magnetic fields, it's possible to limit the scope of waste production, optimize sorbent recovery and eliminate filter caking / blocking. γ -Fe₂O₃ nanoparticles are compatible with magnetic filtration and have been identified as suitable candidates for magnetic drug delivery applications due to their ease in preparation, biocompatibility and lack of toxicity.³⁴³ Embedding the γ -Fe₂O₃ nanoparticles within the 50-poly(*S-r*-canola) matrix should create a composite with the ability to remove pollutants from water and then be isolated by magnetic filtration.

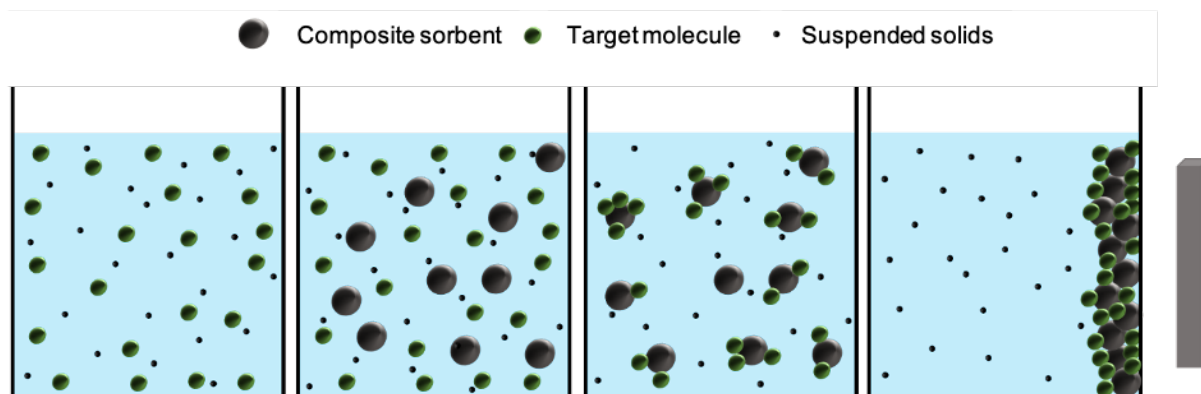


Figure 143 – Diagram describing the process of magnetic filtration.

5.3.4 Microwave heating of ferromagnetic composite materials

The ferromagnetic particles used in the composite synthesis ($\gamma\text{-Fe}_2\text{O}_3$ nanoparticles) are known to produce heat upon microwave irradiation.³⁴⁴ Bregar *et al.* demonstrated that composite materials containing nanoscale ferromagnetic particles can absorb microwave radiation and undergo rapid heating.³⁴⁵ Microwaves consist of a magnetic field component and an electric field component. Typical microwave heating occurs due to the alternating dielectric field component causing any molecule with an electrical dipole moment to re-orient itself to align with the alternating field. The resulting friction and collisions that occur between particles during this re-alignment process results in heat loss, known as dielectric losses.^{346, 347} Due to the magnetic field component of the microwaves, magnetic losses also contribute to microwave heating. These magnetic losses have been shown to be up to four times more effective at heating ferrite samples than typical dielectric losses.³⁴⁶ Magnetic losses are the combination of various energy dissipation mechanisms that occur when a magnetic material is subjected to a time varying external magnetic field.³⁴⁸ This is due to the irreversible nature of the magnetization process which results in energy being lost by the system in the form of heat.³⁴⁸ The mechanisms for heat loss of magnetic materials includes conduction loss as well as added losses from hysteresis, eddy currents, domain wall resonance and electron spin resonance.³⁴⁹ Sulfur-sulfur exchange reactions are known to occur within 50-poly(*S-r*-canola) at temperatures as low as 70 °C.²¹⁹ As microwave irradiation is known to rapidly heat composite materials containing nanoparticles, it was hypothesised that microwave irradiation could also be utilized to facilitate rapid reactive compression moulding. This proposal, outlined in Figure 144, was evaluated in this study.

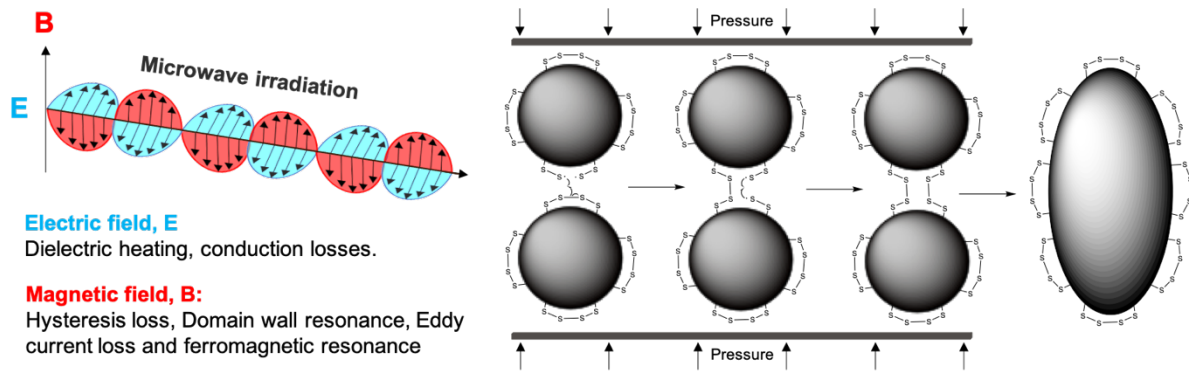


Figure 144 – Diagram demonstrating the concept of utilising the heat loss mechanisms of magnetic composite materials to facilitate reactive compression moulding.

5.3.5 Magnetic composites in electrical and mechanical applications

Magnetic materials and their composites have previously found use within the industrial and automotive fields in switching power supplies,^{294, 350-360} as filter inductors,^{294, 350-353, 356-358, 360} smoothing chokes,¹⁸⁵ transformers,³⁵⁵ coupling devices,³⁵⁸ magnetic sensors¹⁸⁵ and information storage mediums.¹⁸⁵ The heat loss mechanisms mentioned above are useful in some applications however they can have a negative impact on the materials performance in others. This is especially true for high frequency electrical applications. Because of this magnetic composite materials have typically been used in low frequency / high power applications such as sonar transducers, motors, hydraulic actuators, active vibrational dampeners and shape memory alloys such as Nitinol.¹⁸⁴ The incorporation of semiconductors and other advancements into electrical and mechanical systems has resulted in the need for magnetic materials that can be used effectively at higher AC frequencies.^{291, 292, 294} Concurrently, the need to save energy combined with the growing demand for cheaper and more efficient materials and manufacturing processes is driving the increase in interest in sustainable alternatives to these materials.¹⁸⁵ To work efficiently at higher frequencies, the magnetic material requires a lower hysteresis loss and higher magnetic permeability. SMMs or ferromagnets, are therefore ideal for these applications as their anisotropy is very low which results in higher permeabilities and the lower hysteresis losses.^{292, 294} Eddy current losses also negatively impact the materials effectiveness in higher frequency applications. To reduce the losses associated with eddy current production, an electrically insulating material can be used to coat the magnetic particles effectively eliminating the effect of eddy current on efficiency. By encapsulating a SMM in an insulating layer, the hysteresis losses are reduced as well as the eddy current losses. This insulating layer can also offer additional benefits such as a specific chemical reactivity, tailored mechanical properties and easier processability to suit the desired

application. These materials are called soft magnetic powder cores and due to their reduced iron losses they have been investigated for use in higher frequency electrical applications.²⁹¹ We hypothesise that by combining the electrically insulating 50-poly(*S-r*-canola) polymer with the soft magnetic γ -Fe₂O₃ nanoparticles, a multifunctional composite will be formed which is easier to form and mould into desired shapes and sizes and reduces the hysteresis and eddy current losses making it suitable as a component in these high frequency electronic applications. To demonstrate this, the magnetic composite will be moulded into a component of a solenoid valve switch and its effectiveness to replace the existing magnetic component within the switch will be evaluated.

5.4 Experimental

5.4.1 General considerations

5.4.1.1 FTIR analysis

Infrared (IR) spectra were recorded on a Fourier Transform spectrophotometer using the ATR method. Transmission maxima (ν_{\max}) are reported in wavenumbers (cm⁻¹).

5.4.1.2 STA analysis

Approximately 100 mg samples of composite material containing 25, 50, 75 and 90 wt% γ -Fe₂O₃ nanoparticles were crushed into powder form. 10 mg of each sample was placed into a crucible and placed in the STA. The temperature was held constant at 30 °C for 5 minutes, ramped up to 800 °C at a rate of 20 °C per minute and then held at 800 °C for 5 minutes.

5.4.1.3 XPS analysis

X-Ray Photoelectron Spectroscopy was performed on a Leybold Heraeus LHS-10 with a SPECS XR-50 dual anode source operating at 250 W. All spectra were taken with the 1253.6 eV Mg-K α anode with the analyser pass energy set to 20 eV.

5.4.1.4 XRD analysis

Powder X-ray diffraction (XRD) patterns were recorded on a Bruker D8 Advance Eco diffractometer (Bragg-Brentano geometry) using Co-K α radiation ($\lambda = 1.78897 \text{ \AA}$). The Bragg angle (2θ) was varied from 10° to 90° with a step size of 0.019°, measurement time of 0.45 s per step and sample rotation at 15 rpm. The XRD patterns were collected on a silicon low background sample holder, where powder samples were deposited onto the surface of the holder.

5.4.1.5 ^1H NMR spectroscopy

Proton nuclear magnetic resonance (^1H NMR) were recorded on a 600 MHz spectrometer. All chemical shifts are quoted on the δ scale in ppm using residual solvent as the internal standard (^1H NMR: $\text{C}_5\text{D}_5\text{N}$ $\delta = 7.22, 7.58, 8.74$).

5.4.2 Composite synthesis design

5.4.2.1 Preparation of 50-poly(S-*r*-canola) / $\gamma\text{-Fe}_2\text{O}_3$ magnetic composite mats

1.0 gram of $\gamma\text{-Fe}_2\text{O}_3$ nanoparticles (<50 nm) were added to a 50 mL centrifuge tube along with 6.5 grams of 50-poly(S-*r*-canola). The tube was then inverted multiple times to mix the iron nanoparticles and the polymer together. This mixture was then placed into the 10 × 10 cm stainless steel mould between two sheets of PTFE paper. The mould was then placed into the S15 Devils press 10-ton hydraulic heated press that was previously heated up to 100 °C. Once the temperature of the system had equilibrated at 100 °C, the pressure was increased to 40 MPa. The pressure immediately starts to fall due to the moulding reducing the volume of the material. Once the pressure dropped and stabilised the pressure was increased back up to 40 MPa. After 10 minutes, the pressure was relieved, and the mould was removed from the press. The mould was opened and the resulting 50-poly(S-*r*-canola) / $\gamma\text{-Fe}_2\text{O}_3$ composite mat was removed from the PTFE paper.

5.4.2.2 Preparation of 50-poly(S-*r*-canola) / $\gamma\text{-Fe}_2\text{O}_3$ magnetic composite powder

A magnetic composite mat was ground up into a fine powder. It was observed that the powder did not seem to smudge or stick to the container walls as much as the nanoparticles did.

5.4.2.3 Comparison of 50-poly(S-*r*-canola) / $\gamma\text{-Fe}_2\text{O}_3$ blend with different ratios of $\gamma\text{-Fe}_2\text{O}_3$

1.0 gram of $\gamma\text{-Fe}_2\text{O}_3$ nanoparticles (<50 nm) were added to a 50 mL centrifuge tube along with 6.5 grams of 50-poly(S-*r*-canola). The tube was then inverted multiple times to mix the iron nanoparticles and the polymer together. This was repeated using 2.0 grams of $\gamma\text{-Fe}_2\text{O}_3$ nanoparticles.

5.4.2.4 Preparation of composite with different ratios of $\gamma\text{-Fe}_2\text{O}_3$

To increase the nanoparticle content, the composite powder (1.0 gram of $\gamma\text{-Fe}_2\text{O}_3$, 6.0 grams of 50-poly(S-*r*-canola)) prepared above was added into a new 50 mL centrifuge tube. To this tube an extra 1.0 grams of $\gamma\text{-Fe}_2\text{O}_3$ nanoparticles was added and the mixture was shaken to ensure

optimal surface coverage of γ -Fe₂O₃ nanoparticles on the polymers surface. This mixture was then placed into the 10 × 10 cm stainless steel mould between two sheets of PTFE paper. The mould was then placed into the S15 Devils press 10-ton hydraulic heated press that was previously heated up to 100 °C. Once the temperature of the system had equilibrated at 100 °C, the pressure was increased to 40 MPa. The pressure immediately starts to fall due to compression reducing the volume of the material and therefore the pressure. Once the pressure stabilised it was increased back up to 40 MPa. This was repeated until the pressure was stabilised at 40 MPa. After 10 minutes, the pressure was relieved, and the mould was removed from the press. The mould was opened and the resulting 50-poly(S-*r*-canola) / γ -Fe₂O₃ composite mat was removed from the PTFE paper. The mat was then ground back up into a powder to form the magnetic composite powder shown below.

5.4.2.5 Direct preparation of magnetic composite at any concentration

1.0 gram of 50-poly(S-*r*-canola) was added to 0.33 grams of γ -Fe₂O₃ nanoparticles and mixed to homogenize. The mixture was then placed into the 10 × 10 cm mould in between two sheets of PTFE. The lid was added to the mould and the entire system was placed into the heated press at 100 °C. Once the mould equilibrated at 100 °C the pressure was increased to 20 MPa gradually over 1 minute. After remaining at 20 MPa at for 1 minute the pressure was increased to 40 MPa. After 1 minute at 40 MPa, the pressure was increased a third and final time to 60 MPa. The mould was left under 60 MPa pressure at 100 °C for 10 minutes. At this point the pressure was removed and the lid and top layer of PTFE sheeting was removed to reveal the mat formed inside the mould. It was noticed that the mat formed was not homogenous, and areas existed very high nanoparticles to polymer ratios. The sample was broken up within the mould using a metal spatula and mixed briefly within the mould. The top sheet of PTFE was re-added along with the mould lid and the process of moulding at 60 MPa was repeated. After repeating this process 2 times a solid mat had formed with limited defects. The above process was repeated using 1.0, 3.0, and 9.0 grams of γ -Fe₂O₃ nanoparticles to achieve composite mats with 25, 50, 75 and 90 wt% γ -Fe₂O₃ nanoparticles content.

5.4.3 Characterisation of composites

5.4.3.1 STA analysis of composites synthesis

Thermogravimetric analysis (TGA) and differential scanning calorimetry (DSC) were carried out on a 449 F5 Jupiter simultaneous thermal analyser. A sample size between 4-5 mg was used in each run. The furnace was purged at 20 mL/min with nitrogen and equilibrated for 1

minute at 30 °C before each run. Heating was carried out up to 600 °C using a 20 °C/min heating rate. The temperature was held isothermally at 600 °C at the end of each experiment to oxidize remaining organic matter.

5.4.3.2 Sample preparation for XPS analysis

For each γ -Fe₂O₃ concentration composite, a 1 × 1 cm square was cut out from a mat of each γ -Fe₂O₃ content. A sample of 100% γ -Fe₂O₃ nanoparticles was also moulded for 20 minutes at 100 °C at 40 MPa. This resulted in a thin film of γ -Fe₂O₃ on the surface of the Teflon paper. A 1 × 1 cm square was cut from the Teflon sheet and tested as an iron control. A 1 × 1 cm square was also cut from a 100% 50-poly(S-*r*-canola) control mat.

5.4.3.3 Sample preparation for thermal conductivity of powdered composite

7.5 grams of 50-poly(S-*r*-canola) was added into a 500 mL plastic container. 2.5 gram of γ -Fe₂O₃ nanoparticles were added to the 50-poly(S-*r*-canola) and the container was inverted 10 times to mix the 50-poly(S-*r*-canola) and the γ -Fe₂O₃ nanoparticles. A 10 × 10 cm PTFE sheet was added into the stainless-steel mould followed by the mixture of 50-poly(S-*r*-canola) / γ -Fe₂O₃ nanoparticles. A second 10 × 10 cm PTFE sheet was added on top before the lid to the mould was added. The mould was added to the preheated press at 100 °C. Once the temperature equilibrated at 100 °C the pressure was increased to 40 MPa. After 10 minutes the pressure was released, and the mould was removed. The composite mat was ground back into a powder remixed and remoulded at 40MPa, 100 °C for a further ten minutes. The resulting mat was then removed from the mould and separated from the PTFE sheets. The mat was then ground up into a powder form. The above process was repeated 4 times to get approximately 40.0 grams of magnetic composite powder. 20.0 grams of this powder was added to a plastic container and packed in tight to ensure that the conductivity probe would have good contact with the composite particles. This sample was labelled as the powdered sample.

5.4.3.4 Sample preparation for thermal conductivity of moulded composite

20.0 grams of the composite was transferred into the 10 × 10 cm stainless-steel mould between two PTFE sheets and placed in the hot press pre-heated to 100 °C. Once the temperature had reached 100 °C the pressure was increased to 40 MPa and held for 20 minutes. After this time the pressure was released, and the mould was removed from the press. The composite mat was the removed from the mould and separated from the PTFE sheets. This was repeated to prepare a second 20.0 gram mat. Finally, a 10 × 10 cm PTFE sheet was added into the stainless-steel

mould followed by the first pre-prepared mat. On top of this mat, along the diagonal, was placed the stainless-steel thermal conductivity meter probe casing. The second 20.0 gram mat was placed on top of the first and the probe casing followed by a second PTFE mat. The lid was placed on the mould before it was placed in the hot press that was pre-heated to 100 °C. Once the temperature had equilibrated at 100 °C the pressure was increased to 10 MPa and held for 60 minutes. The lower pressure is used to ensure the metal probe casing wasn't damaged during the moulding process. After 60 minutes the pressure was released, the mould was then removed from the press and the composite mat was removed from the mould and separated from the PTFE sheets. This formed a 40.0 gram mat with the stainless-steel thermal conductivity meter case embedded within it.

5.4.3.5 Thermal conductivity experiment

Powdered sample: A TLS thermal conductivity probe was used to perform the measurements. After calibration the thermal conductivity probe was coated in a ceramic thermal compound paste (Arctic Silver Arctic Alumina) before being inserted into the composite powder sample. The system was left to equilibrate to room temperature for 15 minutes. After this time the measurement was made. This process was repeated three times to gain triplicate measurements.

Moulded sample: A TLS thermal conductivity probe was used to perform the measurements. After calibration the thermal conductivity probe was coated in a ceramic thermal compound paste (Arctic Silver Arctic Alumina) before being inserted into the thermal conductivity meter case embedded within the composite mat formed in (5.4.3.3). The system was left to equilibrate to room temperature for 15 minutes. After this time the measurement was made. This process was repeated three times to gain triplicate measurements.

5.4.4 Magnetic filtration

5.4.4.1 Magnetic filtration of magnetic composite powder

1.0 gram of 50-poly(S-*r*-canola) / γ -Fe₂O₃ magnetic composite powder was added to a 50 mL centrifuge tube along with 30 mL of D.I. water. The lid was placed onto the tube and the entire tube was placed on a rotary mixer for 5 minutes. After 5 minutes had passed the tube was removed from the mixer and a magnet was used to draw the polysulfide to the bottom of the flask and the remaining solution was decanted off.

5.4.4.2 Magnetic filtration of composite material from fine tailings in HgCl₂ doped solution

3.0 grams of fine tailings was added to a 6 × 50 mL centrifuge tubes. To 3 of these tubes 1.0 grams of the 50-poly(*S-r*-canola) / γ -Fe₂O₃ nanoparticles composite was added. To each of these tubes 20 mL of HgCl₂ solution (~5 ppm) was added and the 6 tubes (3 control, 3 treated) were transferred into a rotary end over end mixer at 25 rpm for 24 hours. After 24 hours the mixing was stopped, and the solutions removed from the mixer. Control samples were filtered, and the remaining liquid was transferred to a storage container for further analysis. For the remaining solutions (treated with composite) a magnet was used to draw the composite to the sides of the centrifuge tube and the remaining solution/tailings was decanted off into a clean 50 mL centrifuge tube. A magnet was applied to wall of the new tube and no particles were observed to stick to the wall suggesting that no magnetic composite was in this mixture. This mixture was then filtered, and the remaining solution was transferred into a 20 mL glass vial for analysis. The composite remaining in the original tube had 50 mL of clean DI water added and the new mixture was mixed thoroughly. The magnet was then reapplied, and the composite was drawn to the wall. The remaining sand was again decanted off with the water leaving only the composite remaining. The composite was left in the fume hood to dry overnight. All decanted mixture was added to the same waste beaker. After all samples where cleaned, the magnet was applied to the side of the waste beaker and a small amount of polysulfide was observed to stick to the walls of the beaker. The remaining mixture was again decanted off and the composite extracted from the waste beaker was also left in the fume hood to dry for 24 hours. Once dry the magnetic composite samples were weighed to determine yield. To separate the remaining composite from any residual sand, the magnet was sealed inside 4 × 6 cm plastic bag. The magnet was then placed over the top of the dry solid recovered from previous filtration leaving behind the non-magnetic sand particles. This effectively separated the magnetic composite from any remaining solid. The composite particles stuck to the plastic bag surrounding the magnet and were removed from the bag by simply removing the magnet from the wall of the bag and allowing the composite particles to drop into a storage container.

5.4.4.3 Magnetic separation of composite filler material from magnetic composite

4.0 grams of 25% magnetic composite powder was added to 1.0 gram of waste PVC shavings in a plastic container. This mixture was inverted to create a homogenous mixture and then added to a 10 × 10 cm steel mould in between two sheets of PTFE. The mould was added to the heated press, which was pre-heated to 100 °C. Once the temperature had equilibrated at

100 °C the pressure on the press was increased up until 40 MPa. The pressure was maintained at 40 MPa for 20 minutes. After 20 minutes the pressure was released, and the mould was removed from the press. The resulting composite mat was removed from the mould and separated from the PTFE sheets. This mat was then ground back up into a powder. Once ground into a powder, physical magnetic separation was performed to remove any magnetic composite from any non-magnetic filler materials (I.e. waste PVC shavings). The separated filler material was weighed and stored. The separated magnetic composite was ground back up into a powder and magnetic separation was performed again and the separated composite and filler were weighed. This process repeated until all the filler material had been recovered from the composite. This took a total of 10 repeats. The remaining PVC particles still had residual magnetic composite bound to them at this point. The PVC / composite particles were then further ground up and the magnetic separation was performed again. Any remaining polymer particles were then removed and added to the composite previously separated. The final composite and waste PVC weights were recorded, and final yields determined.

5.4.5 Microwave heating

5.4.5.1 Microwave heating: Composite, 50-poly(*S-r*-canola) and γ -Fe₂O₃ nanoparticle control

0.8 grams of magnetic composite was placed on a 10 × 10 cm sheet of PTFE paper. An IR thermometer (Stanley, ≤1mW, 630-660nm) was used to measure the temperature. The thermometer was scanned over the surface of the material and the highest temperature observed during the scan was recorded as the temperature. This was done before irradiation to establish the initial room temperature of the material. This was repeated three times for triplicate measurements. A standard household microwave (1100W) was used to irradiate the samples. The microwave tray in the household microwave was observed to heat up under microwave irradiation introducing the possibility of heat transfer from the tray to the sample. The tray was therefore removed from the microwave to eliminate other potential heat sources. The sample was then placed in the microwave and irradiated for 10 seconds. At ten seconds the door was opened, the sample was quickly moved onto the benchtop and the temperature was recorded using the IR thermometer. Again, the thermometer was scanned over the surface of the sample and the highest value was recorded. Once the sample had cooled back to room temperature this was repeated two more times to get triplicate values for 10 seconds irradiation time. This process was repeated, in triplicate, for irradiation times of 20, 30, 40 seconds. This process was repeated using 50-poly(*S-r*-canola) powder, γ -Fe₂O₃ nanoparticles and PTFE sheet as controls.

5.4.5.2 FLIR imaging of composite after 20 seconds of microwave irradiation

0.75 grams of composite material was placed onto 10 × 10 cm PTFE sheet and placed into the microwave. The sample was heated for 20 seconds. After the radiation the sample was immediately removed from the microwave and placed directly on the bench and imaged using the FLIR camera. The Images were taken every 10 seconds for 3 minutes. This was repeated with 0.75 grams of composite material in a thin mat (~1mm thick), a composite disk (~13 mm diameter, ~ 0.6 cm thick) and the 50-poly(S-*r*-canola) / γ -Fe₂O₃ nanoparticle mixture used to prepare the composite.

5.4.5.3 Difference in temperature after 5 seconds of microwave irradiation

0.5 × 0.5 mm squares of composites materials consisting of 10, 25, 50, 75 and 90% γ -Fe₂O₃ nanoparticle content were placed onto a 5 × 5 cm sheet of PTFE and their initial temperatures were recorded by taking an image of the samples using the FLIR thermal imaging camera. The samples were then placed in the microwave. The samples were heated for 5 seconds, after which time they were instantly imaged with the FLIR thermal imaging camera. Images of the samples were recorded every 10 seconds over 1 minute.

5.4.5.4 Comparison of heating rates against γ -Fe₂O₃ nanoparticles

0.5 × 0.5 mm squares of composites materials consisting of 10, 25, 50, 75 and 90 wt% γ -Fe₂O₃ nanoparticle content were placed onto a 10 × 10 cm sheet of PTFE and their initial temperatures were recorded by taking an image of the samples using the FLIR thermal imaging camera. The samples were then placed in the microwave. The samples were heated for 5, 10, 15, 20, 25 and 30 second time periods. To avoid degradation once a sample had reached 150 °C further irradiation was stopped. The temperature was recorded using the FLIR thermal imaging camera. This process was repeated three times to gain triplicates for each sample and each irradiation time.

5.4.5.5 Comparison of cool down rate

A 0.5 × 0.5 mm square of composites material consisting of 25% γ -Fe₂O₃ nanoparticle content was placed onto a hot plate set to 100 °C. An FLIR thermal imaging camera was used to monitor the temperature of the sample. Once the temperature had reached 100 °C it was transferred onto a 33.0 × 45.7 cm metal tray at room temperature and FLIR thermal images were recorded at t = 0 and then again, every 10 seconds until the sample's temperature had

dropped to below 30 °C. This process was repeated for magnetic composites with 50, 75 and 90% γ -Fe₂O₃ nanoparticle content.

5.4.6 Microwave induced reactive compression moulding

5.4.6.1 Microwave heating polypropylene syringe control

A 5 mL polypropylene syringe was placed into the household microwave and its initial temperature was recorded using a handheld IR thermometer. The polypropylene syringe was then irradiated for 10 seconds, after which the door was immediately opened, and the temperature was recorded using the handheld IR thermometer. This was repeated three times for triplicate measurements. This process was then repeated for irradiation times of 20 and 30 seconds.

5.4.6.2 Reactive compression moulding of composite in microwave

Magnetic composite (2.5 grams) was placed into a 5 mL polypropylene syringe. The plunger was then inserted, and pressure was applied to the composite for 1 minute, compacting it and forcing the particles into contact. The syringe containing the compressed composite was then inserted into the microwave and the sample was irradiated for ~14.0 s. Directly after this, the sample was removed from the microwave and compression was re-applied to the plunger to re-compress the composite. This was done until the sample had cooled back down to 30 °C, determined using IR thermometer (roughly 72.8 seconds). The syringe was then placed back into the microwave and the sample was irradiated for ~12.3 s. This process was repeated 3 times to ensure maximum moulding was achieved. After the final irradiation cycle, the composite was removed from the syringe by firstly withdrawing the syringe to draw the composite to the back of the syringe, using a scalpel to cut the end of the syringe off and finally removing the composite by forcing it out the removed end of the syringe using the plunger.

5.4.6.3 Moulding composite into cylinders and disks using reactive compression moulding in the microwave

All samples prepared using the above protocol (5.4.6.2). First 0.8 grams of 25% composite were added into a 20 mL polypropylene syringe. The plunger was inserted, and the composite was compressed within the syringe by applying constant pressure to the plunger. Pressure was applied for 1 minute before placing the entire syringe into an empty household microwave (1100W) and performing the above protocol (5.4.6.2). This process was repeated using a syringe with a smaller radius to achieve disks of different radius. This process was repeated in the 5 mL and 10 mL syringes using 3.2 grams of 25% composite to form composite cylinders.

5.4.6.4 Preparation of magnetic composite using microwave irradiation

1.0 gram of γ -Fe₂O₃ nanoparticle (<50 nm) were added to a 50 mL centrifuge tube along with 6.5 grams of 50-poly(S-*r*-canola). The tube was then inverted multiple times to mix the γ -Fe₂O₃ nanoparticles and the polymer together. 3.0 grams of this mixture were added into a 5 mL syringe. The syringe was then compressed to force the polymer and γ -Fe₂O₃ nanoparticle together. It was then placed directly into the microwave and heated for 20 seconds. The system was then removed and allowed to cool to room temperature whilst pressure was applied by pushing the syringe in by hand. The 20 second irradiation followed by cool down under pressure was repeated 8 more times. After this period the syringe plunger was pulled out drawing the composite tube further down the syringe. The end of the syringe was then cut off using a scalpel and the composite cylinder was pushed out the end using the plunger.

5.4.7 Composites use in mechanical and electrical systems

5.4.7.1 Magnetic actuator from composite material

4.0 grams of magnetic composite was placed into a 5 mL syringe and the compressed by pushing the syringe closed. The entire syringe was then placed into the microwave and irradiated for 20 seconds in the microwave. The whole system was left to cool back to room temperature whilst applying constant pressure on the sample by pushing the plunger in. Once cooled back down to room temperature the system was placed back into the microwave and irradiated for a further 20 seconds in the microwave followed by applying pressure and allowing it to cool back to room temperature. This was repeated 1 more time for a total of 3 irradiation / cooldown cycles. Once the system had returned to room temperature the plunger was draw out pulling the formed cylinder back down the syringe. The end of the syringe was cut off using a scalpel and the resulting cylinder was pushed through the syringe and out of the end. The resulting cylinder was left to cure in an oven pre-heated to 100 °C for 2 hours.

5.4.7.2 Preparation of magnetic composite cylinder for solenoid valve component

2.0 grams of magnetic composite was placed into a 3 mL syringe and the compressed by pushing the syringe closed. The entire syringe was then placed into the microwave and irradiated for 20 seconds in the microwave. The whole system was left to cool back to room temperature whilst applying constant pressure on the sample by pushing the plunger in. Once cooled back down to room temperature the system was placed back into the microwave and irradiated for a further 20 seconds followed by applying pressure and allowing it to cool back to room temperature. This was repeated 1 more time for a total of 3 irradiation / cooldown

cycles. Once the system had returned to room temperature the plunger was drawn out pulling the formed cylinder back down the syringe. The end of the syringe was cut off using a scalpel and the resulting cylinder was pushed through the syringe and out of the end. The resulting cylinder was left to cure in an oven pre-heated to 100 °C for 2 hours.

5.4.7.3 Construction of magnetic solenoid valve

The valve body was taken apart and the original operator was removed. A new spring was added into the tube which will be later placed into the solenoid. The new operator, magnetic composite cylinder, was then placed in the tube against the spring. The tube, with operator and spring inserted was screwed back into the main body of the valve.

5.4.7.4 Testing the use of the magnetic solenoid valve with magnetic composite component

50 mL of FeCl₃ solution was added to a 500 mL dropping funnel. Plastic tubing was used to connect the outlet of the dropping funnel with the inlet of the solenoid valve. Plastic tubing was also inserted into the outlet of the solenoid valve. The valve was held up by a retort stand and the pressure on the system was altered by changing the height of the dropping funnel with respect to the valve. The valve was positioned so that the liquid would flow through the valve vertically and a beaker was placed below the valve to catch the running liquid. The compression springs used did not display their spring constants. Different springs were tested. Most of the springs in the set were too rigid and the force produced on the composite by the solenoid coil was not strong enough to compress the springs and open the valve. The weakest spring in the set demonstrated a small amount of give when the solenoid was turned on. By firstly stretching the spring, effectively reducing the number of coils per unit area, and secondly shortening its length to fit the system, the solenoid coil was able to draw the composite material up against the spring with enough force to open the valve slightly and allow water flow.

5.5 Results and Discussion

5.5.1 Preparation of 50-poly(*S-r*-canola) / γ -Fe₂O₃ composite

To combine the 50-poly(*S-r*-canola) polymer and the γ -Fe₂O₃ nanoparticles, reactive compression moulding was investigated. Initially the γ -Fe₂O₃ nanoparticles were simply mixed with the 50-poly(*S-r*-canola) polymer. It was noted that the addition of 1.0 gram of γ -Fe₂O₃ nanoparticles to 6.5 grams of 50-poly(*S-r*-canola) powder followed by mixing resulted in a relatively homogenous mixture in which the γ -Fe₂O₃ nanoparticles adhered to the surface of

the 50-poly(*S-r*-canola) particles. Performing reactive compression moulding of this mixture at 100 °C resulted in a composite material whereby the γ -Fe₂O₃ nanoparticles were embedded into the 50-poly(*S-r*-canola) matrix.

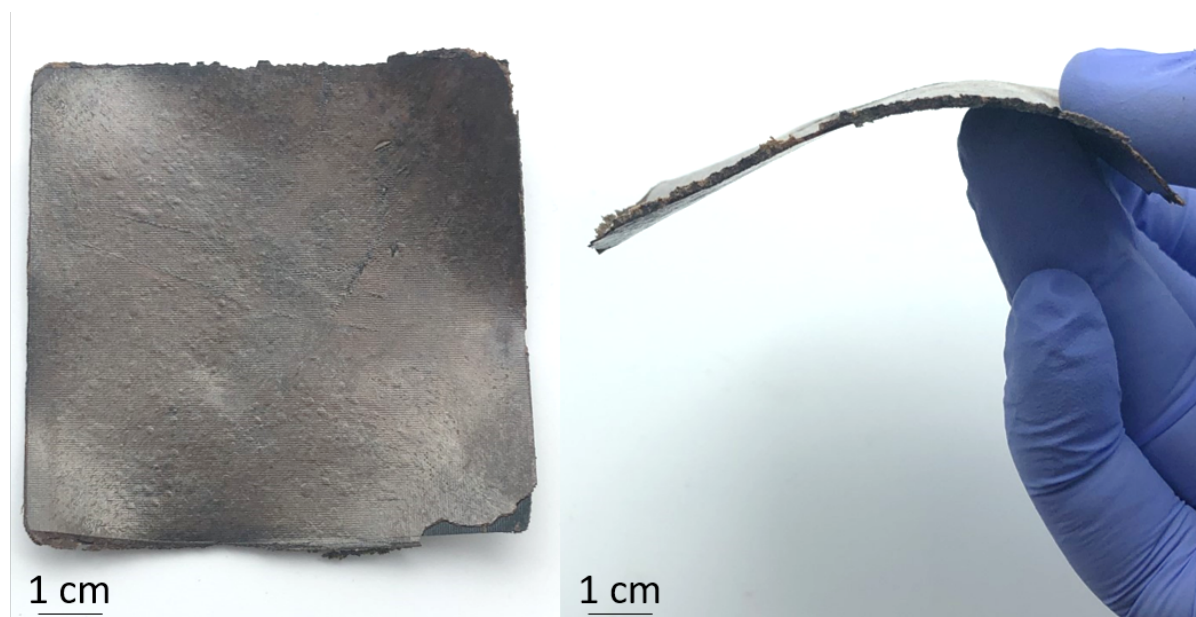


Figure 145 – Magnetic 50-poly(*S-r*-canola) / γ -Fe₂O₃ composite mat.

This mat (Figure 145) was shown to maintain its magnetic properties by demonstrating its affinity towards a permanent magnet (Figure 146).

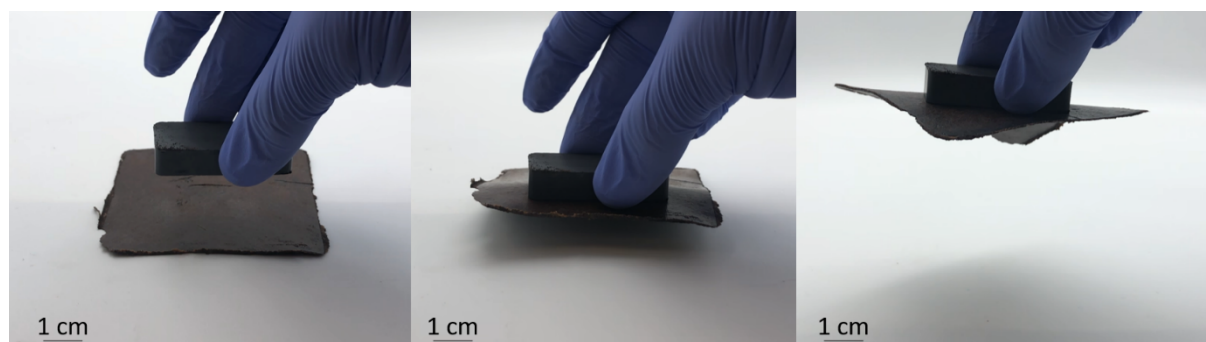


Figure 146 – Images showing the magnetic 50-poly(*S-r*-canola) / γ -Fe₂O₃ composite mat's magnetic attraction towards a magnet.



Figure 147 – A) γ -Fe₂O₃ nanoparticles, B) 50-poly(*S-r*-canola) particles, C) Blend of A and B, D) Magnetic γ -Fe₂O₃ nanoparticles encapsulated in 50-poly(*S-r*-canola).

The nanoparticles observed under SEM in Figure 148 seem to coat the surface of the 50-poly(*S-r*-canola) when blended (Figure 149).

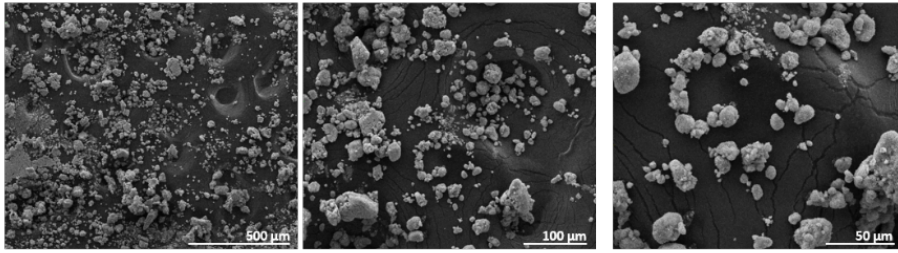


Figure 148 – SEM analysis of γ -Fe₂O₃ nanoparticles.

SEM of γ -Fe₂O₃ nanoparticles revealed that the particles size is highly dispersed with particles as big as 100 μm being observed.

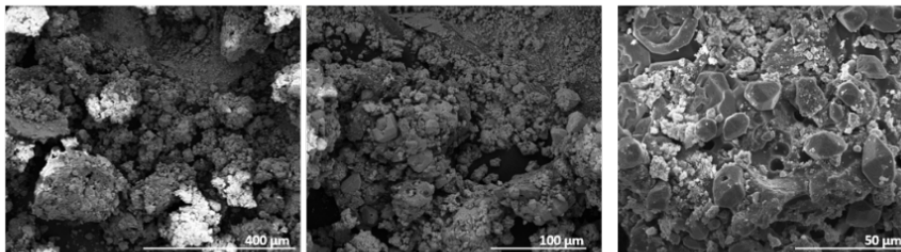


Figure 149 – SEM analysis of γ -Fe₂O₃ / 50-poly(*S-r*-canola) polymer blend.

SEM analysis of the blend (Figure 149) showed that the γ -Fe₂O₃ nanoparticles were coating the surface of the 50-poly(*S-r*-canola) polymer.

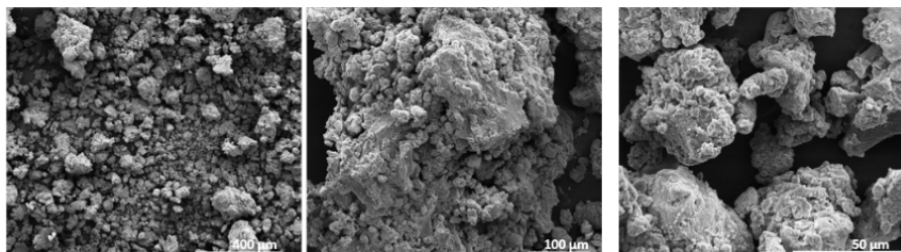


Figure 150 – SEM analysis of γ -Fe₂O₃ / 50-poly(*S-r*-canola) polymer composite.

It appears that after moulding the γ -Fe₂O₃ nanoparticles had been embedded into the 50-poly(*S-r*-canola) polymer matrix forming a composite (Figure 150). To ensure this was the case, EDX analysis was performed (Figure 15). It revealed that the signal for Fe covered most of the surface with strong signals for sulfur only observed in regions where the nanoparticles weren't present. After moulding the regions of strong sulfur signals became more uniformly dispersed across the surface and the sulfur signals increased. This suggested that the nanoparticles are embedded under the 50-poly(*S-r*-canola) polymers surface.

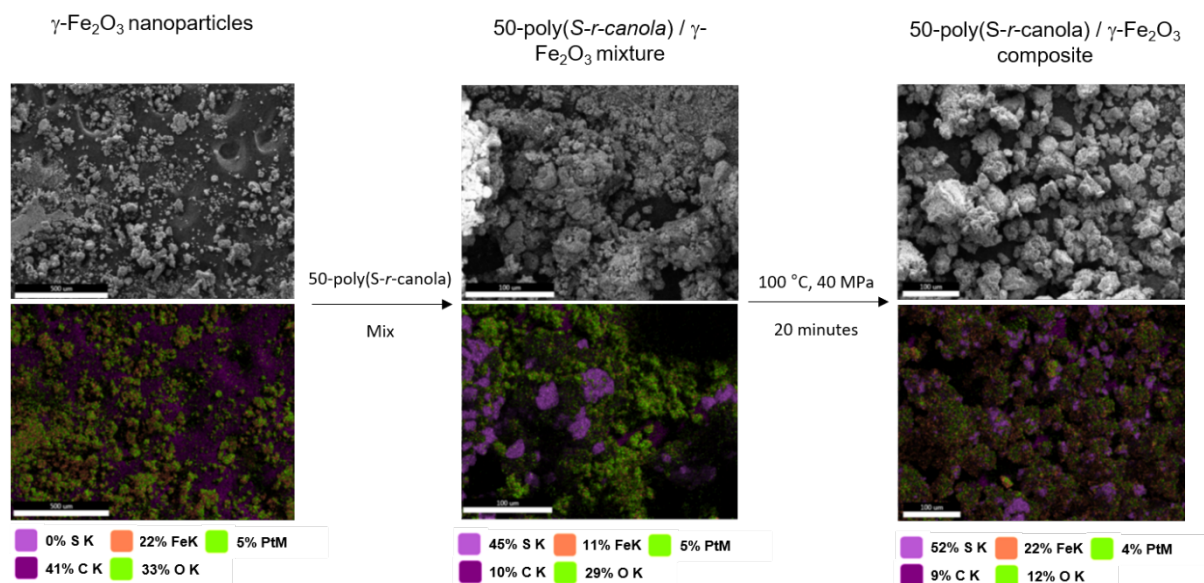


Figure 151 – EDX analysis of γ -Fe₂O₃ nanoparticles and the 50-poly(*S-r-canola*) / γ -Fe₂O₃ blend before and after moulding.

The addition of more than 1.0 gram of nanoparticles to 6.5 grams of 50-poly(*S-r-canola*) resulted in free nanoparticles not bound to the surface of 50-poly(*S-r-canola*) particles. When moulded a uniform distribution of nanoparticles was not observed in the polymer matrix. Instead, the resulting composite mat had areas with no filler material and just nanoparticles. This is highlighted in Figure 152.

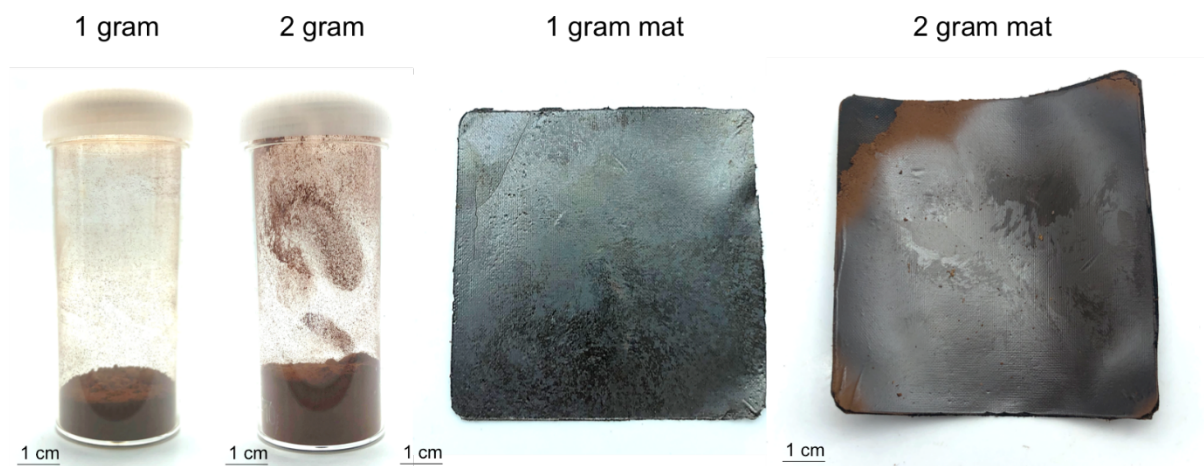


Figure 152 – 6.5 grams of 50-poly(*S-r-canola*) with 1.0 gram of γ -Fe₂O₃ nanoparticles added, 6.5 grams of 50-poly(*S-r-canola*) with 2.0 grams of γ -Fe₂O₃ nanoparticles added and the corresponding mats.

5.5.2 Direct preparation of composite materials with varying Fe₂O₃ content

To ensure the distribution of iron throughout the polymer was uniform and homogenous a new method was established. The second method consisted of adding the desired ratio of γ -Fe₂O₃

nanoparticles to 50-poly(*S-r*-canola) polymer and performing reactive compression moulding on the mixture at 100 °C. The resulting mat, which doesn't have uniform γ -Fe₂O₃ nanoparticle distribution, was broken into a powder inside the mould by using a metal spatula to break the mat apart. Reactive compression moulding was then performed again at 100 °C. This was repeated one more time for a total of three moulding periods. This method is outlined below in Figure 153.

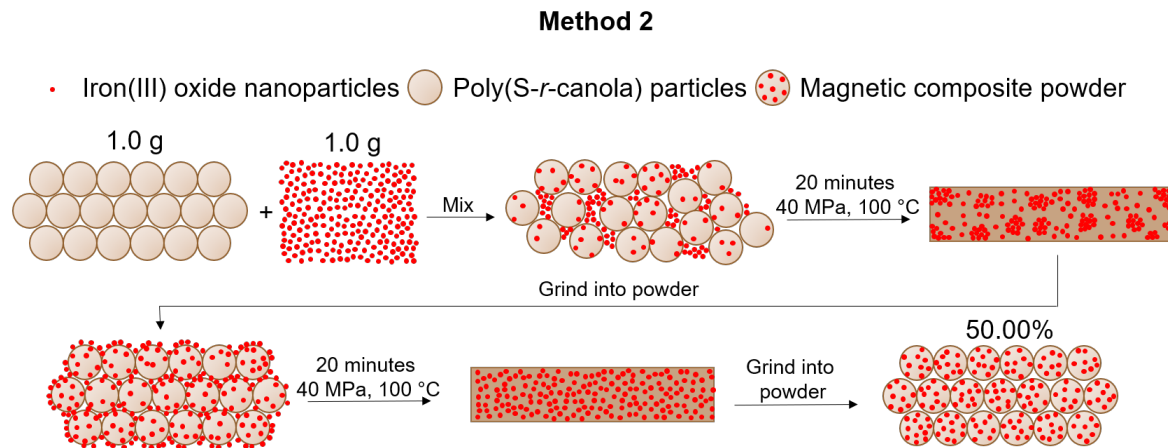


Figure 153 – Diagram describing the process used to make composites with uniformly distributed nanoparticles.

This resulted in a composite material with uniform distribution of γ -Fe₂O₃ nanoparticles at their desired content. Using this method composite materials with up to 90 wt% γ -Fe₂O₃ nanoparticles were prepared. These are shown in Figure 154. The 25wt% composite was similar in mechanical properties to the 0wt% control. The rigidity of the mats increased as the γ -Fe₂O₃ content increased. The mats formed up to 50wt% were mechanically sound and retained some of the elastic properties of the 0wt% control. The 75% composite was more brittle than the 50wt% and would break upon bending. At 90wt% γ -Fe₂O₃ content the composite was far more brittle with cracks appearing in all mats formed.

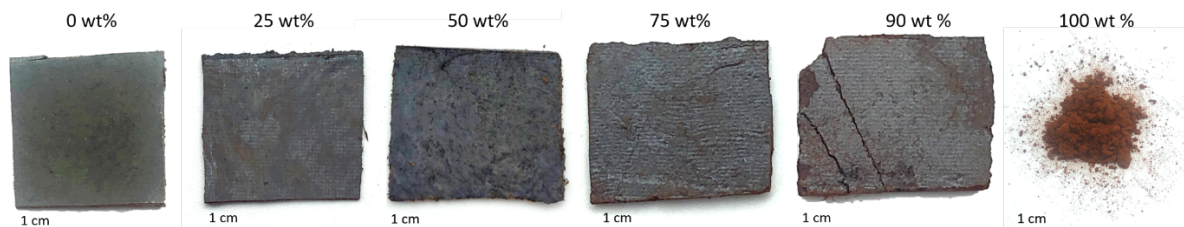


Figure 154 – Images of composites formed by reactive compression moulding of mixtures of 50-poly(*S-r*-canola) and γ -Fe₂O₃ nanoparticles.

5.5.3 Characterization of 50-poly(*S-r-canola*) / γ -Fe₂O₃ nanoparticles

The distribution of nanoparticles was observed via SEM / EDX analysis to be evenly distributed throughout the bulk material. The SEM images and EDX mappings of the cross-sections and surfaces for the 25% composite is shown in Figure 155.

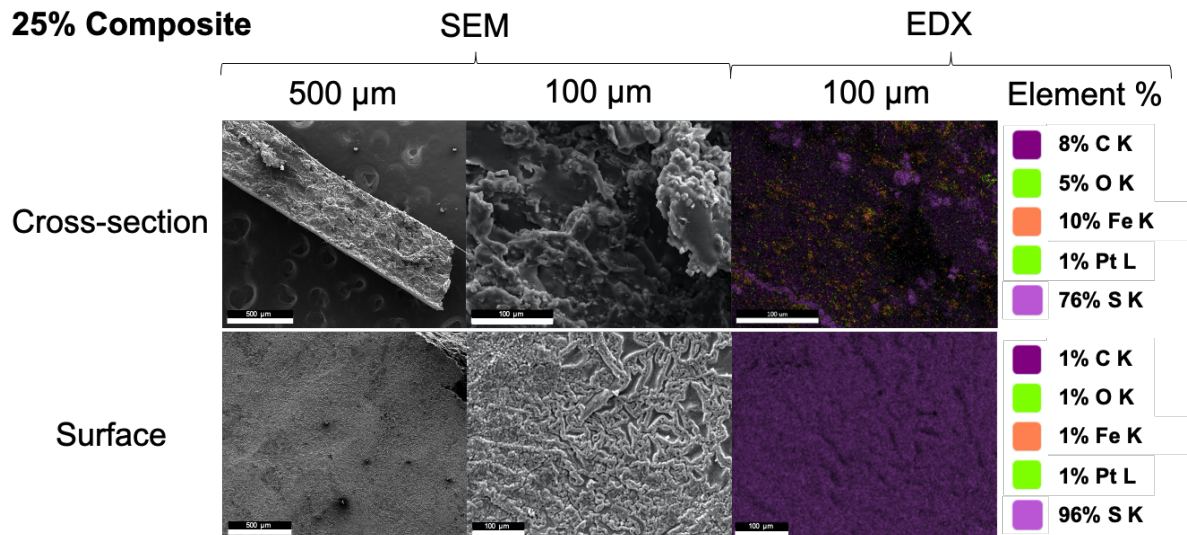


Figure 155 – SEM / EDX analysis of cross-section and surface of 25% composite mat.

EDX analysis reveals that the 25% composite's surface consisted almost entirely of sulfur. Chapter 4 revealed that when the 50-poly(*S-r-canola*) polymer underwent reactive compression moulding, unreacted sulfur within the polymer migrates through the bulk of the material to the surface where it combines to form a high sulfur content surface layer. This explains the high sulfur content signal on the surface of the 25% γ -Fe₂O₃ composite sample. These results suggest that the sulfur surface layer is prominent for samples with γ -Fe₂O₃ below 25%. While the formation of this sulfur layer was not an intentional outcome, it is possible that it could provide an insulating and protective layer for the composite.

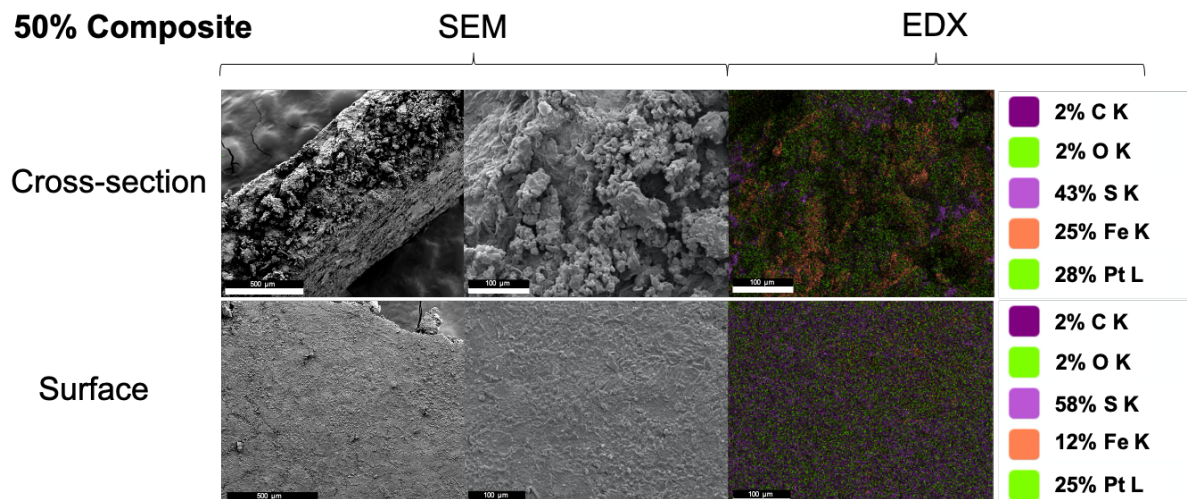


Figure 156 – SEM / EDX analysis of cross-section and surface of 50% composite mat. As the $\gamma\text{-Fe}_2\text{O}_3$ content is increased to 50% (Figure 156) the $\gamma\text{-Fe}_2\text{O}_3$ starts to become incorporated into the high sulfur content surface layer and the signal for Fe increased. It was also noted that the Fe and S signals appeared to be relatively uniformly distributed across the surface.

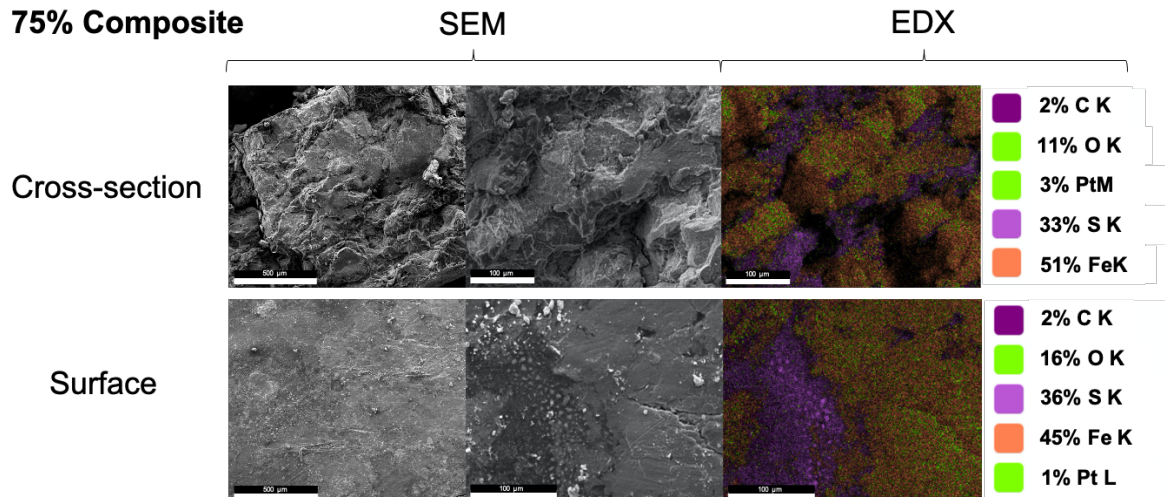


Figure 157 – SEM / EDX analysis of cross-section and surface of 75% composite mat.

The signal for Fe increased as its content increased to 75% (Figure 157) however the distribution across the surface wasn't as uniform as it was for the 50% sample.

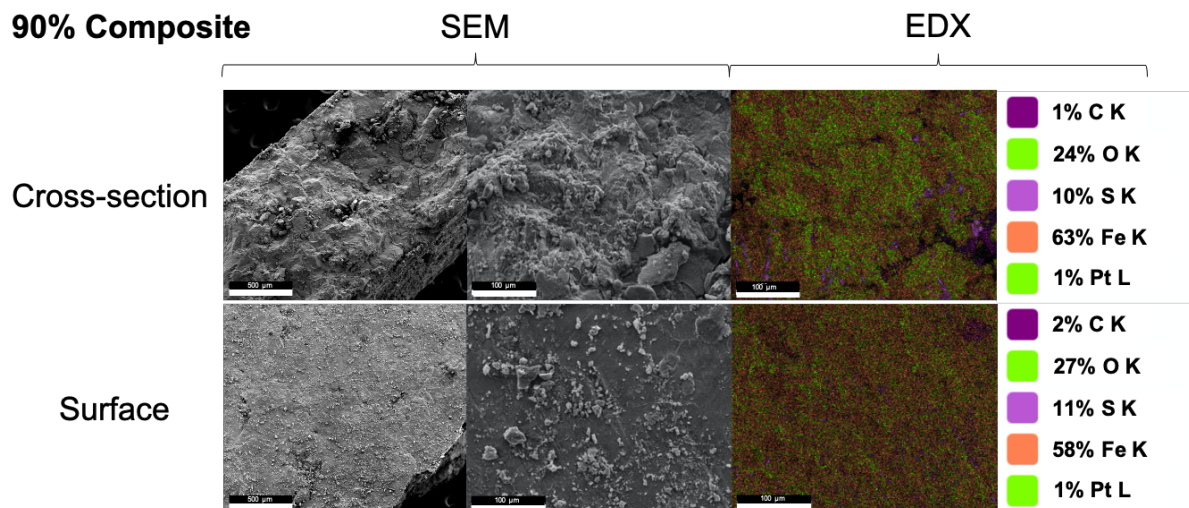


Figure 158 – SEM / EDX analysis of cross-section and surface of 90% composite mat.

The 90% sample (Figure 158) consisted mainly of signals from Fe and O however S signals were distributed across the surface. The distribution of $\gamma\text{-Fe}_2\text{O}_3$ nanoparticles throughout the bulk of the material was relatively uniform in all samples with the least uniformity being shown in the 75% composite. Next to investigate the thermal properties of the composites, simultaneous thermal analysis was performed (Figure 159). It was noted that a large percentage

of each material remained after heating to 800 °C. The mass remaining after heating increased with and corresponded to the γ -Fe₂O₃ content of the composite tested.

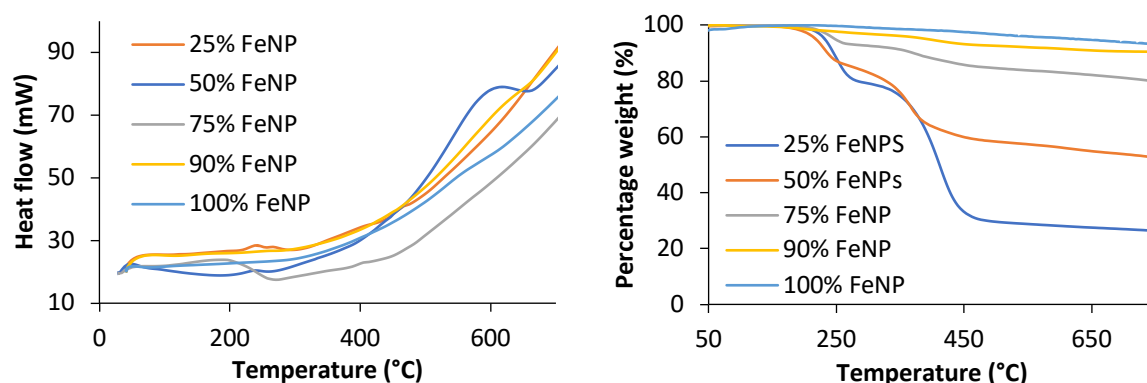


Figure 159 – DSC (left) and TGA (right) plots for composites with varying γ -Fe₂O₃ contents.

STA also demonstrated that the different composition materials react relatively similarly in terms of heat flow. Next the chemical structures of the various composites were investigated. Initially FTIR analysis was performed (Figure 160).

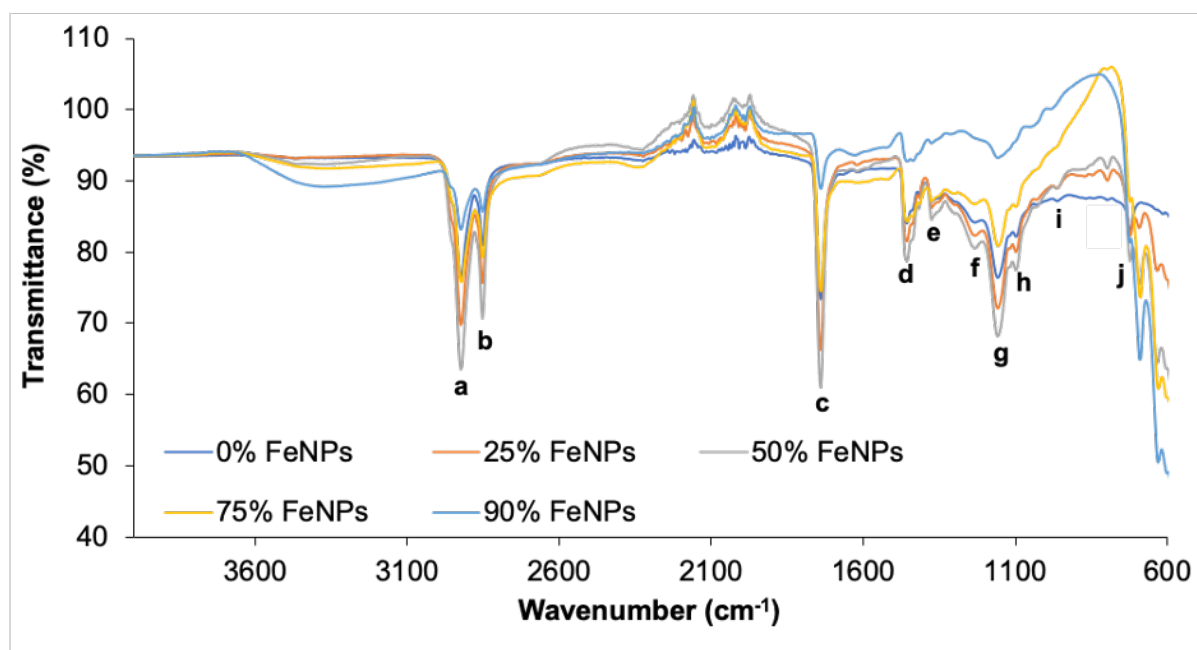


Figure 160 – FTIR analysis of composites containing from 25-90% γ -Fe₂O₃ nanoparticles in a 50-poly(S-*r*-canola) matrix as well as the 0 and 100% controls.

All expected peaks for the 50-poly(S-*r*-canola) polysulfide were observed. The only significant difference observed was the transmittance peaks between 600 and 800 cm⁻¹ which appears to increase in intensity with an increase in γ -Fe₂O₃ content. These results showed no indication that the γ -Fe₂O₃ nanoparticles and the 50-poly(S-*r*-canola) polymer reacted during the preparation of the composite material. To further investigate the possibility of a chemical

reaction occurring, as opposed to just physical encapsulation, STA analysis was repeated on the starting materials under the reaction conditions used to prepare the composites (Figure 161). Any clear changes in the heat flow profile, not observed by the samples individually, could suggest that a chemical reaction, other than the S-S exchange reaction of the 50-poly(S-r-canola), is occurring.

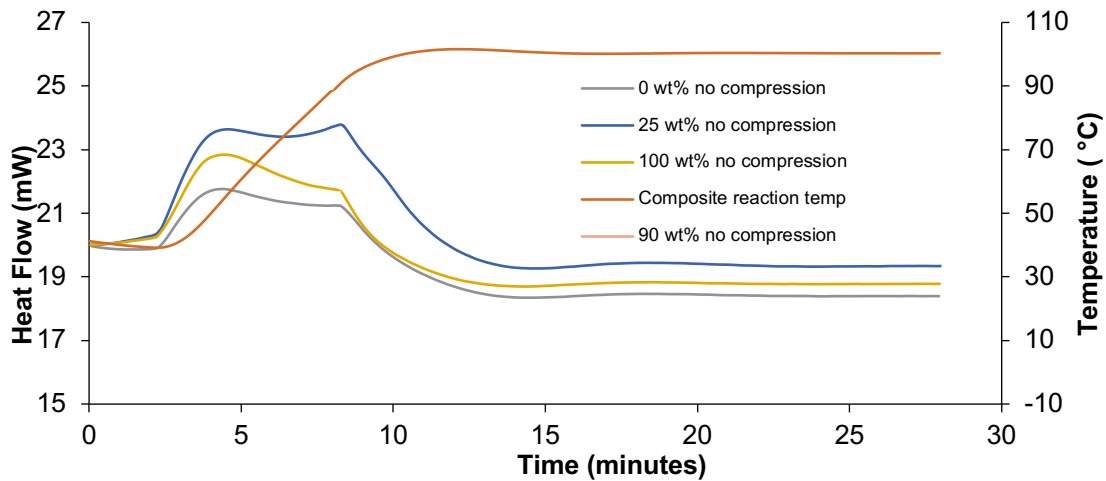


Figure 161 – DSC analysis of composites individual components under reaction conditions without pressure applied.

It's clear that no significant difference is observed between the different samples suggesting that no reaction was occurring under the heat conditions alone. The small differences observed are likely due to differences in thermal conductivities of the samples. To determine whether the pressure had played a role in the reaction, each sample underwent compression at 40 MPa for 20 minutes before being placed in the DSC. Results are shown in Figure 162.

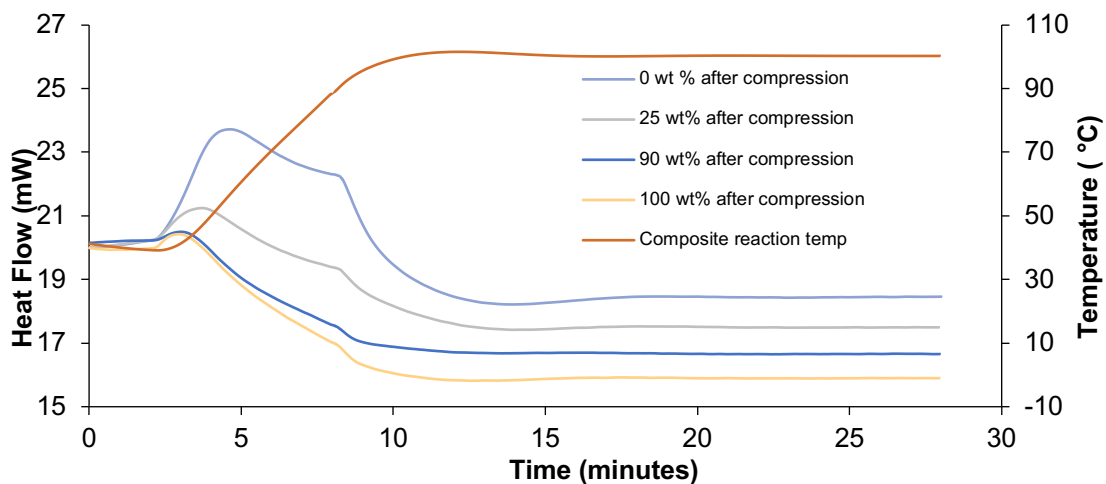


Figure 162 – DSC analysis of composites individual components under reaction conditions with 40 MPa pressure applied to sample before analysis.

It was clear from these results that compression resulted in an obvious difference in heat flow profiles throughout the reaction conditions used. Interestingly the 50-poly(*S-r*-canola) polymer controls heat profile did not change significantly after moulding. The γ -Fe₂O₃ sample showed the largest change in heat flow with the 90% composite and 25% composites decreasing in heat flow by an amount which corresponded to the amount of γ -Fe₂O₃ contained within the composite. These results provide further evidence to suggest that a reaction is occurring between the γ -Fe₂O₃ nanoparticles when pressure was applied at 100 °C. As compression of a material is shown to result in a change in observed thermal conductivity, it's important to determine whether the differences observed by STA analysis were due to a chemical change or a physical change. To determine this the thermal conductivities of the different samples were investigated. Both powdered and moulded 20% composite samples were investigated and compared with that of the 50-poly(*S-r*-canola) polymer. For powdered samples 20.0 g of composite was packed in 50 mL plastic vials. For moulded samples, two 20.0 g composite mats were prepared. It was noted that inserting the conductivity probe into these samples resulted in fractures and breaks to the material. To ensure that an accurate thermal conductivity measurement was obtained, a metal sleeve specifically calibrated for use with the thermal conductivity probe was sandwiched between two pre-made 20.0 gram composite mats. Extended time and reduced pressure (10 MPa, 100 °C, 60 minutes) were used in this case to limit any possible damage caused to the metal sleeve during moulding. Images of the prepared samples are shown in Figure 163.

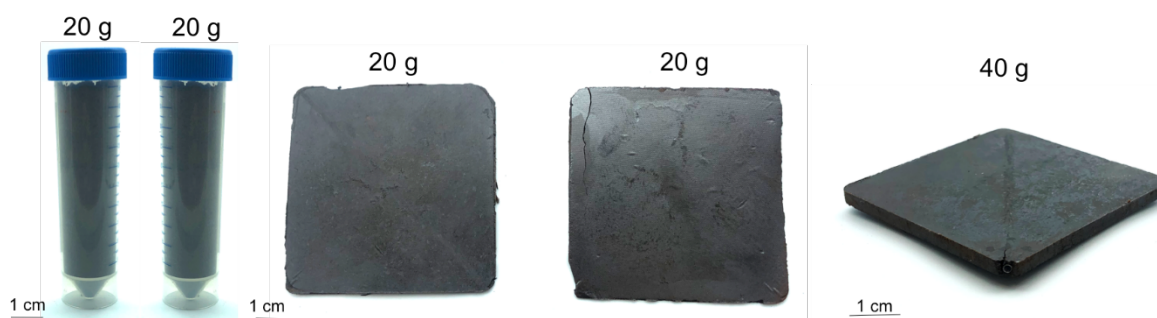


Figure 163 – Images of powdered composite (left), 20.0 g composite mats (middle) and the 40.0 g composite mat with the metal thermal conductivity meter probe casing embedded within it (right).

For the powdered samples the particles were lightly compressed to ensure maximal contact with the probe. The probe was then placed directly in the centre of the powder ensuring that the probe wasn't in contact with the walls of the tube. For the moulded sample the probe was inserted directly into the metal sleeve embedded in the moulded composite mat. In both cases

the probe was coated in ceramic thermal compound paste (Arctic Silver Arctic Alumina) before being inserted ensuring that maximum contact was achieved between the sample and the probe. The samples with the probes inserted are shown in Figure 164.



Figure 164 – Image showing the samples with probe inserted for thermal conductivity measurement.

The thermal conductivity and resistivity results for both the powders and mats are shown below in Figure 165 and 166.

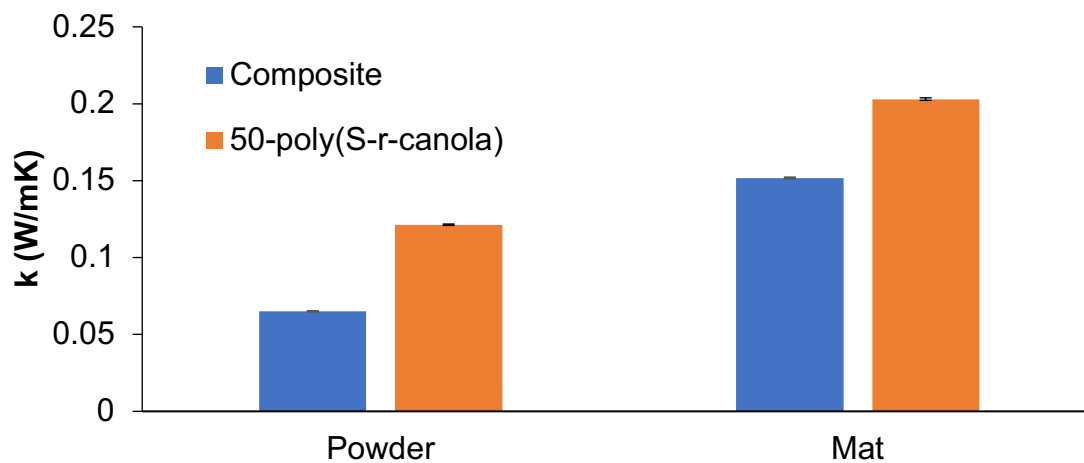


Figure 165 – Thermal conductivity results for the magnetic composite and the 50-poly(S-r-canola) mats and powder.

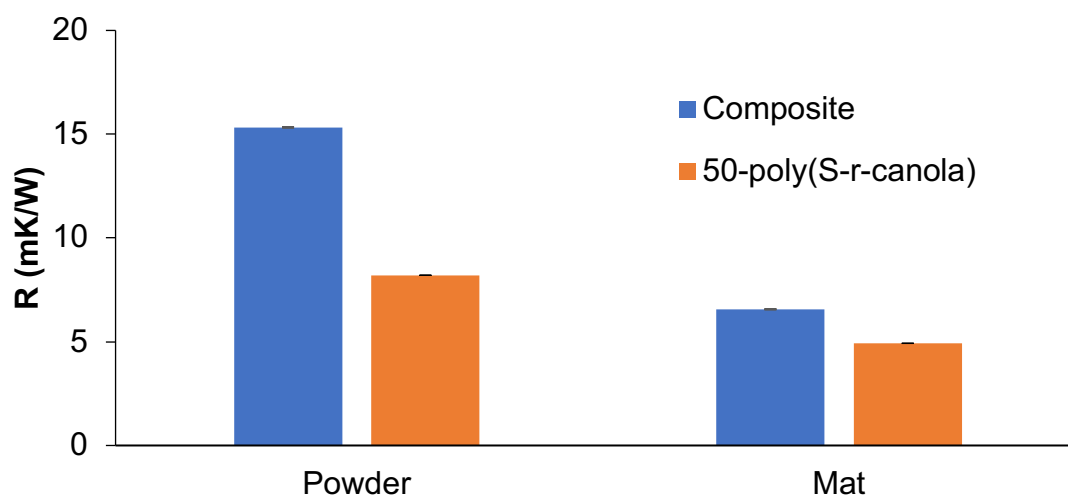


Figure 166 – Thermal resistivity results for the magnetic composite and 50-poly(S-*r*-canola) mats and powder.

The powder was shown to have a lower thermal conductivity than the mat. This was expected as in a powder the heat must transfer through the air between particles whereas in the moulded sample the heat is only transferred directly through the material. The thermal conductivity of air is $0.020 \text{ W}\cdot\text{m}^{-1}\cdot\text{K}^{-1}$ resulting in a substantial decrease in observed thermal conductivity.³⁶¹ For this reason, the thermal conductivity of the moulded sample gives a more accurate reading into the thermal conductivity value of these composites than the powder's value. The thermal conductivity value for the powder is still important as it gives an insight into how quickly this material will heat up and cool down when in powdered form or bulk form. The 50-poly(S-*r*-canola) showed larger thermal conductivity than the 25% composite. This result can be used to explain the DSC results above. The higher thermal conductivity of the 50-poly(S-*r*-canola) polymer leads to smaller heat flow values. Although STA analysis was inconclusive evidence from FTIR prompted further investigation into the chemical structure of the composites. XPS analysis was performed on the sample and the results are shown below.

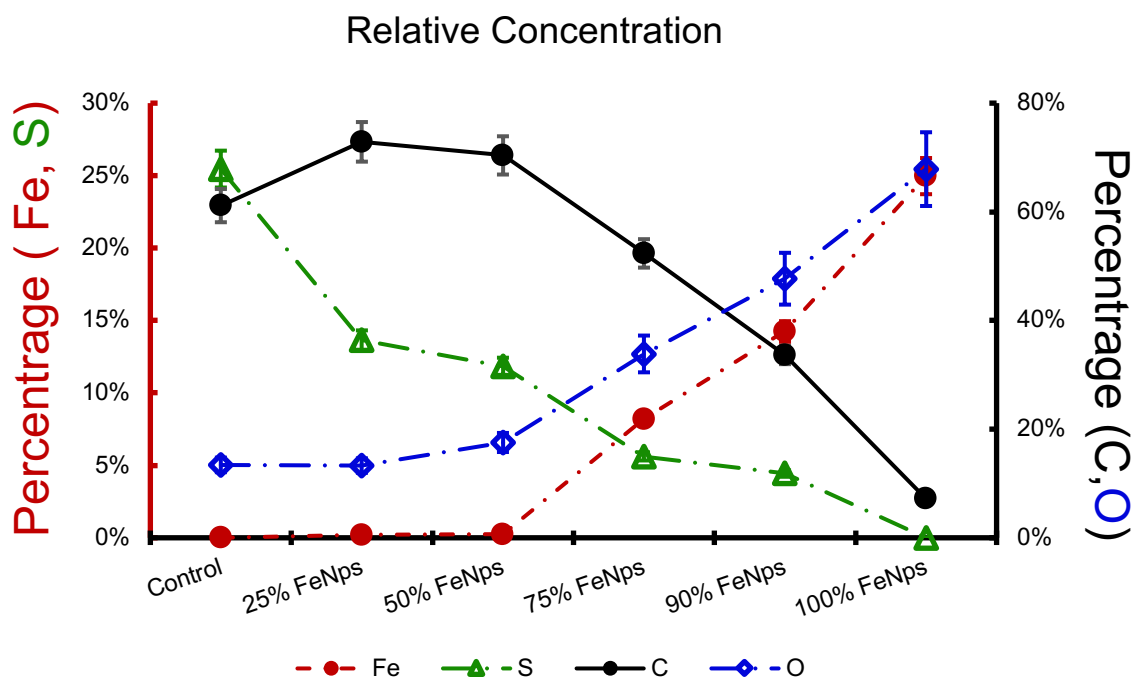


Figure 167 – XPS results showing the relative concentrations of different atoms on the composites surface.

Initially the relative intensities of each atom in the samples were compared (Figure 167). The Fe content on the surface was very low until approximately 50%. This is likely due to the formation of the sulfur layer, on the surface, observed under SEM, blocking direct measurement of the Fe below it. Above 50 wt%, the Fe content is large enough that it is incorporated into the sulfur layer and it can be seen under XPS. As the Fe₂O₃ nanoparticles content increased, the carbon and sulfur signals decreased whilst the signals for oxygen and iron increased, as expected. The different species of carbon observed in the samples is shown in Figure 168.

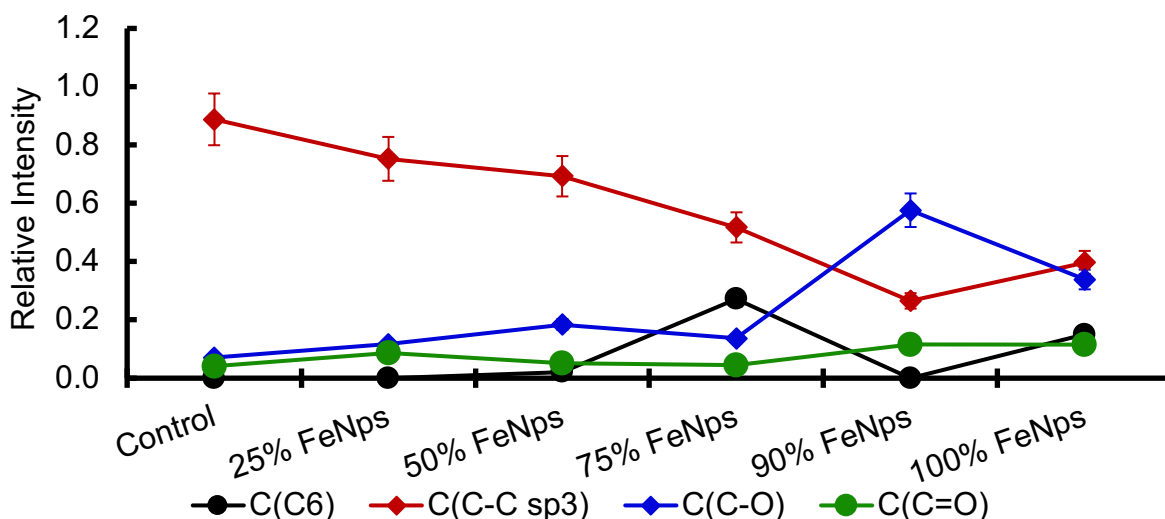


Figure 168 – XPS results showing the relative concentrations of different carbon centered functional groups present on the surface of the composite mats.

As expected, the C-C bonds decreased with increasing γ -Fe₂O₃ content. Unexpectedly the signal corresponding to C-O groups increased as the γ -Fe₂O₃ content increased. A possible explanation for this is that the presence of γ -Fe₂O₃ disrupts the migration of sulfur to the surface resulting in a higher C-O and C=O signal being observed. Next the signals corresponding to different sulfur species were investigated (Figure 169).

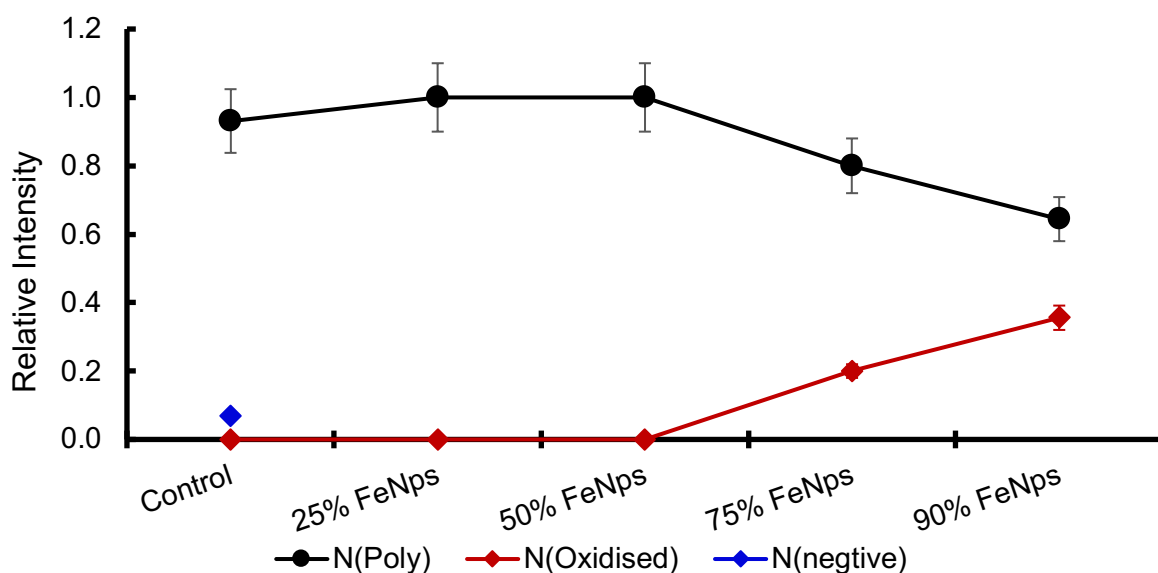


Figure 169 – XPS results showing the relative concentrations of different sulfur centered functional groups present on the surface of the composite mats.

From 0-50 wt% γ -Fe₂O₃, the polymeric high sulfur content layer blocks the bulk material being observed. Above 50 wt% an oxidised form of sulfur was observed. This species could potentially be of the form SO_x. This result suggest that the polymeric sulfur is being oxidised

by the γ -Fe₂O₃ nanoparticles or air. Finally, the different Fe species were investigated (Figure 170).

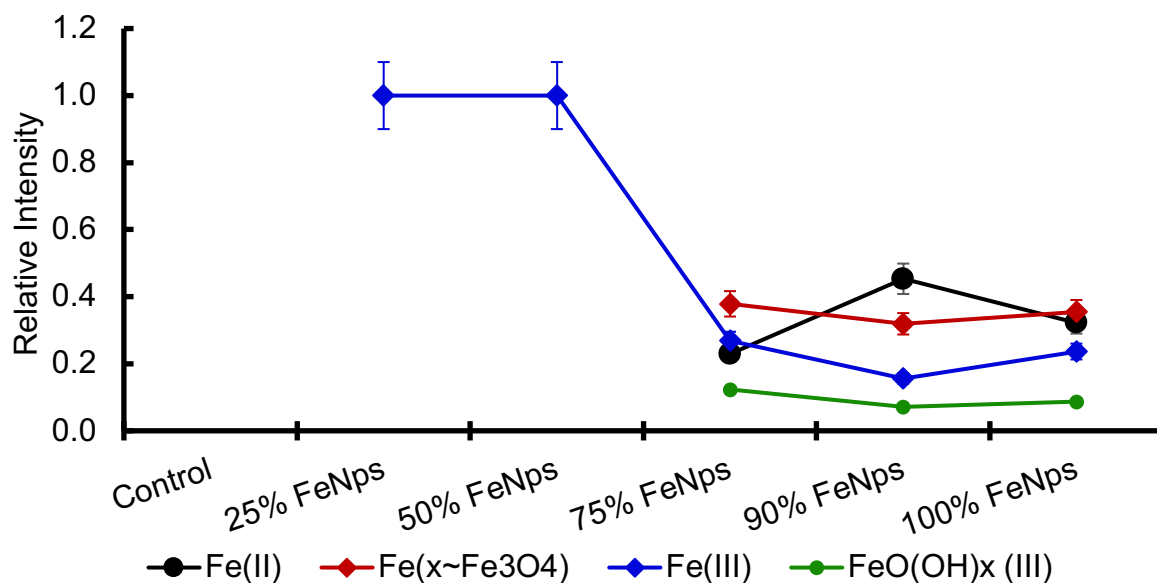


Figure 170 – XPS results showing the relative concentrations of different carbon centred functional groups present on the surface of the composite mats.

Up to 50 wt % γ -Fe₂O₃ content, the only Fe species observed by XPS was Fe(III). Above 50 wt% the species Fe(II), Fe(x~Fe₃O₄) and FeO(OH)_x were also observed. It should be noted that the 100% sample also contains all 4 of these species suggesting that a reduction reaction is taking place between the γ -Fe₂O₃ nanoparticles under reactive compression moulding conditions resulting in the formation of Fe(II) species. Each Fe species showed a decreased signal at 90 wt% compared to the pure sample except for the Fe(II) signal. This is the only peak which signal that shows a significant difference to the control suggesting if a reaction is taking place between the γ -Fe₂O₃ nanoparticles and the polymer, its likely an oxidation of sulfur converting Fe(III) into Fe(II). SEM / EDX suggests that the γ -Fe₂O₃ nanoparticles aggregate forming bulk γ -Fe₂O₃ particles during the reactive compression moulding process. This is shown in Figure 171. The iron is shown with EDX analysis and appears to have aggregated into a layer on the surface. To confirm that the nanoparticles had aggregated into bulk material XRD analysis was performed on the samples (Figure 171).

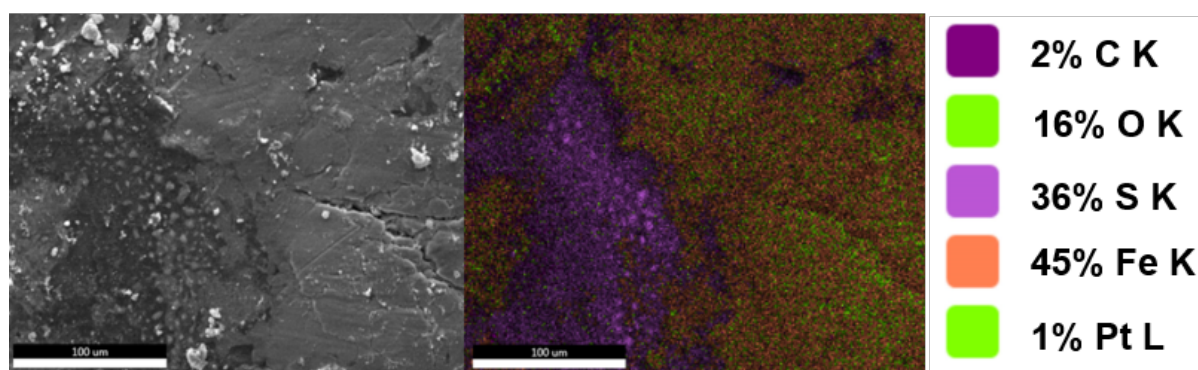


Figure 171 – SEM / EDX analysis highlighting regions on the composites surface whereby the γ -Fe₂O₃ nanoparticles appear to have aggregated.

XRD analysis was used to investigate any differences in the crystal structures for the Fe₂O₃, 50-poly(*S-r*-canola) and any other species formed during their reaction.

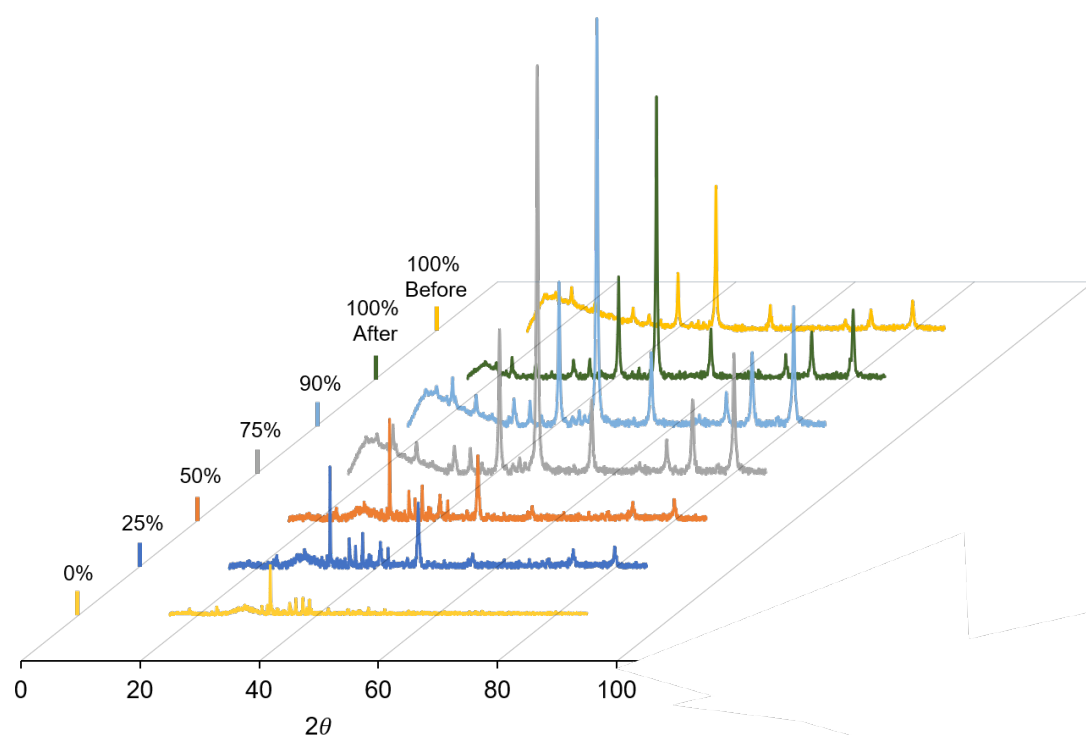


Figure 172 – XRD plots for 0-90% composite powders and 100% γ -Fe₂O₃ nanoparticles before and after moulding.

XRD analysis (Figure 172) revealed that the signals corresponding to the starting material do not change significantly after moulding suggesting little to no reaction has occurred. These same signals are present in all samples with their intensities decreasing with a decrease in Fe content. The inverse is true for the 50-poly(*S-r*-canola) signals whereby they decrease in signal as their wt% in the composite decreases. These results indicated that there was no change in chemical structure. In summary whilst FTIR and XPS provided some evidence to suggest a reaction had occurred, XRD and STA did not. The small amount of evidence gained suggests that if any

reactions are occurring, it is likely some form of polysulfide oxidation. XPS suggested the reaction could be an oxidation of sulfur to form SO_x groups (sulfoxides, thiosulfinate, thiosulfonates, etc). Fe_2O_3 has been shown to act as a catalyst in the solid-state oxidation of soot through direct contact.³⁶² It's possible that under the high pressure and temperature conditions used to prepare the composites (100 °C, 40 MPa), the Fe_2O_3 particles partially oxidised a small extent of the 50-poly(*S-r*-canola) polymer resulting in the increases in oxidised sulfur signals observed. It is also possible that sulfur oxidation occurred under these conditions due to air and not the Fe_2O_3 particles. These sulfur oxidation signals may have also been present on the surface only and not within the bulk. Further investigation would be required to determine the exact mechanism of this sulfur oxidation. As iron is known to react with sulfur under elevated temperatures we hypothesised that the polysulfide may bind directly with the iron during composite preparation.³⁶³ No evidence of Fe-S bond formation was observed. These results suggest that whilst a small amount of sulfur oxidation could be occurring, it is likely that the Fe_2O_3 particles are being physically embedded within the polymer matrix and not chemically binding with it. While any chemical differences would be interesting to investigate, they didn't affect the materials functionality and for this reason these differences were left for future work and focus shifted back towards applications of these composites.

5.5.4 Applications: Magnetic filtration

The use of these materials for magnetic filtration was investigated. The composite with the lowest $\gamma\text{-Fe}_2\text{O}_3$ nanoparticle content (~13.33%) was ground into a fine powder suspended in water. A magnet was then used to filter the composite particles from the water resulting in complete removal of the composite from the water (Figure 173).

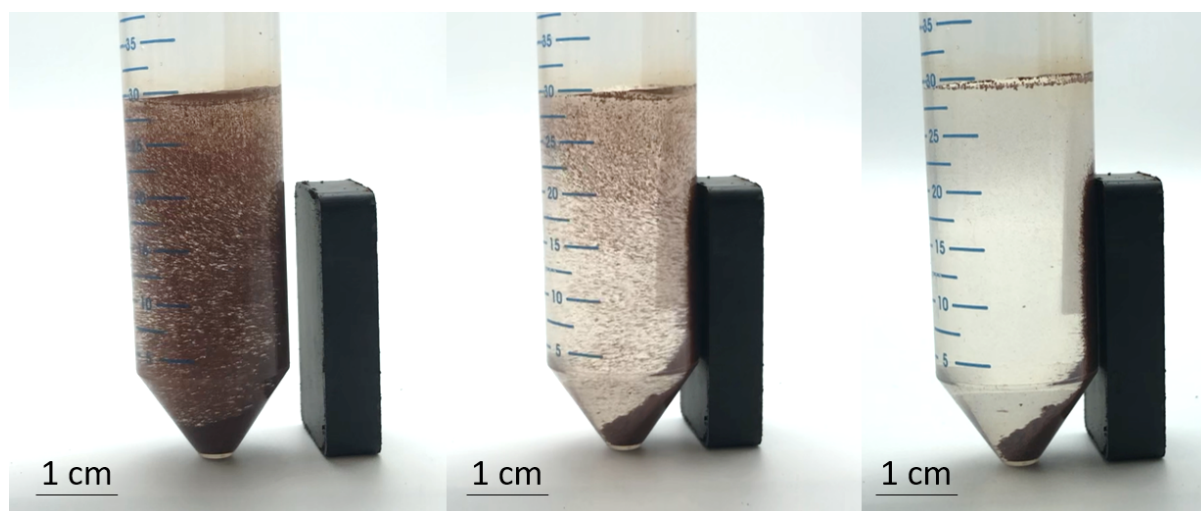


Figure 173 – Images demonstrating the ability to filter out the composite particles using magnetic filtration.

Using this composite for magnetic filtration was investigated further by treating a solution of HgCl_2 (150 ppm) containing insoluble mine tailings (Figure 174).



Figure 174 – Images demonstrating the magnetic filtration and separation of the composite powder from a tailings / water slurry.

The magnetic composite effectively removed 98.6% of the HgCl_2 before being removed via magnetic filtration followed by magnetic separation from the solid ore. It should be noted that this is 98.6% of the HgCl_2 remaining in solution after the addition of the fine tailings. The amount remaining after addition of fine tailings is shown in Table 7 as the control sample. HgCl_2 concentrations before and after treatment were determined using cold vapor atomic absorption (CVAA) spectroscopy. The treatment results are shown in Table 7.

Sample	Concentration (ppm)
Initial	9.3 ± 0.16
Control	0.48 ± 0.15
Treated	0.0067 ± 0.0066

Table 7 – Results from mercury treatment

The composite powders after magnetic filtration are shown below in Figure 175. It was noted that small amounts of remanent ore was present and not removed upon the first magnetic filtration step.



Figure 175 – Images showing the composite material directly after magnetic filtration / separation from the sand / water slurry.

The separated sorbent material contained some remanent ore which wasn't removed during the magnetic filtration process. To further isolate the magnetic composite material from the ore, magnetic separation was performed on the physical mixture of ore and composite powder.

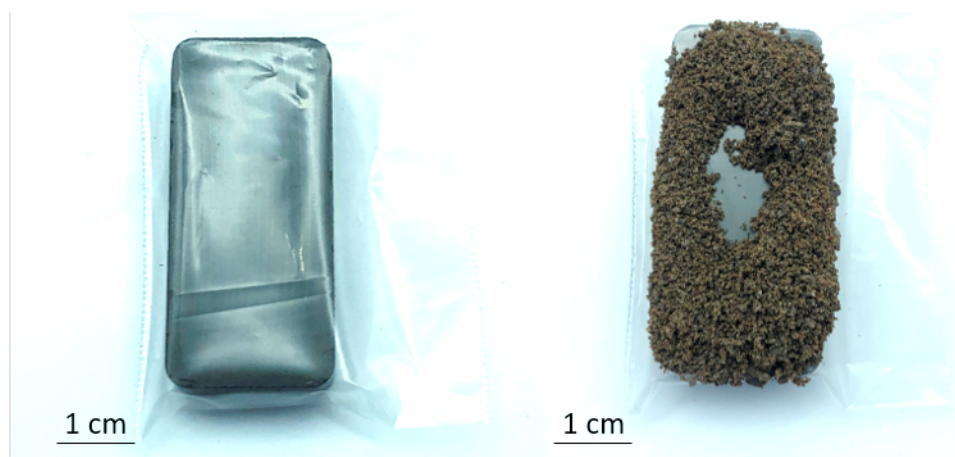


Figure 176 – A) 47 × 22 mm ceramic magnet in plastic zip lock bag before separation, B) Image showing the magnetic composite bound to the plastic bag with a magnet inside it shown in A.

A plastic bag was placed over the magnet (Figure 176) to ensure a simple removal of magnetic composite through simple removal of the magnet from the bag. This protected magnet was then used to magnetically separate the sand from the composite material. This is shown in Figure 177.

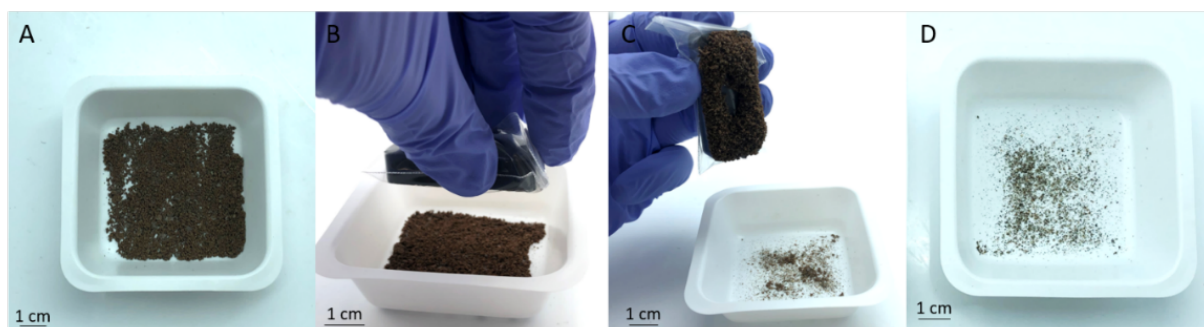


Figure 177 – A) Magnetic composite contaminated with sand, B), Magnet inside a Ziplock bag being used to magnetically separate the composite from the sand C), Magnetic composite material stuck to the magnet leaving only sand behind D), Sand remaining after separation step. Shown above, by simply passing the bag containing the magnet over the sand / composite mixture, the composite powder was magnetically attracted, and pulled up into contact with the bag. The sand wasn't magnetic and remained in the container effectively separating the particles from one another. The final percentage of recovered composite was 99%. Finally, the ability to use this magnetic functionality to separate the magnetic / 50-poly(*S-r*-canola) from other components in a multicomponent composite material. To do this, 20 wt% composite powder was formed into a composite with waste PVC shavings. This is shown below in figure 178. Once formed the composite was ground back up into a fine powder and the magnetic separation process used above was performed.

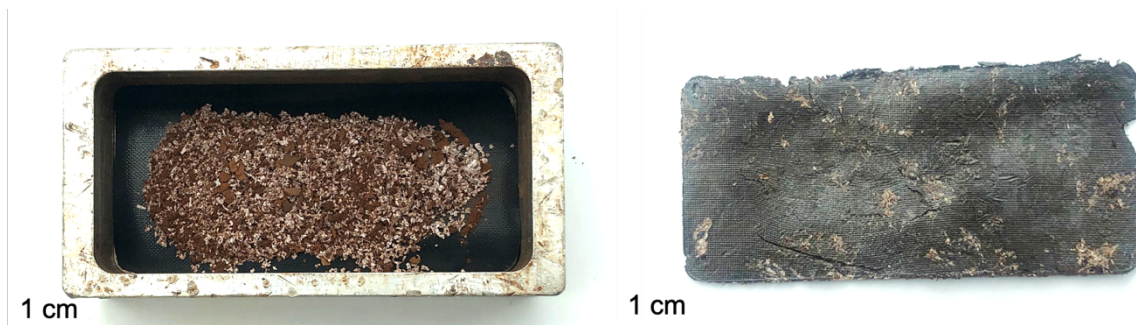


Figure 178 – 50-poly(*S-r*-canola) / Fe_2O_3 / PVC blend before (left) and after (right) being moulded into a composite mat.

The mat was then ground back into a fine powder and magnetic separation was used to separate the magnetic composite from the PVC shavings. The magnetic separation process is shown in Figure 179.

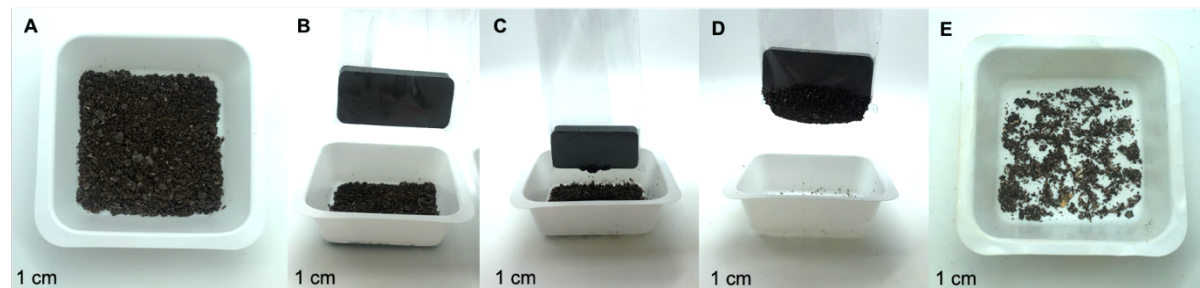


Figure 179 – Images showing the process of magnetically separating the composite from other components in a solid-solid mixture.

The small PVC pieces had small portions of composite material stuck to their surface after grinding back into a powder. This meant that although the PVC particles were not magnetic the small portions of composite bound to their surface were. This meant that the PVC particle still felt a small force under a magnetic field. In order to ensure that the PVC particles were not recovered with the composite the magnet was held further away from the mixture (3 cm) meaning that only the composite material not bound to the heavy PVC particles would be drawn into the air and stick to the magnet. The recovered composite and the PVC/composite waste is shown in Figure 180.

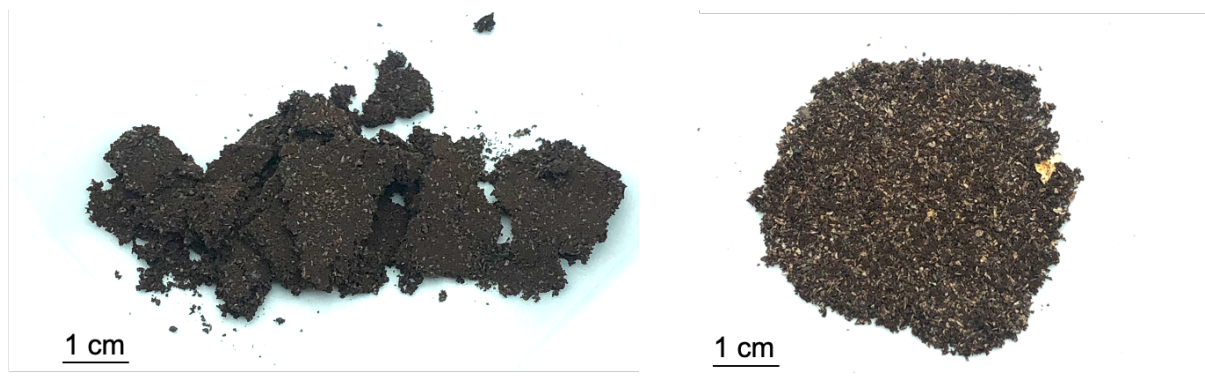


Figure 180 – Magnetic composite (left) and PVC with fine composite coating (right)

Most of the PVC was removed from the composite with only very small particles remaining. The recovered particles are shown in Figure 180. These particles could have potentially been removed using a finer particle size grinder method or by repeating the process multiple times. This is the first time that magnetic filtration has been utilized to recycle individual components within a composite material.

5.5.5 Applications: Microwave heating

Another interesting application of these magnetic composite materials is their ability to undergo direct heating through microwave irradiation. Magnetic $\gamma\text{-Fe}_2\text{O}_3$ nanoparticles can undergo both dielectric heating and magnetorestrictive heating under the influence of microwave irradiation. Due to the high content of $\gamma\text{-Fe}_2\text{O}_3$ nanoparticles, the ability to heat this composite using microwave irradiation was investigated. The heating of the composite was compared to its individual constituents over 40 seconds.



Figure 181 – **A**) 0.1 grams of γ -Fe₂O₃ nanoparticles (<50nm), **B**) 0.65 grams of 50-poly(S-*r*-canola) polysulfide, **C**) 0.75 grams of 50-poly(S-*r*-canola) / γ -Fe₂O₃ composite material.

The samples were first placed on PTFE paper (Figure 186) as it did not show any temperature increase under microwave irradiation and therefore wouldn't transfer extra heat to the samples during testing. These sheets were placed directly into a household microwave with the temperature being monitored before and after irradiation using a handheld IR thermometer. The magnetic composite powder, 50-poly(S-*r*-canola) polymer and γ -Fe₂O₃ nanoparticle were investigated (Figure 182).

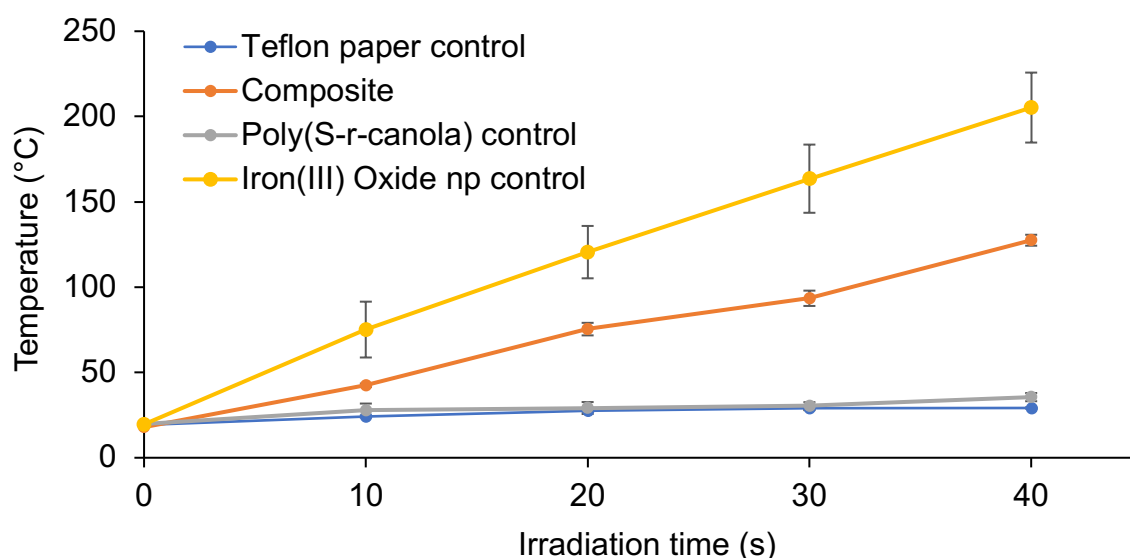


Figure 182 – Temperature profile for 0 - 40 seconds of microwave irradiation for PTFE paper, 50-poly(S-*r*-canola), γ -Fe₂O₃ nanoparticle control and 50-poly(S-*r*-canola) / γ -Fe₂O₃ composite.

The γ -Fe₂O₃ nanoparticle control demonstrated the highest temperature increase under microwave irradiation followed by the 20% composite powder. The 50-poly(S-*r*-canola) powder was almost identical to the PTFE control not showing any significant heating and remained constant in temperature throughout the irradiation. This demonstrated how the

addition of $\gamma\text{-Fe}_2\text{O}_3$ nanoparticles facilitates the microwave heating of 50-poly(*S-r*-canola) polymers, something which wasn't previously possible. It was noted that over 40 seconds of irradiation resulted in degradation of the composite material (Figure 183).



Figure 183 – Image showing the magnetic composite before (left) and after (right) 50 seconds of microwave irradiation. This demonstrates that under 50 seconds of irradiation the composite will start to decompose.

The temperature being measured by the handheld IR thermometer is the temperature on the surface of the composite. As the 50-poly(*S-r*-canola) polymer doesn't heat up under microwave irradiation the only source of heat is from the nanoparticles. The heat produced from the nanoparticles during microwave irradiation must then transfer to the 50-poly(*S-r*-canola) polymer and through its bulk to the surface before being measured. This means that the temperature at the nanoparticle / 50-poly(*S-r*-canola) interface would be higher than the temperature being observed at the surface. Although the temperature measured after 40 seconds was ~ 127 seconds, the nanoparticle control had reached $200\text{ }^{\circ}\text{C}$ meaning that the temperature at the 50-poly(*S-r*-canola) interface would be approaching degradation temperature. This should be avoided as degradation is a fire hazard and would lead to the generation of toxic SO_2 gas. As microwave heating is possible with this material, the ability to perform reactive compression moulding in the microwave was investigated. A syringe was used to compress composite particles into a cylinder shape (Figure 184). Irradiation time of 20 s was initially used, followed by 2 more irradiation times of 15 seconds, to ensure the reaction completed.

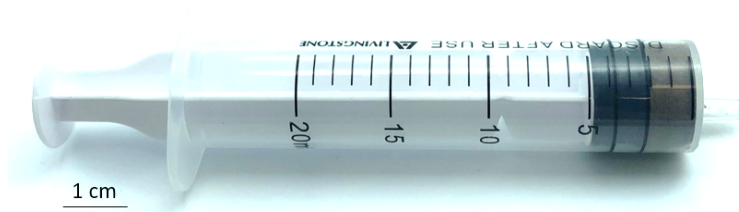


Figure 184 – Syringe with composite in before moulding into disk.



Figure 185 – Images showing the composite disks made from the magnetic composite using reactive compression moulding in the microwave.

Using this method magnetic composite disks (Figure 185) and cylinders (Figure 186) could be prepared.



Figure 186 – Syringe containing un moulded composite (Left) and the resulting moulded composite cylinder (Right).

This cylinder was shown to retain its magnetic properties after moulding. This was demonstrated by showing its affinity towards a permanent magnet (Figure 187).

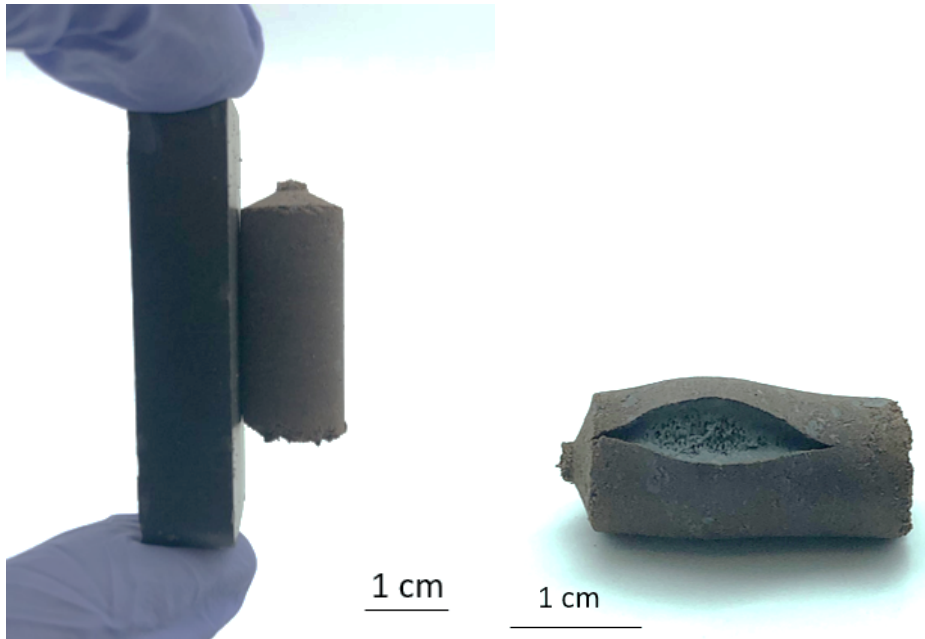


Figure 187 – A) Image demonstrating the ability to pick up the magnetic composite cylinder using a magnet, **B)** Image of composite cylinder after an additional 20 seconds of heating.

Although the initial sample was irradiated for 20 seconds without issue, the final bulk material decomposed when heated for 20 seconds. This is half the 40 seconds required for the powder in earlier experiments. This corresponds well with the results from the thermal conductivity experiments which showed that the powdered composite displayed double the thermal conductivity compared to the bulk form. To highlight this difference, the same experiment was repeated comparing the 50-poly(*S-r*-canola) / γ -Fe₂O₃ blend with the 50-poly(*S-r*-canola) / γ -Fe₂O₃ composite in both powder and bulk form (Figure 188).

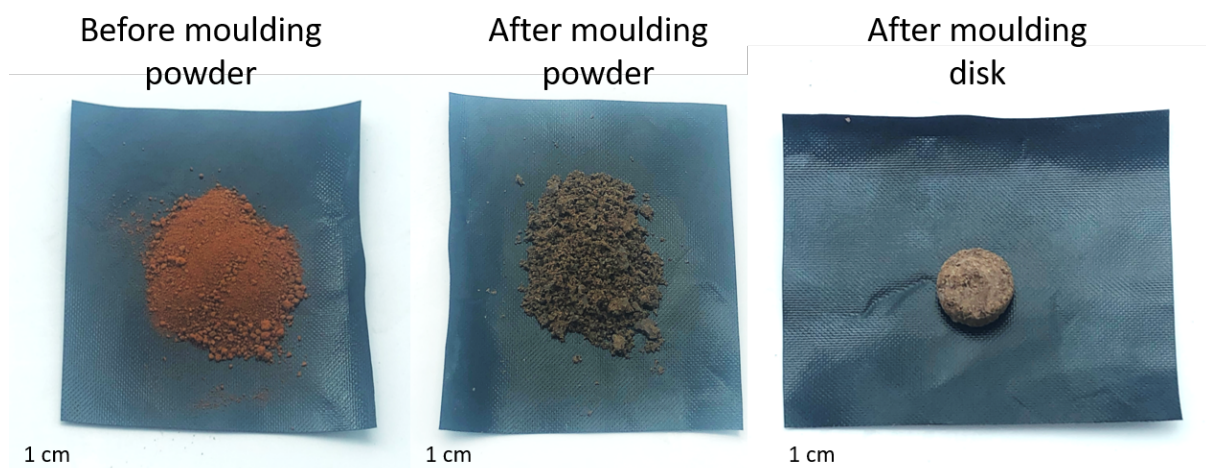


Figure 188 – Images of the 50-poly(*S-r*-canola) blend before moulding (Left), the powdered composite (middle) and the composite moulded into small disk (right).

The samples were placed on PTFE paper and placed inside a household microwave. The temperature of the samples after 20 seconds irradiation was recorded using a FLIR thermal imaging camera in hotspot mode.

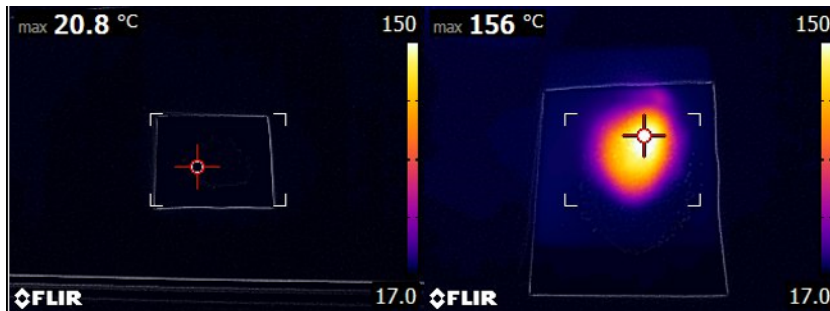


Figure 189 – FLIR thermal imaging of unmoulded blend before and after microwave irradiation for 20 seconds.

The blend (Figure 189) demonstrated the highest observed temperature increase (135.2 °C). This was expected as the γ -Fe₂O₃ nanoparticles cover the surface of the 50-poly(*S-r*-canola) polymer and the temperature measured is that of the nanoparticles directly.

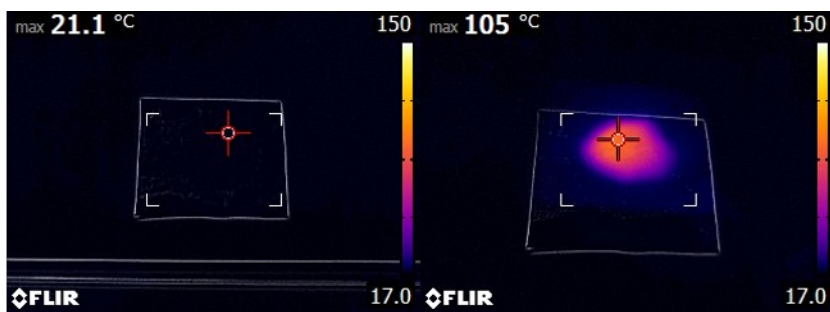


Figure 190 – FLIR thermal imaging of composite powder before and after microwave irradiation for 20 seconds.

As expected, the composite powder (Figure 190) showed a decreased temperature increase in comparison to the blend, increasing in temperature by 73.9 °C.

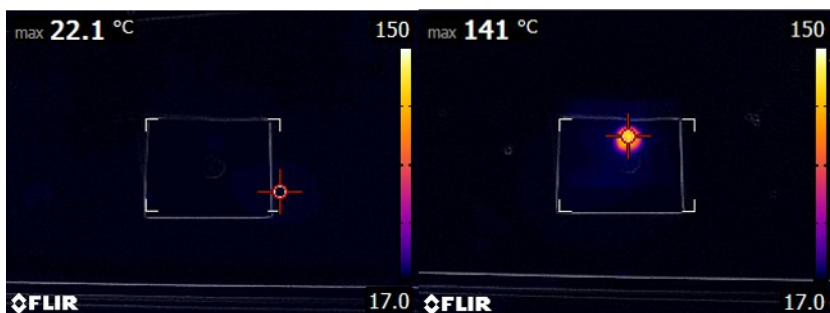


Figure 191 – FLIR thermal imaging of composite disk before and after microwave irradiation for 20 seconds.

The composite disk (Figure 191) showed a significantly higher recorded temperature than the composite powder. This is because the 50-poly(*S-r*-canola) is a thermal insulator and holds the heat generated by the Fe nanoparticles under microwave irradiation. Heat does not need to transfer through the air between particles to contribute to other particles heating up, it does so directly through the composite. This results in a higher number of heat sources contributing to the temperature increase at each location on the material. This results in the higher temperature observed. The temperature observed by the disk was smaller than that observed by the blend. This was expected as in the case of the blend the nanoparticles were measured directly whereas in the composite the surface temperature of the 50-poly(*S-r*-canola) was instead measured. The microwave irradiation heating rate of the various γ -Fe₂O₃ composites were investigated. Thermal conductivity measurements revealed that powdered samples conduct heat differently to bulk samples and therefore heating experiments were performed on 0.5 × 0.5 cm square composite mats of equal thickness (approximately 2 mm). It was demonstrated that the rate of heating under microwave irradiation was directly proportional to the number of γ -Fe₂O₃ nanoparticles the composite contained (Figure 192). The heating profiles for each composite were recorded and used to create an equation which allows one to calculate the irradiation time required for a composite to reach a specific temperature depending on its γ -Fe₂O₃ content. This was important to ensure that degradation could be avoided to minimize both the hazards involved and any damage to the samples.

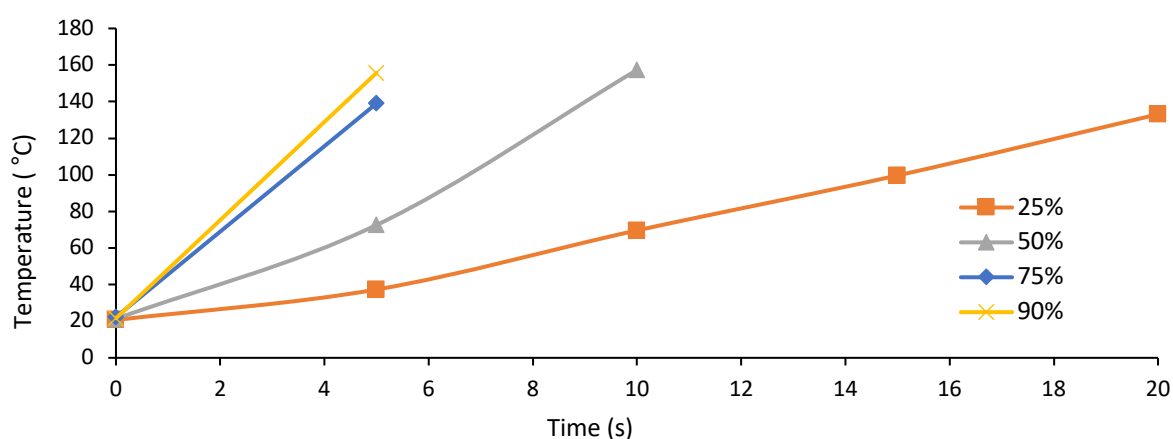


Figure 192 – Plot of temperature against microwave irradiation time (s) for each composite.

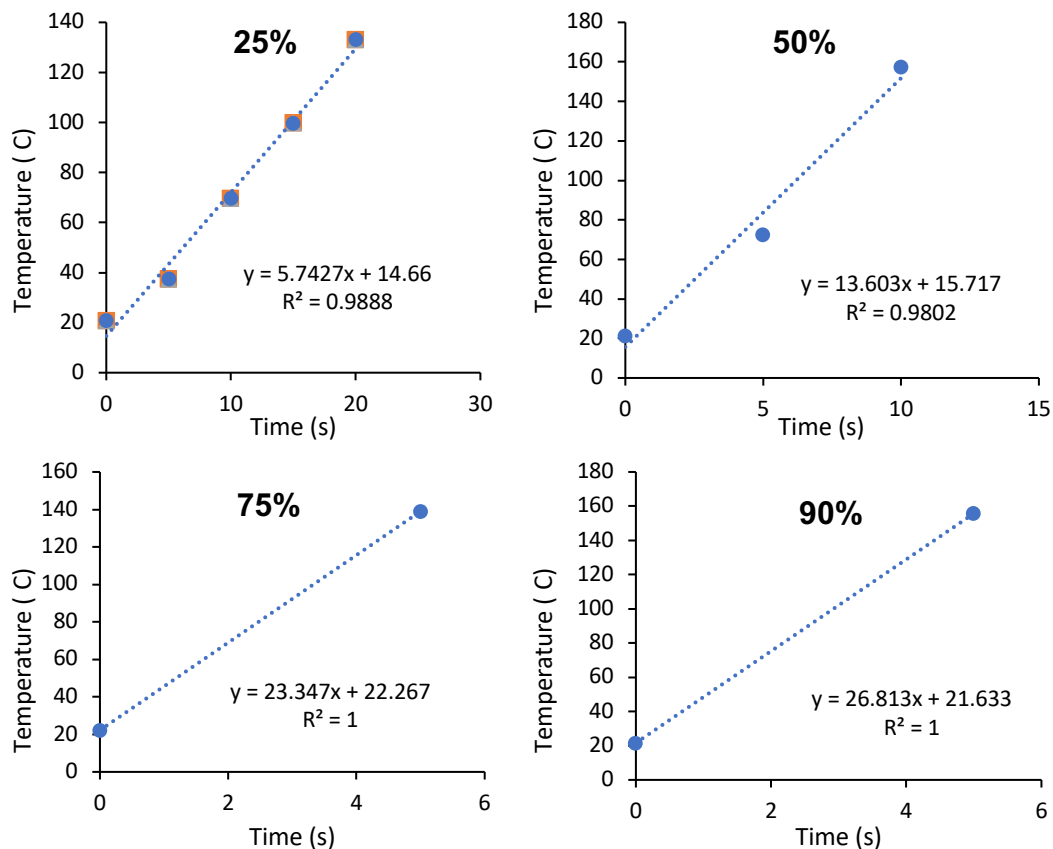


Figure 193 – Plots for temperature vs time for each $\gamma\text{-Fe}_2\text{O}_3$ content composite with a linear line of best fit added.

The slope for the lines of best fit for the plots in Figure 193 are equivalent to the heating rate under microwave irradiation.

Fe Content (wt%)	Rate ($^{\circ}\text{C/s}$)
25	6
50	14
75	23
90	27

Table 8 – Results for heating rate of composite materials with different $\gamma\text{-Fe}_2\text{O}_3$ contents.

The weight percentages of $\gamma\text{-Fe}_2\text{O}_3$ nanoparticle were plotted against their corresponding heating rates (Figure 194) shown in Table 8. This demonstrated a linear relationship with an R^2 value of 0.9947.

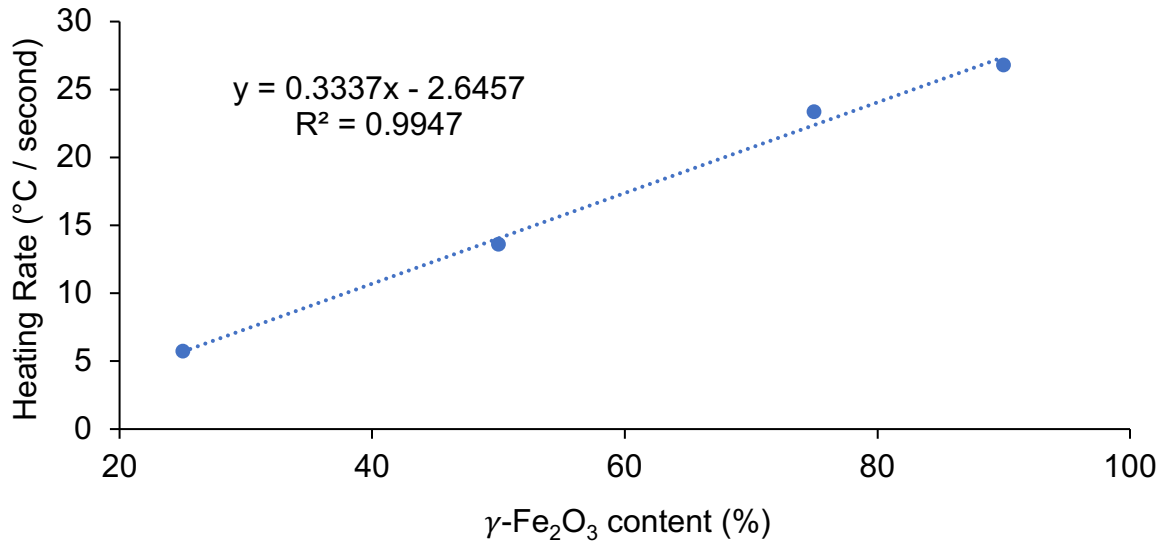


Figure 194 - Microwave heating rate of the composite against the $\gamma\text{-Fe}_2\text{O}_3$ content of the composite material.

A simple linear model was used to estimate the time required to get the polymer to 100 °C:

$$\text{Heating rate} = 0.3337 \times (\text{Fe}_2\text{O}_3\%) - 2.6457 \quad \text{Equation 9}$$

Therefore, to increase temperature by 100 °C:

$$100 = (\text{Heating rate}) \times T$$

Or

$$100 = (0.3337 \times (\text{Fe}_2\text{O}_3\%) - 2.6457) \times T$$

Therefore

$$T = \frac{100}{0.3337 \times (\text{Fe}_2\text{O}_3\%) - 2.6457} \quad \text{Equation 10}$$

Using this equation, it is possible to estimate the irradiation time required to heat bulk composite to 100 °C depending on the $\gamma\text{-Fe}_2\text{O}_3$ content. It's important to note that this equation is only applicable to bulk sample and not powdered samples. Powdered samples would require a higher irradiation time to achieve the same temperature as the bulk. This was observed in the previous heating experiment whereby the powdered composite did not increase in temperature as much as the bulk sample under the same irradiation times. Although reactive compression moulding starts with a powdered form of the composite, the process involves compressing the particles into a bulk form in which case the equation is applicable. This equation can therefore be used to determine the optimised irradiation time required for a sample of given $\gamma\text{-Fe}_2\text{O}_3$

content to undergo reactive compression moulding under microwave irradiation without overheating the sample.

5.4.6 Applications: Electrical and mechanical components

Another application of magnetic composites is in electronics and robotics. These fields require new, inexpensive lightweight materials which can work efficiently in their desired applications. To demonstrate the use of our 50-poly(*S-r*-canola) / γ -Fe₂O₃ composite material in these fields, the 75% composite was moulded into a cylinder by compacting the composite within a 5 mL syringe and using reactive compression moulding in the microwave under the previously defined optimized conditions. This composite cylinder was then investigated for use as the active magnetic component of a solenoid valve switch. To do this a solenoid valve, whose schematics are shown below, was deconstructed. The operator (part that responds to magnetic fields) was replaced with the composite cylinder and the valve was reconstructed. A small steel spring was added to the top of the composite cylinder to ensure that the cylinder remained closed when the solenoid was not on. The cylinder was placed inside a plastic cylinder (radius = 1.0 cm, thickness = 0.2 cm) before being placed into the solenoid coil. This was to ensure that the composite cylinder fitted tightly, and no leaks were possible. The construction process is depicted in Figure 195.

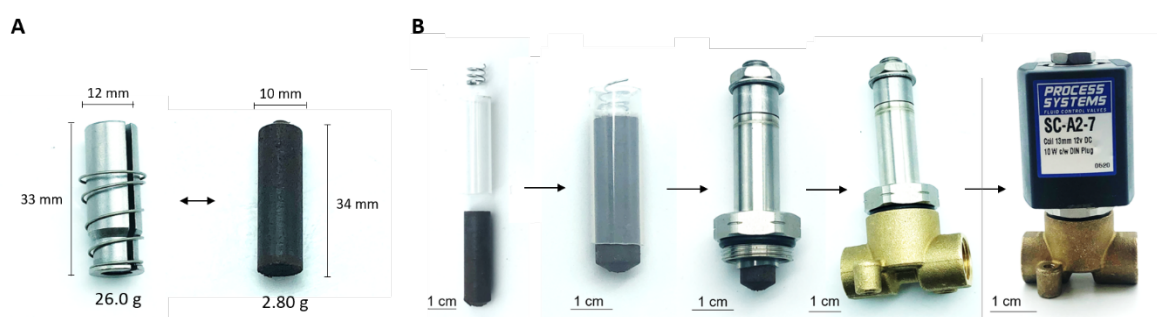


Figure 195 – A) Image of initial operator inside solenoid valve and its replacement prepared by the composite material. **B)** Images describing the process of re-constructing the solenoid valve with the magnetic composite material used as the composite material.

After replacing the solenoid valve switch's operator, the solenoid valve setup was clamped in a vertical position and plastic tubing was used to connect the inlet of the solenoid to a dropping funnel. A second piece of tubing was attached to the outlet of the solenoid valve. A beaker was placed below the outlet tube to catch the flow through. To better visualize the experiment, a coloured FeCl_{3(aq)} solution was added into the dropping funnel. The funnel was opened to allow the solution to meet the closed inlet on the valve. The power to the solenoid valve was turned

on and the valve was switched to the on position. The $\text{FeCl}_3(\text{aq})$ solution flowed through the solenoid valve and into the beaker. This is shown in Figure 196.

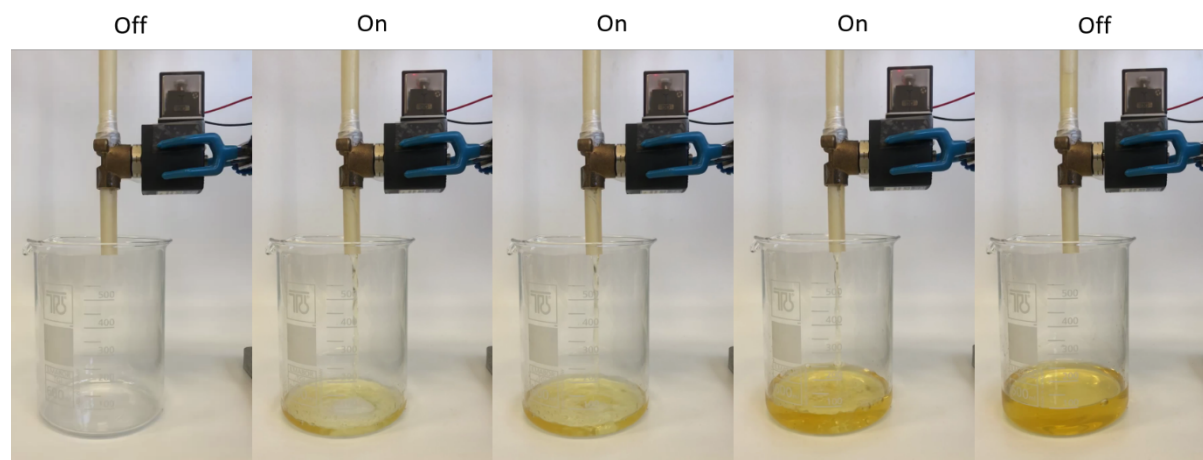


Figure 196 – Images showing the working solenoid valve with magnetic composite replacing the operator inside it.

When the valve was turned back off, the flow of the FeCl_3 stopped. This suggested that the composite cylinder was able to effectively act as the operator in a magnetic solenoid valve. This simple demonstration illustrates how the composite made by reactive compression moulding can be used as a component in a mechanical device such as a solenoid.

5.5 Conclusions

A sustainable multifunctional magnetic composite material is prepared directly from 50-poly(*S-r*-canola) polymer and $\gamma\text{-Fe}_2\text{O}_3$ nanoparticles using a process called reactive compression moulding. This involves blending 50-poly(*S-r*-canola) polymer with $\gamma\text{-Fe}_2\text{O}_3$ nanoparticles then placing the mixture in a hot press at 40 MPa at 100 °C for 20 minutes. The composite material was shown to retain 50-poly(*S-r*-canola) polymers chemical reactivity towards HgCl_2 whilst the incorporation of the $\gamma\text{-Fe}_2\text{O}_3$ nanoparticles facilitated magnetic filtration further simplifying the remediation process whilst reducing solid waste production. The magnetic properties of the nanoparticles facilitate rapid heating under microwave irradiation. The process used to prepare and mould the composite material, reactive compression moulding, has been demonstrated to occur rapidly using microwave irradiation as the heating source. The rate of heating of the composite was shown to be directly proportional to the $\gamma\text{-Fe}_2\text{O}_3$ content of the composite. Reactive compression moulding using microwave irradiation was utilized to prepare a cylinder of 75 wt% $\gamma\text{-Fe}_2\text{O}_3$ composite material which was shown to replace the original magnetic component of a commercial solenoid valve. This

reduced the weight of the component 10-fold and demonstrated the potential to use these magnetic composites as components in electrical and mechanical systems.

6.0 Conclusions and outlook

The synthesis of a sustainable polymeric material from sulfur and canola oil has been demonstrated using the process termed inverse vulcanisation. These polymers were prepared with varying amounts of sulfur, with and without porosity and through both conventional and microwave heating strategies. The rapid synthesis of these polymers using microwave heating was an important discovery as it not only reduced the time required to prepare these polymers, but it also facilitated their preparation in places with limited resources expanding the materials viability. This is also the only example of microwave heating being utilised for initiating the inverse vulcanisation reaction. This is because sulfur will not heat upon microwave irradiation alone, the microwave irradiation heats the canola oil which transfers to the sulfur to initiate the reaction. After preparing and characterising these materials, their use as iron pollution sorbents was investigated. These materials have been investigated as sorbents in mercury remediation previously however this was the first instance where iron pollution has been investigated. There remains a small amount of heavy metal pollutants in which these sulfur polymers have not been investigated already as sorbent materials. Investigating the interactions of these polymers with different metals and the various complex's they form in aqueous solution is the next step for future work. The sustainable 50-poly(S-*r*-canola) polymer was also shown to be an effective support material for powdered activated carbon, increasing its safety profile and facilitating its use within continuous flow and filtration-based systems. The 50-poly(S-*r*-canola) / PAC blend was demonstrated to be an effective sorbent material for the remediation of the persistent organic pollutants, PFOA and PFOS from water. Future work in this field would be to determine a suitable method to recover the PFOS and PFOA from the sorbent material after remediation. A method for reforming and remoulding the 50-poly(S-*r*-canola) polymer, termed reactive compression moulding was created and then investigated as a potential method for recycling the material after use. This method was demonstrated to work effectively even when waste 50-poly(S-*r*-canola) sorbent, previously saturated with Fe(III), was used. This is the first time in literature that a heat induced sulfur exchange reaction has been used to facilitate the recycling and reforming of these thermoset sulfur polymers. Although saturation of the polymer with Fe(III) showed no impact on the reactive compression moulding process, the effects of saturation with other compounds should be investigated as future work. Reactive compression moulding was also utilised as a method for preparing composite materials from sulfur polymers. Filler materials were simply mixed in with the 50-poly(S-*r*-canola) polymer particles before moulding to form the desired composite. It was shown that the use of different types and amounts of filler materials allowed one to control the resulting mechanical properties

of the moulded mats. This was important as it allows for the tailoring of the materials properties to suit specific applications. Future work would encompass the use of various other filler materials and compositions to optimise the materials use in specific applications. Next, by using $\gamma\text{-Fe}_2\text{O}_3$ nanoparticles as the filler material, multifunctional magnetic composite materials were prepared. In these composites the magnetic nanoparticles were encapsulated by the 50-poly(*S-r*-canola) polymer forming a relatively homogenous composite mat after undergoing reactive compression moulding. By crushing this mat up into a powder, it was able to be used efficiently to treat HgCl_2 solution as well as be removed from solution using magnetic filtration. This was an important discovery as it adds further capabilities and scope to using 50-poly(*S-r*-canola) polymers in remediation processes. The inclusion of the magnetic nanoparticles also facilitated the microwave heating of the composite mats, something which was not possible with the 50-poly(*S-r*-canola) polymer on its own. This allowed for the rapid, reactive compression moulding of the composite materials using microwave irradiation. The heating rates for each composite were shown to share a linear relationship with the amount of nanoparticles present in the composite. Using this relationship, the optimal reaction conditions were determined and reactive compression moulding was implemented to form magnetic composite disks and cylinders. To demonstrate the potential use of these magnetic composite materials in mechanical and electrical systems, the active magnetic component of a solenoid valve was replaced with one made from the magnetic composite material. The solenoid valve was demonstrated to work with the magnetic composite component replacing the original component and in turn reducing its weight tenfold. Future work will investigate the use of these composites as components in various other mechanical and electrical systems.

7.0 References

1. Zhu, Y.; Romain, C.; Williams, C. K. *Nature* **2016**, 540, 354-362.
2. Sieffert, Y.; Huygen, J. M.; Daudon, D. *J. Clean. Prod.* **2014**, 67, 125-138.
3. Galvan, A. M.; Hanson, R.; George, D. R. *J. Community Health* **2018**, 43, 944-946.
4. Lu, J. Y.; Zhu, Q. Y.; Zhang, X. X.; Zhang, F. R.; Ding, X. Z.; Xia, L. Q.; Huang, W. T.; Luo, H. Q.; Li, N. B. *Ecotoxicol Environ Saf* **2018**, 160, 273-281.
5. Mohajerani, A.; Vajna, J.; Cheung, T. H. H.; Kurmus, H.; Arulrajah, A.; Horpibulsuk, S. *Constr. Build. Mater.* **2017**, 156, 443-467.
6. Rhodes, C. J. *Sci Prog* **2018**, 101, 207-260.
7. Worthington, M. J. H.; Shearer, C. J.; Esdaile, L. J.; Campbell, J. A.; Gibson, C. T.; Legg, S. K.; Yin, Y.; Lundquist, N. A.; Gascooke, J. R.; Albuquerque, I. S.; Shapter, J. G.; Andersson, G. G.; Lewis, D. A.; Bernardes, G. J. L.; Chalker, J. M. *Adv. Sustain. Syst.* **2018**, 2, 1800024.
8. Arancon, R. A. D.; Lin, C. S. K.; Chan, K. M.; Kwan, T. H.; Luque, R. *Energy Sci. Eng.* **2013**, 1, 53-71.
9. Mata, T. M.; Martins, A. A.; Caetano, N. S., Valorization of Waste Frying Oils and Animal Fats for Biodiesel Production. In *Advanced Biofuels and Bioproducts*, Lee, J. W., Ed. Springer New York: New York, NY, **2013**, pp 671-693.
10. Sormunen, P.; Kärki, T. *J. Build. Eng.* **2019**, 24, 100742.
11. G U, R.; Kumarappa, S.; Gaitonde, V. *J. Mater. Environ. Sci* **2012**, 3, 907-916.
12. Bu Najmah, I.; Lundquist, N. A.; Stanfield, M. K.; Stojcevski, F.; Campbell, J. A.; Esdaile, L. J.; Gibson, C. T.; Lewis, D. A.; Henderson, L. C.; Hasell, T.; Chalker, J. M. *ChemSusChem*.
13. Arancon, R. A.; Barros Jr, H. R.; Balu, A. M.; Vargas, C.; Luque, R. *Green chem.* **2011**, 13, 3162-3167.
14. Russ, W.; Meyer-Pittroff, R. *Crit. Rev. Food Sci. Nutr.* **2004**, 44, 57-62.
15. Stenmarck, Å.; Jensen, C.; Quested, T.; Moates, G.; Buksti, M.; Cseh, B.; Juul, S.; Parry, A.; Politano, A.; Redlingshofer, B., *Estimates of European food waste levels*. IVL Swedish Environmental Research Institute: **2016**.
16. Parfitt, J.; Barthel, M.; Macnaughton, S. *Philos. Trans. R. Soc. Lond., B, Biol. Sci.* **2010**, 365, 3065-3081.
17. Cabeza, L. F.; Taylor, M. M.; DiMaio, G. L.; Brown, E. M.; Marmer, W. N.; Carrió, R.; Celma, P. J.; Cot, J. *J. Waste Manag.* **1998**, 18, 211-218.

18. Teuber, R.; Jensen, J., *Food losses and food waste: Extent, underlying drivers and impact assessment of prevention approaches*. **2016**.
19. Mannu, A.; Garroni, S.; Ibanez, J.; Mele, A. *Processes* **2020**, 8, 366.
20. Mannu, A.; Ferro, M.; Pietro, M. E. D.; Mele, A. *Sci. Prog.* **2019**, 102, 153-160.
21. Kawentar, W. A.; Budiman, A. *Energy Procedia* **2013**, 32, 190-199.
22. Lapuerta, M.; Herreros, J. M.; Lyons, L. L.; García-Contreras, R.; Briceño, Y. *Fuel* **2008**, 8, 3161-3169.
23. Zhang, Y.; Dubé, M. A.; McLean, D. D.; Kates, M. *Bioresour. Technol.* **2003**, 89, 1-16.
24. Zhang, Y.; Dubé, M. A.; McLean, D. D.; Kates, M. *Bioresour. Technol.* **2003**, 90, 229-240.
25. Wang, Y.; Pengzhan Liu, S. O.; Zhang, Z. *Energy Convers. Manag.* **2007**, 48, 184-188.
26. Phan, A. N.; Phan, T. M. *Fuel* **2008**, 87, 3490-3496.
27. Karmakar, G.; Ghosh, P.; Sharma, B. *Lubricants* **2017**, 5, 44.
28. Ahmed, R. B.; Hossain, K. *Construc. Build. Mater.* **2020**, 230, 116985.
29. Rinaldi, L.; Wu, Z.; Giovando, S.; Bracco, M.; Crudo, D.; Bosco, V.; Cravotto, G. *Green Process. and Synth.* **2017**, 6, 425-432.
30. Mas'ud, Z. A.; Farid, M.; Surya, H.; Bambang, S. *IOP Conf. Ser.: Mater. Sci. Eng* **2019**, 509, 012083.
31. Chandelkar, S. R.; Karadbhajne, V. Y. *Int. J. ChemTech Res.* **2014**, 6, 481-486.
32. Chung, W. J.; Griebel, J. J.; Kim, E. T.; Yoon, H.; Simmonds, A. G.; Ji, H. J.; Dirlam, P. T.; Glass, R. S.; Wie, J. J.; Nguyen, N. A.; Guralnick, B. W.; Park, J.; Somogyi, A.; Theato, P.; Mackay, M. E.; Sung, Y. E.; Char, K.; Pyun, J. *Nat. Chem.* **2013**, 5, 518-24.
33. Gunstone, F. D., *Rapeseed and canola oil: production, processing, properties and uses*. CRC Press: **2004**.
34. Rapeseed oil production, 2014; Crops/Regions/World list/Production Quantity; unofficial data. UN Food and Agriculture Organization, C. S. D. F., Ed. **2017**.
35. Gary, J. H., Petroleum Refining. In *Encyclopedia of Physical Science and Technology (Third Edition)*, Meyers, R. A., Ed. Academic Press: New York, **2003**, pp 741-761.
36. Mayer, R., Elemental Sulfur and its Reactions. In *Organic Chemistry of Sulfur*, Oae, S., Ed. Springer US: Boston, MA, **1977**, pp 33-69.
37. Tobolsky, A. V. *J. Polym. Sci. Part C: Polym. Symp.* **1966**, 12, 71-78.
38. Ren, Y.; Shui, H.; Peng, C.; Liu, H.; Hu, Y. *Fluid Phase Equilib.* **2011**, 312, 31-36.

39. Kozhevnikov, V. F.; Kozhevnikov, V. F.; Payne, W. B.; Olson, J. K.; McDonald, C. L.; Inglefield, C. E. *J. Chem. Phys.* **2004**, 121.
40. Bacon, R. F.; Fanelli, R. *J. Am. Chem. Soc.* **1943**, 65, 639-648.
41. Tamura, K.; Seyer, H. P.; Hensel, F. *Berichte der Bunsengesellschaft für physikalische Chemie* **1986**, 90, 581-586.
42. Greer, S. C. *J. Chem. Phys.* **1986**, 84, 6984-6988.
43. Bellissent, R.; Bellissent, R.; Descotes, L.; Boué, F.; Pfeuty, P. *Phy. Rev. B: Condens. Matter* **1990**, 41, 2135-2138.
44. Kalampounias, A. G.; Andrikopoulos, K. S.; Yannopoulos, S. N. *J. Chem. Phys.* **2003**, 118, 8460-8467.
45. Steudel, R.; Passlack-Stephan, S.; Holdt, G. *Zeitschrift für anorganische und allgemeine Chemie* **1984**, 517 7-42.
46. Worthington, M. J. H.; Kucera, R. L.; Chalker, J. M. *Green Chem.* **2017**, 19, 2748-2761.
47. Bartlett, P. D. *J. Chem. Educ.* **1966**, 43, A1096.
48. Penczek, S.; ŚLazak, R.; Duda, A. *Nature* **1978**, 273, 738-739.
49. Duda, A.; Penczek, S. **1980**, 181, 995-1001.
50. Blight, L. B.; Currell, B. R.; Nash, B. J.; Scott, R. T. M.; Stillo, C. *Polym. J.* **1980**, 12, 5-11.
51. Tsuda, T.; Takeda, A. *Chem. Comm.* **1996**, 1317-1318.
52. Ding, Y.; Hay, A. S. *J. Polym. Sci.* **1997**, 35, 2961-2968.
53. Wen, Q.; Wu, Y.; Wang, X.; Zhuang, Z.; Yu, Y. *Hydrometallurgy* **2017**, 171, 77-85.
54. Sakuda, A.; Ohara, K.; Fukuda, K.; Nakanishi, K.; Kawaguchi, T.; Arai, H.; Uchimoto, Y.; Ohta, T.; Matsubara, E.; Ogumi, Z.; Okumura, T.; Kobayashi, H.; Kageyama, H.; Shikano, M.; Sakaebe, H.; Takeuchi, T. *J. Am. Chem. Soc.* **2017**, 139, 8796-8799.
55. Artemkina, S. B.; Grayfer, E. D.; Kozlova, M. N.; Poltarak, P. A.; Poltarak, A. A.; Fedorov, V. E. 41st International Convention on Information and Communication Technology, Electronics and Microelectronics (MIPRO), 21-25 May, **2018**, pp 0036-0039.
56. Chalker, J. M.; Worthington, M. J. H.; Lundquist, N. A.; Esdaile, L. J. *Top. Cur. Chem.* **2019**, 377, 16.
57. Meyer, B. *Chem. Rev.* **1976**, 76, 367-388.
58. Abraham, A.; Pillai, V.; Lonkar, S.; Al Hassan, S. **2017**, *J. Am. Chem. Soc.* pp PMSE-332.

59. Anyszka, R.; Kozanecki, M.; Czaderna, A.; Olejniczak, M.; Sielski, J.; Sicinski, M.; Imiela, M.; Wreczycki, J.; Pietrzak, D.; Gozdek, T.; Okraska, M.; Szyrkowska, M. I.; Malinowski, P.; Bielinski, D. M. *J. Sulfur Chem.* **2019**, *40*, 587-597.
60. Arslan, M.; Kiskan, B.; Cengiz, E. C.; Demir-Cakan, R.; Yagci, Y. *Eur. Polym. J.* **2016**, *80*, 70-77.
61. Choudhury, S.; Srimuk, P.; Raju, K.; Tolosa, A.; Fleischmann, S.; Zeiger, M.; Ozoemena, K. I.; Borchardt, L.; Presser, V. *Sustain. Energy Fuels* **2018**, *2*, 133-146.
62. Cui, W. Organic composite material including inorganic nano-material and preparation method and use. WO2002092638A1, **2002**.
63. Dirlam, P. T.; Park, J.; Simmonds, A. G.; Domanik, K.; Arrington, C. B.; Schaefer, J. L.; Oleshko, V. P.; Kleine, T. S.; Char, K.; Glass, R. S.; Soles, C. L.; Kim, C.; Pinna, N.; Sung, Y.-E.; Pyun, J. *ACS Appl. Mater. Interfaces* **2016**, *8*, 13437-13448.
64. Dirlam, P. T.; Simmonds, A. G.; Kleine, T. S.; Nguyen, N. A.; Anderson, L. E.; Klever, A. O.; Florian, A.; Costanzo, P. J.; Theato, P.; Mackay, M. E.; Glass, R. S.; Char, K.; Pyun, J. *RSC Adv.* **2015**, *5*, 24718-24722.
65. Eder, M. L.; Jenkins, C. **2019**, *J. Am. Chem. Soc.*, POLY-0336.
66. Gomez, I.; Leonet, O.; Blazquez, A.; Mecerreyes, D. **2017**, *J. Am. Chem. Soc.* POLY-433.
67. Gomez, I.; Leonet, O.; Blazquez, J. A.; Mecerreyes, D. *ChemSusChem* **2016**, *9*, 3419-3425.
68. Gomez, I.; Mecerreyes, D.; Blazquez, J. A.; Leonet, O.; Ben Youcef, H.; Li, C.; Gomez-Camer, J. L.; Bundarchuk, O.; Rodriguez-Martinez, L. *J. Power Sources* **2016**, *329*, 72-78.
69. Griebel, J. J.; Li, G.; Glass, R. S.; Char, K.; Pyun, J. *J. Polym. Sci. A. Polym. Chem.* **2015**, *53*, 173-177.
70. Hoefling, A.; Nguyen, D. T.; Lee, Y. J.; Song, S.-W.; Theato, P. *Mater. Chem. Front.* **2017**, *1*, 1818-1822.
71. Jiang, Q.; Li, Y.; Zhao, X.; Xiong, P.; Yu, X.; Xu, Y.; Chen, L. *J. Mater. Chem. A* **2018**, *6*, 17977-17981.
72. Li, Z.; Fang, C.; Qian, C.; Zhou, S.; Song, X.; Ling, M.; Liang, C.; Liu, G. *ACS Appl. Polym. Mater.* **2019**, *1*, 1965-1970.
73. Liu, X.; Lu, Y.; Zeng, Q.; Chen, P.; Li, Z.; Wen, X.; Wen, W.; Li, Z.; Zhang, L. *ChemSusChem* **2020**, *13*, 715-723.

74. Moritomo, H.; Shibata, Y. Voltage-driven devices, batteries, displays, magnetic control apparatus, and inversion symmetry control units using cyano-crosslinked metal complexes. JP2010113892A, **2010**.
75. Oleshko, V. P.; Herzing, A. A.; Soles, C. L.; Griebel, J. J.; Chung, W. J.; Simmonds, A. G.; Pyun, J. *Microsc. Microanal.* **2016**, 22, 1198-1221.
76. Oleshko, V. P.; Kim, J.; Schaefer, J. L.; Hudson, S. D.; Soles, C. L.; Simmonds, A. G.; Griebel, J. J.; Glass, R. S.; Char, K.; Pyun, J. *MRS Commun.* **2015**, 5, 353-364.
77. Pyun, J. **2018**, Am. Chem. Soc. pp CHED-1981.
78. Pyun, J.; Zhang, Y.; Carothers, K.; Glass, R.; Char, K. **2017**, Am. Chem. Soc. pp POLY-594.
79. Shukla, S.; Ghosh, A.; Roy, P. K.; Mitra, S.; Lochab, B. *Polymer* **2016**, 99, 349-357.
80. Simmonds, A. G.; Griebel, J. J.; Park, J.; Kim, K. R.; Chung, W. J.; Oleshko, V. P.; Kim, J.; Kim, E. T.; Glass, R. S.; Soles, C. L.; Sung, Y.-E.; Char, K.; Pyun, J. *ACS Macro Lett.* **2014**, 3, 229-232.
81. Wadi, V. S.; Jena, K. K.; Khawaja, S. Z.; Ranagraj, V. M.; Alhassan, S. M. *RSC Adv.* **2019**, 9, 4397-4403.
82. Wang, Z.; Rao, G.; Jiang, Z.; Shang, X.; Yi, J.; Chen, S.; Zhang, X.; Xu, R. Reciprocal network structure of nano sio composite electrolyte and its preparation method. CN105355972A, **2016**.
83. Wei, Y.; Li, X.; Xu, Z.; Sun, H.; Zheng, Y.; Peng, L.; Liu, Z.; Gao, C.; Gao, M. *Polym. Chem.* **2015**, 6, 973-982.
84. Yesilot, S.; Kucukkoylu, S.; Demir, E.; Demir-Cakan, R. *Polym. Chem.* **2020**, 11, 4124-4132.
85. Zhang, Y.; Griebel, J. J.; Dirlam, P. T.; Nguyen, N. A.; Glass, R. S.; MacKay, M. E.; Char, K.; Pyun, J. *J. Polym. Sci., Part A: Polym. Chem.* **2017**, 55, 107-116.
86. Zhao, F.; Li, Y.; Feng, W. *Small Methods* **2018**, 2, 1-34.
87. Kuwabara, J.; Oi, K.; Watanabe, M. M.; Fukuda, T.; Kanbara, T. *ACS Appl. Polym. Mater.* **2020**, 2, 5173-5178.
88. Griebel, J. J.; Nguyen, N. A.; Namnabat, S.; Anderson, L. E.; Glass, R. S.; Norwood, R. A.; Mackay, M. E.; Char, K.; Pyun, J. *ACS Macro Lett.* **2015**, 4, 862-866.
89. Liu, P.; Gardner, J. M.; Kloo, L. *ChemComm.* **2015**, 51, 14660-14662.
90. Bear, J. C.; Peveler, W. J.; McNaughten, P. D.; Parkin, I. P.; O'Brien, P.; Dunnill, C. W. *ChemComm.* **2015**, 51, 10467-10470.
91. Martin, T.; Mazzio, K.; Hillhouse, H.; Luscombe, C. *ChemComm.* **2015**, 51.

92. McNaughter, P. D.; Bear, J. C.; Mayes, A. G.; Parkin, I. P.; O'Brien, P. **2017**, 4, 170383.
93. Zhang, C.; Yan, C.; Xue, Z.; Yu, W.; Xie, Y.; Wang, T. **2016**, 12, 5320-5328.
94. Valle, S. F.; Giroto, A. S.; Klaic, R.; Guimarães, G. G. F.; Ribeiro, C. *Polymer Degradation and Stability* **2019**, 162, 102-105.
95. do Valle, S. F.; Giroto, A. S.; Reis, H. P. G.; Guimarães, G. G. F.; Ribeiro, C. *Journal of Agricultural and Food Chemistry* **2021**, 69, 2392-2402.
96. Liu, Y.-H.; Wang, T.-J.; Qin, L.; Jin, Y. *Powder Technology* **2008**, 183, 88-93.
97. Mann, M.; Kruger, J. E.; Andari, F.; McErlean, J.; Gascooke, J. R.; Smith, J. A.; Worthington, M. J. H.; McKinley, C. C. C.; Campbell, J. A.; Lewis, D. A.; Hasell, T.; Perkins, M. V.; Chalker, J. M. *Org. Biomol. Chem.* **2019**, 17, 1929-1936.
98. Crockett, M. P.; Evans, A. M.; Worthington, M. J.; Albuquerque, I. S.; Slattery, A. D.; Gibson, C. T.; Campbell, J. A.; Lewis, D. A.; Bernardes, G. J.; Chalker, J. M. *Angew. Chem. Int. Ed. Engl.* **2016**, 55, 1714-8.
99. Tikoalu, A. D.; Lundquist, N. A.; Chalker, J. M. *Adv. Sustain. Sys.* **2020**, 4, 1900111.
100. Worthington, M. J. H.; Kucera, R. L.; Albuquerque, I. S.; Gibson, C. T.; Sibley, A.; Slattery, A. D.; Campbell, J. A.; Alboaiji, S. F. K.; Muller, K. A.; Young, J.; Adamson, N.; Gascooke, J. R.; Jampaiah, D.; Sabri, Y. M.; Bhargava, S. K.; Ippolito, S. J.; Lewis, D. A.; Quinton, J. S.; Ellis, A. V.; Johs, A.; Bernardes, G. J. L.; Chalker, J. M. *Chem. Eur. J.* **2017**, 23, 16219-16230.
101. Fu, Y.; Yang, C.; Zheng, Y.; Jiang, J.; Sun, Y.; Chen, F.; Hu, J. *J. Mol. Liq.* **2021**, 328, 115420.
102. Wadi, V. S.; Mittal, H.; Fosso-Kankeu, E.; Jena, K. K.; Alhassan, S. M. *Colloid. Surf. A-Physicochem. Eng. Asp.* **2020**, 606, 125333.
103. Zhang, B.; Dodd, L. J.; Yan, P.; Hasell, T. *React. Funct. Polym.* **2021**, 161, 104865.
104. Je, Sang H.; Buyukcakir, O.; Kim, D.; Coskun, A. *Chem* **2016**, 1, 482-493.
105. Deng, Z.; Hoefling, A.; Théato, P.; Lienkamp, K. *Macromol. Chem. Phys.* **2018**, 219, 1700497.
106. Lee, J.-Sing M.; Parker, D. J.; Cooper, A. I.; Hasell, T. *J. Mater. Chem. A.* **2017**, 5, 18603- 18609.
107. Bear, J. C.; McGettrick, J. D.; Parkin, I. P.; Dunnill, C. W.; Hasell, T. *Microporous and Mesoporous Mater.* **2016**, 232, 189-195.
108. Bear, J. C.; McGettrick, J. D.; Parkin, I. P.; Dunnill, C. W.; Hasell, T. J. M. *Microporous Mesoporous Mater.* **2016**, 232, 189-195.

109. Lee, J.-S. M.; Parker, D. J.; Cooper, A. I.; Hasell, T. J. *J. Mater. Chem. A* **2017**, *5*, 18603-18609.
110. Liu, Y.; Chen, Y.; Zhang, Y.; Chen, Y.; Wang, L.; Zan, X.; Zhang, L. *Polymers* **2020**, *12*.
111. Bear, J.; Peveler, W.; McNaughter, P.; Parkin, I.; O'Brien, P.; Dunnill, C. *ChemCommun.* **2015**, 51.
112. Kim, E. T.; Chung, W. J.; Lim, J.; Johe, P.; Glass, R. S.; Pyun, J.; Char, K. *Polym. Chem.* **2014**, *5*, 3617-3623.
113. Zhuo, S.; Huang, Y.; Liu, C.; Wang, H.; Zhang, B. *ChemComm.* **2014**, *50*, 11208-11210.
114. Yu, S.; Kwon, H.; Noh, H. R.; Park, B.-I.; Park, N. K.; Choi, H.-J.; Choi, S.-C.; Kim, G. D. *RSC Adv.* **2015**, *5*, 36030-36035.
115. Gupta, V.; Ghosh, S.; Phapale, V. *Phosphorus, Sulfur, and Silicon and the Related Elements* **2018**, *193*, 752-758.
116. Couture, R.-M.; Wallschläger, D.; Rose, J.; Van Cappellen, P. *Environ. Chem.* **2013**, *10*.
117. Bonfield, W. **1988**.
118. Thorn, G.; Ludwig, R. *The dithiocarbamates and related compounds.* **1962**.
119. Li, G.; Zhao, Z.; Liu, J.; Jiang, G. *J. hazard. mater.* **2011**, *192*, 277-283.
120. Richardson, J. M.; Jones, C. W. *J. Catal.* **2007**, *251*, 80-93.
121. Yu, M.; Tian, W.; Sun, D.; Shen, W.; Wang, G.; Xu, N. *Anal. Chim. Acta.* **2001**, *428*, 209-218.
122. Lagadic, I. L.; Mitchell, M. K.; Payne, B. D. *Environ. sci. technol.* **2001**, *35*, 984-990.
123. Hernández, G.; Rodríguez, R. *J. non-cryst. solids* **1999**, *246*, 209-215.
124. Lezzi, A.; Cobiacono, S.; Roggero, A. *J.f Polym. Sci. A. Polym. Chem.* **1994**, *32*, 1877-1883.
125. Okamoto, K.; Kanbara, T.; Yamamoto, T.; Wada, A. *Organometallics.* **2006**, *25*, 4026-4029.
126. Kagaya, S.; Sato, E.; Masore, I.; Hasegawa, K.; Kanbara, T. *Chem. lett.* **2003**, *32*, 622-623.
127. Akrivos, P. D. *Coord. Chem. Rev.* **2001**, *213*, 181-210.
128. Kluiber, R. W. *Inorg.* **1965**, *4*, 829-833.
129. Akaiwa, M.; Kanbara, T.; Fukumoto, H.; Yamamoto, T. *J. organomet. chem.* **2005**, *690*, 4192-4196.

130. Koizumi, T.-a.; Teratani, T.; Okamoto, K.; Yamamoto, T.; Shimoi, Y.; Kanbara, T. *Inorganica chim. acta* **2010**, 363, 2474-2480.
131. Kuwabara, J.; Kanbara, T. *J. Photopolym. Sci. Technol.* **2008**, 21, 349-353.
132. Sloodmaekers, B.; Manessi-Zoupa, E.; Perlepes, S.; Desseyn, H. *Spectrochim. Acta A. Mol. Biomol. Spectrosc.* **1996**, 52, 1255-1273.
133. De Beukeleer, S. H.; Desseyn, H. O. *Spectrochim. Acta A. Mol. Spectrosc.* **1994**, 50, 2291-2309.
134. Raper, E. S. *Coord. chem. rev.* **1994**, 129, 91-156.
135. Chuen-Ying, L.; Huan-Tsung, C.; Cho-Chun, H. *Inorganica chim. acta.* **1990**, 172, 151-158.
136. Martin, R.; Masters, A. **1975**, 14, 885-892.
137. Hyder, M. M. Z.; Ochiai, B. *Chem. Lett.* **2017**, 46, 492-494.
138. Nagai, D.; Imazeki, T.; Morinaga, H.; Oku, H.; Kasuya, K. I. *J. Polym. Sci. A. Polym. Chem.* **2010**, 48, 845-851.
139. Ochiai, B.; Ogihara, T.; Mashiko, M.; Endo, T. *J. Am. Chem. Soc.* **2009**, 131, 1636-1637.
140. Nagai, D.; Imazeki, T.; Morinaga, H.; Nakabayashi, H. *J. Polym. Sci. A. Polym. Chem.* **2010**, 48, 5968-5973.
141. Kai, T.; Hagiwara, T.; Haseba, H.; Takahashi, T. *Ind. eng. chem. res.* **1997**, 36, 2757-2759.
142. Zuo, G.; Muhammed, M. *React. Polym.* **1995**, 24, 165-181.
143. Jiang, Y.; Zhang, H.; He, Q.; Hu, Z.; Chang, X. *Microchim. Acta* **2012**, 178, 421-428.
144. Mikysek, T.; Švancara, I.; Vytrás, K.; Banica, F. G. *Electrochem. commun.* **2008**, 10, 242-245.
145. Hinchcliffe, A.; Hughes, C.; Pears, D.; Pitts, M. *Org. Process Res. Dev.* **2007**, 11, 477-481.
146. Nikbin, N.; Ladlow, M.; Ley, S. V. *Org. Process Res. Dev.* **2007**, 11, 458-462.
147. Girgis, M. J.; Kuczynski, L. E.; Berberena, S. M.; Boyd, C. A.; Kubinski, P. L.; Scherholz, M. L.; Drinkwater, D. E.; Shen, X.; Babiak, S.; Lefebvre, B. G. *Org. Process Res. Dev.* **2008**, 12, 1209-1217.
148. Ni, C.; Yi, C.; Feng, Z. *J. Appl. Polym. Sci.* **2001**, 82, 3127-3132.
149. Abd El-Rehim, H.; Hegazy, E.; Ali, A. E.-H. *React. Funct. Polym.* **2000**, 43, 105-116.
150. Kinemuchi, H.; Ochiai, B. *Adv. Mater. Sci. Eng.* **2018**, 3729580.

151. Kagaya, S.; Miyazaki, H.; Ito, M.; Tohda, K.; Kanbara, T. *J. hazard. mater.* **2010**, 175, 1113-1115.
152. Yantasee, W.; Warner, C. L.; Sangvanich, T.; Addleman, R. S.; Carter, T. G.; Wiacek, R. J.; Fryxell, G. E.; Timchalk, C.; Warner, M. G. *Environ. sci. technol.* **2007**, 41, 5114-5119.
153. Qu, Y.; Zhang, X.; Wu, Y.; Li, F.; Hua, J. *Polym. Chem.* **2014**, 5, 3396-3403.
154. Khulbe, K. C.; Matsuura, T. *Appl. Water Sci.* **2018**, 8, 19.
155. Jones, M. M. *Sulfur Reports* **1985**, 4, 119-150.
156. Lundquist, N. A.; Worthington, M. J. H.; Adamson, N.; Gibson, C. T.; Johnston, M. R.; Ellis, A. V.; Chalker, J. M. *RSC Adv.* **2018**, 8, 1232-1236.
157. Wu, X.; Smith, J. A.; Petcher, S.; Zhang, B.; Parker, D. J.; Griffin, J. M.; Hasell, T. *Nat. Comm.* **2019**, 10, 647.
158. Hasell, T.; Parker, D. J.; Jones, H. A.; McAllister, T.; Howdle, S. M. *ChemCommun.* **2016**, 52, 5383-5386.
159. Parker, D. J.; Jones, H. A.; Petcher, S.; Cervini, L.; Griffin, J. M.; Akhtar, R.; Hasell, T. *J. Mater. Chem. A.* **2017**, 5, 11682-11692.
160. Thielke, M.; Bultema, L.; Brauer, D.; Richter, B.; Fischer, M.; Theato, P. *Polymers* **2016**, 8, 266.
161. Abraham, A. M.; Kumar, S. V.; Alhassan, S. M. *Chem. Eng. J.* **2018**, 332, 1-7.
162. Akay, S.; Kayan, B.; Kalderis, D.; Arslan, M.; Yagci, Y.; Kiskan, B. **2017**, 134, 45306.
163. Chalker, J. M., Worthington, M. J. H., Haldane J. Metal Adsorbent Material And Uses Thereof. WO/2017/181217, 26.10.2017, **2017**.
164. Griebel, J. J.; Nguyen, N. A.; Astashkin, A. V.; Glass, R. S.; Mackay, M. E.; Char, K.; Pyun, J. *ACS Macro Letters* **2014**, 3, 1258-1261.
165. Duan, L.; Kong, W.; Yan, W.; Li, C.-H.; Jin, Z.; Zuo, J.-L. *Sustain. Energy Fuels.* **2020**, 4, 2760-2767.
166. Amamoto, Y.; Otsuka, H.; Takahara, A.; Matyjaszewski, K. **2012**, 24, 3975-3980.
167. Tonkin, S. J.; Gibson, C. T.; Campbell, J. A.; Lewis, D. A.; Karton, A.; Hasell, T.; Chalker, J. M. *Chem.l Sci.* **2020**, 11, 5537-5546.
168. Rekondo, A.; Martin, R.; Ruiz de Luzuriaga, A.; Cabañero, G.; Grande, H. J.; Odriozola, I. *Mater. Horiz.* **2014**, 1, 237-240.
169. Caraballo, R.; Rahm, M.; Vongvilai, P.; Brinck, T.; Ramström, O. *ChemComm.* **2008**, 6603-6605.

170. Lei, Z. Q.; Xiang, H. P.; Yuan, Y. J.; Rong, M. Z.; Zhang, M. Q. *Chem. Mater.* **2014**, 26, 2038-2046.
171. Sarma, R. J.; Otto, S.; Nitschke, J. R. *Chem. Eur. J.* **2007**, 13, 9542-9546.
172. Gao, W.; Bie, M.; Liu, F.; Chang, P.; Quan, Y. *ACS Appl. Mater. & Interfaces.* **2017**, 9, 15798-15808.
173. Otsuka, H.; Nagano, S.; Kobashi, Y.; Maeda, T.; Takahara, A. *ChemComm.* **2010**, 46, 1150-1152.
174. Fairbanks, B. D.; Singh, S. P.; Bowman, C. N.; Anseth, K. S. *Macromolecules* **2011**, 44, 2444-2450.
175. Martin, R.; Rekondo, A.; de Luzuriaga, A. R.; Casuso, P.; Dupin, D.; Cabañero, G.; Grande, H. J.; Odriozola, I. *Smart Mater. Struct.* **2016**, 25, 084017.
176. Lin, H.-K.; Liu, Y.-L. *Macromol. Rapid Commun.* **2017**, 38, 1700051.
177. Thiounn, T.; Lauer, M. K.; Bedford, M. S.; Smith, R. C.; Tennyson, A. G. *RSC Adv.* **2018**, 8, 39074-39082.
178. Smith, A. D.; Thiounn, T.; Lyles, E. W.; Kibler, E. K.; Smith, R. C.; Tennyson, A. G. *J. Polym. Sci. A. Polym. Chem.* **2019**, 57, 1704-1710.
179. Hernández, M.; Grande, A. M.; Dierkes, W.; Bijleveld, J.; van der Zwaag, S.; García, S. J. *ACS Sustain. Chem. Eng.* **2016**, 4, 5776-5784.
180. Parker, D. J.; Chong, S. T.; Hasell, T. *RSC Adv.* **2018**, 8, 27892-27899.
181. Arslan, M.; Kiskan, B.; Yagci, Y. *J. Sci. rep.* **2017**, 7, 1-11.
182. Lin, H.-K.; Liu, Y.-L. *Macromol. Rapid Commun.* **2017**, 38, 1700051.
183. Ghosh, A.; Shukla, S.; Khosla, G. S.; Lochab, B.; Mitra, S. J. *J. Sci. rep.* **2016**, 6, 25207.
184. Kamila, S. *Am. J. Appl. Sci.* **2013**, 10, 876.
185. Gramatyka, P.; Kolano-Burian, A.; Kolano, R.; Polak, M. *J. Achiev. Mater. Manuf. Eng.* **2006**, 18, 99-102.
186. Zhang, S.; Pan, L.; Xia, L.; Sun, Y.; Liu, X. *Reac. Funct. Polym.* **2017**, 121, 8-14.
187. Xin, Y.; Peng, H.; Xu, J.; Zhang, J. *Adv. Funct. Mater.* **2019**, 29, 1808989.
188. Kutney, D. G., *Sulfur: History, Technology, Applications and Industry*. 2 ed.; ChemTec Publishing: **2013**.
189. Kimball, S. J. a. S. M., Mineral Commodity Summaries. United States Department of the Interior, U. S. G. S., Ed. **2016**, pp 165–166.
190. çimrin, K.; Turan, M.; Kapur, B. *Fresenius Environ. Bull.* **2007**, 16, 1113-1120.
191. Lee, T. G.; Eom, Y.; Lee, C. H.; Song, K. S. *J. Air Waste Manag. Assoc.* **2011**, 61, 1057-1062.

192. Adamache, I. I. Recovery of elemental sulphur from products containing contaminated elemental sulphur by froth flotation. US4952307A, 1990-08-28, **1990**.
193. Smith, J. A.; Green, S. J.; Petcher, S.; Parker, D. J.; Zhang, B.; Worthington, M. J. H.; Wu, X.; Kelly, C. A.; Baker, T.; Gibson, C. T.; Campbell, J. A.; Lewis, D. A.; Jenkins, M. J.; Willcock, H.; Chalker, J. M.; Hasell, T. **2019**, 25, 10433-10440.
194. Chen, Y.; Yasin, A.; Zhang, Y.; Zan, X.; Liu, Y.; Zhang, L. *Materials* **2020**, 13, 632.
195. Scheiger, J. M.; Direksilp, C.; Falkenstein, P.; Welle, A.; Koenig, M.; Heissler, S.; Matysik, J.; Levkin, P. A.; Theato, P. *Angew. Chem. Int. Ed. Eng.* **2020**, 59, 18639-18645.
196. Sharma, S.; Bhattacharya, A. *Applied Water Science* **2017**, 7, 1043-1067.
197. Warneck, P. *Phys. Chem. Chem. Phys.* **2018**, 20, 4020-4037.
198. Ko, D.; Lee, J. S.; Patel, H. A.; Jakobsen, M. H.; Hwang, Y.; Yavuz, C. T.; Hansen, H. C. B.; Andersen, H. R. *J. Hazard. Mater.* **2017**, 332, 140-148.
199. Thielke, M. W.; Bultema, L. A.; Brauer, D. D.; Richter, B.; Fischer, M.; Theato, P. *Polymers* **2016**, 8, 266.
200. Albukhari, S. M.; Hussein, M. A.; Abdel Rahman, M. A.; Marwani, H. M. *Des. Monomers Polym.* **2020**, 23, 25-39.
201. Prasad, T. D.; Danso-Amoako, E. *Procedia Eng.* **2014**, 70, 1353-1361.
202. Armand, H.; Stoianov, I. I.; Graham, N. J. D. *Urban Water J.* **2017**, 14, 263-277.
203. Shewan, F. A. S. a. M. J. *Aquat. microb. Academic Press*, **1978**.
204. Ohimain, E. *Am. J. Environ. Prot.* **2014**, 3, 59.
205. Sajid, A. *Int. J. Agric. Biol.* **2007**, 9, 333-337.
206. agency, U. S. E. P. Drinking Water Regulations and Contaminants. <https://www.epa.gov/dwregdev/drinking-water-regulations-and-contaminants>. (26 October),
207. Agency, U. S. E. P. National Pollutant Discharge Elimination System (NPDES). <https://www.epa.gov/npdes/industrial-wastewater>. (26 October),
208. Khatri, N. Tyagi, S. Rawtani, D. *J. Water Proc. Eng.* **2017**, 19, 291-304.
209. Ellis, D.; Bouchard, C.; Lantagne, G. *Desalination.* **2000**, 130, 255-264.
210. Carey, E.; Taillefert, M. *Limnol. Oceanogr.* **2005**, 50, 1129-1141.
211. Jameel, P. *J. Water Pollut. Control Fed.* **1989**, 61, 230-236.
212. Vitvitsky, V.; Yadav, P. K.; An, S.; Seravalli, J.; Cho, U.-S.; Banerjee, R. *J. Biol. Chem.* **2017**, 292, 5584-5592.

213. Rickard, D.; Luther, G. W. *Chem. Rev.* **2007**, 107, 514-562.
214. Rohman, A.; Windarsih, A.; Riyanto, S.; Sudjadi; Shuhel Ahmad, S. A.; Rosman, A. S.; Yusoff, F. M. *Int. J. Food Prop.* **2016**, 19, 680-687.
215. Steudel, R.; Chivers, T. *Chem. Soc. Rev.* **2019**, 48, 3279-3319.
216. Trofimov, B. A.; Sinegovskaya, L. M.; Gusarova, N. K. *J. Sulfur Chem.* **2009**, 30, 518-554.
217. Van Wart, H. E.; Lewis, A.; Scheraga, H. A.; Saeva, F. D. *Proc. Natl. Acad. Sci. USA.* **1973**, 70, 2619-2623.
218. Hoefling, A.; Lee, Y. J.; Theato, P. *Macromol. Chem. Phys.* **2017**, 218, 1600303.
219. Lundquist, N. A.; Tikoalu, A. D.; Worthington, M. J. H.; Shapter, R.; Tonkin, S. J.; Stojcevski, F.; Mann, M.; Gibson, C. T.; Gascooke, J. R.; Karton, A.; Henderson, L. C.; Esdaile, L. J.; Chalker, J. M. *Chem. Eur. J.* **2020**, 26, 10035-10044.
220. Benchoam, D.; Cuevasanta, E.; Möller, M. N.; Alvarez, B. *Antioxidants.* **2019**, 8, 48.
221. Agency, U. S. E. P., Drinking Water Regulations and Contaminants. Agency, U. S. E. P., Ed. **2017**.
222. Liu, L.; Luo, X.-B.; Ding, L.; Luo, S.-L., 4 - Application of Nanotechnology in the Removal of Heavy Metal From Water. In *Nanomaterials for the Removal of Pollutants and Resource Reutilization*, Luo, X.; Deng, F., Eds. Elsevier: **2019**; pp 83-147.
223. Munter, R.; Ojaste, H.; Sutt, J. *J. Environ. Eng.* **2005**, 131, 1014-1020.
224. Philibert, M.; Zacchi, C. M.; Pottier, C.; Sacareau, D.; Baudin, I. *Water and Environment Journal* **2020**, 34, 381-389.
225. Cooke, M., Technical Fact Sheet – Perfluorooctane Sulfonate (PFOS) and Perfluorooctanoic Acid (PFOA). (EPA), E. P. A., Ed. Office of Land and Emergency Management, **2017**.
226. Banks, R. E.; Smart, B. E.; Tatlow, J., *Organofluorine chemistry: principles and commercial applications*. Springer Science & Business Media: **2013**.
227. Da Silva-Rackov, C. K. O.; Lawal, W. A.; Nfodzo, P. A.; Vianna, M. M. G. R.; do Nascimento, C. A. O.; Choi, H. *Appl. Catal. B.* **2016**, 192, 253-259.
228. C. Kunacheva, S. Fujii, Shuhei Tanaka, S. Seneviratne, N. P. H. Lien, M. Nozoe, K. Kimura, B. R. Shivakoti, H. Harada *Water Sci. Technol.* **2012**, 66, 2764-2771.
229. Anderson-Mahoney, P.; Kotlerman, J.; Takhar, H.; Gray, D.; Dahlgren, J. *NS.* **2008**, 18, 129-143.
230. Miner, K. R.; Clifford, H.; Taruscio, T.; Potocki, M.; Solomon, G.; Ritari, M.; Napper, I. E.; Gajurel, A. P.; Mayewski, P. A. *Sci. Total Environ.* **2021**, 759, 144421.

231. Grandjean, P.; Clapp, R. *NS*. **2015**, 25, 147-163.
232. Gallo, V.; Leonardi, G.; Genser, B.; Lopez-Espinosa, M.-J.; Frisbee, S. J.; Karlsson, L.; Ducatman, A. M.; Fletcher, T. J. *Environ. Health Perspect.* **2012**, 120, 655-660.
233. Barry, V.; Winqvist, A.; Steenland, K. *Environ. Health Perspect.* **2013**, 121, 1313-1318.
234. Melzer, D.; Rice, N.; Depledge, M. H.; Henley, W. E.; Galloway, T. S. *Environ. Health Perspect.* **2010**, 118, 686-692.
235. Lopez-Espinosa, M.-J.; Mondal, D.; Armstrong, B.; Bloom, M. S.; Fletcher, *Environ. Health Perspect.* **2012**, 120, 1036-1041.
236. Li, K.; Gao, P.; Xiang, P.; Zhang, X.; Cui, X.; Ma, L. Q. *Environ Int.* **2017**, 99, 43-54.
237. Morrissey Donohue, J.; Moore Duke, T.; Wambaugh, J. *Health Effects Support Document for Perfluorooctanoic Acid (PFOA); EPA 822-R-16-003: 2016.*
238. Deng, S.; Nie, Y.; Du, Z.; Huang, Q.; Meng, P.; Wang, B.; Huang, J.; Yu, G. *J. Hazard. Mater.* **2015**, 282, 150-157.
239. Xia, C.; Liu, J. *J. Nanoparticle Res.* **2020**, 22.
240. *Environmental Engineering Science* **2020**, 37, 472-481.
241. Ochoa-Herrera, V.; Sierra-Alvarez, R. *Chemosphere* **2008**, 72, 1588-1593.
242. Pramanik, B. K.; Pramanik, S. K.; Suja, F. *Environ. Technol.* **2015**, 36, 2610-2617.
243. Romchat Rattanaoudom, C. V., Suwanna Kitpati Boontanon. *J. Water Sustain.* **2012**, 2, 245 - 258.
244. Zhang, Q.; Deng, S.; Yu, G.; Huang, J., *Removal of perfluorooctane sulfonate from aqueous solution by crosslinked chitosan beads: Sorption kinetics and uptake mechanism.* **2010**; Vol. 102, p 2265-71.
245. Du, Z.; Deng, S.; Bei, Y.; Huang, Q.; Wang, B.; Huang, J.; Yu, G. *J. Hazard. Mater.* **2014**, 274C, 443-454.
246. Chen, W.; Zhang, X.; Mamadiev, M.; Wang, Z. *RSC Adv.* **2017**, 7, 927-938.
247. Lagergren, S. *Kungliga Svenska Vetenskapsakademiens Handlingar*, **1898**. 24, 1-39.
248. McBirney, S. E.; Trinh, K.; Wong-Beringer, A.; Armani, A. M. *Biomed. Opt. Express.* **2016**, 7, 4034-4042.
249. Duchesne, A. L.; Brown, J. K.; Patch, D. J.; Major, D.; Weber, K. P.; Gerhard, J. I. *Environ. Sci. Technol.* **2020**, 54, 12631-12640.
250. Siriwardena, D. P.; James, R.; Dasu, K.; Thorn, J.; Iery, R. D.; Pala, F.; Schumitz, D.; Eastwood, S.; Burkitt, N. *J Environ. Manage.* **2021**, 289, 112439.
251. Rahimi, A.; García, J. M. *J. Nat. Rev.* **2017**, 1, 1-11.

252. Morales Ibarra, R., Chapter 20 - Recycling of thermosets and their composites. In *Thermosets (Second Edition)*, Guo, Q., Ed. Elsevier: **2018**, pp 639-666.
253. Fortman, D. J.; Brutman, J. P.; De Hoe, G. X.; Snyder, R. L.; Dichtel, W. R.; Hillmyer, M. A. *ACS. Sustain. Chem. Eng.* **2018**, 6, 11145-11159.
254. Fortman, D. J., Brutman, Jacob P., De Hoe, Guilhem X., Snyder, Rachel L., Dichtel, William R., Hillmyer, Marc A. *ACS Sustain. Chem. Eng.* **2018**, 6, 14.
255. Canadell, J.; Goossens, H.; Klumperman, B. *Macromolecules* **2011**, 44, 2536-2541.
256. Lafont, U.; van Zeijl, H.; van der Zwaag, S. *ACS Appl. Mater. Interfaces.* **2012**, 4, 6280-6288.
257. Chakma, P.; Konkolewicz, D. *Angew. Chem.* **2019**, 58, 9682-9695.
258. Michal, B. T.; Jaye, C. A.; Spencer, E. J.; Rowan, S. J. *ACS Macro Lett.* **2013**, 2, 694-699.
259. Imbernon, L.; Oikonomou, E. K.; Norvez, S.; Leibler, L. *Polym. Chem.* **2015**, 6, 4271-4278.
260. Karunarathna, M. S.; Lauer, M. K.; Thiounn, T.; Smith, R. C.; Tennyson, A. G. *J. Mater. Chem. A.* **2019**, 7, 15683-15690.
261. Lauer, M. K.; Estrada-Mendoza, T. A.; McMillen, C. D.; Chumanov, G.; Tennyson, A. G.; Smith, R. C. *Adv. Sustainable Syst.* **2019**, 3, 1900062.
262. Zhang, Y.; Konopka, K. M.; Glass, R. S.; Char, K.; Pyun, J. *Polym. Chem.* **2017**, 8, 5167-5173.
263. Zhang, B.; Petcher, S.; Hasell, T. *ChemComm.* **2019**, 55, 10681-10684.
264. Arslan, M.; Kiskan, B.; Yagci, Y. *Sci Rep* **2017**, 7, 5207.
265. Hasell, T.; Yan, P.; Zhao, W.; Zhang, B.; Jiang, L.; Petcher, S.; Smith, J.; Parker, D.; Cooper, A.; Lei, J. *Angew. Chem. Int. Ed.* **2020**, 59.
266. Akkus, B.; Kiskan, B.; Yagci, Y. *Polym Chem* **2019**, 10, 5743-5750.
267. Xin, Y.; Peng, H.; Xu, J.; Zhang, J. **2019**, 29, 1808989.
268. Westerman, C. R.; Jenkins, C. L. *Macromolecules* **2018**, 51, 7233-7238.
269. Wu, M. S.; Centea, T.; Nutt, S. R. *Adv. Manuf.: Polym. Compos. Sci.* **2018**, 4, 1-12.
270. Bilgili, E.; Dybek, A.; Arastoopour, H.; Bernstein, B. *J. Elastomers Plast.* **2003**, 35, 235-256.
271. Denk, M. K. *Eur. J. Inorg. Chem.* **2009**, 1358-1368.
272. Shukla, S.; Ghosh, A.; Roy, P. K.; Mitra, S.; Lochab, B. *Polymer* **2016**, 99, 349-357.

273. Yuan, L.; Yuan, H.; Qiu, X.; Chen, L.; Zhu, W. *J. Power Sources* **2009**, 189, 1141-1146.
274. Han, S. C.; Song, M. S.; Lee, H.; Kim, H. S.; Ahn, H. J.; Lee, J. Y. *J. Electrochem. Soc.* **2003**, 150, A889-A893.
275. Wei, W.; Wang, J.; Zhou, L.; Yang, J.; Schumann, B.; Nuli, Y. *Electrochem. Commun.* **2011**, 13, 399-402.
276. Zeng, S.-Z.; Zeng, X.; Tu, W.; Huang, H.; Yu, L.; Yao, Y.; Jin, N.; Zhang, Q.; Zou, J. *ACS App. Mater. Interfaces.* **2018**, 10, 22002-22012.
277. Wang, H.; Yang, Y.; Liang, Y.; Robinson, J. T.; Li, Y.; Jackson, A.; Cui, Y.; Dai, H. *Nano Lett.* **2011**, 11, 2644-2647.
278. Zheng, G.; Yang, Y.; Cha, J. J.; Hong, S. S.; Cui, Y. *Nano Lett.* **2011**, 11, 4462-4467.
279. Wang, J.; Yang, J.; Wan, C.; Du, K.; Xie, J.; Xu, N. *Adv. Func. Mater.* **2003**, 13, 487-492.
280. Sun, M.; Zhang, S.; Jiang, T.; Zhang, L.; Yu, J. *Electrochem. Commun.* **2008**, 10, 1819-1822.
281. Doan, T. N. L.; Ghaznavi, M.; Zhao, Y.; Zhang, Y.; Konarov, A.; Sadhu, M.; Tangirala, R.; Chen, P. *J. Power Sources* **2013**, 241, 61-69.
282. Puthirath, A. B.; Baburaj, A.; Kato, K.; Salpekar, D.; Chakingal, N.; Cao, Y.; Babu, G.; Ajayan, P. M. *Electrochim. Acta* **2019**, 306, 489-497.
283. Gwon, S.; Shin, M. *Constr. Build. Mater.* **2019**, 228, 116784.
284. Schwartz, M. A.; Llewellyn, T. O., Sulfur in Construction Materials. In *New Uses of Sulfur*, Am. Chem. Soc. **1975**; Vol. 140, pp 75-84.
285. Jafari, M.; Kadivar, M.; Keramat, J. *J. Am. Oil Chem. Soc.* **2009**, 86, 103-110.
286. Reding, F. P.; Walter, E. R.; Welch, F. J. *J. Polym. Sci.* **1962**, 56, 225-231.
287. Wani, A. L., Ara, A., Usmani, J. A., *Interdiscip Toxicol.* **2015**, 8, 55-64
288. Hasell, T.; Parker, D. J.; Jones, H. A.; McAllister, T.; Howdle, S. M. *ChemComm.* **2016**, 52, 5383-5386.
289. Lundquist, N. A.; Chalker, J. M. *SM&T.* **2020**, 26, e00222.
290. Griebel, J.; Namnabat, S.; Kim, E.; Himmelhuber, R.; Moronta, D.; Chung, W.; Simmonds, A.; Kim, K.-J.; van der Laan, J.; Nguyen, N.; Dereniak, E.; Mackay, M.; Char, K.; Glass, R.; Norwood, R.; Pyun, J. *Adv. mater.* **2014**, 26.
291. Saito, T.; Tsuruta, H.; Watanabe, A.; Ishimine, T.; Ueno, T. *AIP Adv.* **2018**, 8, 047708/1-047708/6.

292. McHenry, M. E., Magnetic Steels. In *Encyclopedia of Materials: Science and Technology*, Buschow, K. H. J.; Cahn, R. W.; Flemings, M. C.; Ilshner, B.; Kramer, E. J.; Mahajan, S.; Veyssi re, P., Eds. Elsevier: Oxford, **2001**; pp 4961-4964.
293. Kotnala, R. K.; Shah, J., Chapter 4 - Ferrite Materials: Nano to Spintronics Regime. In *Handbook of Magnetic Materials*, Buschow, K. H. J., Ed. Elsevier: **2015**; Vol. 23, pp 291-379.
294. Grybos, D.; Leszczynski, J.; Swieboda, C.; Kwiecien, M.; Rygal, R.; Soinski, M.; Pluta, W. In *Magnetic properties of composite cores made of nanocrystalline material for high frequency inductors and transformers*, 2018 Innovative Materials and Technologies in Electrical Engineering (i-MITEL), 18-20 April, **2018**; pp 1-6.
295. Sun, H.; Zhang, L.; Chen, Y.; Chen, F.; Qu, X.; Xie, C.; Zhang, L. *J. Mater.* **2019**, 486, 165287.
296. Chen, Y.; Zhang, L.; Sun, H.; Chen, F.; Zhang, P.; Qu, X.; Fan, E. *J. Alloys Compd.* **2020**, 813, 152205.
297. Mehdinia, A.; Haddad, H.; Mozaffari, S. *J. sep. sci.* **2016**, 39, 3418-27.
298. Wu, H.; Zhang, H.; Zhang, W.; Yang, X.; Zhou, H.; Pan, Z.; Wang, D. *Chemosphere* **2019**, 219, 66-75.
299. Wu, S.; Sun, A.; Lu, Z.; Cheng, C. *Mater. Chem. Phys.* **2015**, 153, 359-364.
300. Li, D.-S.; Liu, B.; Wang, Y.-F.; Liu, W.-L.; Ren, M.-M.; Kong, F.-G.; Wang, S.-J.; Yue, K.; Meng, Q. *J. Solgel Sci. Technol.* **2019**, 92, 124-133.
301. Streckova, M.; Bures, R.; Faberova, M.; Medvecky, L.; Fuzer, J.; Kollar, P. *Chin. J. Chem. Eng.* **2015**, 23, 736-743.
302. Koll r, P.; Bir akov , Z.; F zer, J.; Bureš, R.; F berov , M. *J. Magn. Magn. Mater.* **2013**, 327, 146-150.
303. T.A, L.; Manna, S.; B.G, F.; N, V. *Physics Procedia.* **2015**, 75, 1396-1403.
304. Zhang, H.; Huang, R.; Li, Y.; Li, H.; Wu, Z.; Huang, J.; Yu, B.; Gao, X.; Li, J.; Li, L. *Polymers.* **2019**, 11, 1335.
305. Aikawa, Y. Iron aluminum silicon soft magnetic powder for magnetic core. JP2004128327A, **2004**.
306. Fan, X.; Luo, Z.; Li, G.; Li, Y. Multiple insulating layer iron silicon-based soft magnetic powder core for electronic component and preparation method thereof. CN108899152A, **2018**.
307. Guo, X.; Zhang, Y.; Xiao, Q.; Xu, F.; Zhou, J.; Liu, H.; He, K. Silicone resin. WO2019029145A1, **2019**.

308. Huang, J.; Wang, Z. Method for preparing iron-silicon-aluminum soft magnet magnetic core through warm pressing. CN105344993A, **2016**.
309. Li, J.; Sun, Y. Iron-silicon soft magnetic powder, its preparation method and application in preparation of iron-silicon magnetic powder core. CN111370197A, **2020**.
310. Li, J.; Sun, Y.; Jin, Z. Iron-silicon-aluminum soft magnetic powder, its preparation method and application in preparation of magnetic powder core. CN111370194A, **2020**.
311. Li, X.; Pang, J.; Ji, J.; Jiang, Z. Iron-silicon-aluminum magnetic core and its preparation method. CN108597714A, **2018**.
312. Luo, Y.; Pei, X.; Liu, C.; Zhang, J.; Li, T. Iron-silicon-aluminum-nickel soft magnetic powder core with effective magnetic conductivity of 90 for switch power supply and preparation method thereof. CN110853907A, **2020**.
313. Luo, Y.; Pei, X.; Wang, F.; Bao, W.; Xu, C.; Cao, H. Preparation method of iron-silicon-aluminum-nickel soft magnetic powder core with effective magnetic permeability of 125 for boost inductor. CN110853858A, **2020**.
314. Sun, A.; Wu, S.; Zou, C.; Dong, J.; Yang, J.; Xing, Y. Silicone-ferrite composite coated soft magnetic powder core and preparation method thereof. CN103151134A, 2013.
315. Tang, F.; Tong, X.; Zou, Z.; Su, H.; Ma, J.; Du, Y. Method for preparing iron silicon metal soft magnetic powder core. CN107275032A, **2017**.
316. Tang, F.; Zou, Z.; Tong, X.; Su, H.; Ma, J.; Du, Y. Annealing method for improving DC bias property of iron-silicon-aluminum soft magnetic powder core. CN107119174A, **2017**.
317. Yan, L.; Yan, B. Preparation method of high-silicon steel-ferrite composite soft magnetic powder core. CN106409462A, **2017**.
318. Yao, C.; Xiong, W.; Shen, J. Method for preparing ferro-silicon-aluminum soft magnetic powder core with $\mu=150-250$. CN109680210A, **2019**.
319. Yao, G. Preparation of iron-silicon-aluminum soft magnetic powder. CN105014065A, **2015**.
320. Guo, Z.; Wang, J.; Chen, W.; Chen, D.; Sun, H.; Xue, Z.; Wang, C. J. M.; Design. **2020**, 108769.
321. Larumbe, S.; Gómez-Polo, C.; Pérez-Landazábal, J. I.; Pastor, J. M. *J. Phys. Condens. Matter*. **2012**, 24, 266007.

322. Lee, S. H.; Lee, D. H.; Jung, H.; Han, Y.-S.; Kim, T.-H.; Yang, W. *Curr. Appl. Phys.* **2015**, 15, 915-919.
323. Pham, X.-H.; Eunil, H.; Kim, H.-M.; Son, B.; Jo, A.; An, J.; Thi, T.; Nguyen, Q.; Jun, B.-H. *Nanomaterials* **2020**, 10, 117.
324. Dey, C.; Das, A.; Goswami, M. M. *ChemistrySelect.* **2019**, 4, 12190-12196.
325. Wang, J.; Wu, Z.; Li, G. *J Adv. Powder Technol.* **2016**, 27, 1189-1194.
326. Zhao, F.; Liang, W.; Li, Z.; Li, K.; Deng, P. Method for preparing metal soft magnetic powder core by using SiO₂ coated metal powder and metal soft magnetic powder core prepared with the method. CN107020373A, **2017**.
327. Sunday, K. J.; Taheri, M.; Darling, K.; Hanejko, F., *PowderMet Conference Proceedings.* **2015**.
328. Peng, Y.; Yi, Y.; Li, L.; Yi, J.; Nie, J.; Bao, C. *Mater. Des.* **2016**, 109, 390-395.
329. Duan, C.-L.; Deng, Z.; Cao, K.; Yin, H.-F.; Shan, B.; Chen, R. J. *Vac. Sci. Technol.* **2016**, 34, 04C103.
330. Li, K.; Liu, S.; Xue, Y.; Zhang, L.; Han, Y. *J. Mater. Chem. B.* **2019**, 7, 5265-5276.
331. Yao, H.; Fan, M.; Wang, Y.; Luo, G.; Fei, W. *J. Mater. Chem. A.* **2015**, 3, 17511-17524.
332. Fu, W.; Yang, H.; Chang, L.; Hari, B.; Li, M.; Zou, G. *Colloid. Surf. A-Physicochem. Eng. Asp.* **2006**, 289, 47-52.
333. Shahid, M.; McDonagh, A.; Kim, J.; Shon, H. K. *Desalination Water Treat.* **2014**, 54, 1-24.
334. De Matteis, L.; Custardoy, L.; Fernández-Pacheco, R.; Magén, C.; de la Fuente, J. M.; Marquina, C.; Ibarra, M. R. *Chem. Mater.* **2012**, 24, 451-456.
335. Tan, D.; Jin, J.; Guo, C.; Dhanjai; Chen, J. *Environ. Chem. Lett.* **2020**
336. Xiao, L.; Fan, H.; Cheng, W.; Li, Z.; Li, M. *Proc. Inst. Mech. Eng.* **2019**, 233, 1134-1144.
337. Safarikova, M. *J. chromatogr. B Biomed. sci. appl* **1999**, 722, 33-53.
338. Raghavarao, K.; Dueser, M.; Todd, P. *Adv. biochem. engin./biotechnol.* **2000**, 68, 139-90.
339. Liberti, P. A.; Feeley, B. P., Analytical- and Process-Scale Cell Separation with Bioreceptor Ferrofluids and High-Gradient Magnetic Separation. In Cell Separation Science and Technology, *Am. Chem. Soc.* **1991**, Vol. 464, pp 268-288.
340. Svoboda, J. *Magnetic Separation News* **1989**, 2.
341. Bahaj, A.; James, P. A. B.; Moeschler, F. D. *IEEE Trans. Magn.* **1996**, 32, 5106-5108.
342. Deng, T.; Prentiss, M.; Whitesides, G. M. **2002**, 80, 461-463.

343. Pankhurst, Q. A.; Connolly, J.; Jones, S. K.; Dobson, J. *J. Phys. D Appl. Phys.* **2003**, 36, R167-R181.
344. Hsieh, T.-H.; Ho, K.; Bi, X.; Han, Y.-K.; Chen, Z.-L.; Hsu, C.-H.; Chang, Y. *Euro. Polym. J.* **2009**, 45, 613-620.
345. Bregar, V. *IEEE Trans. Magn.* **2004**, 40, 1679-1684.
346. Sun, J.; Wang, W.; Yue, Q. *Materials* **2016**, 9, 231.
347. Priece, P.; Lopez-Sanchez, J. A. *ACS Sustain. Chem. Eng.* **2019**, 7, 3-21.
348. Bertotti, G.; Fiorillo, F., Magnetic Losses. In *Reference Module in Materials Science and Materials Engineering*, Elsevier: **2016**.
349. Mishra, R. R.; Sharma, A. K. *Composites Part A: Applied Science and Manufacturing* **2016**, 81, 78-97.
350. Endo, I.; Tatsumi, H.; Otsuka, I.; Yamamoto, H.; Shintani, A.; Koshimoto, H.; Yagi, M.; Murata, K. *i-MITEL*. **2000**, 36, 3421-3423.
351. Hilzinger, R.; Rodewald, W., *Magnetic materials: fundamentals, products, properties, applications*. Vacuumschmelze: **2013**.
352. Iqbal, Y.; Davies, H.; Gibbs, M.; Woodcock, T.; Todd, I.; Major, R. *J. Magn. Magn. Mater.* **2002**, 242, 282-284.
353. Liu, Y.; Yi, Y.; Shao, W.; Shao, Y. *J. Magn. Magn. Mater.* **2013**, 330, 119-133.
354. Mazaleyrat, F.; Léger, V.; Lebourgeois, R.; Barrué, R. *IEEE Trans. Magn.* **2002**, 38, 3132-3134.
355. McLyman, C. W. T., *Transformer and inductor design handbook*. Dekker New York,, USA: **1988**.
356. Nikolov, G. T.; Valchev, V. C. *Procedia Earth and Planetary Science* **2009**, 1, 1357-1361.
357. Nowosielski, R.; Wysocki, J.; Wnuk, I.; Gramatyka, P. *J. Mater. Process. Technol.* **2006**, 175, 324-329.
358. Raja, M. M.; Ponpandian, N.; Majumdar, B.; Narayanasamy, A.; Chattopadhyay, K. *J. Mater. Sci Eng.* **2001**, 304, 1062-1065.
359. Rylko, M. S.; Hartnett, K. J.; Hayes, J. G.; Egan, M. G. Magnetic Material Selection for High Power High Frequency Inductors in DC-DC Converters, *Twenty-Fourth Annual IEEE Appl. Power Electron. Conf. Expo.* **2009**, pp 2043-2049.
360. Zhang, Y.; Sharma, P.; Makino, A. *IEEE Trans. Magn.* **2014**, 50, 1-4.

361. Zare, S.; Kargari, A., 4 - Membrane properties in membrane distillation. In *Emerging Technologies for Sustainable Desalination Handbook*, Gude, V. G., Ed. Butterworth-Heinemann: **2018**, pp 107-156.
362. Wagloehner, S.; Kureti, S. *Appl. Catal. B.* **2012**, 125, 158-165.
363. Yuan, Y.; Wang, L.; Gao, L. *Front. Chem.* **2020**, 8.